

ON THE DESIGN AND DEVELOPMENT OF ROBOTIC MECHANISMS FOR LAPAROSCOPIC SURGERY

by

Te-mei Li
B. Sc. Tamkang University, 1988
M. Sc. University of Missouri – Columbia, 1991

THESIS SUBMITTED IN PARTIAL FULFILLMENT OF
THE REQUIREMENTS FOR THE DEGREE OF
DOCTOR OF PHILOSOPHY

In the School
of
Engineering Science

© Te-mei Li 2006
SIMON FRASER UNIVERSITY
Spring 2006

All rights reserved. This work may not be
reproduced in whole or in part, by photocopy
or other means, without permission of the author

APPROVAL

Name: Te-mei Li
Degree: Doctor of Philosophy
Title of Thesis: On the Design and Development of Robotics
Mechanisms for Laparoscopic Surgery

Examining Committee:

Chair: Dr. Shawn Stapleton
Professor, School of Engineering Science

Dr. Shahram Payandeh, Senior Supervisor
Professor, School of Engineering Science

Dr. John Dill
Professor, School of Engineering Science

Dr. Bonnie Gray
Assistant Professor, School of Engineering Science

Dr. John Jones, Internal Examiner
Associate Professor, School of Engineering Science

Dr. Nariman Sepehri, External Examiner
Professor, Department of Mechanical and Industrial
Engineering, University of Manitoba

Date Defended/Approved: December, 16, 2005



DECLARATION OF PARTIAL COPYRIGHT LICENCE

The author, whose copyright is declared on the title page of this work, has granted to Simon Fraser University the right to lend this thesis, project or extended essay to users of the Simon Fraser University Library, and to make partial or single copies only for such users or in response to a request from the library of any other university, or other educational institution, on its own behalf or for one of its users.

The author has further granted permission to Simon Fraser University to keep or make a digital copy for use in its circulating collection, and, without changing the content, to translate the thesis/project or extended essays, if technically possible, to any medium or format for the purpose of preservation of the digital work.

The author has further agreed that permission for multiple copying of this work for scholarly purposes may be granted by either the author or the Dean of Graduate Studies.

It is understood that copying or publication of this work for financial gain shall not be allowed without the author's written permission.

Permission for public performance, or limited permission for private scholarly use, of any multimedia materials forming part of this work, may have been granted by the author. This information may be found on the separately catalogued multimedia material and in the signed Partial Copyright Licence.

The original Partial Copyright Licence attesting to these terms, and signed by this author, may be found in the original bound copy of this work, retained in the Simon Fraser University Archive.

Simon Fraser University Library
Burnaby, BC, Canada

Abstract

Laparoscopic surgery is performed in the abdominal area of a patient, through small incisions. Despite advantages to patients, surgeons have difficulties such as loss in manipulation ability, reduction in dexterity and sensation of touch, and indirect vision. Laparoscopic surgery requires the surgeons to learn a new form of hand-eye coordination and to become skillful in the manipulation of instruments.

The objective of this research is in the synthesis, design, and development of new robotic mechanisms to assist surgeons to overcome surgical difficulties. These robotic mechanisms solve existing surgical problems such as inaccuracy in positioning of endoscopic tools, lack of force/tactile feedback, reduced dexterity and pneumoperitoneum.

First, to solve the problem of positioning of endoscopic tools, a compact automated surgical tool-holding mechanism was designed and developed as a four DOF surgical robotic arm. This mechanism manipulates and positions the surgical tools or a laparoscopic camera automatically and thus eliminates the need for human assistance. The design parameters are optimized for a maximal workspace. The kinematics and numerical examples are presented.

Second, to solve lack of force/tactile feedback problem, both gimbal and spherical parallel type devices are designed and developed to provide four DOF force feedback in surgical training or telesurgery. The spherical parallel types utilize a passive support component to support the weight and reduce inertia. The direct and inverse kinematics are discussed with direct kinematics solved by a neural network model for real time application.

Third, design for manufacturing and cost structure model for haptic devices are analyzed. This design for manufacturability is implemented after which the bill of materials, machining process, and analysis of tolerance and accuracy are presented.

Fourth, supporting mechanisms such as a local master-slave mechanism and abdominal surgical space maker are designed. The local master-slave mechanism contains two rotational DOF to increase surgical dexterity for difficult surgical tasks. This mechanism is manually actuated without motor. The abdominal surgical space maker is a foldable structure that can be folded in a tube and inserted into the patient's abdominal wall to expand and create space.

Acknowledgements

Thanks to my senior supervisors, Dr. Shahram Payandeh, for his advice and support throughout this thesis work. This work would not be possible without his enthusiasm and knowledge of inter-disciplinary research. I also appreciate the time and efforts he put into all my writings.

Thanks to Dr. John Dill for his advice and support throughout this thesis. Thanks to Dr. Bonnie Gray for being my thesis committee. Also thanks to Dr. John Jones for examining this thesis and Dr. Shawn Stapleton for chairing my defence. Thanks to Dr. Nariman Sepehri from University of Manitoba to be my External Examiner.

It is grateful that Mr. Hendrik Van der Wal in machine technology center spared his time on the prototyping different project and taught me practical manufacturing knowledge. I would also like to thank Dr. Alan Lomax for his invaluable surgery expertise, comments, and suggestions on the design and evaluation of the haptic device. Thanks to Qingguo Li for helping me for sharing his helpful experience. I also thank all my fellow colleagues in Experimental Robotics Lab (ERL) and those students who have worked in ERL. I have gained many help from them, both in technical aspect and daily life. Thanks to all my dear friends at SFU for making my life here a great and precious time.

Finally, I want to thank my family for their spiritual support and love.

Table of Contents

Approval	ii
Abstract.....	iii
Acknowledgements	v
Table of Contents	vi
List of Figures.....	ix
List of Tables	xv
Glossary	xvi
Acronym.....	xix
1. Introduction.....	1
1.1. Minimally Invasive Surgery	1
1.2. Problem Statement and Robotic Assistance	3
1.3. Objectives and Outline.....	9
1.4. Contributions.....	11
2. Design of Surgical Tool-Holding and Tele-Operation Mechanism	13
2.1. Design Objectives and Related Research	14
2.2. Design Process	20
2.2.1. Function Specification	20
2.2.2. Type Synthesis	22
2.2.3. Characteristics and Classification of Parallel Device	29
2.2.4. Comparison of Serial and Parallel Mechanism.....	30
2.3. Mechanical Structural Design.....	32
2.4. Kinematic Model	42
2.5. Workspace optimization of Genetic Algorithm	49
2.6. Kinematics Analysis	54
2.6.1. Inverse Kinematics.....	54
2.6.2. Numerical Example of Inverse Kinematics	58

2.6.3.	Direct Kinematics	61
2.6.4.	Collision Determination.....	64
2.6.5.	Linear motion Analysis.....	67
2.7.	Integration and Experimental setup	68
2.8.	Discussion	70
3.	Design of Surgical Haptic Force Feedback Device	73
3.1.	Introduction.....	74
3.1.1.	Mechanical Characteristics and Design Objectives	75
3.1.2.	Previous Research.....	76
3.2.	Mechanical Design.....	77
3.2.1.	Square Frame Gimbal Type (SFGT).....	78
3.2.2.	Ring Frame Gimbal Type (RFGT)	84
3.2.3.	Hybrid Parallel Support Type (HPST).....	90
3.2.4.	Spherical Parallel Ball Support Type (SPBS).....	98
3.2.5.	Two handed Type (THT)	105
3.3.	Kinematic Modeling	107
3.3.1.	Inverse Kinematic of SPBS	112
3.3.2.	Numerical Example of Inverse Kinematics	115
3.3.3.	Direct Kinematics of SPBS.....	120
3.3.4.	Numerical Example of Direct Kinematics	123
3.3.5.	Experimental setup and measurement result.....	129
3.3.6.	Neural Network Method to solve DK.....	131
3.4.	Discussion	138
4.	Design for Manufacturing.....	140
4.1.	Design Guidelines for Manufacture and Assembly.....	142
4.2.	Bill of Materials	152
4.3.	Machining Processes.....	154
4.4.	Modeling of Manufacturing Cost.....	156
4.5.	Tolerance and Accuracy Analysis	160

5. Master-slave and Supporting Mechanisms	164
5.1. Two-DOF Local Master-Slave Mechanism.....	169
5.2. Abdominal Space Maker.....	183
5.3. Discussion	190
6. Conclusion	193
6.1. Summary and Contributions	193
6.2. Future Work Suggestion	197
Appendix A Drawings of Assembly and Parts	201
Appendix B Design for Manufacturing Guidelines	205
Reference list	207

List of Figures

Figure 1-1 Minimally invasive surgery- Laparoscopic.....	1
Figure 1-2 Various monitor positions (USC department of Surgery).....	4
Figure 1-3 Intuitive surgical robot set up in operation room.....	8
Figure 2-1 The laparoscopic operation room set up	14
Figure 2-2 Laparoscopic surgical tools.....	15
Figure 2-3 Four DOF concentric multi link spherical joint.....	16
Figure 2-4 Osaka University robotic laparoscope positioning system	16
Figure 2-5 Sketch of Endo Assist	17
Figure 2-6 LER	18
Figure 2-7 Kinematics diagram of Da Vinci robot	18
Figure 2-8 Surgical robotic arm developed by Intuitive Surgical.....	19
Figure 2-9 Four DOF requirements of laparoscopic tool or camera.....	21
Figure 2-10 Structure of type synthesis	22
Figure 2-11 Ball joint type three DOF.....	25
Figure 2-12 Serial type three rotational DOF	26
Figure 2-13 Hybrid type three rotational DOF	27
Figure 2-14 Three DOF spherical parallel type	28
Figure 2-15 Kinematics structure of serial and parallel mechanism.....	31
Figure 2-16 Mechanical design of tool-holding mechanism	32
Figure 2-17 Nested linkage.....	34
Figure 2-18 Orthogonal axes platform.....	35
Figure 2-19 270 mm arm length	35
Figure 2-20 Concentric actuating axes	36
Figure 2-21 Concentric parallel spur gears	37
Figure 2-22 Photograph of the tool-holding mechanism	38
Figure 2-23 Comparing the link size of first and second mechanism.....	39
Figure 2-24 Revolute middle joint.....	40
Figure 2-25 Lead screw linear motion design module.....	40
Figure 2-26 Concentric link module	41

Figure 2-27 Schematic drawing of the three DOF spherical platform.....	42
Figure 2-28 Link angles.....	43
Figure 2-29 World coordinate frame	44
Figure 2-30 Angle of actuating coordinate frame.....	44
Figure 2-31 Link coordinate frame	45
Figure 2-32 Platform coordinate frame.....	46
Figure 2-33 Camera/Tool Coordinate frame.....	46
Figure 2-34 Branch link radii.....	47
Figure 2-35 Actuating angles.....	48
Figure 2-36 Middle revolute angle	48
Figure 2-37 Workspace volume.....	51
Figure 2-38 GA flow chart.....	51
Figure 2-39 An example of Crossover model.....	52
Figure 2-40 Flow chart of solving inverse kinematics.....	55
Figure 2-41 Spherical triangle	57
Figure 2-42 Top view of platform home position.....	59
Figure 2-43 Link platform angles	63
Figure 2-44 Collision range of branch 1	66
Figure 2-45 Collision range of branch 2	66
Figure 2-46 Collision range of branch 3	67
Figure 2-47 Experimental setup of tool holding mechanism.....	68
Figure 3-1 Friction of surgical tool.....	75
Figure 3-2 CAD model of SFGT	79
Figure 3-3 Prototype of SFGT	79
Figure 3-4 Base frame with brackets	80
Figure 3-5 Primary bracket and platform of square frame gimbal type	81
Figure 3-6 The section view of square frame gimbal type	83
Figure 3-7 Prototype of RFGT (Photo I)	84
Figure 3-8 Prototype of RFGT (Photo II).....	85
Figure 3-9 Lower frame assembly of RFGT.....	86
Figure 3-10 Two-DOF platform with handle of RFGT	87

Figure 3-11 Crank slider type (a) and (b)	87
Figure 3-12 Force component of crank slider.....	88
Figure 3-13 Prototype of crank slider type and close view of slider	89
Figure 3-14 Motor s and pulley system for Z-axis	89
Figure 3-15 CAD model of HPST	91
Figure 3-16 Rendering image from side and top view	92
Figure 3-17 Photograph of HPST prototype.....	92
Figure 3-18 Design of one branch of HPST	93
Figure 3-19 Linear motion design.....	94
Figure 3-20 Three rotational DOF yoke type passive supporting mechanism .	95
Figure 3-21 Symmetrical motor alignment.....	96
Figure 3-22 Prototype of HPSTA	97
Figure 3-23 Schematic diagram of the spherical parallel platform.....	98
Figure 3-24 CAD model of SPBS (iso and front view).....	99
Figure 3-25 Mechanical structure of SPBS (one branch)	100
Figure 3-26 Photograph of SPBS prototype	101
Figure 3-27 Torque and force of active link	102
Figure 3-28 Displacement calculation of active link	103
Figure 3-29 The active link with slot.....	104
Figure 3-30 CAD model of two-handed type	105
Figure 3-31 Prototype of two-handed type	106
Figure 3-32 Connecting pin of Two handed type	107
Figure 3-33 World coordinate frame	108
Figure 3-34 World coordinate frame and Platform coordinate frame	109
Figure 3-35 Handle coordinate frame	110
Figure 3-36 Kinematic notation diagram of SPBS	110
Figure 3-37 Middle joint vector of SPBS	111
Figure 3-38 Link arc angle.....	111
Figure 3-39 Mapping between kinematic	112
Figure 3-40 Two possible solutions of middle joint vector	114
Figure 3-41 Active cam rotation direction.....	115

Figure 3-42 Front and top view of home position	116
Figure 3-43 Direct kinematics link angle (shown on one branch).....	121
Figure 3-44 Home position of SPBS (top and side view).....	124
Figure 3-45 The configurations corresponding to the eight solution.....	127
Figure 3-46 The CAD model of corresponding solutions	128
Figure 3-47 Experimental setup for measurement.....	129
Figure 3-48 Diagram of the neural network for haptic device.....	133
Figure 3-49 Network approximation of spiral trajectory	135
Figure 3-50 Network approximation error of direct kinematics	136
Figure 3-51 Comparison of neural network model and experiment	137
Figure 3-52 Error between neural network model and experiment	138
Figure 4-1 Engineering design circles	141
Figure 4-2 Taxonomy of DFM&A Guidelines	143
Figure 4-3 Number of parts and manufacturing cost between generations	145
Figure 4-4 Components of RFGT	145
Figure 4-5 Components of SPBS linear guide.....	147
Figure 4-6 Customized bearing and components of RFGT bracket	148
Figure 4-7 Symmetrical branch design of haptic device	149
Figure 4-8 Platform of SPBS and THT.....	150
Figure 4-9 Connecting pin of THT	151
Figure 4-10 Platform support of HPST and THT	151
Figure 4-11 Automated machines.....	155
Figure 4-12 Alignment for link arrangement in machining.....	156
Figure 4-13 Breakdown of manufacturing cost analysis	157
Figure 4-14 Cost structure of SPBS.....	159
Figure 4-15 Manufacturing time of SPBS	160
Figure 4-16 Error model of devices.....	162
Figure 4-17 percentage of design and manufacturing difference for SPBS ...	163
Figure 5-1 Suturing tasks	165
Figure 5-2 schematic of remote master-slave relationship	166
Figure 5-3 Master end of UCB telesurgical workstation.....	167

Figure 5-4 Slave manipulator of UCB telesurgical workstation.....	167
Figure 5-5 Instiutive surgical master end and Immersion Endo Wrist.....	168
Figure 5-6 Two additional DOF of local master-slave surgical tool	169
Figure 5-7 Schematic of local master-slave relationship.....	170
Figure 5-8 Serial type of two-DOF master end	171
Figure 5-9 Serial type two for X and Z axis rotation.....	171
Figure 5-10 Two-DOF spherical parallel type master end	172
Figure 5-11 Master end spherical joint and arc frame	173
Figure 5-12 Front and section view of master end	173
Figure 5-13 First two-DOF slave end with section view.....	174
Figure 5-14 Hinge pulley type slave end.....	175
Figure 5-15 Nine different postures of slave end type II.....	176
Figure 5-16 Gimbal type local master-slave mechanism.....	176
Figure 5-17 Transmisson of master-slave.....	177
Figure 5-18 Local master-slave type II.....	179
Figure 5-19 Local master-slave type III.....	179
Figure 5-20 Force feedback gimbal type master end.....	181
Figure 5-21 Six DOF force feedback haptic device.....	181
Figure 5-22 Six DOF slave end surgical robot arm	182
Figure 5-23 Six DOF remote master-slave mechanism schematic.....	182
Figure 5-24 Wire and hook type space maker	184
Figure 5-25 Fishing rod type abdominal wall lifter	184
Figure 5-26 Fan type abdominal wall lifting device.....	185
Figure 5-27 Folded EASM status	187
Figure 5-28 Compressed and extended status.....	187
Figure 5-29 EASM Extended status	188
Figure 5-30 Folded DASM	188
Figure 5-31 DASM semi assembly status.....	189
Figure 5-32 DASM assembled status	189
Figure 5-33 kinematic of local master-slave mechanism	192
Figure 6-1 Integration of research objective.....	193

Figure 6-2 Design of single surgical arm with three tools.....	197
Figure 6-3 Integration of 4 DOF haptic device with tool-holding mechanism for tele-operation	198
Figure 6-4 The integration of tooling-holding and haptic device	199

List of Tables

Table 1-1 Various types of minimally invasive surgery	2
Table 1-2 Endoscopic surgical problems, solution and researches.....	6
Table 1-3 Comparison between human surgeons and surgical robots [21].....	7
Table 2-1 Joint type synthesis.....	23
Table 2-2 List of kinematics' joint number	24
Table 2-3 Actuating axes dimension data.....	36
Table 2-4 Parameters of GA workspace volume	54
Table 2-5 Active link rotation direction judgment	58
Table 2-6 DH Table of tool-holding mechanism.....	62
Table 2-7 Test Result with $Z=5.2$ cm	69
Table 3-1 Denavit Hartenberg table of SPBS	113
Table 3-2 Position of the moving platform of the eight solutions	126
Table 3-3 Samples of the measuring data for NN training	131
Table 4-1 Platform of SPBS and THT.....	150
Table 4-2 BOM of SPBS	153
Table 4-3 List of SPBS manufacturing and materials cost.....	158
Table 4-4 Three level machining tolerance	161

Glossary

Architecture Designation: Open kinematic chains are usually described by the sequence of their kinematic pairs (joints), where the following notation is used for the kinematic pairs: P: prismatic; R: revolute; S: spherical.

Branch set: One of the several solutions of the inverse kinematic problem.

Compact: Closely and firmly united or packed together. Occupying little space compared with others of its type.

Configuration: The combined positions and orientations of all links and the mobile platform. Similar Terms: posture.

Device: A contrivance or an invention serving a particular purpose, especially a machine used to perform one or more relatively simple tasks.

Dexterity: Skill and grace in physical movement, especially in the use of the hands.

Direct kinematics: The problem of finding the generalized coordinates from the joint ones. Similar Terms: direct kinematic problem, forward kinematics.

Endoscope: An instrument for examining visually the interior of a bodily canal or a hollow organ such as the colon, bladder, or stomach.

Force Feedback: Relating to the mechanical production of information sensed by the human kinesthetic system.

Haptic: Relating to the sense of touch.

Hybrid Parallel Mechanism: Parallel mechanism with an n -DOF end-effector connected to the base by m ($m < n$) independent kinematic chains, each having one or more actuated joints.

Inverse kinematics: The problem of finding the joint coordinates from the generalized ones. Similar Terms: inverse kinematic problem, reverse kinematics.

Joint coordinates: The variables describing the actuated joints. Similar Terms: joint variables, input variables.

Kinematic chain: Assemblage of links and joints.

Machine: Mechanical system that performs a specific task, such as forming of material and the transference and transformation of motion and force.

Manipulator: A machine, the mechanism of which usually consists of a series of segments, jointed or sliding relative to one another, for the purpose of grasping and/or moving objects usually in several degrees of freedom.

Mechanism: A machine or mechanical appliance. The arrangement of connected parts in a machine.

Maximal workspace: The set of all positions that can be attained by any point for at least one orientation of the mobile platform. Similar Terms: reachable workspace.

Orientational parallel mechanism: Parallel mechanism for which all points on the mobile platform describe paths that are located on concentric spheres. Similar terms: parallel wrist mechanism.

Parallel mechanism: Closed loop mechanism in which the end effector (mobile platform) is connected to the base by at least two independent kinematic chains. Similar terms: parallel robot, parallel manipulator, parallel-link mechanism, closed-loop mechanism, in-parallel mechanism, Parallel Kinematic Machine (PKM).

Pneumoperitoneum: The presence of air or gas in the peritoneal cavity because of disease or for the treatment of certain conditions.

Pose: The position and orientation of the mobile platform.

Robot: Mechanical system under automatic control that performs operations such as handling and automation.

Spherical mechanism: Mechanism in which all points of its links describe paths located on concentric spheres.

Surgical tool/instruments: Tools used to perform surgical tasks such as knives, scissors, forceps, graspers, retractors, clips and staplers.

Tactile: Pertaining to the cutaneous sense but more specifically the sensation of pressure rather than temperature or pain.

Tool dexterity: the relative orientation of the tools with respect to each other and the surgical site.

Trocar: A sharp-pointed surgical instrument, used with a cannula to puncture a body cavity for fluid aspiration.

Acronym

BOM: Bill of materials

CAD: Computer aided design

CAM: Computer aided manufacturing

COM: Center of mass

DK: Direct kinematic

DOF: Degrees of freedom

GA: Genetic algorithm

MIS: minimally invasive surgery

NC: Numerical control

NN: Neural networks

SFGT: square frame gimbal type haptic device

RFGT: ring frame gimbal type haptic device

HPST: Hybrid parallel support type haptic device

HPSTA: Hybrid parallel support type-A haptic device

SPBS: Spherical parallel ball support haptic device

THT: Two handed type haptic device

DFM: Design for manufacturing

DFA: Design for assembly

1. Introduction

1.1.Minimally Invasive Surgery

Minimally invasive surgery (MIS) is carried out by entering the body through a body cavity or an anatomical opening with the smallest damage to these structures. MIS is performed with less operative trauma for the patient. MIS requires special medical equipment such as endoscopic cameras and special surgical instruments handled via tubes which are inserted into the body through small openings. The images of the interior are transmitted to a monitor by the endoscopic camera so that surgeons visually recognize the features inside the patient's body.



Figure 1-1 Minimally invasive surgery- Laparoscopic

MIS types include arthroscopic surgery, coronary surgery, percutaneous surgery, stereotactic surgery, and laparoscopic surgery as shown in Table 1-1.

Table 1-1 Various types of minimally invasive surgery

Surgical Type	Description
Arthroscopic surgery	Examine the interior of a joint using an arthroscope
Coronary surgery	Access to the coronary circulation and blood-filled chambers of the heart using a catheter
Stereotactic surgery	Use 3D coordinate system to locate small targets inside the body and to perform on them some action such as ablation (removal), biopsy, lesion, injection, stimulation, implantation
Laparoscopic surgery	Operations within the abdomen or pelvic cavity

MIS approaches to the esophagus, stomach, bowel, spleen and adrenal gland have been specified as laparoscopic surgery, shown in Figure 1-1. MIS have been extended to other surgical specialties such as urology, gynecology, thoracic surgery, and otolaryngology and orthopedics surgery. MIS has also been applied to "closed-chest" coronary artery bypass surgery[1].

Compared to open surgery, MIS offers numerous advantages. The patient's benefits include less trauma (tiny 10 mm marks vs. 160-250 mm scar), less pain, shorter hospital stay (1-3 days vs. 7-10 days), faster recovery (1-2 weeks vs. 8 weeks or more) and lower risk of wound infection. In addition to quality of life benefits, shorter hospital stays save money. Allen [2] studied the economic of laparoscopic surgery and pointed out that the average direct cost per case was about \$1,400 of laparoscopic cholecystectomies and an

average of \$5,300 each for 53 open cholecystectomies. MIS also benefits children as effectively as the open procedure[3].

MIS [4] shows significant advances in the operative and post-operative care of patients. The technical aspects of laparoscopy have taken a lot of the credit for this. MIS procedures have been adopted and became standard methods for cholecystectomy rapidly. Demand from patients has also rapidly increased the evolution of this technology. More than 90% of cholecystectomy surgeries are now done through MIS.

1.2.Problem Statement and Robotic Assistance

Though advantage on patients, MIS is difficult for surgeons as the direct manual operation and freely visible organs is no longer possible. Compared to traditional open surgery, surgeons performing MIS lose both manipulation ability and direct vision. The surgeon's sense of touch and dexterity are highly reduced due to the use of long stem surgical instruments. Endoscopic surgery requires the surgeon to have new hand-eye coordination and instrument manipulation skills as the perform surgery by looking at the endoscopic image on a monitor. These skills are not easy and performing such surgical procedures requires a considerable amount of training and experimentation prior to the actual operation.

Surgeons have to observe the image from the monitor in order to manipulate the long instrument and perform surgical tasks. Hand-eye coordination and motion without haptic feedback is difficult. Surgeons require extensive training and experience to ensure successful and safe operations. In addition, instrument exchanges increase the risk of accidental tissue damage and decrease surgical efficiency[5].

Surgeons have several limitations such as indirect vision of the operation area, reduced dexterous manipulation, and lack of force feedback and difficult control of surgical instruments. The visual feedback is based on an endoscopic camera inserted into the patient's body to take the image from interiors of the body and display the image on a monitor. Utilizing endoscopic camera has several disadvantages: 1) Limited viewing due to the view-field of laparoscopic camera[6]. 2) Difficulty in depth perception due to loss of 3D stereo vision on 2D image display[7]. 3) Unnatural view angle due to position and orientation constraint of the endoscopic camera. Limited view-field problem can be improved by wide-angle endoscopic camera. Now surgical 3D endoscopic cameras have been developed to overcome such depth-recognition problems.

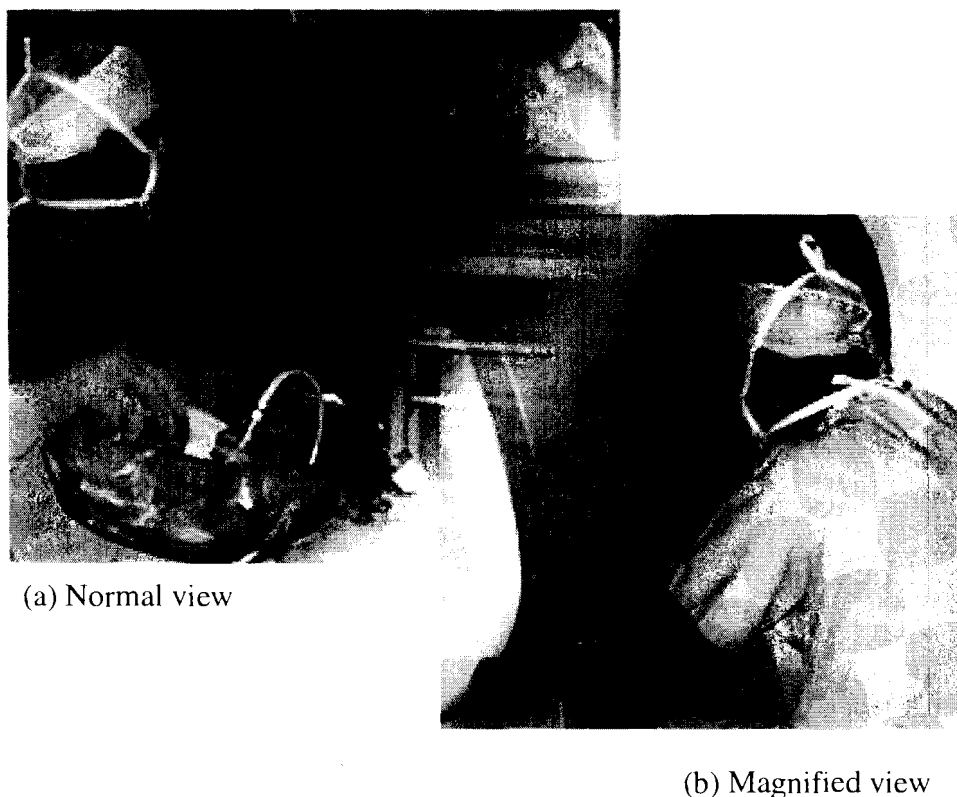


Figure 1-2 Various monitor positions (USC department of Surgery)

Advantages for using endoscopic camera includes: 1) position and orientation of monitor can be adjusted to fit surgeon's requirement. Shown in Figure 1-2 (a), the surgeon can stand beside and look at the monitor. In Figure 1-2 (b), the surgeon sits and looks at the monitor with a comfortable posture. This feature allows surgeons to manipulate surgical tasks with a variety of postures. 2) zoom-in or zoom-out function, so that a small surgical area can be magnified on monitor for clearer view.

The problems of laparoscopic surgery in kinematics perspective include: 1) Reduced motion DOF (Degrees of freedom) because of from a rigid surgical tools in trocar; therefore, the kinematics motion will be reduced. 2) Increased problem of dexterity due to reduced DOF motion. The four DOF limits complex surgical tasks requiring higher dexterity such as suturing, knotting. 3) Motion scale problem, it is caused by the long rigid stem tool pivot with respect to the incision point. The tool length is the sum of the length inserted into patient's body adding the tool length outside patient's body. The motion scale relays on the tool length and the inserted length which is studied by[8]. 4) Haptic sensation problem; surgeons cannot use hand to palpate and the force/tactile sensation are lost.

Due to the numbers advantages of MIS, surgeons are demanded to overcome more difficulties in performing such surgeries. The endoscopic surgical problems, solution approaches, and related researches are listed in Table 1-2 which includes different categories of endoscopic problems. These problems lead to a wide research area for engineers to explore. Engineers also play in important role in development of new technologies that can assist surgeon to overcome these problems. The coordination between engineers and surgeons for engineers realize the practical needs of surgeons. The research work explores the problems 1, 2, 3, and 7 listed in Table 1-2. The discussion of related research for each surgical problem is provided in later chapters.

Table 1-2 Endoscopic surgical problems, solution and researches

	Surgical problems	Solution approach	Related research
1	Position of endoscopic/tools	Robotic arm	End Assist[9], Osaka U[10]
2	Lack of force/tactile feedback	Haptic device	Phantom[11], Immersion LSW
3	Reduced dexterity	Wrist on tool tip	Endo Wrist, Berkeley [12]
4	Complexity of tasks (e.g. suturing)	Spherical proposed tool	SFU[13], RPI [14]
5	Reduced DOF	Flexible stem	SFU[13], Sturges [15]
6	Direction reverse motion, scaling of motion	Training system, rubber model, animals	VEST System One, kismet Medical
7	Pneumoperitoneum	Gasless surgery	Lifting device [16] [17] [18]
8	Distance	Telesurgery	Da Vinci[19], Zeus[20], Endo Via

Robotic surgery is a fast developing research area that integrates the advantages of robotic technology to solve surgical problems listed in Table 1-2. To identify the difference between human surgeons and surgical robots, a comparison of their characteristics is given in Table 1-3[21]. This comparison identifies each of their strengths and limitations. From the comparison, it is clear the major strength of surgical robots is in high precision, accuracy, stability, and scale motion. These features allow more precision in surgical tasks than by human surgeons. In addition, the surgical robot

can be controlled remotely to perform tele-surgery with surgeon and patient at different locations. Engineers can improve the limitations of surgical robot. For example, the limited dexterity can be improved by increasing DOF of surgical robot. An artificial intelligence can be developed to assist surgical robots making judgments. In addition, surgical robots are in experimental stage, that only advanced medical school or hospitals have done clinical trails. The high cost can be reduced if surgical robots become popular and production quantities increases.

Table 1-3 Comparison between human surgeons and surgical robots [21]

Human surgeon	Surgical robot
Strengths	
Strong hand-eye coordination Good judgment Flexible	High geometrical accuracy Stability with no tremor Scale motion Not tired (can work 24 hr/day) Remote control Unaffected by radiation
Limitations	
Lower geometrical accuracy Limited Dexterity Fatigue	Limited dexterity No judgment Problem of reliability Requirement of support engineer Expensive Experimental trial

The surgical robot, Da Vinci, can be integrated with the surgical procedures to assist the surgeon[22]. Da Vinci consists of a surgeon's console, patient-side cart, instruments, and image processing equipment. Figure 1-3 shows an operation with robotics assistance. The surgeon uses the console to operate while seated; viewing an image of the surgical

site. The surgeon's hand controls the master device. The system translates the surgeon's hand, wrist, and finger movements into movements of the endoscope arms and moves the surgical tool or endoscopic camera. The instruments are designed with seven degrees of motion that mimic the dexterity of the human arm and wrist.

Master device –
Surgeon's console

Slave end - Surgical
robotic arm

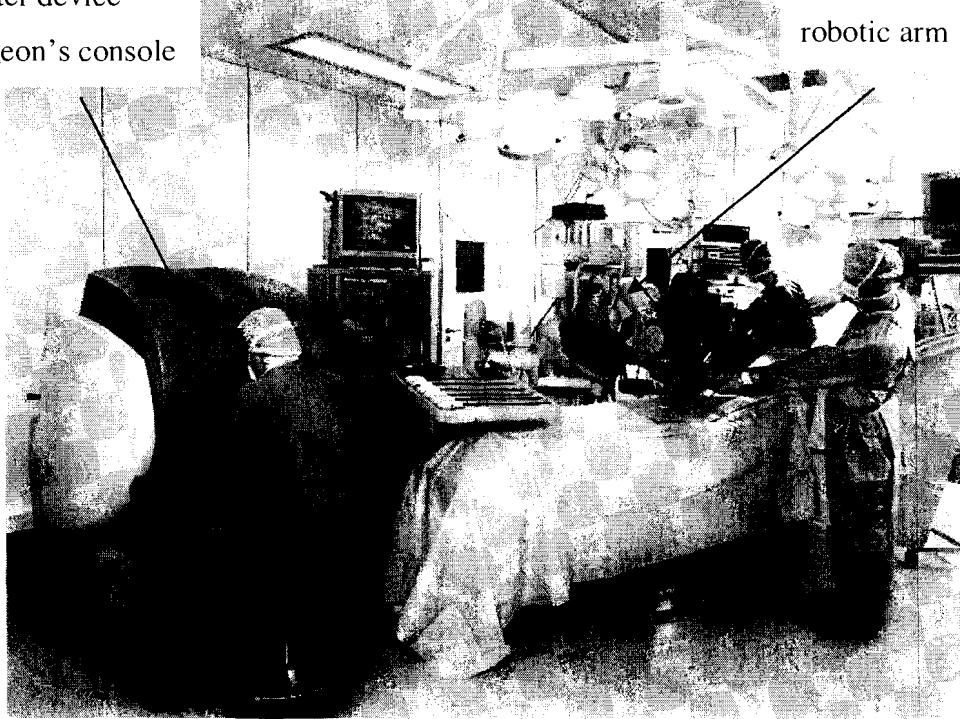


Figure 1-3 Intuitive surgical robot set up in operation room

Drawbacks of the current surgical robot are complexity of the system and mechanical design. In addition, the surgical robotic arm occupies a great space, thus causing collision in certain surgical procedures.

1.3.Objectives and Outline

The purpose of this research is concentrated on the mechanical design needed to build compact surgical robotic mechanisms such as surgical tool-holding mechanism, haptic force feedback device, and local master-slave device. These mechanisms can utilize different mechanical structures to solve the laparoscopic surgical problems from a mechanical perspective. The surgical problems are identified by consulting with surgeons and observing surgical processes. The design and development of a laparoscopic surgical robotic assistance system integrates the following devices with their specific goals.

The main research objective can be expressed as following: First, design and develop a surgical tool-holding mechanism that is compact in size and automated by motor. The mechanism can function as a four DOF surgical robotic arm to replace human assistance that manipulates surgical tools. Second, design and develop a haptic device that is compact, lightweight, and low of inertia. The haptic device has four DOF that can provide force feedback to help surgeons gain force sensation in laparoscopic surgery. Third, analyze the design for manufacturing and assess the development process of the engineering device. The concept of concurrent engineering is implemented to integrate the entire process from concept to design and manufacturing of the engineering product. In addition, manufacturing cost modeling will be discussed. Fourth, supporting mechanisms for local master-slave mechanism and abdominal surgical space maker are designed. The surgical mechanism has two rotational DOF which can be integrated with master or slave devices to increase dexterity. In addition, the abdominal surgical space maker creates surgical space inside patient's abdominal wall without gas. This gasless process can reduce the side effects from current technology.

The objective for this research is to design and develop novel robotic mechanisms that assist the laparoscopic surgery. In addition, this research is focusing on design and

manufacturing process. Automatic control, integration with software and networking can be developing in the future.

A description of the design of the surgical tool-holding mechanism is presented in Chapter 2, where the design synthesis, mobility, mechanism structure, and kinematic analysis are discussed and a special case of the kinematic calculation example is described.

Chapter 3 presents the designs of surgical haptic force feedback devices. In the subsequent sections, both gimbal and spherical parallel types of haptic devices are developed. The design synthesis and mechanical design are proposed. Direct and inverse kinematics is presented along with numerical examples. The experiment and simulation for direct kinematics using neural network is also presented.

Chapter 4 presents general guidelines for manufacture and adoption to the haptic devices. In addition, the manufacturing processes, bill of materials and manufacturing cost structure are analyzed.

In chapter 5, two types of supporting mechanisms are designed in order to enhance surgical dexterous condition. Local master-slave mechanism increases the dexterous ability by adding two-DOF wrist on surgical tool tip. The foldable/ extendable abdominal space maker increases the surgical workspace inside the patients' body without using gas to inflate patients' abdominal wall.

In Chapter 6, the conclusion and contributions of the research work are laid out. Suggestions for future research are presented.

1.4. Contributions

The major contributions of this research are summarized as:

- **Automatic surgical tool-holding mechanism:** The new four DOF tool-holding mechanism is able to replace the surgical assistant in laparoscopic surgery or work as a slave end of the surgical robot to perform surgical tasks. This patented design comprises a novel application of a spherical parallel mechanism. The optimization of workspace, direct kinematic and inverse kinematic are analyzed.
- **Haptic force feedback device:** The new kinematic structures of four DOF haptic force feedback devices are able to help surgeons regain a sense of touch. Both gimbal type and spherical parallel type are designed, manufactured, and evaluated. The unique new design of spherical parallel mechanism with various passive support components is presented. The passive support is able to carry the weight of moving parts and reduce inertia.
- **Design for manufacturing analysis:** Not only design but also manufacturing and design for manufacturing are studied. Therefore, the engineering manufacturing for innovation technology are analyzed that includes design for manufacturing and assembly, manufacturing cost modeling, bill of materials, machining process and accuracy.
- **Local master–slave and supporting mechanism:** The mechanism has two-DOF wrist attached on the tip of surgical tool. The master has finger rings for pivoting the connecting tendon to actuate the slave end. Local master slave mechanism is able to increase the maneuvering ability by adding two-DOF wrist. Supporting mechanisms such as abdominal space maker are designed that can be deployed

easily inside the patient's abdominal wall. To increase the visible and workable space for surgery, two types of abdominal space makers are designed: 1) Extendable abdominal space maker, 2) Deployable abdominal space maker.

2. Design of Surgical Tool-Holding and Tele-Operation Mechanism

This chapter presents a design of surgical tool-holding or tele-operation mechanism with four DOF for laparoscopic surgery. The mechanism can be used as a robotic arm attached to the surgical table to replace human assistance in the operating room. In addition, surgeons may control these mechanisms from a different location so that the mechanisms are utilized as surgical robots can operate surgery on the patient. The distance can be as short as next room or thousand miles away.

This chapter is organized as follows: In section 2.1 the design objectives and prior works are reviewed. In section 2.2, the design processes, including function specification, type synthesis, number synthesis, and topological synthesis are presented. After completing the synthesis processes, spherical parallel mechanism are chosen. The characteristics and classification of spherical parallel mechanism are reviewed. In section 2.3, the supportive analysis of workspace optimization analysis by genetic algorithm is discussed. In section 2.4, the four DOF mechanical design of the tool-holding mechanism is presented. Design characteristics and features are introduced. In section 2.5 and 2.6 the kinematic model, both direct and inverse are presented. Section 2.7 includes the discussions.

2.1.Design Objectives and Related Research

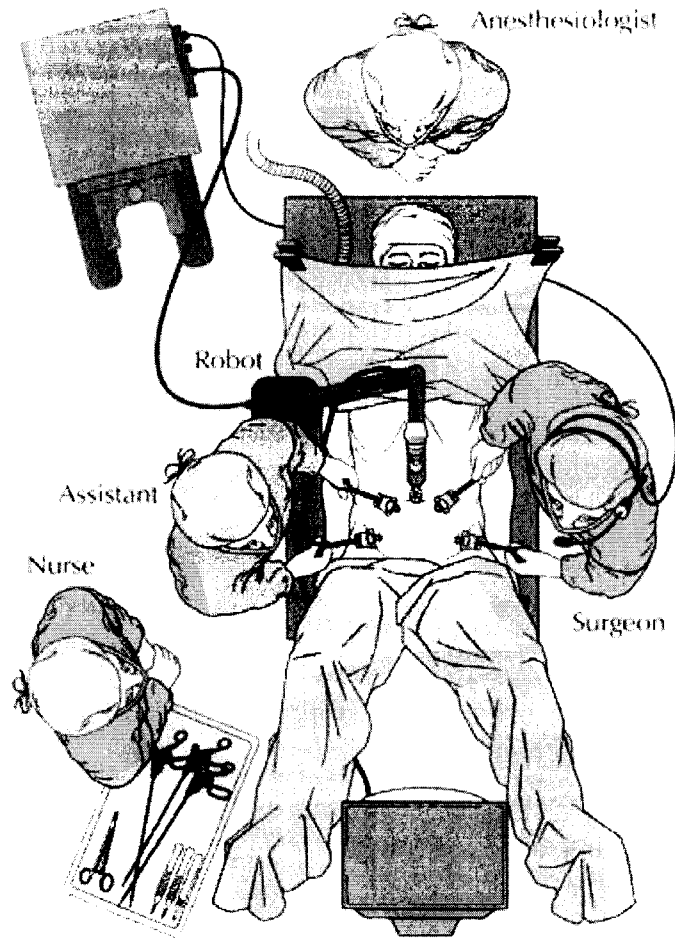


Figure 2-1 The laparoscopic operation room set up

Shown in Figure 2-1, in laparoscopic operation room, surgeons manipulate long surgical tools to achieve procedures such as excisional, ablative and reconstructive[23]. To manipulate different types of surgical tools, it is necessary for the surgeon to practice for a long time to be acquainted with complex surgical tasks. The surgical tools, developed by Karl Storz, are shown in Figure 2-2. At the same time, the surgical assistant holds the endoscopic tools or camera and follows the surgeon's instruction to adjust the position

and orientation. Thus, the camera takes an image of the surgical area and displays on the monitor screen. Holding and manipulating the endoscopic camera is an exhausting and tedious work for the human assistant. However, manipulation of the endoscopic camera can be replaced by a robotic assistant so that the human assistant can contribute to other more valuable work. Therefore, the concept of developing a robotic assistant or robotic arm to perform this task was initiated in late 1990's[24]. The object is to design a mechanism that can hold the surgical tool/ camera firmly and free the operators' hands. This kinematic motion of mechanism must satisfy the physical constraints that will be analyzed in section 2.2.1.

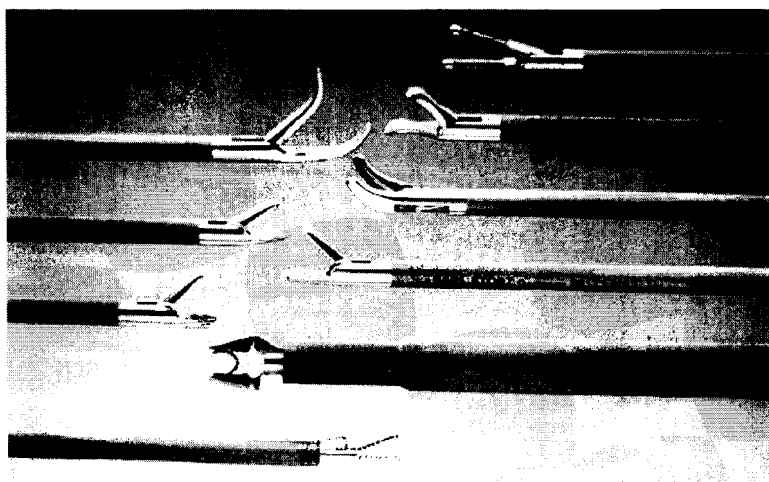


Figure 2-2 Laparoscopic surgical tools

The automated control of tool-holding mechanism to the camera position and orientation is a new fast developing research area. Faraz et al. [8] developed the laparoscopic extender with three rotational DOF and one linear DOF, shown in Figure 2-3. The concentric multi link spherical joint is a novel design that has been optimized for workspace and links. This mechanism has four DOF that can pivot three rotational DOF with the incision and one linear DOF. This mechanism is semi-automatic such that two rotational DOF (A and B in Figure 2-3) are pneumatically controlled and the rotation about C and linear motion about D are can be controlled manually by tide set screws.

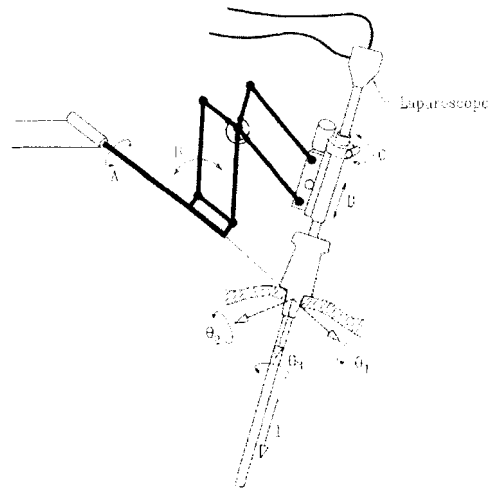


Figure 2-3 Four DOF concentric multi link spherical joint

Osaka University [10] developed a robotic laparoscope positioning system with the automatic control interface. Shown in Figure 2-4, the experiment was carried out to evaluate the performance.

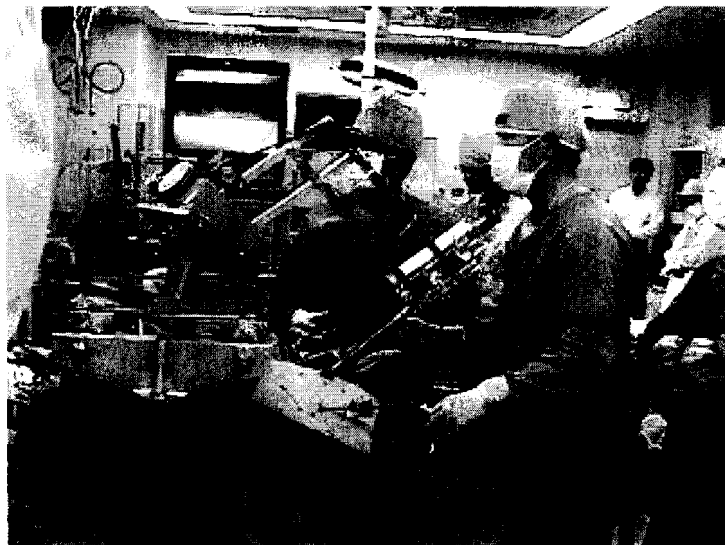


Figure 2-4 Osaka University robotic laparoscope positioning system

End Assist [9] is designed with an articulation and specifically intended for the needs of laparoscopic surgery. The robot contains a four DOF cylindrical geometry manipulator, with an additional linkage added to make its movements pass through a single point as illustrated in Figure 2-5.

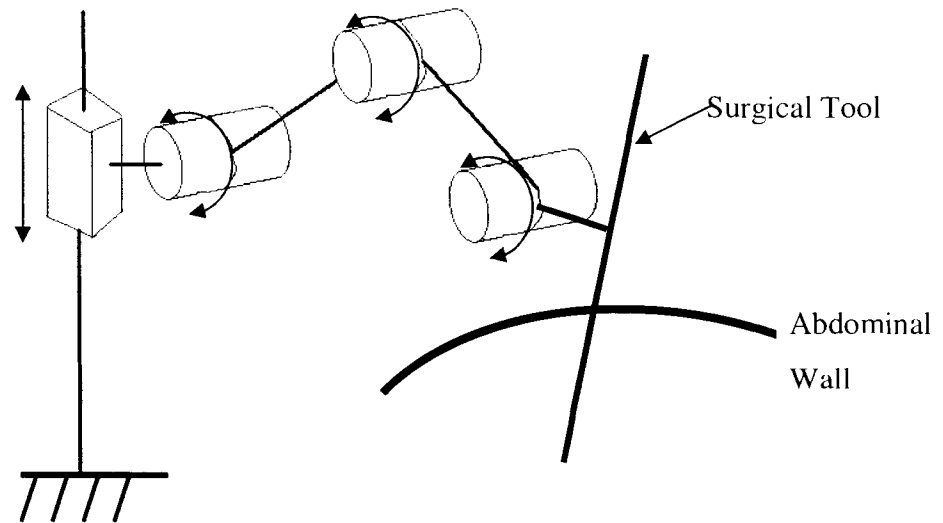


Figure 2-5 Sketch of Endo Assist

Charoenkrung Pracharak Hospital [25] developed a serial manipulator for laparoscopic camera by utilizing an adjustable desk lamp. Surgeons or assistants must lock/unlock the setscrew to adjust the position of the camera holder manually. A two rotational and one linear DOF device, LER, was developed[26]. Shown in Figure 2-6, this design is simple and compact with no rotation about Z-axis.

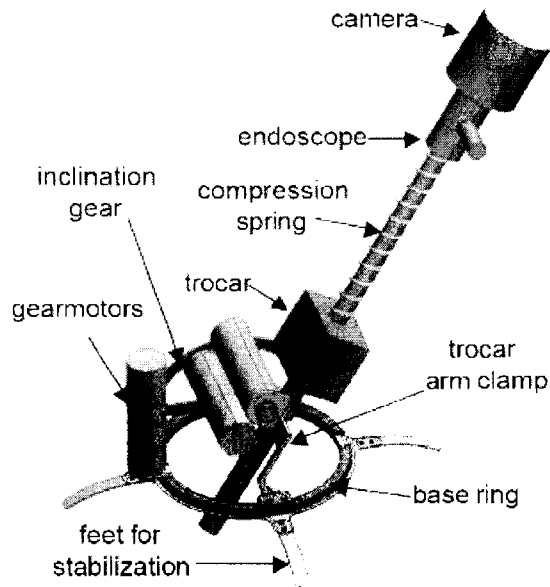


Figure 2-6 LER

Commercial products are available, such as “Da Vinci”, a surgical robot developed by intuitive surgical company has been experimented at hospitals[27], [28], [29] and[30]. The kinematics of Da Vinci is similar to the Endo assist shown in Figure 2-7, the only difference being the linear motion on the distal end. Computer Motion developed a surgical robot, AESOP, to hold the laparoscope and alter its position in response to a surgeon’s verbal commands. The robotic arm attaches directly to the operation table, weighs about 18 kg (40 lb), and can move at a maximum speed of 7.5 cm/sec.

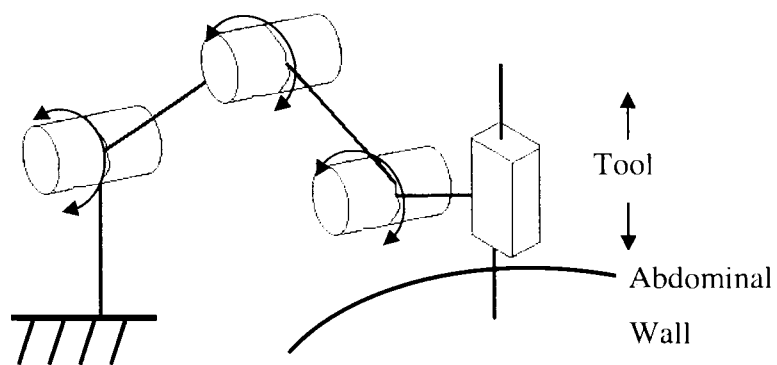


Figure 2-7 Kinematics diagram of Da Vinci robot

Automated, voice or footpad can be utilized to control the tool-holding mechanism. There is a number of research on the ease of control of automated robotic assistance mechanisms[31],[32]. Zhang [33] developed an automated image tracking method so that the endoscopic camera can trace a marker attached to the surgical tool automatically.

Although many assisting mechanisms have been developed, the major design criterion of “arm size” has not been considered. Shown in Figure 2-8, these surgical robotic arms are bulky and occupy a lot of the space above the patient’s body. The rotation angles of robotic arms are very limited. The angles between the robotic arms are small. This small collision-free workspace also motivates us to develop new compact kinematic structures that can overcome the limited workspace problem.



Figure 2-8 Surgical robotic arm developed by Intuitive Surgical

2.2.Design Process

The design process has been developed for tool-holding mechanism. This process was developed to ensure that the new design is suitable from different engineering perspectives. The design process has been divided into three major steps: (1) function specification and planning stage, (2) conceptual synthesis design stage and (3) practical/detailed design stage. In the function specification and planning stage, the design requirements were identified and converted into engineering specifications. In the conceptual synthesis design stage, various achievable design types were generated to explore the model feasibility. In the practical design stage, design analysis, design optimization for workspace, engineering drawings, material section, geometrical, and dimension tolerance are specified. Finally, the prototypes are manufactured and function test are presented.

2.2.1. Function Specification

For laparoscopic surgery, the required four DOF of laparoscopic tool or camera is shown in Figure 2-9. It has to achieve three spherical DOF with respect to the incision point at abdominal wall (three rotations about X, Y, Z-axes at the incision point). One linear DOF is added to move the surgical tool in and out along the Z-axis. The mechanism's pivot center has to be located exactly at the incision point so that the movement of mechanism will not stretch the patient's abdominal wall.

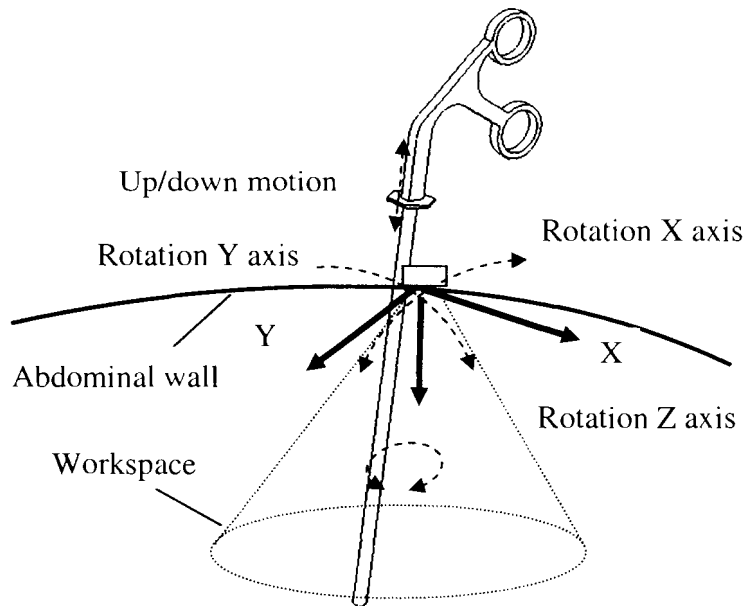


Figure 2-9 Four DOF requirements of laparoscopic tool or camera

The kinematic motion can be defined to achieve yaw, pitch, and twist the three rotational DOF and one linear DOF. The critical design requirements include:

- The mechanism should have three rotational and one linear DOF with respect to incision point.
- The yaw motion (rotation with respect to X-axis) can reach 45° from center to both sides.
- The pitch motion (rotation with respect to Y-axis) can reach 45° from center to both sides.
- The twist motion (rotation with respect to Z-axis) can reach 70° from center to both sides.
- The linear movement stroke is able to reach 150 mm along Z-axis.
- The mechanism must locate and move on the upper hemisphere with respect to the incision point to avoid interference.

2.2.2. Type Synthesis

Synthesis problems are thought of as one of system identification[34]. Angeles [35] defined synthesis problems as those related to function generation, rigid body guidance and path generation. Type synthesis classifies and determines mechanisms that fit the application purpose[36]. Several different mechanisms are explored to identify the mechanism that can meet the special design requirements in previous section. This procedure consists of several steps to find the feasible mechanism type. Shown in Figure 2-10, type synthesis contains number synthesis and topological synthesis[37].

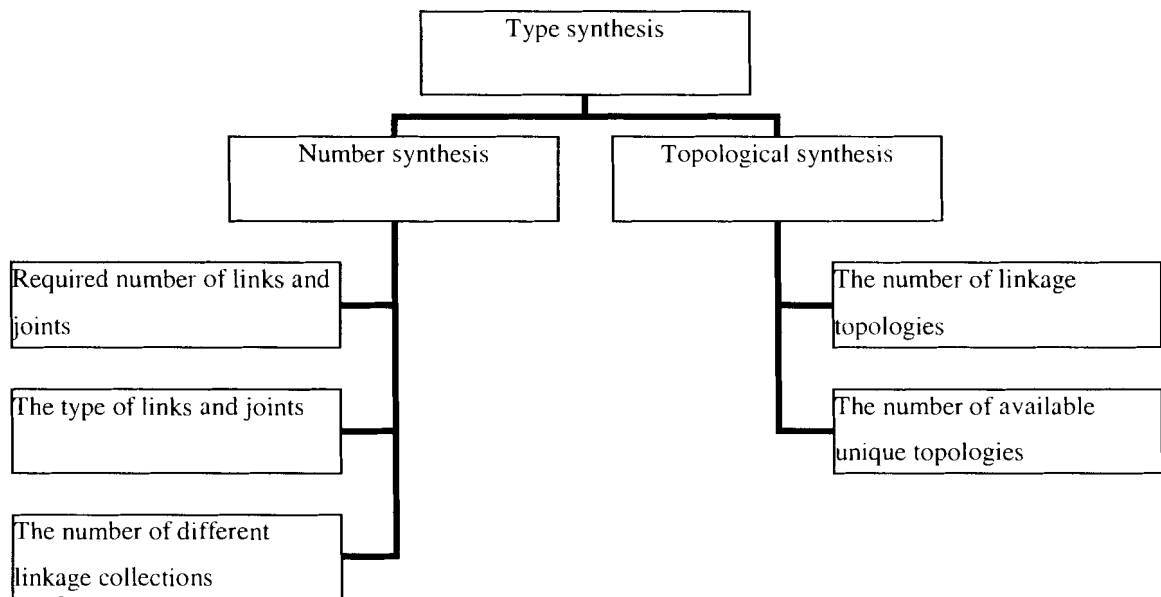

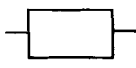

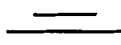

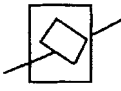


Figure 2-10 Structure of type synthesis

Number synthesis is the determination of all kinematic chains of a given number of links or the number of links in a chain[38]. The popular kinematic pairs are initially for number synthesis (in Table 2-1) that includes revolute, prismatic, helix, cylinder, spherical and planar joints. Eight frequently used kinematic pairs are listed by Tsai[39]. Waldron listed six different lower pair joints is similar to Table 2-1[40]. The

classification of kinematics pair notation from Dukkupati [38] was applied to build the table for number synthesis.

Table 2-1 Joint type synthesis

Class symbol	P1			P2	P3	
Letter Symbol	R	P	H	C	S	PL
DOF	1	1	1	2	3	3
RTH ⁽¹⁾	100	010	001	110	300	030
Sketch Symbol						
Names	Revolute; Hinge;	Prismatic joint; Sliding pair	Screw; Helical joint	Cylinder joint;	Spherical joint; Ball joint;	Planar joint

⁽¹⁾R: Revolute type, T: Translational type, H: Helical type, 1: available, 0: not available

In number synthesis, the mechanism search was limited to lower pair joints. Higher pair joints such as one DOF cylinder roller, two-DOF cam pair, or three DOF rolling ball will not be included in this number synthesis. The mechanism must follow mobility criterion or equation.

Table 2-2 List of kinematics' joint number

Number of links	Type	Number	Kind
4	4P1	14	4R, 4P, 4H, 3R+[1P, 1H], 2R+[2P, 2H, 1P+1H], 1R+[3P, 3H, 2P+1H, 1P+2H], 3P+1H, 3H+1P
3	2P1+1P2	3	2R+[1C], 2P+[1C], 2H+[1C]
2	1P1+1P3	6	1R+[1S, 1PL], 1P+[1S, 1PL], 1H+[1S, 1PL]
2	2P2	1	2C

Twenty-four different kinematic types have been listed in Table 2-2 for four DOF mechanisms. 3R+ [1P, 1H], 1P+ [1S] and 1H+ [1S] of Table 2-2 can reach the design requirement of three rotational and one linear DOF.

Topological synthesis:

To meet the three spherical DOF design requirement (in Figure 2-9), ball joint type linkage is used which is the spherical DOF linkage type, advantages of this type include straightforward, compact mechanical structure with the fewest parts (ground and end effector) and manufacture of a ball joint is a simple process. It is also necessary to actuate the spherical joint with a three DOF spherical actuator or three motors with complex transmission system (linkage, tendon, or pulley wire). Only experimental type spherical motors are available [41] and the additional transmission system will defeat the simple kinematic purpose.

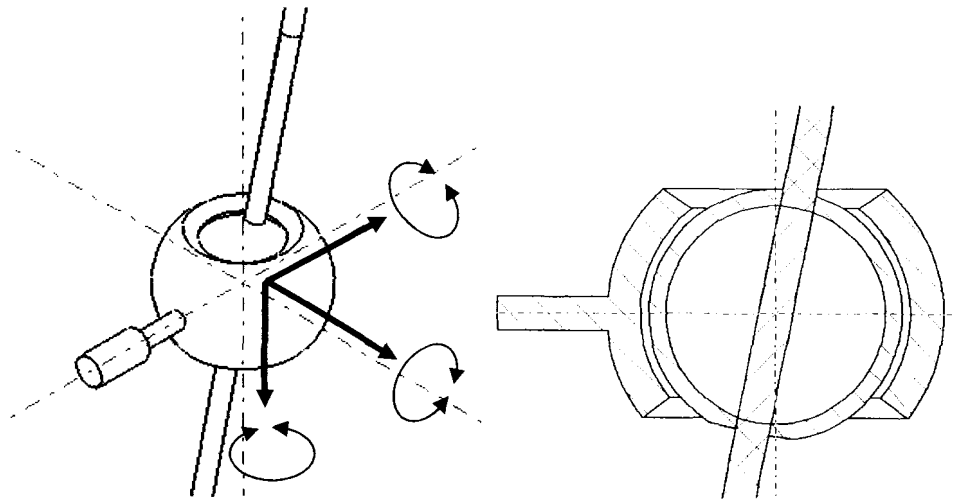


Figure 2-11 Ball joint type three DOF

Serial type linkage: As shown in Figure 2-12, the serial kinematic three DOF contains three revolute joints to achieve three DOF with respect to X, Y and Z-axis. The advantages are simple control, large workspace, and ease of manufacture. The actuator can be installed on the revolute joint to actuate the link. Disadvantages include low accuracy, low rigidity, and occupation of large space during movement. Let F be the number of DOF of the mechanism, l be number of links (including the ground), j be total number of joints, f_i be the mobility of joint i . Let λ be the operator in which the mechanism is intended to operate; $\lambda=3$ for planar and spherical motions and $\lambda=6$ for spatial motion. The DOF of the mechanism is governed by the mobility equation (2-1) which is suggested by Freudenstein and Maki[42]:

$$F = \lambda(l - j - 1) + \sum_{i=1}^j f_i \quad (2-1)$$

The mobility of serial type linkage can be calculated as $F = 3(4 - 3 - 1) + (1 + 1 + 1) = 3$.

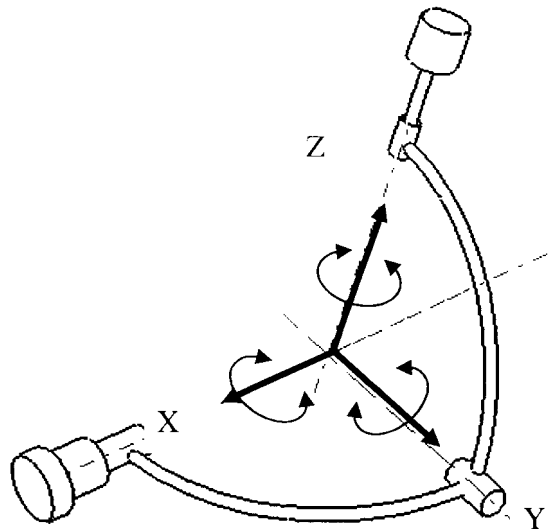


Figure 2-12 Serial type three rotational DOF

Hybrid type linkage: As shown in Figure 2-13, this linkage is the combination of open and closed chain linkage to achieve three spherical DOF. In this configuration, two revolute joints are attached to the ground and can be perpendicular to each other with their actuating axes meet at the center. The intermediate joint has two-DOF with respect to X and Y-axis. One rotational DOF can be attached to the intermediate joint to create two-DOF. The DOF of the intermediate joint is governed by the mobility equation (2-1).

The mobility of hybrid type linkage can be calculated as

$$F = 3(5 - 5 - 1) + (1 + 1 + 1 + 1 + 1) = 2$$

One additional DOF is attached to the intermediate joint to contribute to total three rotational DOF. In order to actuate this mechanism, two motor can be installed to be stationary and an additional motor can be installed on the intermediate joint to actuate the Z-axis rotational DOF.

The advantages include high stiffness, low deformation. Disadvantages include more links, more machining processes, and limited workspace.

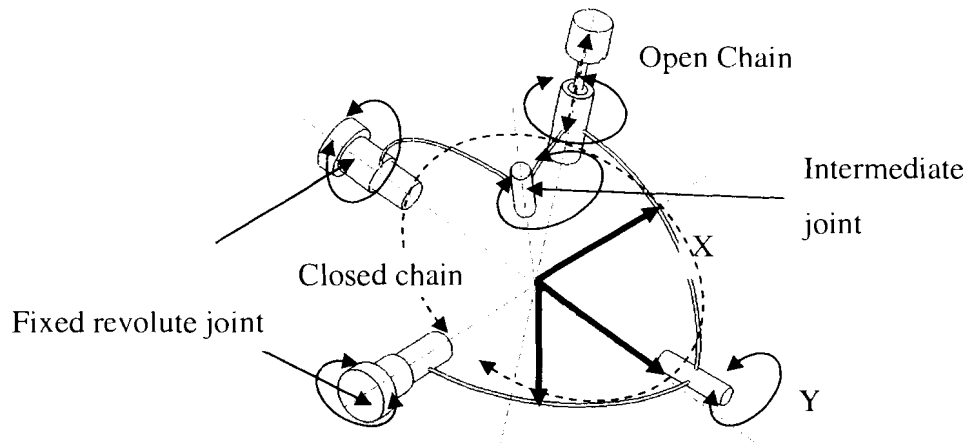


Figure 2-13 Hybrid type three rotational DOF

Parallel type linkage: As shown in Figure 2-14, the kinematic configuration of three DOF parallel linkages also meets the three rotational DOF requirement. There are three branches connected to the end effector. Each branch contains three revolute joints.

The DOF of the end effector is governed by the mobility equation (2-1). The mobility of spherical parallel type linkage can be calculated as

$$F = 3(8 - 9 - 1) + (1 + 1 + 1 + 1 + 1 + 1 + 1 + 1) = 3$$

Advantages of this mechanism include the actuation that can be fixed on ground, rigid structure, less deformation. Limitations of this mechanism include complex kinematics without analytical solution, higher number of links and limited workspace.

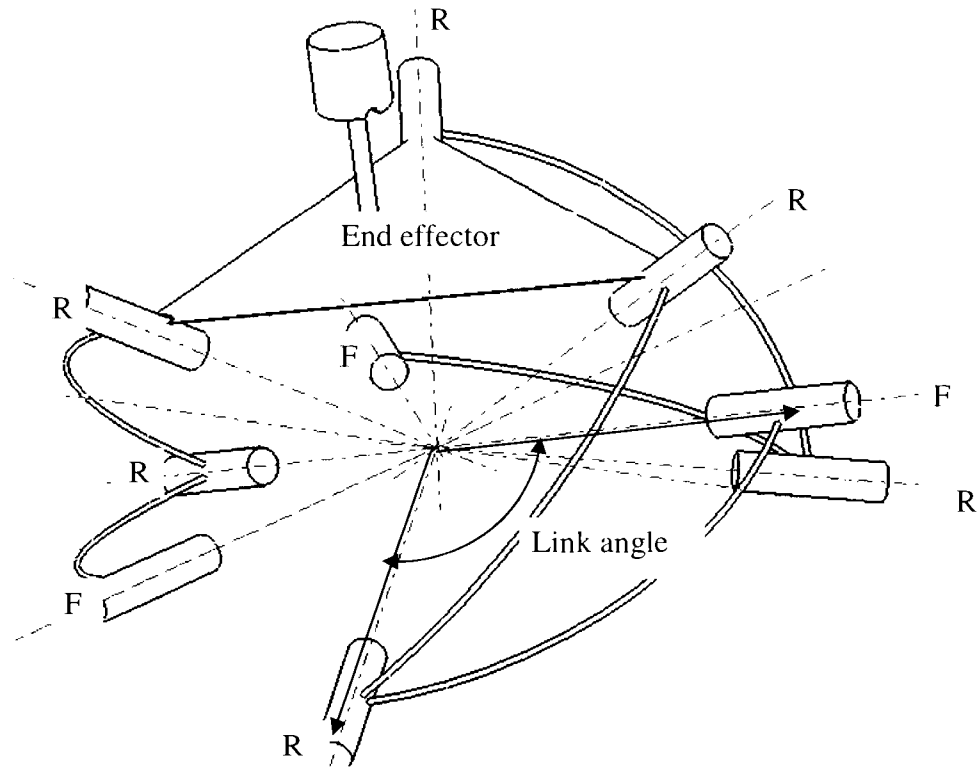


Figure 2-14 Three DOF spherical parallel type

F: Fixed revolute joint R: Revolute joint

Based on previous synthesis, the spherical parallel type was chosen to be the basic design structure because the advantages satisfy the design requirement that include 1) three rotational DOF with respect to the incision point, 2) feasible workspace, 3) motor that can be fixed on ground to provide more workable space.

Spherical parallel mechanism is suitable for this design because spherical mechanism has three DOF with respect to the incision point on patient's abdominal wall for laparoscopic surgery. Parallel mechanism can have the motor fixed on a remote base to save surgical space for surgeons. Therefore, this mechanism has been chosen to develop further design detail.

2.2.3. Characteristics and Classification of Parallel Device

Since the parallel manipulator is chosen from the type synthesis process in section 2.2.2, it consists of a moving platform connected to a fixed base by several linkages (branches). The number of linkages is equal to the number of DOF of the moving end effector and each linkage requires one actuator that can be mounted on a fixed base. The chain is closed if every link of a kinematics chain is coupled with at least two other links[35]. Gosselin [36] defined a parallel robot that is fully parallel when the number of legs is greater or equal to the number of DOF of the moving platform, with each parallel chain having a single actuator. Merlet [43] defined the characteristic of parallel manipulators as: 1) support for the end effector with least two chains, 2) the number of actuators to be equal to the number of DOF of the end effector, 3) the mobility of the manipulator to be zero when the actuators are locked. Tsai [44] classified parallel manipulators as planar, spherical and spatial. However, the classification of DOF and joint types are based on different methods for the parallel manipulators. The parallel manipulator can be classified in to kinematics type, joint type and movement type. Kinematics type includes two-DOF, three DOF, four DOF, five DOF, and six DOF. Joint type includes linear joint, revolute joint, universal joint and ball joint. Movement type includes translational, rotational, spherical, and spatial.

Spherical parallel mechanism has the kinematics characteristic of spherical mechanism that all linkages move with fixed distance with respect to the common stationary center point[45]. The locus of any link is contained in a spherical surface. This spherical mechanism perfectly fits this particular design requirement.

For spherical parallel mechanism, several researches have been studied. Gosselin [46] [47] [48] [49] developed the Agile eye and ShaDe haptic devices that are three DOF parallel devices. Liu studied [50] the stiffness to select the link lengths of three DOF spherical parallel manipulators for operational performance.

2.2.4. Comparison of Serial and Parallel Mechanism

In this section, the comparison of serial and parallel mechanism is presented to discuss the feasibility of parallel mechanism for our design objective. The major difference between parallel mechanisms and serial mechanisms are in their kinematic structures. Parallel mechanisms are composed of at least two closed kinematic chains. These chains connect a moving platform to a fixed base. Parallel mechanism permits the location of the actuator to be away from the moving platform. The actuator must be mounted at every joint along the serial linkage of serial mechanism. These actuators located at each joint will increase a significant payload to the whole mechanism which reduces the power to move the load on end effector. On the other hand, the actuators of parallel mechanism can utilize all of their power to move the platform instead of other weight of links or actuators. This feature makes the platform lightweight and fast to respond. Therefore, the parallel mechanism can be lighter in weight than serial mechanism. An earlier parallel mechanism application is "Stewart Platform" which was proposed by Stewart to be a flight simulation mechanism[51].

Kinematics structures: serial mechanism contains open loop kinematics while parallel mechanism contains closed loop mechanism. Shown in Figure 2-15, the moving platform for parallel mechanism contains three supporting branches while that of serial mechanism contains only one.

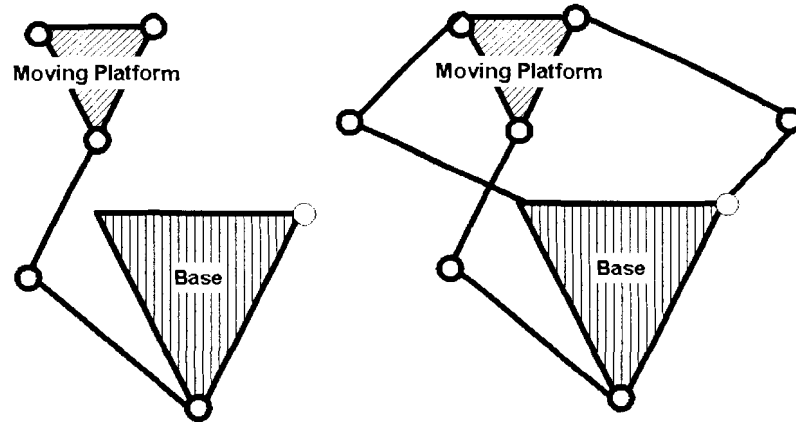


Figure 2-15 Kinematics structure of serial and parallel mechanism

Workspace: A serial manipulator contains larger workspace volume than a parallel manipulator does. For serial manipulator, each link can be moved independently; therefore, the end effector can reach a large workspace. For parallel manipulator, the end effector is connected by several links and workspace must be compromised due to constraints of all links[44]. Design for optimal workspace is an important issue for parallel manipulator.

Load (robot mass ratio): For serial manipulator, the end effector and load are located at the distal end. Every actuator has to exert enough torque and power to move all distal links and overhead actuators. Therefore, the actuator must be strong and heavy. A parallel manipulator does not have this feature. Actuators of a parallel manipulator can be placed on ground to support stronger payload than a serial manipulator.

Accuracy: For parallel manipulator, the geometrical errors are not added, as all the branches are connected to the end effector. The dimension accuracy of each link must be high so that the position and orientation of end effector is more accurate than serial manipulator. For serial manipulator, the geometrical errors will accumulate error of each link. Therefore, the end effector of serial manipulator will have lower position accuracy.

Repeatability: The repeatability of parallel manipulator is more accurate than serial manipulator because of higher dimensional accuracy of parallel manipulator.

2.3.Mechanical Structural Design

Based on the synthesis in section 2.3, the mechanical structure design was developed. The mechanical design configuration is shown in Figure 2-16. This design consists of a three DOF rotating platform with one additional linear DOF mechanism.

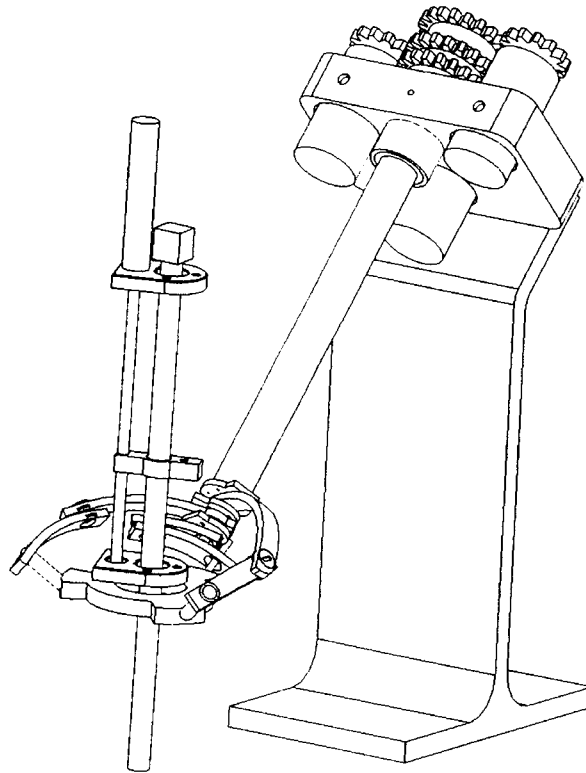


Figure 2-16 Mechanical design of tool-holding mechanism

The platform is connected to the actuating axis via three branches. Each branch contains two arc links. These two links are connected by middle joint joining the passive link (the link connecting to the platform) and the active link (the link connecting to active axes). The moving platform is attached to three passive links via revolute joints. Three active links are attached to the concentric actuating axis. Three motors are geared with the actuating axis and fixed on a distal plate. The remote motor location is placed away from the surgical area, in order to provide more working space for surgeons. For the first prototype, links and platform are made by high stress engineering plastic to reduce weight and maintain high stiffness of structure. The major purpose of lightweight links is to maintain fixed distance between the actuating axes and the moving platform without deflection. The precision position is critical in parallel manipulators to ensure smooth movement.

This mechanism has the following design characteristics: 1) spherical parallel structure, 2) optimized asymmetric linkages, 3) nested link radius, 4) orthogonal platform frame link axes, 5) remote motor location, 6) concentric actuating axes, 7) gear reduction.

1) Spherical parallel mechanism: The platform of tool-holding mechanism is based on the spherical parallel kinematics. All of the components move on the upper semispherical surface to avoid interference with patient's body. The spherical center is the incision point of the patient.

2) Optimized asymmetric linkages: The workspace of spherical parallel manipulator is very limited; therefore, the link angles are optimized for maximal workspace in section 2.3. However, in section 2.3 the result is based on theoretical parameters (link angles). In the practical design stage, additional physical limitations affect these parameters. For example, the surgical tool on the platform is modeled as a vector to check the interference with the links. In practical design, the surgical tool with linear motion device occupies

more space above the platform that may interfere with the links while rotating. Therefore, three branches are not symmetric with six different link angles.

3) Nested linkage: The six different link radii are shown in Figure 2-17. The radii are nested (120, 113, 106, 99, 92, 85 mm), so that each link moves on a different radii surface in order to avoid collision between links. This design feature increases workspace of parallel manipulator. The thickness of the link is 6 mm and a 1 mm distance exists between passive and active link.



Figure 2-17 Nested linkage

4) Orthogonal axis platform: As shown in Figure 2-18, the three branch platform vectors (v_1, v_2, v_3) are perpendicular to each other. The advantage of the perpendicular platform frame is ease in both direct and inverse kinematic calculation. The vector v_3 is the cross product of vectors v_1 and v_2 . In manufacturing process, this orthogonal axis requires precision setup to ensure the correct angles of the platform.

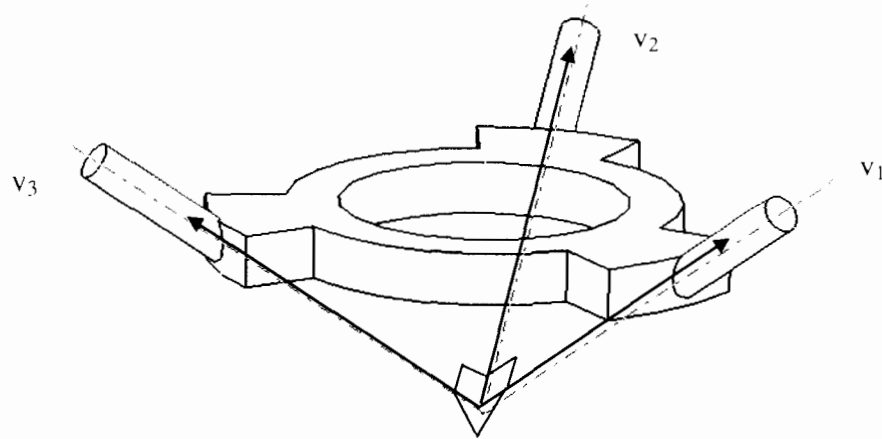


Figure 2-18 Orthogonal axes platform

5) Remote motors location: The benefit of remote motor location is better workable space for surgeons. Three motors are fixed on a distant plate and one small motor attached on the moving platform. These three motors are parallel to the actuating axis with different distance from the base plate. The torque transmits from motor to driving gear, driven gear, active rod, and active link. The length of actuating axis is 270 mm which can be extended if necessary.

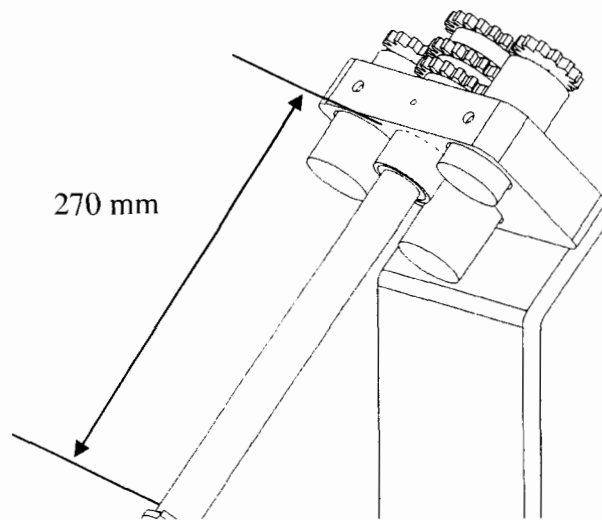


Figure 2-19 270 mm arm length

6) Concentric actuating axis: As shown in Figure 2-20, the special advantage of concentric actuating axes is minimized space occupation with three independent rotations. Three concentric actuating axes are separated by bearings. The stainless solid inner rod is supported by three bearings inside the middle tube. These three bearings are allocated to the front, middle and end to distribute loading evenly on middle tube. The middle tube is supported by two bearings in the outer tube. There is only one 19 mm diameter external tube. This tube is smaller size than any other surgical robotics arm. A detail dimension of axes and bearing is shown in Table 2-3.

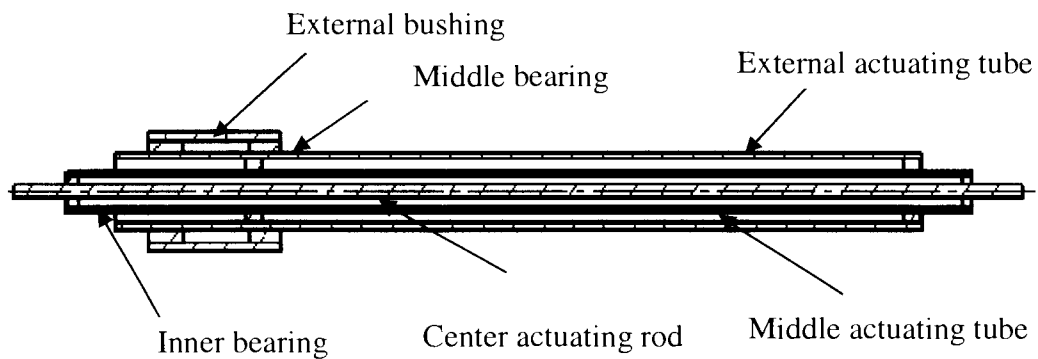


Figure 2-20 Concentric actuating axes

Table 2-3 Actuating axes dimension data

	ID(mm)	OD (mm)	Length (mm)	Material
Center rod	n/a	3.175	300	Stainless
Middle tube	7.9375	9.525	270	Stainless
External tube	15.875	19.05	240	Brass
Inner bearing	3.175	7.9275	3	Deep groove ball bearing
Middle bearing	9.525	15.875	5	Deep groove ball bearing
Outer bushing	19.05	25.4	12.75	Deep groove ball bearing
Base plate	25.4	n/a	12.5	Aluminum

7) Gear reduction: Spur gears are used to transmit torque from the motor to active link. To increase the torque, a 56:24 (driven: driving) gear ratio is applied. This ratio is based on the distance between motor axis and active axis that increases torque to 2.4 times so that smaller motor can be chosen. The three driven spur gears are concentric and parallel.

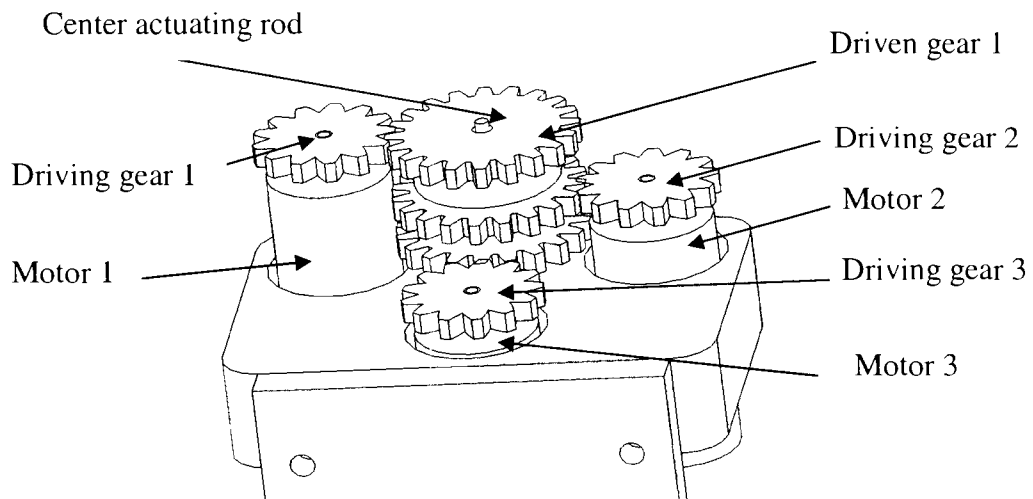


Figure 2-21 Concentric parallel spur gears

Shown in Figure 2-22, the tool-holding mechanism contains features of compact size platform, aluminum alloy links and platform, all revolute joints and small linear drive mechanism. The prototype of spherical parallel mechanism with revolute joints. It is actuated by three permanent geared DC motor (Pitman GM8724S023) that are connected to the driving gears. The spherical parallel design has benefits of both speed and workspace[52]. The parallel manipulator offers high stiffness, high precision, and light weight. High stiffness takes heavier load with less deflection; therefore, applying load on the surgical tool will not deform the structure. A high precision robot can manipulate the end effector with less error which means that the position can be more accurate. The moving parts of manipulator are light weight because all actuators are fixed to the ground. Three brush motors are attached on a distal plate. Actuating axes are located at the center

of three motors. The actuating axis is composed of two hollow tubes and one solid rod. Metal tubes and rods are concentric and separated by three sets of ball bearings. The supporting bearings separate the two tubes for turning and one rod to reduce friction.

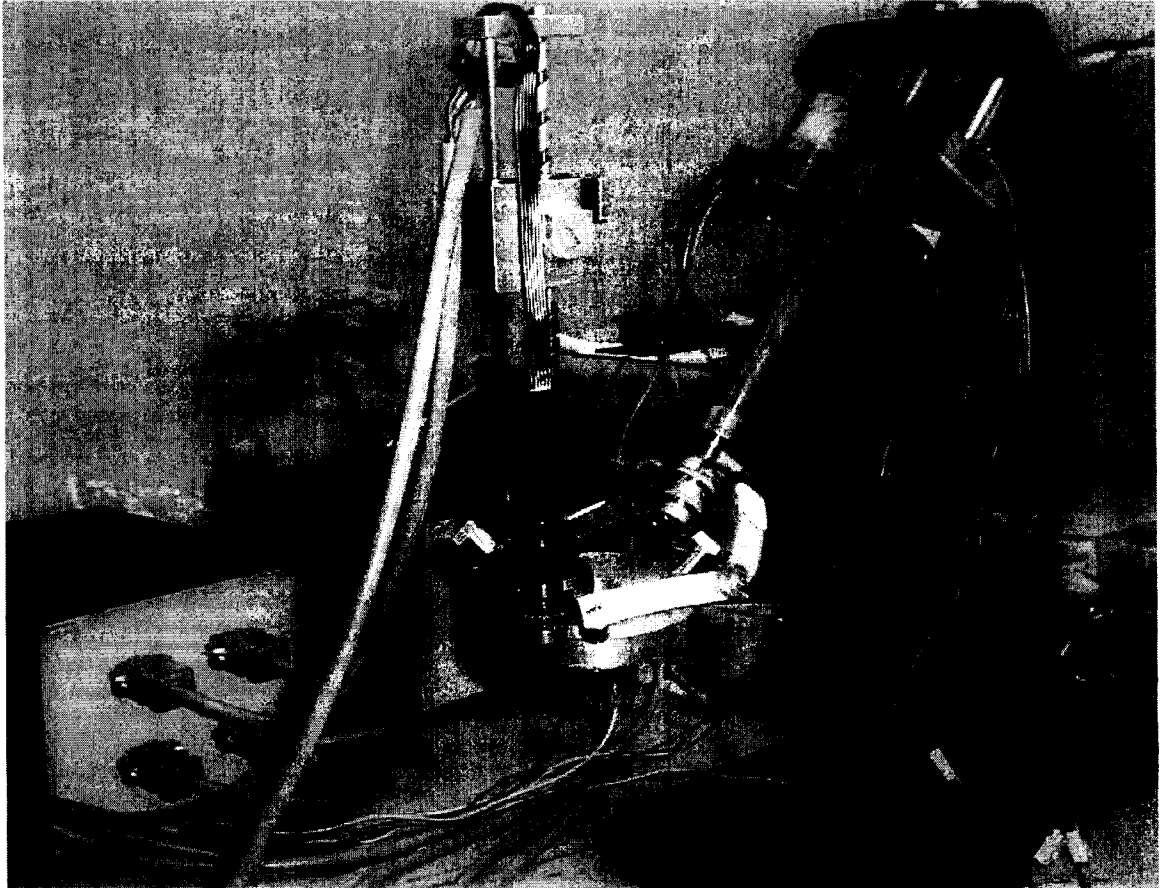


Figure 2-22 Photograph of the tool-holding mechanism

Shown in Figure 2-22, the tool-holding mechanism is a compact mechanism with link radii 33% smaller than the earlier prototype. This small link-radius reduces overall size and space. Not only is the radius reduced, the linkage thickness is also reduced from 6 mm to 4 mm. The links and platform are made of aluminum alloy (AL 6061) which is high in strength, light in weight and a common alloy used in aerospace industry. The high strength engineering plastic material used in the earlier version is strong. According

to the input from machine shop, machining tools were broken while machining the fiber reinforced high-stress engineering plastic.

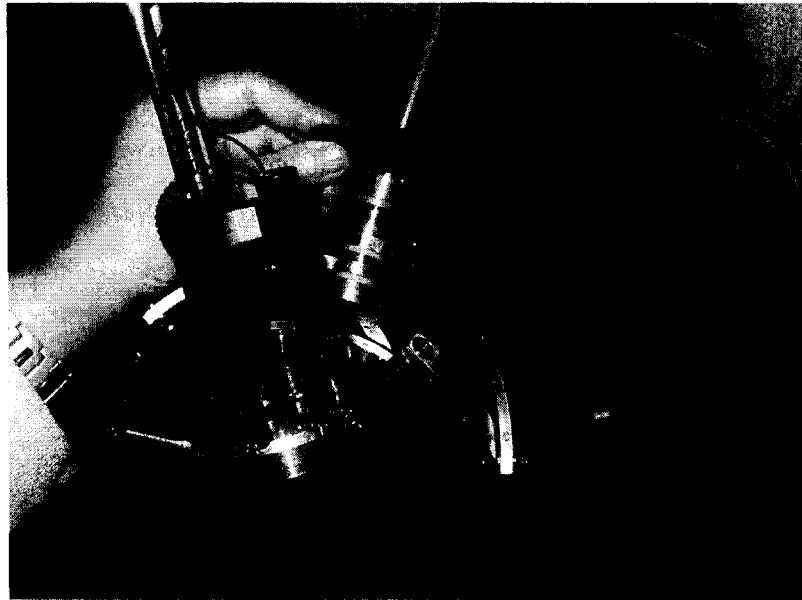


Figure 2-23 Comparing the link size of first and second mechanism

Shown in Figure 2-24, all joints are revolute which were high in demand for this mechanism in order to ensure the kinematics behavior. A cylindrical bushing passes through 8 mm diameter bores of active and passive link. One 1-mm thickness washer is placed between links to maintain distance between.

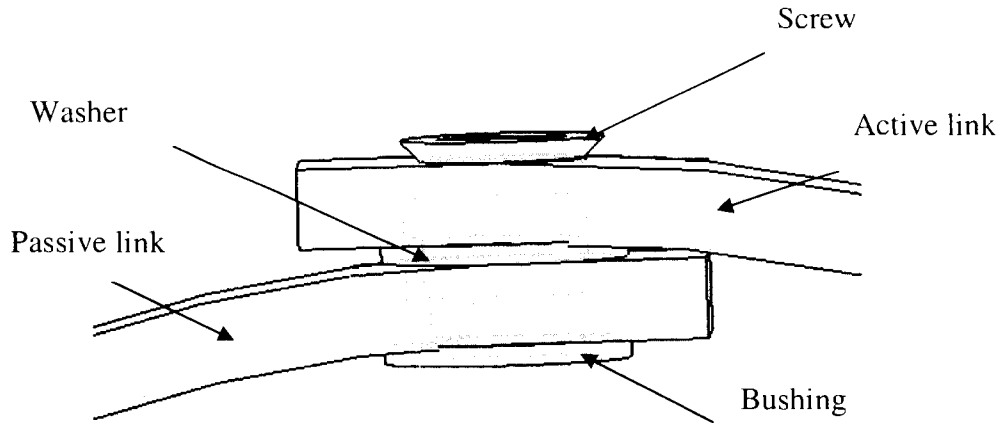


Figure 2-24 Revolute middle joint

A lead screw is used to convert rotary motion into linear motion. Back driving produces the load pushing axially on the screw or nut to create rotary motion. Advantages include self-locking capability, good for vertical application, low cost, ease of manufacture. Limitations of lead screw include lower efficiencies, requirement of larger motor and high friction force. Shown in Figure 2-25, lead screw linear motion design module was modified to reduce dimension in order to avoid the collision with links by reduced size.

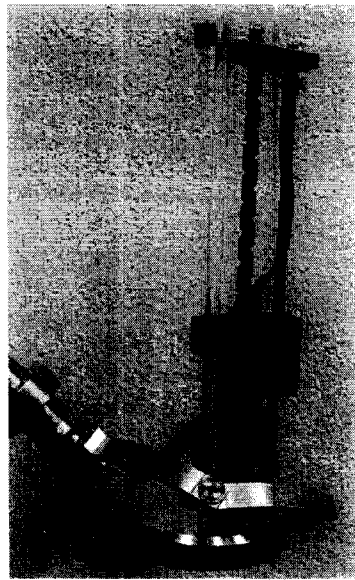


Figure 2-25 Lead screw linear motion design module

Shown in Figure 2-26, the concentric link module connecting active rods with active links were built to ensure the concentric feature. The active link of each branch is fixed to the module by four screws.

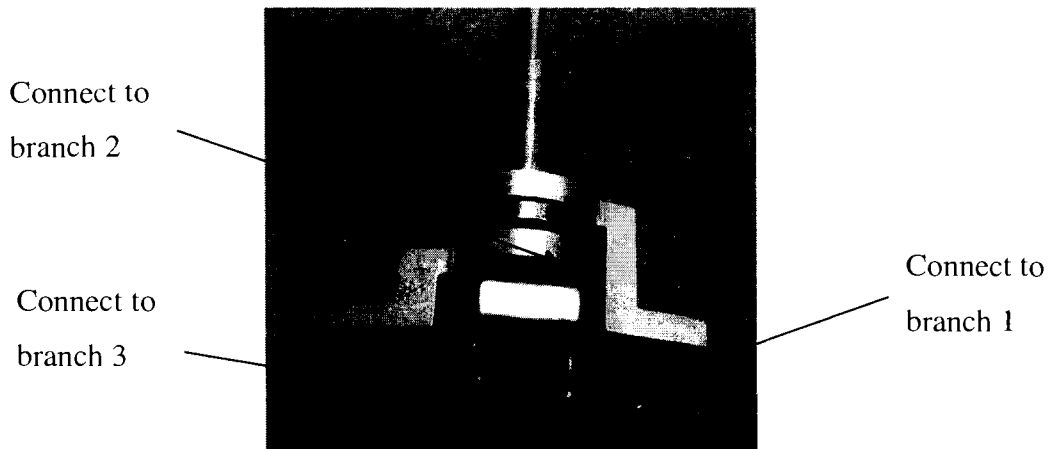


Figure 2-26 Concentric link module

The platform of tool-holding mechanisms is cantilever design. The endoscopic camera and linear motion mechanism is mounted on the platform. The weight of platform with linear device is measured about 750 grams and the maximal deflection of the actuating link can be calculated as:

$$\text{Deflection } (\delta_{\max}) = \frac{pl^3}{3EI}$$

Moment of inertia of the tube $I = \frac{\pi(OD^4 - ID^4)}{4}$, Substituting p, l, E and I leads to

$$\delta_{\max} = \frac{p \times l^3}{3 \times E \times I} = \frac{100 \times 240^3}{3 \times 101 \times 10^3 \times \frac{3.1415 \times (9.525^4 - 7.9375^4)}{4}} = 0.1363 \text{ (mm)}$$

Since the deflection of actuating shaft caused by platform, weight can be considered insignificant. No compensate methods are designed for further kinematic analysis.

2.4. Kinematic Model

In general, kinematic analysis can be divided into direct (forward) kinematic and inverse kinematics. The direct kinematics problems obtain the position and orientation of the manipulator by knowing the input joint variables. Inverse kinematics problems involve taking the known position and orientation of the manipulator and solving for the joint variables.

The kinematic diagram is shown in Figure 2-27. The unit vector v_a directs along the concentric actuating axis. The unit vectors p_1, p_2, p_3 are the axes of the revolute joints connected to the platform. The unit vectors corresponding to revolute joints connecting passive link and active link on each branch are $m_1, m_2,$ and m_3 . The link angle of passive links are defined as $\alpha_{1i}, (i=1, 2, 3)$. The link angle of active links are $\alpha_{2i}, (i=1, 2, 3)$. To solve both direct and inverse kinematic problems, kinematic methods from Craig and Sciavicco are used[45, 53].

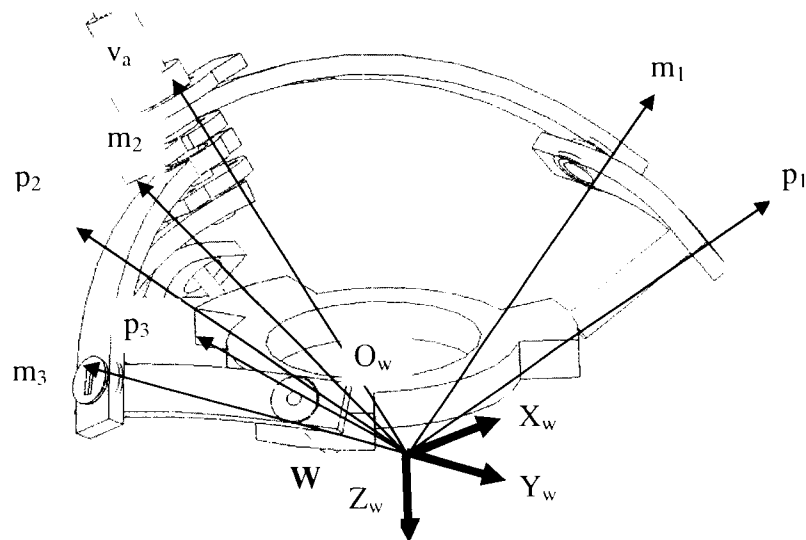


Figure 2-27 Schematic drawing of the three DOF spherical platform

Link angles ($\alpha_{11}, \alpha_{21}, \alpha_{31}, \alpha_{12}, \alpha_{22}, \alpha_{32}$): These six angles represent two links of three branches. Shown in Figure 2-28, angles α_{11}, α_{21} and α_{31} are the angles of passive link L_{ij} that are the angles between moving platform vectors and the corresponding middle revolute joints. α_{11}, α_{21} and α_{31} are passive link angles. $\alpha_{12}, \alpha_{22}, \alpha_{32}$ are active link angles that are the angles between the middle revolute joints and actuating axis.

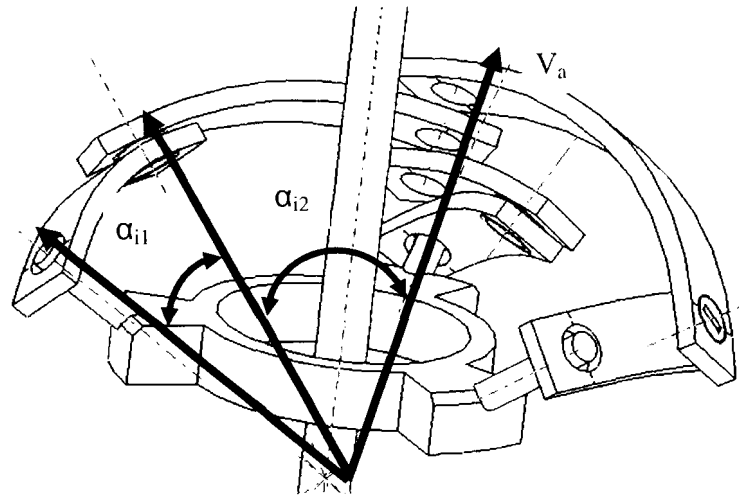


Figure 2-28 Link angles

World coordinate frame (W): World coordinate frame is a fixed frame, with reference to which, other frames are defined. Shown in Figure 2-29, the origin point O of the world coordinate frame is located at the pivot center of the moving platform. This center is the incision point on the abdominal wall of patient. Three coordinate axes, X_w, Y_w and Z_w , are defined. Positive Z-axis is defined towards into the abdominal wall. The revolute joint vectors and actuating axes meet at this origin point. The bottom of platform is 25 mm above the abdomen. This distance between the bottom of platform and the abdomen is a balanced number that should be kept. The purpose of keeping the distance is to avoid interference between the moving parts and abdomen. This distance of 25 mm can be increased or reduced depending on the surgical application. If this distance increases, the diameter of platform and links must be increased.

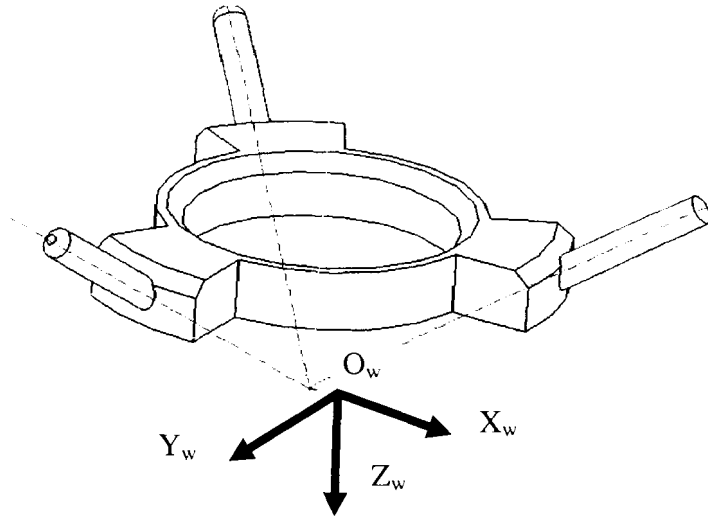


Figure 2-29 World coordinate frame

Actuating coordinate frame (A): Actuating coordinate frame is a fixed frame. Shown in Figure 2-30, the origin point O_a of actuating coordinate frame is located at the same position as the origin point of world coordinate frame. In this figure, β represents the angle ($3/4\pi$) between Z-axis of the world frame and actuating frame. The rotation matrix

of actuating coordinate frame can be expressed as $R_a^W = \begin{bmatrix} 1 & 0 & 0 \\ 0 & \cos \beta & -\sin \beta \\ 0 & \sin \beta & \cos \beta \end{bmatrix}$

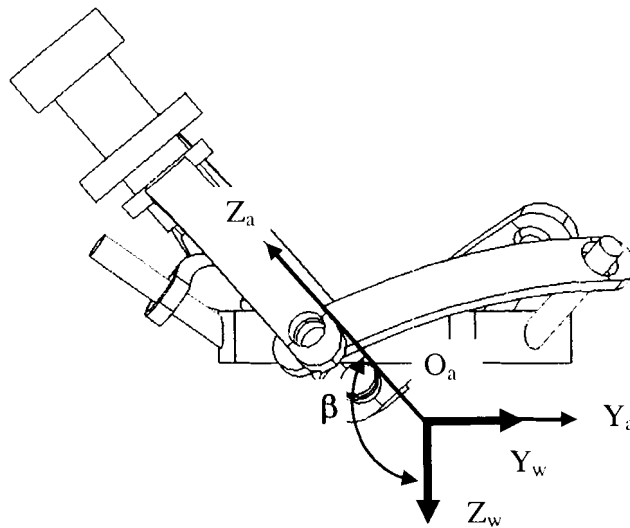


Figure 2-30 Angle of actuating coordinate frame

Link coordinate frame (L): link coordinate frame is attached to each link in order to determine local coordinate position, shown in Figure 2-31. The Z-axis is pointing to spherical center and X-axis is parallel to link arc.

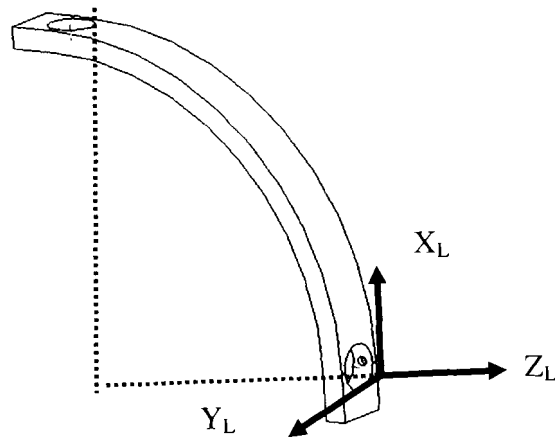


Figure 2-31 Link coordinate frame

Platform coordinate frame (P): In Figure 2-32, the platform coordinate frame is attached to the moving platform and defined by three branch vectors. The platform coordinate frame shares its origin point with that of the world coordinate frame and rotates with respect to world coordinate frame same as translation. This special design characteristic of orthogonal platform vectors has been introduced in section 2.3. The benefit of this design is that the third vector of the platform (z_p) can be calculated easily as the cross product of vector x_p and y_p .

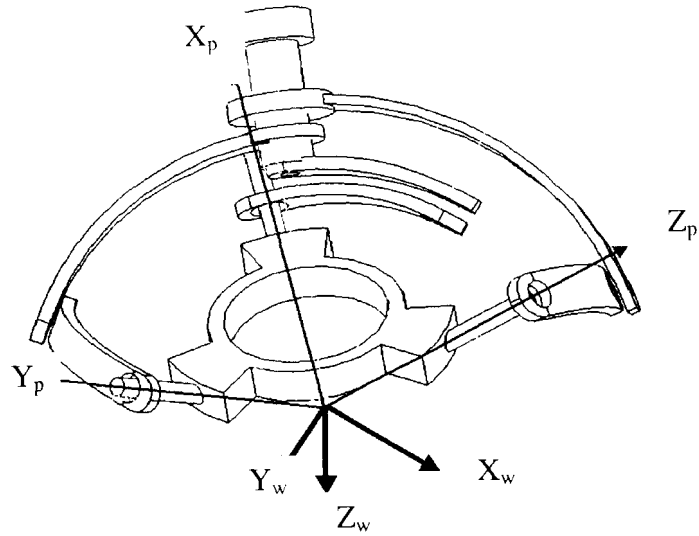


Figure 2-32 Platform coordinate frame

Tool (camera) coordinate frame (T): Shown in Figure 2-33, a moving coordinate frame is attached to the tip of endoscopic camera or surgical tool. It is convenient to describe camera/tool motion with respect to the camera frame rather than the world frame. Since the camera is attached to the moving platform, the camera frame has only one linear DOF with respect to platform and four DOF with respect to world frame.

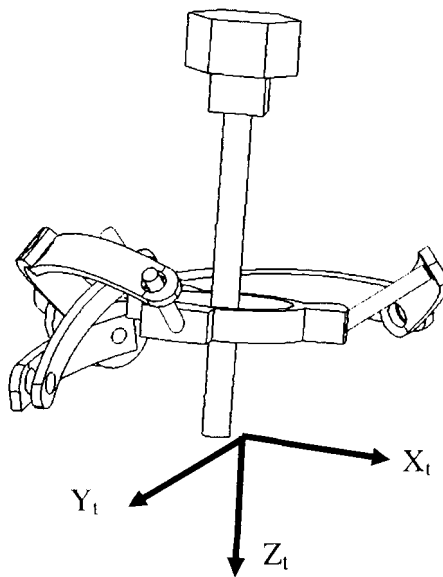


Figure 2-33 Camera/Tool Coordinate frame

Branch link radii ($r_{11}, r_{21}, r_{31}, r_{12}, r_{22}, r_{32}$): These six radii are nested for three branches. Shown in Figure 2-34, r_{11}, r_{21} and r_{31} are the radius of passive link L_{i1} and r_{12}, r_{22}, r_{32} are those of active link L_{i2} . The tool-holding mechanism has branch link radii (80, 75, 70, 65, 60, 55) mm.

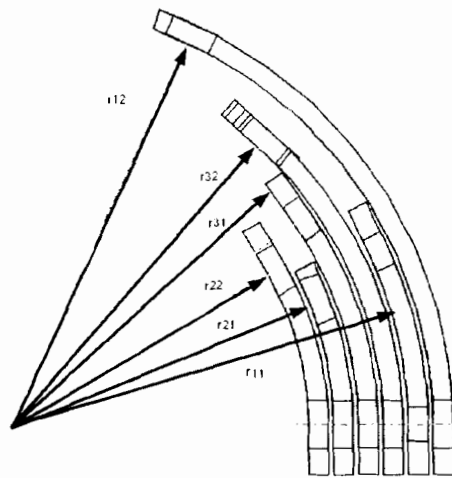


Figure 2-34 Branch link radii

Active link rotation angles ($\theta_{1a}, \theta_{2a}, \theta_{3a}$): Shown in Figure 2-35, active link rotation angle is measured between the X-axis of actuating frame and the X-axis of link coordinate frame of L_{21}, L_{22} and L_{23} . This angle is positive for counter clockwise and negative for clockwise. The angles are driven by motor with the gear ratio of (56:24).

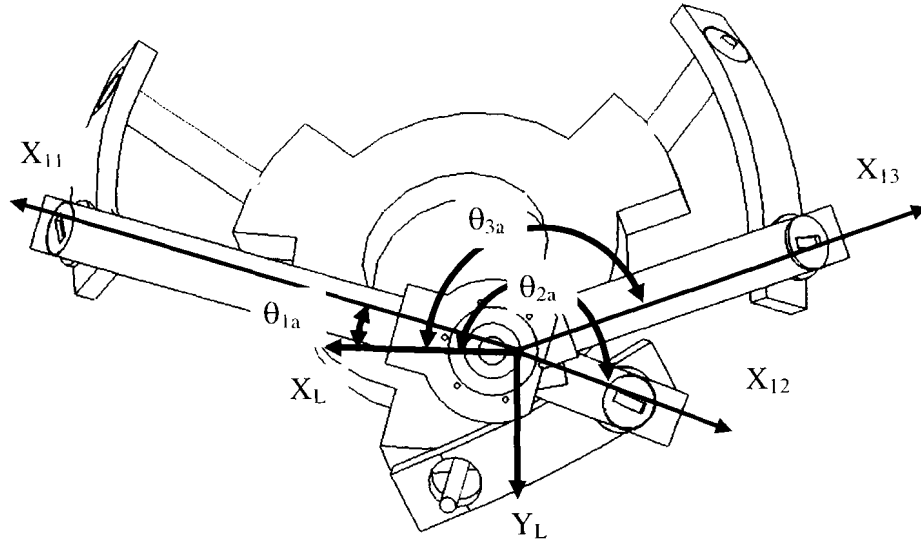


Figure 2-35 Actuating angles

Middle revolute angles (θ_{1m} , θ_{2m} , θ_{3m}): Shown in Figure 2-36, middle revolute angles are measured between passive and active links. The angle between axis X_i and X_p about axis Z_i is positive when rotation is counter clockwise. Middle revolute angles are passive which can be calculated from kinematic formulations or measured by potentiometer.

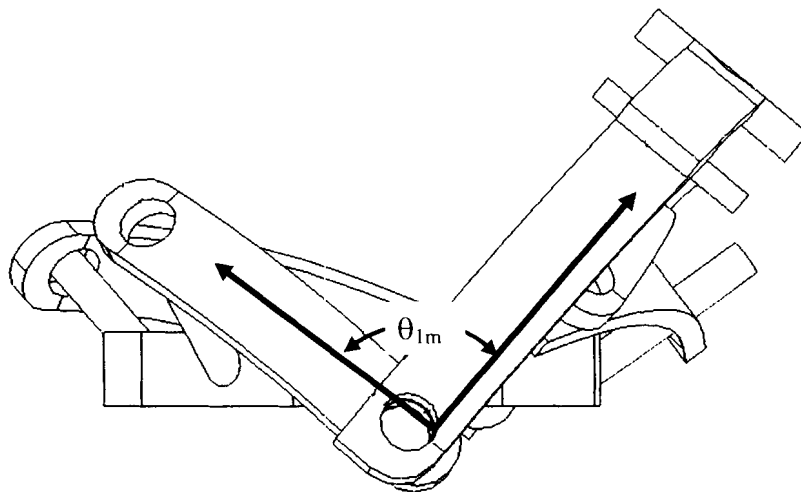


Figure 2-36 Middle revolute angle

2.5. Workspace optimization of Genetic Algorithm

Since the spherical parallel structure is chosen (in section 2.1) and the limited workspace is a main disadvantage (in section 2.2), it is necessary to analyze and maximize the workspace to ensure the mechanism is able to reach the design specification. The purpose of supportive analysis is to ensure the feasible design in addition to the design synthesis. Genetic algorithm (GA) is chosen to optimize the workspace volume because of the advantages.

Limited workspace is the main disadvantage of parallel manipulator. Oblak [54] studied manipulator workspace of the Jacobian analysis with one or more joints achieving the limit position. Hay [55] applied a synthesis for determining a manipulator design so that the workspace corresponds to a prescribed workspace by numerical method. Liu [56] studied the solution space of spherical 3-DOF serial wrists, classified the reachable workspaces and investigated the dexterous workspaces for spherical four bar wrists mechanism. Majid [57] studied the size and shape of workspace for a three-PPSR (prismatic-prismatic-spherical-revolute joint) manipulator that provides numerically a larger workspace than Stewart platform. Stamper[58] suggested a parallel manipulator design for maximum workspace volume that might not be the optimal design for practical applications. The optimal design is the synthesis and integration of all design parameters to achieve the special function.

Genetic algorithm (GA) is a stochastic global search method that mimics natural biological evolution[59]. GA was selected as an optimizing tool because it has the advantages of both weak and strong search methods[60]. Strong methods, such as numerical optimization procedures, perform search in an informed manner by function gradients. Weak methods such as random or exhaustive procedures search in the

uninformed method by extensively sampling the design space. Weak methods are expensive but more likely to find global optima; strong methods are inexpensive but more likely to settle by local sub optima. GA is operated with strong progression toward improved designs, together with the weak operations of probabilistic selection, crossover, and mutation. GA has been successfully applied to optimization problems like scheduling, optimal control, transportation problems and engineering design[61], [62], and [63]. This method is robust because it simultaneously evaluates many points in the search space and converges toward the global optimal solution.

At this stage, the spherical parallel mechanism is chosen with the parameters affecting workspace volume, branch position angles, and link angles (Figure 2-28). GA is applied for the workspace with the same parametric variable as in heuristic optimization. The goal is to find the maximal workspace volume. In GA approach, the design parameters (link angles) are chromosome strings. First, the program randomly generates 100 sets of different design parameters (link angles) as the first generation parents. Then, the workspace volume with respect to each set of design parameters is calculated. While calculating the workspace volume, the collision detection among all the links with the tool/endoscope is checked to prevent collision; the detail calculation of which is in[64]. The reachable workspace is defined as the space that normal vector of platform can reach without collision. For given design parameter, the workspace volume is described by the loci of the normal vector of the moving platform (Figure 2-37). From the kinematic equations, normal direction of moving platform can be calculated. A general form of equation that can describe the workspace volume is given as:

$$\text{Workspace Volume} = 1/3\pi\sin(\lambda)^2\cos\lambda .$$

Where λ is the boundary loci of normal vector corresponding to the symmetric centerline of workspace.

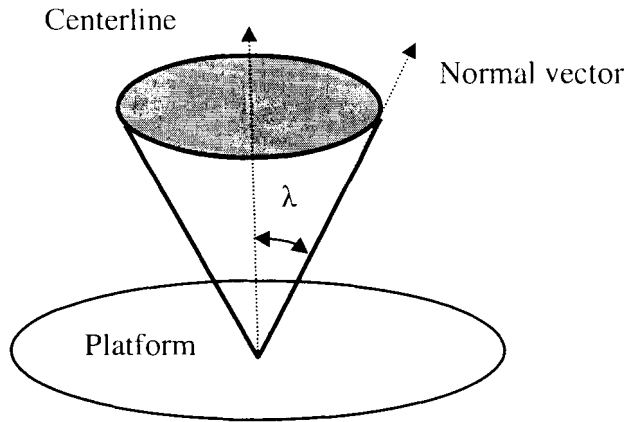


Figure 2-37 Workspace volume

Third, the workspace volume ranked the parents. The parent with larger workspace volume has higher ranked value in the rank list. Parents were selected by ranked value to produce offspring. GA repeats previous steps until designated generate number is reached.

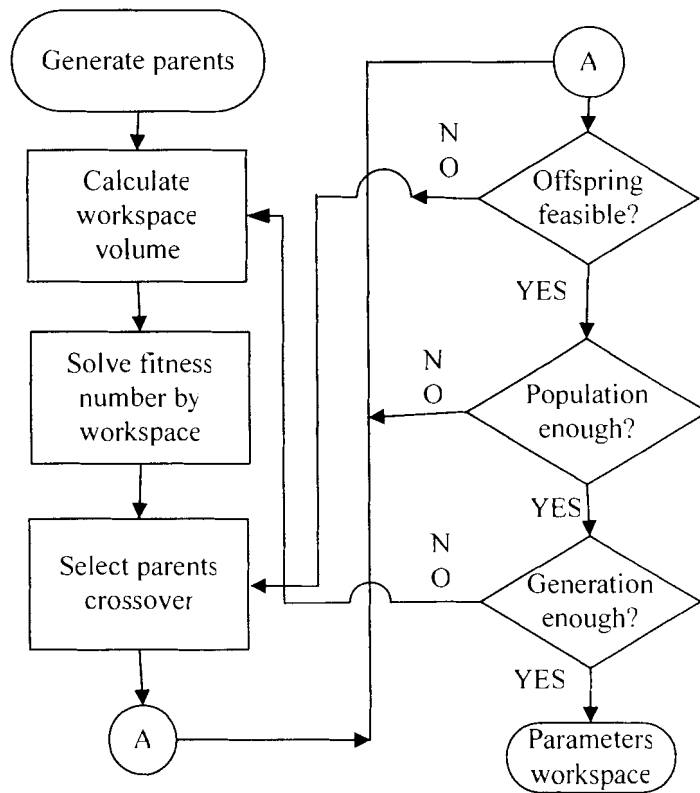


Figure 2-38 GA flow chart

GA operates a population of potential solutions by applying the principle of survival of the fittest to produce better solution. For each generation, the process of selecting parents produces a new set of approximations. GA analyzes simultaneously a number of potential solutions called populations, consisting of encoded parameter sets. Typically, a population is composed of a range of solutions between 30 and 100.

Shown in Figure 2-38, the GA formulation for workspace analysis has the following steps:

Selection: Selection is proportional to the fitness from the population of parents. Good parents contain larger workspace volume than bad parents do. It is necessary to balance the "good parents" and "bad parents" because different chromosomes are needed from both good and bad parents. The chromosomes are link angles. The workspace volume of each member in the population is calculated to represent fitness number. The population is ranked in fitness number for crossover. At the selection stage, a fitness number from the best solution as the highest rank and the worst solution for lowest rank is selected. The parent with higher rank will have a better chance to be selected to perform crossover action.

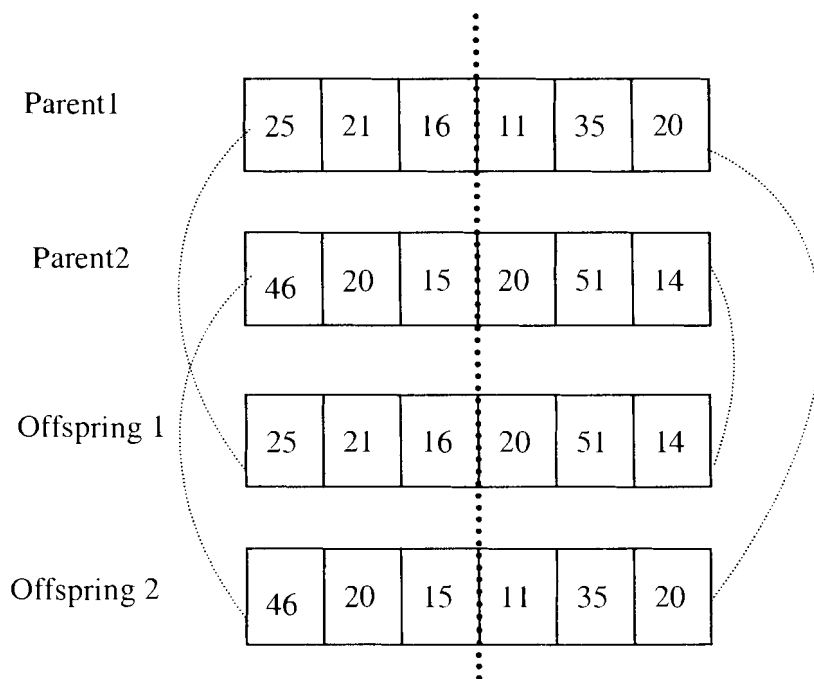


Figure 2-39 An example of Crossover model

Crossover: Shown in Figure 2-39, the crossover action combines different chromosome strings to generate new offspring strings. Goldberg [60] defined the partially mapped crossover (PMO) by using two crossover points. The selection between these points defines an interchange mapping. Two crossover methods are applied: a) Random position where a crossover point was generated randomly by program. This number is greater than one and less than the total number of chromosome b) Middle crossover where the crossover point is at the middle of total chromosome string.

Mutation: Mutation will be applied when the offspring is the same as one of its parents. In general, the mutation works with a single chromosome. A chromosome will be created by randomly reassigning a value to one of its genes. The probability to conduct a mutation depends on the identity of parents and offspring. The chromosome of every offspring will be compared with its parents. The mutation will be performed only when the offspring contains chromosome identical to its parent. If the parent and offspring are identical, the mutation changes any chromosome randomly. The mutation offers versatile solution to prevent offspring converging to local maximum.

Replacement: The replacement produces new generation offspring from the current parents. The best solution of new offspring is compared with the best solution of their parents, with the new generation replacing its parents. If the best offspring is not as good as the best parent is, crossover process will be repeated to generate new offspring. The GA simulation result is shown in Table 2-4 which are design parameters, link angles, of tool-holding mechanism.

Table 2-4 Parameters of GA workspace volume

Link angle	11	12	21	22	21	31
Angle	30	50	15	25	25	65

The simulation result of GA is an optimized value which satisfies the design requirement (in section 2.2.1). For a further step, finding the global optimum by GA can be ensured by implementation of additional GA technology such as parallel GA, breeder GA [65] or by using the exhaustive search procedure. The result from exhaustive search procedure can be used to compare with the result from GA to evaluate the difference between the result from GA and global optimum.

2.6. Kinematics Analysis

Both inverse and direct kinematic are studied in this section. Solving the kinematic problem is the basic requirement to control the motion and orientation of the manipulator. In serial manipulator, inverse kinematics is more complex than direct kinematics because of complex non-linear equations[53]. Parallel manipulators contain un-actuated joints so that their analysis is more complex than serial manipulator[66].

2.6.1. Inverse Kinematics

In the robotic assisted surgery, the mechanism holds the surgical tool and surgeons give command to control the robot through computer. The current position of surgical tool

must be identified and the goal position must be defined to calculate corresponding motor angles. The inverse kinematics (IK) problem consists of the determination of the joint variables corresponding to a given end effector position and orientation[53]. IK is necessary to control the correct posture of camera holding mechanism. Once the position and orientation of the tool is defined, the joint variables (of corresponding motor angles) can be solved. Therefore, inverse kinematics is applied to calculate joint variables. The flow chart of solving inverse kinematics is shown in Figure 2-40.

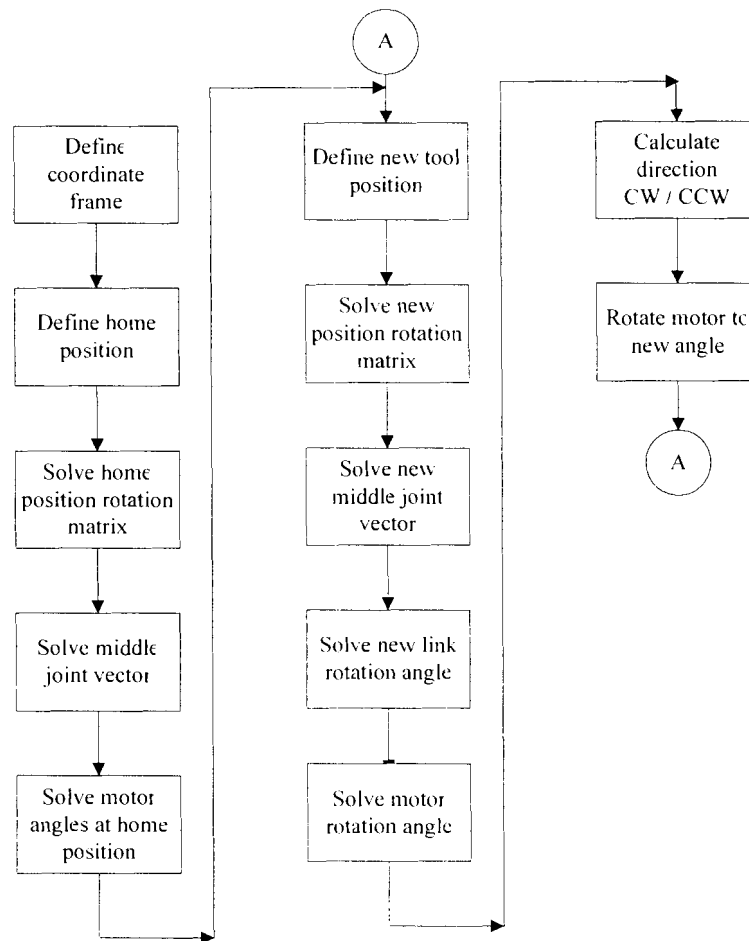


Figure 2-40 Flow chart of solving inverse kinematics

The world coordinate frame (W) and actuating coordinate frame (A) have been defined in the previous section. The next step is to define home position of the tool and the moving

platform. Rotation matrix (R_h) of platform home position can be expressed by platform joint vectors p_1 , p_2 and p_3 .

$$R_h = [p_1 \quad p_2 \quad p_3] \quad (2-2)$$

Substituting p_1 with $[x_{p1}, y_{p1}, z_{p1}]^T$, p_2 with $[x_{p2}, y_{p2}, z_{p2}]^T$, and p_3 with $[x_{p3}, y_{p3}, z_{p3}]^T$ into (2-2) yields to

$$R_h = \begin{bmatrix} x_{p1} & x_{p2} & x_{p3} \\ y_{p1} & y_{p2} & y_{p3} \\ z_{p1} & z_{p2} & z_{p3} \end{bmatrix}$$

Once the platform joint vectors p_i , ($i=1, 2, 3$) are defined, middle joint vectors m_i , $m_1 [x_{m1}, y_{m1}, z_{m1}]^T$, $m_2 [x_{m2}, y_{m2}, z_{m2}]^T$ and $m_3 [x_{m3}, y_{m3}, z_{m3}]^T$, can be solved by cosine laws.

$$\cos \alpha_{i1} = p_i \cdot m_i = x_{pi} \cdot x_{mi} + y_{pi} \cdot y_{mi} + z_{pi} \cdot z_{mi} \quad (2-3)$$

$$\cos \alpha_{i2} = v_a \cdot m_i = x_a \cdot x_{mi} + y_a \cdot y_{mi} + z_a \cdot z_{mi} \quad (2-4)$$

$$x_{mi}^2 + y_{mi}^2 + z_{mi}^2 = 1 \quad (2-5)$$

Two solution sets exist for the middle joint vector of each joint. Therefore, eight different solutions satisfy the previous equation. For three DOF spherical parallel mechanism, eight different configurations are studied by Gosselin[46]. Only one solution matches the physical mechanism configuration. To identify the real solution, a check with the mechanism is done to ensure that the posture of mechanism matches the solution.

By rotating the moving platform to reach a new orientation and a new platform rotation matrix R_n can be obtained. New platform joint vectors p_{1n} , p_{2n} , p_{3n} can be obtained by equation (2-2) and new middle joint vectors m_{in} can be solved by equation (2-3), (2-4) and (2-5).

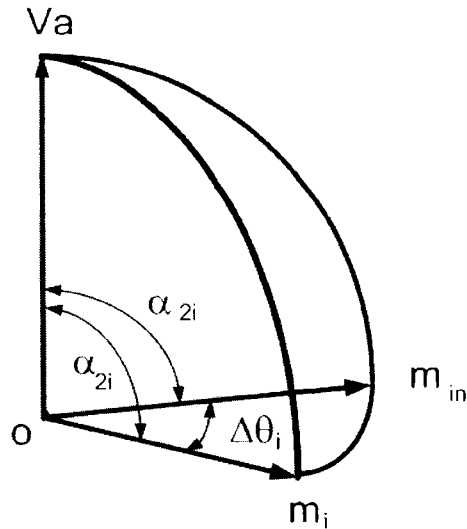


Figure 2-41 Spherical triangle

The next step is to solve the rotation angle $\Delta\theta_i$. $\Delta\theta_i$ is the rotation angle of the i^{th} active link from start position m_i to new position m_{in} . The rotation angle can be obtained by utilizing spherical triangle. Shown in Figure 2-41, let the spherical triangle be drawn on the surface of a unit sphere, centered at a point $O [0, 0, 0]^T$. The vectors from the center of sphere to the vertices are given by v_a , m_i and m_{in} . V_a is the actuating axis vector, m_n is the middle joint vector of start position, m_{in} is the middle joint vector of new position, and α_{i2} is the i^{th} active link angle. The relationship between α_{i2} and $\Delta\theta_i$ can be expressed by cosine law as:

$$\cos \alpha_{i2} = m_i \cdot v_a, \quad \cos \alpha_{i2} = m_{in} \cdot v_a, \quad \cos \Delta\theta_i = m_i \cdot m_{in}$$

Next, rotation angle $\Delta\theta_i$ can be solved as: $\Delta\theta_i = \arccos(m_i \cdot m_{in})$

After obtaining the rotation angle of active link, it is necessary to judge clockwise (CW) or count clockwise (CCW). For Link₁₂, if the Z value of middle joint vector approaches 0, it rotates CCW (positive direction). A selection for CW/CCW is necessary to ensure calculation. For physical condition of branch 1, Link₁₂ rotates CW, the link will raise and z_{m1} value decrease. Table 2-5 shows the rotation direction of the active links.

Table 2-5 Active link rotation direction judgment

	Active link 1(Link ₁₂)	Active link 2 (Link ₁₂)	Active link 3 (Link ₁₂)
Z (moving up)	CW	CCW	CCW
Z (down)	CCW	CW	CW

The last step is to convert gear ratio between motor and active link to get corresponding motor rotating angle. The motor rotation direction is the opposite direction of active link and gear ratio is 24:56. Therefore, the motor rotating angle can be expressed by following equation:

$$\Delta\theta_{motor_i} = -\frac{\Delta\theta_{link_ia} \cdot 56}{24}$$

The $\Delta\theta_{motor_i}$ is the required rotation angle of motor.

2.6.2. Numerical Example of Inverse Kinematics

Shown in Figure 2-42, the home position of tool-holding mechanism is defined as the platform top parallel to ground. At home position, the platform rotation matrix R_h is defined as:

$$R_h = \begin{bmatrix} 0.577350 & 0.211325 & -0.788675 \\ 0.577350 & -0.788675 & 0.211325 \\ -0.5773502 & -0.5773502 & -0.5773502 \end{bmatrix}$$

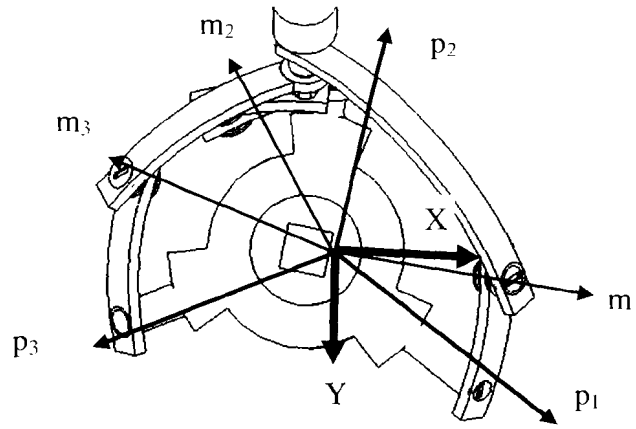


Figure 2-42 Top view of platform home position

Platform joint vectors p_1, p_2, p_3 can be obtained by equation (2-3) of the platform rotation

$$\text{matrix } R_h \cdot p_1 = \begin{bmatrix} 0.577350 \\ 0.577350 \\ -0.577350 \end{bmatrix}, p_2 = \begin{bmatrix} 0.211325 \\ -0.788675 \\ -0.577350 \end{bmatrix}, p_3 = \begin{bmatrix} 0.788675 \\ -0.211325 \\ -0.577350 \end{bmatrix}$$

The actuating axis vector is v_a which is equal to $[0, -0.70710, -0.70710]^T$.

In order to solve middle joint vector $m_1 = [x_{m1}, y_{m1}, z_{m1}]^T$, $\cos \alpha_{11}, \cos \alpha_{12}$ and, p_1 are substitute into equations (2-4) (2-5) and (2-6), which yields

$$\cos \alpha_{11} = m_1 \cdot p_1 = x_{m1} \cdot x_{p1} + y_{m1} \cdot y_{p1} + z_{m1} \cdot z_{p1} \quad (1) \text{ that can be rewritten as:}$$

$$\cos (25\pi/180) = 0.577350x_{m1} + 0.577350y_{m1} - 0.577350z_{m1}$$

$$\cos \alpha_{12} = v_a \cdot m_1 = x_a \cdot x_{m1} + y_a \cdot y_{m1} + z_a \cdot z_{m1} \quad (2)$$

$$\cos (65\pi/180) = 0x_{m1} - 0.7071678100y_{m1} - 0.7071678100z_{m1}$$

$$x_{m1}^2 + y_{m1}^2 + z_{m1}^2 = 1 \quad (3)$$

m_1 can be obtained by equation (1) (2) and (3) and two possible solutions are solved. Hence, for a given position of the platform, there are two configurations for each branch. Solving equations (1) (2) and (3) to obtain $[x_{m1}, y_{m1}, z_{m1}]^T$ for m_1 such that

$$[x_{m1}, y_{m1}, z_{m1}]^T = [0.5232472310, 0.2244257129, -0.8220981904]^T,$$

$$[x_{m1}, y_{m1}, z_{m1}]^T = [0.5232668586, 0.2244257129, -0.8220883766]^T$$

In order to solve $m_2 = [x_{m2}, y_{m2}, z_{m2}]^T$, $\cos \alpha_{21}$ and p_2 are substituted into equations (2-4) (2-5) and (2-6) yield to

$$\cos \alpha_{21} = p_2 \cdot m_2 = x_{p2} \cdot x_{m2} + y_{p2} \cdot y_{m2} + z_{p2} \cdot z_{m2}$$

$$\cos (30\pi/180) = 0.211325x_{m2} - 0.788675y_{m2} - 0.577350z_{m2}$$

$$\cos \alpha_{22} = v_a \cdot m_2 = x_a \cdot x_{m2} + y_a \cdot y_{m2} + z_a \cdot z_{m2}$$

$$\cos (22\pi/180) = 0x_{m2} - 0.707107y_{m2} - 0.707107z_{m2}$$

$$x_{m2}^2 + y_{m2}^2 + z_{m2}^2 = 1$$

The middle joint vector m_2 can be solved as:

$$[x_{m2}, y_{m2}, z_{m2}]^T = [0.1127081991, -0.4030046887, -0.9082312936]^T,$$

$$[x_{m2}, y_{m2}, z_{m2}]^T = [-0.2992483369, -0.8149612248, -0.4962747576]^T$$

In order to solve m_3 , $\cos \alpha_{31}$, $\cos \alpha_{32}$ and p_3 are substituted into equations (2-4) (2-5) and (2-6) yield to

$$\cos \alpha_{31} = p_3 \cdot m_3 = x_{p3} \cdot x_{m3} + y_{p3} \cdot y_{m3} + z_{p3} \cdot z_{m3}$$

$$\cos (35\pi/180) = 0.788675x_{m3} - 0.211325y_{m3} - 0.577350z_{m3}$$

$$\cos \alpha_{32} = v_a \cdot m_3 = x_a \cdot x_{m3} + y_a \cdot y_{m3} + z_a \cdot z_{m3}$$

$$\cos (48\pi/180) = 0x_{m3} - 0.7071678100y_{m3} - 0.7071678100z_{m3}$$

$$x_{m3}^2 + y_{m3}^2 + z_{m3}^2 = 1$$

The middle joint vector m_3 can be solved as:

$$[x_{m3}, y_{m3}, z_{m3}]^T = [-0.3589268957, -0.01301870105, -0.9332748775]^T,$$

$$[x_{m3}, y_{m3}, z_{m3}]^T = [-0.7331464162, -0.3872382215, -0.5590553570]^T$$

2.6.3. Direct Kinematics

The direct kinematics equation of a manipulator expresses the position and orientation of the end effector as a function of joint variables with respect to the world frame[53]. End effector of a manipulator can be calculated by a set of linkage homogeneous transformation. The determination of the direct kinematics of parallel manipulators is difficult but has to be solved for many practical cases. The studies of direct kinematics for parallel robot has been done by Merlet[67]. Direct kinematics of three DOF planar parallel manipulator have been studied by Tsai[68], [69] and[70]. Direct kinematics of general three DOF spherical parallel has been studied by Gosselin[69]. Ji [71] studied a direct algebraic solution of three DOF spherical parallel manipulator and found that the direct kinematics to this parallel manipulator is an eighth polynomial equation.

In tool (or camera) frame, environmental objects can be located relative to the tool tip or gripper. To achieve the related joint motion to move the tool tip properly, the necessary motion trajectory of the end effector with respect to the base frame has to be calculated.

In order to calculate direct kinematics, the world coordinate frame, actuating coordinate frame and Denavit Hartenberg parameters (Table 2-6) are defined. First, the input active link angles ($\theta_1, \theta_2, \theta_3$) must be defined. Second, the middle joint vectors m_i can be obtained by the transformation matrix R and actuating axis vector v_a .

Table 2-6 DH Table of tool-holding mechanism

Branch 1				Branch 2				Branch 3			
a_1	α_1	d_1	θ_1	a_2	α_2	d_2	θ_2	a_3	α_3	d_3	θ_3
0	25	0	θ_{11}	0	30	0	θ_{21}	0	35	0	θ_{31}
0	65	0	θ_{12}	0	22	0	θ_{22}	0	48	0	θ_{32}

To calculate middle joint vector m_i of the i^{th} branch, the parameters of the equations are replaced by active link angle α_{i2} . v_a is actuating axis vector, which is defined by the active coordinate frame. R_{i2} is the rotation matrix of active link.

$$m_i = R_{i2} \cdot v_a \quad (2-6)$$

Where:

$$R_{i2} = \begin{bmatrix} \cos \theta_{i2} & -\sin \theta_{i2} \cos \alpha_{i2} & \sin \theta_{i2} \sin \alpha_{i2} \\ \sin \theta_{i2} & \cos \theta_{i2} \cos \alpha_{i2} & -\cos \theta_{i2} \sin \alpha_{i2} \\ 0 & \sin \alpha_{i2} & \cos \alpha_{i2} \end{bmatrix}$$

$$v_a = \begin{bmatrix} 0 \\ \cos \beta \\ -\sin \beta \end{bmatrix}$$

In order to calculate the i^{th} platform joint vector p_i , the parameters of equation are replaced by passive link angle α_{i1} . and middle joint vector are substituted into equation (2-6) to compute the direct kinematics function as:

$$\begin{aligned}
p_i &= R_{i1} \cdot m_i \\
&= R_{i1} \cdot R_{i2} \cdot v_a \\
&= \begin{bmatrix} \cos \theta_{i1} & -\sin \theta_{i1} \cos \alpha_{i1} & \sin \theta_{i1} \sin \alpha_{i1} \\ \sin \theta_{i1} & \cos \theta_{i1} \cos \alpha_{i1} & -\cos \theta_{i1} \sin \alpha_{i1} \\ 0 & \sin \alpha_{i1} & \cos \alpha_{i1} \end{bmatrix} \cdot \begin{bmatrix} \cos \theta_{i2} & -\sin \theta_{i2} \cos \alpha_{i2} & \sin \theta_{i2} \sin \alpha_{i2} \\ \sin \theta_{i2} & \cos \theta_{i2} \cos \alpha_{i2} & -\cos \theta_{i2} \sin \alpha_{i2} \\ 0 & \sin \alpha_{i2} & \cos \alpha_{i2} \end{bmatrix} \cdot \begin{bmatrix} 0 \\ \cos \beta \\ -\sin \beta \end{bmatrix} \\
(2-7)
\end{aligned}$$

That equation (2-7) contains the unknown (θ_i) i.e. the middle joint angle which is a measurable passive joint.

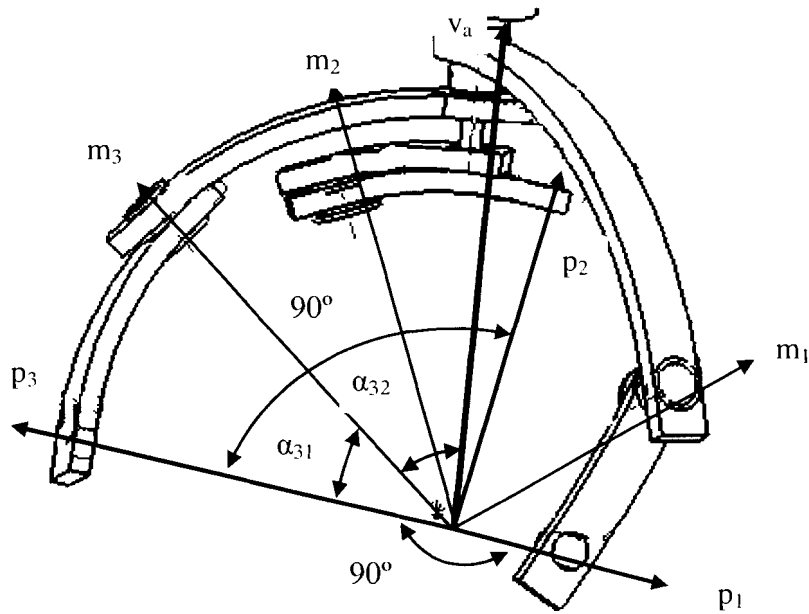


Figure 2-43 Link platform angles

Therefore, solving the direct kinematics of the platform, the relationship between angles can be observed from Figure 2-43, that three platform joint vectors (p_1, p_2, p_3) are orthogonal. Thus, the relationship can be expressed as

$$p_1 \cdot p_2 = \cos\left(\frac{\pi}{2}\right), p_2 \cdot p_3 = \cos\left(\frac{\pi}{2}\right), p_3 \cdot p_1 = \cos\left(\frac{\pi}{2}\right) \text{ which can be rewritten as}$$

$$x_{p1}x_{p2} + y_{p1}y_{p2} + z_{p1}z_{p2} = 0 \quad (2-8)$$

$$x_{p2}x_{p3} + y_{p2}y_{p3} + z_{p2}z_{p3} = 0 \quad (2-9)$$

$$x_{p3}x_{p1} + y_{p3}y_{p1} + z_{p3}z_{p1} = 0 \quad (2-10)$$

By observing the relationship between the middle joint vector and platform joint angle, the cosine law can be applied, that $p_1 \cdot m_1 = \cos \alpha_{11}$, $p_2 \cdot m_2 = \cos \alpha_{21}$, $p_3 \cdot m_3 = \cos \alpha_{31}$ that can be rewritten as:

$$x_{m1}x_{p1} + y_{m1}y_{p1} + z_{m1}z_{p1} = \cos \alpha_{11} \quad (2-11)$$

$$x_{m2}x_{p2} + y_{m2}y_{p2} + z_{m2}z_{p2} = \cos \alpha_{21} \quad (2-12)$$

$$x_{m3}x_{p3} + y_{m3}y_{p3} + z_{m3}z_{p3} = \cos \alpha_{31} \quad (2-13)$$

In addition, the platform joint vectors are unit vectors so that

$\|p_1\| = 1$, $\|p_2\| = 1$, and $\|p_3\| = 1$ This can be rewritten as:

$$x_{p1}^2 + y_{p1}^2 + z_{p1}^2 = 1 \quad (2-14)$$

$$x_{p2}^2 + y_{p2}^2 + z_{p2}^2 = 1 \quad (2-15)$$

$$x_{p3}^2 + y_{p3}^2 + z_{p3}^2 = 1 \quad (2-16)$$

Platform joint vectors p_i can be solved by applying the equations (2-8), (2-9), (2-10), (2-11), (2-12), (2-13), (2-14), (2-15), (2-16). These result in nine equations and nine unknowns (x_{p1} , y_{p1} , z_{p1} , x_{p2} , y_{p2} , z_{p2} , x_{p3} , y_{p3} , z_{p3}). The solutions of these equations represent the direct kinematics problem. A numerical software is used to solve the non-linear equations to obtain eight solution sets.

2.6.4. Collision Determination

The tool-holding mechanism is needed to adjust the posture to reach the goal. When the computer sends a signal to control the mechanism, the goal does not have to be within the reachable workspace. Therefore, the control of the mechanism will be effective to calculate the collision range in advance. Once the goal position of the end effector is defined, a quick check can be applied to verify if the goal is within the collision range. If

it is so, the program can inform the user and reject the goal at the first step itself, which is far more effective since unnecessary calculation is avoided.

The collision of physical limitation of tool-holding mechanism includes: (1) All joints and links above abdominal wall. Under this condition, all the vectors z value must be less than zero. (2) Passive link is not able to fold to other side of active link to avoid singular configuration; therefore, middle joint angle moves between $0-180^\circ$. (3) Platform workspace is a subset of workspace branches 1, 2 and 3.

Based on the condition (1), a Matlab program was developed to calculate the collision ranges for three branches. In this program, the active link from 0° to 360° was calculated so that the corresponding middle joint vectors can be calculated. If the z value of middle joint is greater or equal than 0, the corresponding active link angle is a collision angle. A second calculation of passive link from 0° to 360° based on the collision-free active link angle is applied. The second calculation examines the platform joint vectors of the corresponding angle of passive link. If the z value of platform joint vector is greater or equal to 0, the corresponding passive link angle is within collision range. The collision angles are shown in Figure 2-44, Figure 2-45 and Figure for branch 1, branch 2 and branch 3 respectively. The collision areas (z value greater than 0) are expressed by +. It is clear that shorter branch links ($Link_{12}$ and $Link_{12}$) are able to provide wider collision-free range as compared to other links.

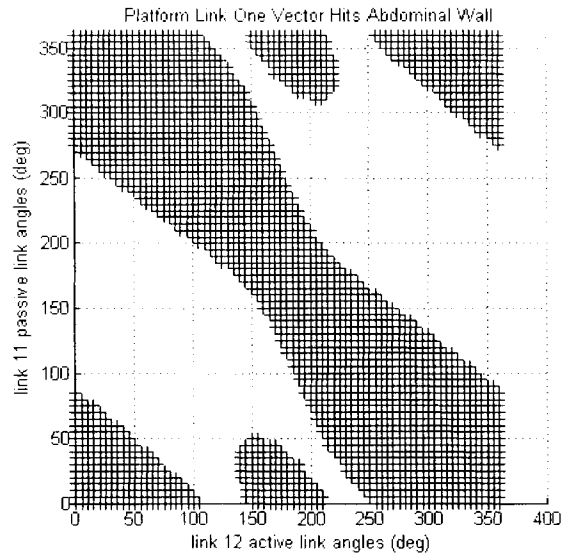


Figure 2-44 Collision range of branch 1

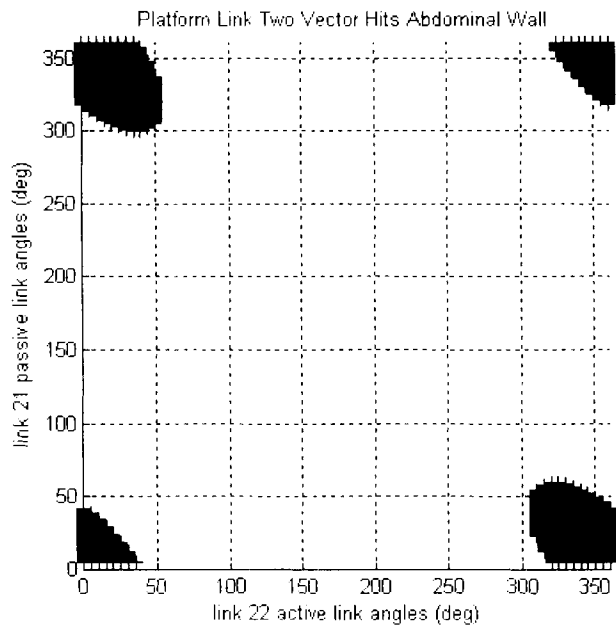


Figure 2-45 Collision range of branch 2

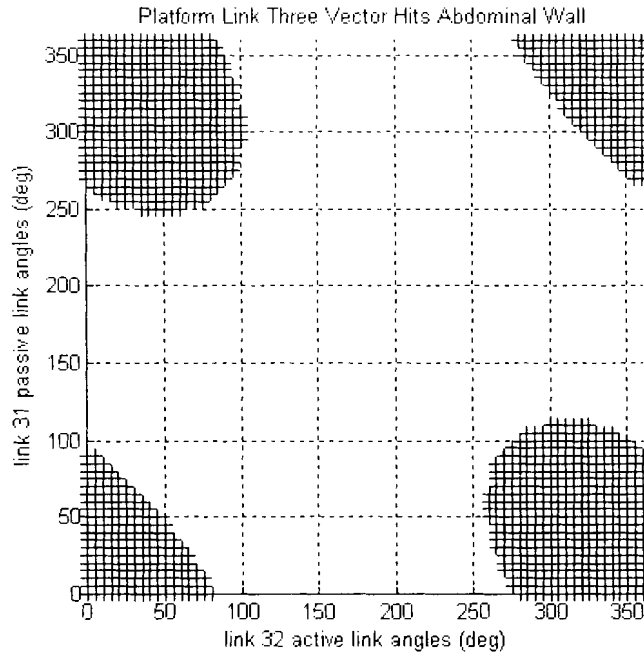


Figure 2-46 Collision range of branch 3

2.6.5. Linear motion Analysis

For linear motion, the only consideration is the distance between tool tip and incision point. At home position, the bottom of platform is 25 mm above incision point and the tool tip is 75 mm below the incision point. The linear motion range is 150 mm; therefore, at the top position, the surgical tool tip is same as the incision point. At bottom point, the tool tip is 125 mm below incision point.

From section 2.6.2, the three rotational DOF orientation can be solved for the platform. The linear motion of surgical tool must be considered in order to achieve the required four DOF. The home position of tool tip is defined at $v_h [0, 0, 1]^T$. The tool tip moves from $v [x, y, z]^T$ to new position $v_n [x_n, y_n, z_n]^T$ which can be of arbitrary length. The linear motion length (L) can be obtained by:

$$L = \sqrt{(x - x_n)^2 + (y - y_n)^2 + (z - z_n)^2}$$

The tool linear motion direction can be calculated by following conditions:

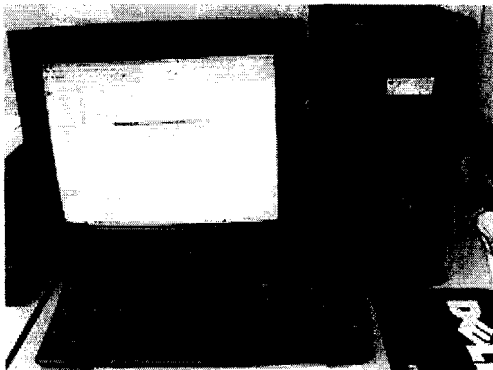
If $z - z_n > 0$, move tool upwards to leave surgical area.

If $z - z_n = 0$, hold the tool without changing position

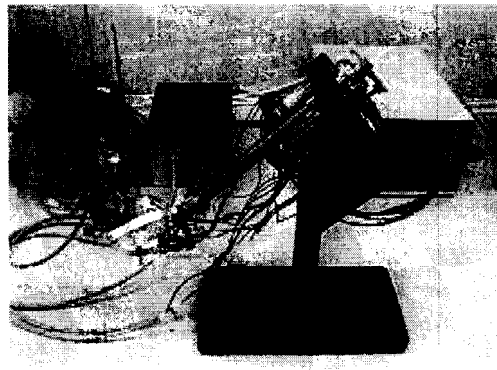
If $z - z_n < 0$, move the tool downward to approach surgical area.

A 13 mm diameter metal-brush DC motor (Maxon 118465) is attached on the linear device to move the surgical tool up and down. That encoder resolution is 16 counts per revolution and the reduction ratio of the gear head is 275:1. The motor drives a lead screw that has a pitch of 1/2 inch per revolution. Based on the condition, the resolution of linear motion can reach 0.0029 mm.

2.7. Integration and Experimental setup



(a) computer site



(b) mechanism site

Figure 2-47 Experimental setup of tool holding mechanism

The experimental setup for position measurement is shown in Figure 2-47. The tool holding and positioning system consists of two PCs with software, a laparoscope, a tool holding mechanism, motor control cards, and servo amplifiers that are combined into the motor control module. The motor control module consists of a PMD MC400 motion control board inside the PC with motor control software, two PMD Breakout 60, one Maxon ADS 50/5 servo amplifier, and three Advanced Motion Controls 12A8 servo amplifiers. This mechanism has been experimented with, and the details of its setup, testing plan, and results are discussed in[72]. The mechanism can be controlled to reach the required position and orientation.

Table 2-7 Test Result with Z=5.2 cm

Z=5.2 cm	Set position (cm)	Actual Position (cm)
Point A	(1, 1, 5.2)	(0.9, 0.5, 5.2)
Point B	(-1.8, 1.8, 5.2)	(-1.3, 0.7, 5.2)
Point C	(-0.5, -1.2, 5.2)	(0., -0.4, 5.2)
Point D	(1.3, -0.5, 5.2)	(1.3, -0.2, 5.2)

The tested result is shown in Table 2-7 and the inaccuracy in position is a problem[72]. It is observed that a few manufactured geometrical dimensions did not meet the requirement of design dimensions. The results show that errors are more than 20%. The sources of error included machining, assembly, deflection, measurement, and control errors. Errors existing in any machined work piece and the actual dimensions will be different from nominal dimensions. These errors should be within the given tolerance limits and determined by the measured dimensions to guarantee accuracy.

An automatic tracking system for laparoscopic surgery was developed and presented[73]. This system controls the laparoscope-holding robot to track a surgical tool and keep it within the view of laparoscope. The image tracking software and the tool-holding mechanism can be integrated for automated tracking. The calibrations can also be expanded.

2.8.Discussion

For laparoscopic tool-holding mechanism, the most important design consideration is the four DOF kinematics motion. Two tool-holding mechanisms are designed and developed to evaluate the design concept of spherical parallel mechanism. This spherical parallel structure has obtained the US patent and a new creative design concept. The mechanism satisfies four DOF motion requirement of laparoscopic surgery.

The nest link design is able to increase the workspace of spherical parallel mechanism and a special feature of gear transmission is applied so that no tendon or wires are used. This feature eliminates the wire-cutting problem. In addition, the link and gear transmission does not have tension or wire-loss problems.

The reachable workspace for Z-axis rotation is limited and rotation is not symmetrical. The motion range reaches 30° CW and 85° CCW. The rotation angle decrease while the rotation angle along X-axis or Y-axis increase that the features can be improved by changing link arc length.

The internal force between links may be enlarged by enlarging the bore on the 4 mm thickness aluminum link. The bore may be worn out due to material properties of

aluminum alloy. Our suggestion is to substitute the material with higher stiffness material such as stainless steel or engineering plastic.

The compact robotic arm size is achieved by concentric acting axis which contains 19 mm diameter external tube. However, it causes difficulties during manufacture, as the 3.175 mm diameter inner rod needs to be connected with the active link. In the assembly process, m2 screws are used to fasten the rod and link. Due to limited space, a 5~8 mm diameter rod is suggested for assembly purpose.

The motor size can be reduced further. In this design, motor selection is not as critical as design condition; therefore, the selection is conservative which means that a powerful motor that can offer high torque by gear reduction (Pittman GM8724S023) was chosen.

Calibration increases the accuracy of manipulator without changing the mechanical structure[74]. For the tool-holding mechanism, the level 1 and level 2 calibrations were examined. For level 1 calibration, the reading from a motor encoder yielded the correct joint displacement was tested to ensure the correct middle joint position. For level 2 calibration, the position and orientation of end effector were examined and the results were corrected. A data-driven method can be used to make correction and calibration of the scope holding mechanism. The data-driven method measures the position and orientation of the end effector with respect to corresponding motor angle. This method does not consider the kinematics of the mechanism.

Singularity is an important consideration to control manipulator motion. Singular configuration will cause the manipulator loses degrees of freedom and comes uncontrollable. This singular configuration can be identified by using the condition number of the Jacobian matrix that studies the instantaneous motion of the end effector. Gosselin [75] analyzed different kinds of singularities encountered in parallel manipulator and described a general classification of these singularities based on the

properties of the Jacobian matrices. It was pointed out that the identification of the singular configurations is particularly relevant for hard automation modules or robotic devices. Angeles [76] discussed a three legs parallel manipulator with both forward and inverse kinematics Jacobian that these relations were applied to the singularity analysis. Goldsmith [77] investigated the kinematics and stiffness of an isotropic three-legged parallel manipulator. Singularities are characterized for the case of concentric u-joints at the tool. These singularities yield the constraint singularities of a related 3-universal-prismatic-universal translational manipulator. Voglewede [78] developed a framework which united the existing measures, provides further understanding for others, and creates new ones. Parenti-Castelli [79] studied a pure translation three DOF parallel manipulator for the optimal geometric design of the manipulator based on static analysis and determination of the singularity loci. This analysis provided a given singularity free workspace. Since our research focuses more on design and manufacturing, this issue, though aware of, can be developed in future. For real time motion control of the tool holding mechanism, the Jacobian matrix of parallel manipulator, the DK and IK singular configuration can be considered.

3. Design of Surgical Haptic Force Feedback Device

Virtual reality (VR) has been applied to surgeries, teleoperation and entertainment field[80]. In surgery, VR can provide a training environment for surgeons to practice their surgical skill. For teleoperation, a robot can be located at remote hazardous area and the user can manipulate the robot from a distance. For aerospace application, NASA uses shuttle training aircrafts to train astronaut pilots to land the space shuttle[81]. Visual, audio and force feedback are the three elements in virtual reality. During recent years, the progress of visual and audio feedback has been developed rapidly. The software development is versatile and rapid. Haptic force feedback hardware generates sensation such as touch, weight, and rigidity. The development of haptic feedback hardware is limited. The design, manufacturing, and evaluation of force feedback hardware are developed in this research. However, there are not many hardware researches focusing on laparoscopic surgical application. Therefore, the research objective is to design and manufacture force feedback hardware device for laparoscopic surgical application.

This chapter is organized as follows: In section 3.1, the advantages and the limitations of VR hardware for laparoscopic surgical application are discussed. The design motivation of haptic electro-mechanical device for endoscopic surgery is also introduced. The review of related design and current research is conducted. The design specifications are defined according to laparoscopic surgical requirement and mechanical properties of haptic devices. Section 3.2 presents the design and manufacture of surgical haptic force feedback devices. These devices are able to provide three rotational and one linear DOF force feedback. Their design features, mechanical structures, advantages, and limitations are presented. In section 3.3, kinematic modeling and notation are presented. Both direct and inverse kinematic problems are analyzed and numerical examples are presented. Neural network (NN) model is applied to solve the kinematics problem. NN is applied

for real time application. The comparison of experimental and simulation results is presented.

3.1. Introduction

The haptic feedback device assists users to feel the contact force between objects and obstacles in VR environment. It has the capability to create "virtual touch." Simulation can be an effective laparoscopic training method for the complete novice, providing significant improvement in skill levels over a relatively short period[82]. Medical training points out that without the sense of touch, training using virtual reality is of limited utility[83, 84]. Lamata [85] investigated the design requirements for endoscopic surgery and proposed using force feedback devices to provide an effective simulator for laparoscopic training. Heng investigated that tactile force feedback can increase accuracy in laparoscopic surgery[86]. Study in telesurgery pointed out that the operation achieved best results with both position and force control[87]. In surgical application, absence of force feedback increases the average force magnitude applied to the tissue by at least 50 % and the peak force magnitude by at least a factor of two[88]. Kazanzides concluded that force feedback provides safety, tactile search capabilities and an improved man machine interface[89].

Since force feedback is able to assist surgical training, the development of electro-mechanical hardware is able to improve the surgical training environment. The objective of this chapter is developing the electrical-mechanical haptic devices that provide force feedback to enhance the surgical realism and teleoperate.

3.1.1. Mechanical Characteristics and Design Objectives

In endoscopic surgery, the tactile sensation is reduced. For example, the surgeon manipulates surgical tool to pull tissue and resistance forces are generated by stretching tissue. Figure 3-1 shows the friction force between trocar and surgical tool stem that reduces user's sensation. For telesurgery, surgeons lose haptic force feedback because the actual surgery is operated by a surgical robot. A haptic device can generate force similar to surgical procedure and enhance tactile force feedback.

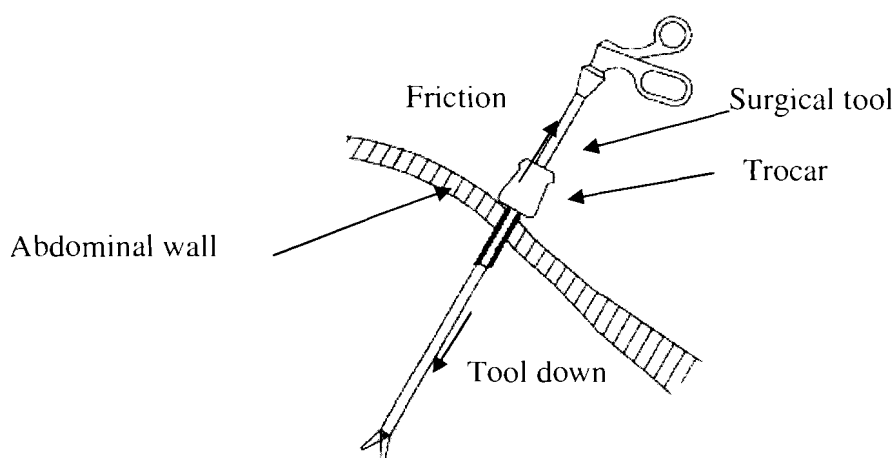


Figure 3-1 Friction of surgical tool

Mechanical properties of haptic devices must be identified for design objectives. Non-force feedback and force feedback are two basic conditions. In non-force feedback, the motor does not exert any power as that the user can manipulate the device without touching the object. In force feedback condition, the motor exerts power to allow the user feel the resistance force. Under the non-force feedback condition, the surgical tool in VR environment can be moved in the space without touching any obstacle. Burdea [80] described non-force feedback as "transparent" with the motor having to respond rapidly without exerting torque. Under force feedback condition, the user feels the resistance forces generated by motor. Research conducted in [11] mechanical characteristics of haptics provided the following conclusions: 1) free space must feel free, 2) solid virtual

objects must feel stiff. The first condition, “Free space must feel free” when translated into design criteria yields 1) low inertia, 2) no unbalance in weight, 3) low friction 4) back drivability. Second condition, “Solid virtual objects must feel stiff” can be a reference that virtual surface with stiffness of at least 20 N/cm or a resistance force of at least 11 N is perceived as solid and immovable by users[90]. The human finger can sense absolute and relative force vibrations of 0.5 N and +/- 7%[91].

Based on the research analysis about the characteristic of haptic device, the objective is to design a four DOF electro mechanical haptic device to provide force feedback for laparoscopic application. The main design requirements for the haptic device are:

- To be low in inertia,
- To have low friction,
- To be compact and lightweight,
- To be back drivable[80],
- To have two angular DOF and the motion range of +/- 70° from vertical axis[8],
- To have one rotational DOF and the motion range of +/- 180° from central position, and
- To have one translational DOF and the motion range at least 15 cm stroke.

3.1.2. Previous Research

Faraz [8] designed the laparoscopic extender which was able to achieve spherical workspace for the kinematic requirement of laparoscopic surgery. Merlet [92] developed a micro parallel robot to offer two rotations and a translation force feedback. Birglen [48] developed a spherical geometry based haptic device with parallel mechanism. Yoon [93] designed a six DOF haptic device by using a parallel mechanism which is composed of

three pantograph mechanisms. Lee [94] proposed six DOF parallel haptic mechanism light in weight and with large workspace. Tsumaki [95] developed a six DOF hybrid parallel mechanism haptic interface with a relatively large workspace, quick motion and compactness. Cauche [49] developed a three DOF rotational force feedback wrist in which the kinematic chain is serial and composed by a Cardan joint corresponding to the pitch and the yaw, followed by a rotational joint for the roll.

Phantom haptic device[11], developed by SensAble Technology, contains six DOF motion and three DOF force feedback. The kinematics of Phantom is similar to PUMA robot. Phantom is driven by DC motor through pulley and cables. The Impulse, developed by Immersion, contains five DOF tracking and three DOF force feedback which is designed for endoscopic surgical procedure simulations. The Impulse applies also pulley/tendon driven mechanism to provide force feedback.

These haptic devices have drawbacks or limitations that are not feasible for laparoscopic surgical purpose. For example, Phantom is not able to provide force feedback for the rotation along surgical tool stem. Immersion haptic device utilizes the tendon driven system that has loosening or slippage problems. The drawbacks of existing haptic devices motivate us to design a novel kinematic four DOF haptic device to be used in laparoscopic surgical training or telesurgery manipulation.

3.2. Mechanical Design

In this section, a number of new haptic devices are designed. In general, gimbal type and spherical parallel type are applied for the four DOF design requirement. For gimbal type haptic device, a two rotational haptic DOF platform with additional one rotational and one linear haptic DOF force. The spherical parallel type implies a three haptic DOF

platform with one linear DOF. In order to achieve the low inertia for haptics, the mass must be low and the center of mass must be close to the pivot center which is important design consideration.

The motor/actuator of haptic device is needed to provide the sensation of resistance force. Without the motor, the device cannot provide force feedback. The device can be used simply as an input device to control surgical robot, at the same time user does not feel any force feedback. Industrial robot could not satisfy haptic force feedback teleoperation because of poor back drivability[96]. The characteristics of the motor affect the user's sensation. The characteristics to select motor should be torque-to-weight ratio, bandwidth, controllability, performance, and cost.

3.2.1. Square Frame Gimbal Type (SFGT)

The design concept of square frame gimbal type (SFGT) is based on gimbal type structure; the CAD model is shown in Figure 3-2. Gimbal type consists of two rings mounted on axes at right angles to each other so that it remains suspended in a certain plane between them. Kinematic movement of SFGT satisfies the DOF for laparoscopic surgery. The pivot center can be the incision point in virtual surgical environment.

The mobility equation (Equation 2-1) can predict the mobility of platform as

$$F = \lambda(l - j - 1) + \sum_{i=1}^j f_i = 3(3-2-1)+1+1=2$$

Where λ is the number of degrees of freedom in space for a mechanism ($\lambda=3$ for spherical motion). l is the number of links in mechanism. j is the number of joints in a mechanism. f_i is the number of degrees of relative motion permitted by joint i .

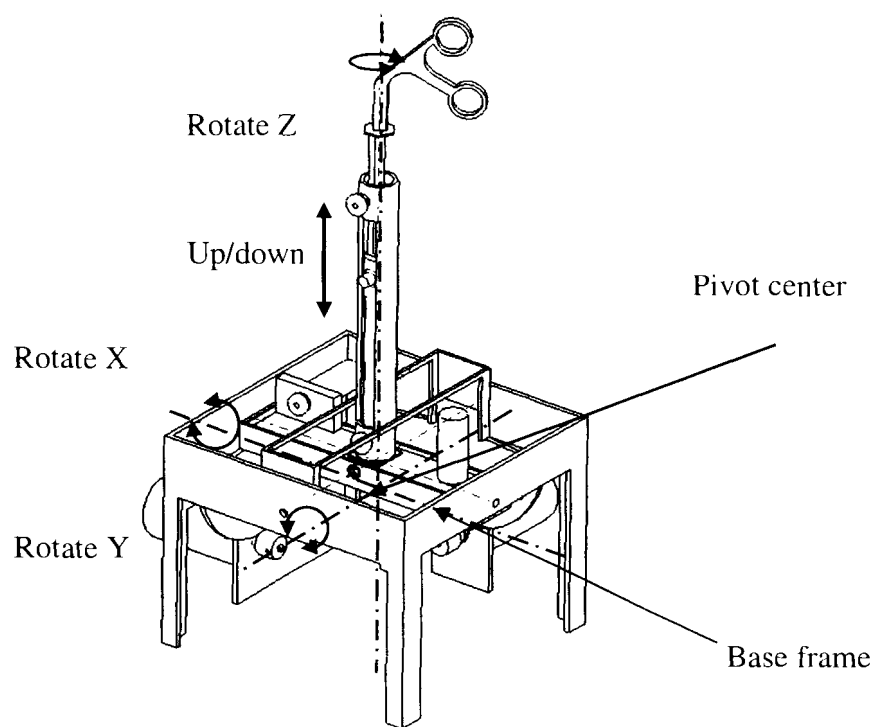


Figure 3-2 CAD model of SFGT

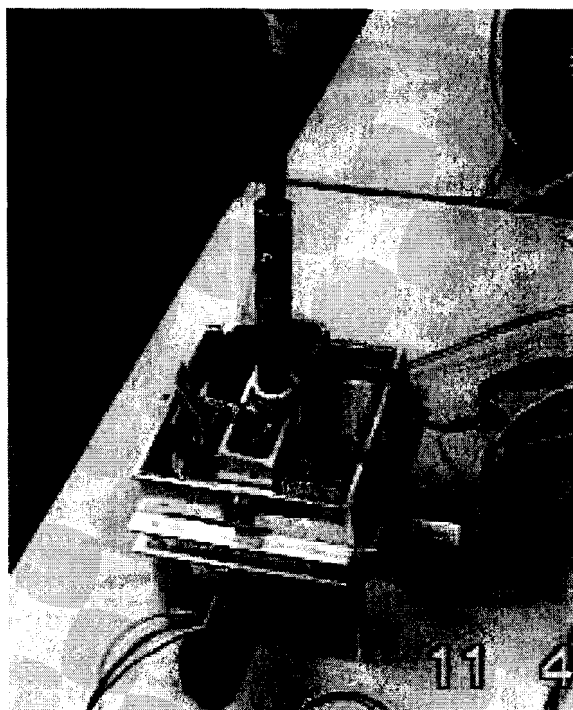


Figure 3-3 Prototype of SFGT

The prototype electrical mechanical haptic device is shown in Figure 3-3. The 15 cm × 15 cm square base frame is manufactured from aluminum alloy (6061-T6) with two stationary motors. The motor axes are perpendicular to each other to provide two-DOF force feedback for X and Y-axis. Figure 3-4 shows the primary bracket mounted on the base frame via ball bearing to rotate along X-axis. The primary bracket also contains two ball bearings to support the platform in order to rotate around Y-axis direction. A secondary bracket constrains the platform to rotate around Y-axis direction. This platform is able to rotate to a maximum of 35° for X-axis and 50° for Y-axis from center position. The limited workspace is caused by the interference between the movable motor and secondary bracket. However, while designing the platform, the main goal is to reduce inertia. Therefore, two movable motors are positioned close to the pivot center to reduce the inertia.

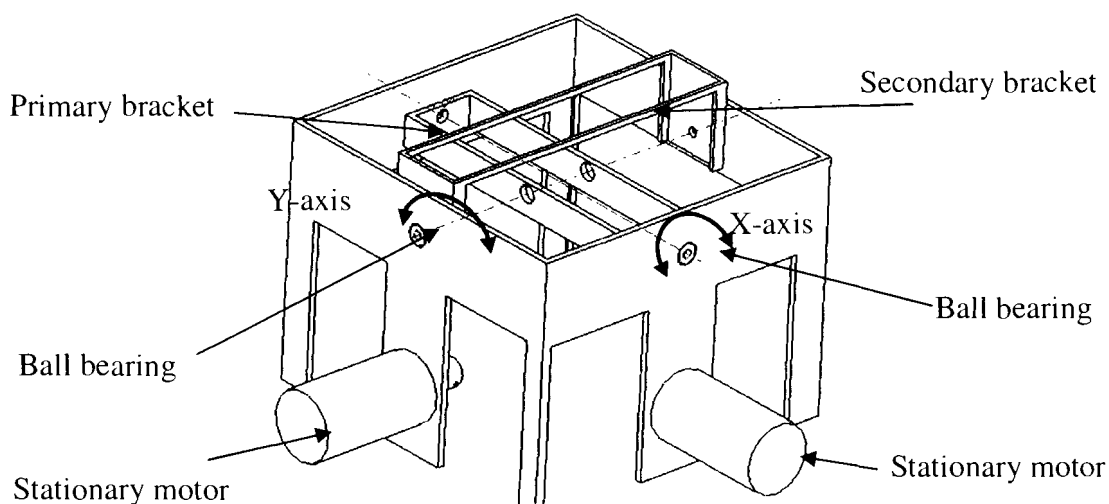


Figure 3-4 Base frame with brackets

Figure 3-5 shows the platform is mounted on the primary bracket by two ball bearings to achieve two rotational DOF. The torque is transmitted from motor to the cam by wire and the primary bracket is pivoted with the cam. Finally, the platform rotates along X axis with primary bracket. The secondary bracket constrains the platform to pivot along

Y-axis. Two small motors, installed on the platform, provide one translational and one rotational force feedback for the end effector (handle).

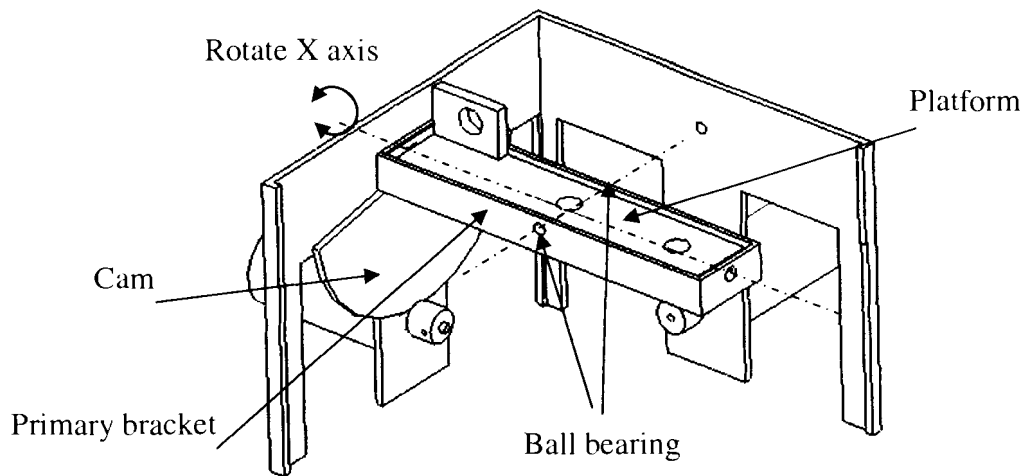


Figure 3-5 Primary bracket and platform of square frame gimbal type

Features of the mechanical design:

Ball bearing: Low inertia and less friction are important features of haptic devices.

Therefore, ball bearings are installed on the base frame and primary bracket to reduce the friction. The main function of the ball bearing is to lower friction (friction coefficient $1\sim 1.5\times 10^{-3}$). Under normal operating condition, bearings have small starting friction coefficient, which is important because the motion of haptic device is slow. The friction

moment for bearings can be expressed by $M = \frac{\mu \cdot P \cdot d}{2}$.

Where M: Friction moment (N-mm), μ : friction coefficient, P: load (N), d: bearing bore diameter (mm).

A 21 N load includes the weight of platform (650 grams) and 15 N applied force. The bore diameter of bearing is 4 mm. The friction moment can be obtained by

$$M = \frac{1.5 \times 10^{-3} \times 21 \times 4}{2} = 0.063 \text{ (N-mm)}$$

The friction moment is very little (0.063N-mm) as compared to the applied force and moment. Therefore, the low friction coefficient of ball bearing design benefits the low inertia for haptic device.

Pulley wire transmission: Pulley type utilizes wires to transmit motion and force from one shaft axis to an offset axis. Pulley wire has the advantages of having a flexible distance between the input and output directions, being lightweight and miniature sized. Limitation includes that wires must maintain minimal tension force to avoid slippage. This tension force increases friction which affects the force feedback. In the SFGT, pulley wire design is applied for 1) rotation of Z-axis, 2) linear motion of Z-axis, 3) between the stationary motor and cam of the X, Y-axis. As shown in Figure 3-6, motor1 rotates the inner tube by the pulley wire. The inner tube is mounted on the platform via a ball bearing so that it rotates to turn end effector (handle) along Z-axis by a key way. For the linear motion of Z-axis, the wire transmits force from motor2 to move the connecting holder and handle up and down. While the connecting holder moves the handle up and down, the handle is able to rotate inside via a ball bearing which is show in Figure 3-13 (b).

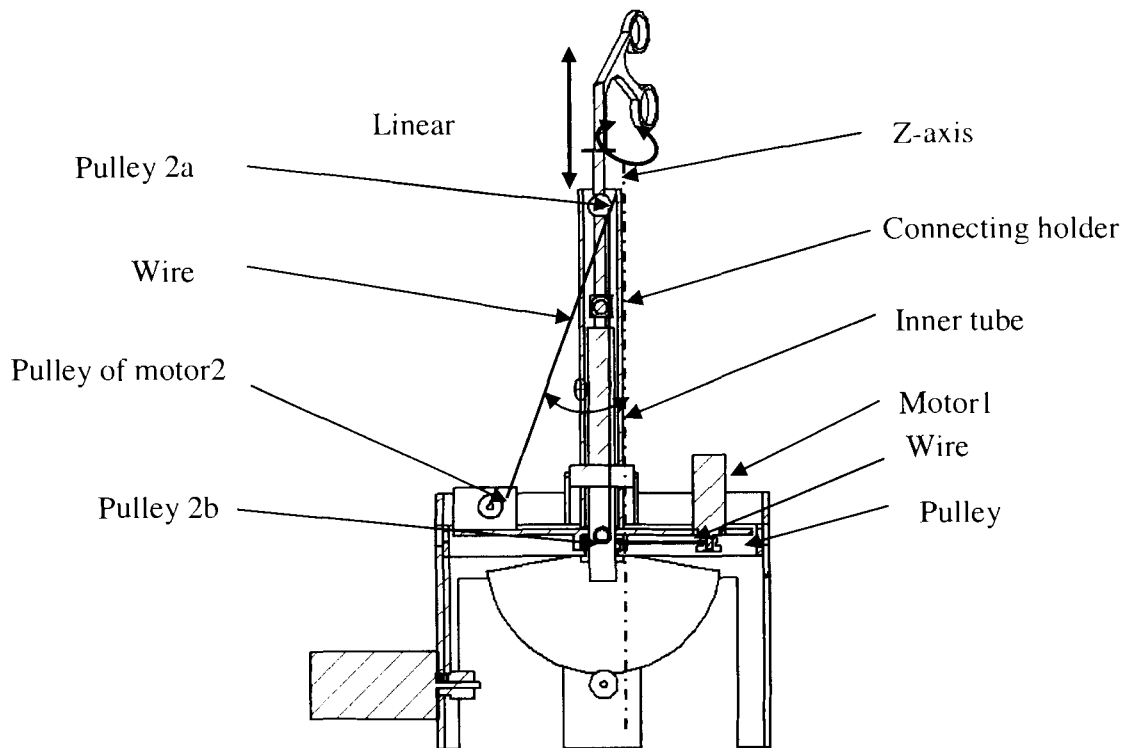


Figure 3-6 The section view of square frame gimbal type

Advantages of SFGT include 1) small (15 × 15 cm) base frame, 2) light weight (low inertia), 3) high power/torque ratio, 4) static balanced platform with two motors. The center of mass of the platform is (-1.9, 14.5, 29.9) mm from pivot center which is close and well balanced.

The limitations of SFGT include 1) friction force of linear motion, 2) limited X Y axes rotational range. Friction force of linear motion is caused by the friction between pulley and wire. The linear motion was smooth with low friction before installing the wire. However, the friction for linear motion increased after installing the wire. The challenge is that tension force (T) must be maintained to avoid slippage but this tension will increase the friction. The tension force also generates a normal force $T\sin(\theta)$ (in Figure 3-6) between handle stem and inner tube. The coefficient of dry friction between aluminum (inner tube) and mild steel (handle stem) is 0.47[97]. For example, a 10 N

linear motion force creates $2.35 (10 \times \sin 30^\circ \times 0.47)$ N friction force. The friction force is greater than 23% which can be improved by next design.

3.2.2. Ring Frame Gimbal Type (RFGT)

Shown in Figure 3-7 and Figure 3-8, the ring frame gimbal type (RFGT) haptic device utilizes similar gimbal kinematic structure as SFGT. RFGT also contains two stationary motors and two movable motors. The brackets are attached to a 300 mm diameter aluminum ring in order to increase the workspace. The maximal rotation angles of X and Y-axis are $\pm 80^\circ$ from neutral position. The neutral position is that in which the tool stem lies on Z-axis (vertical axis). Rotational angle of Z-axis can reach $\pm 180^\circ$ with linear motion range within 150 mm.

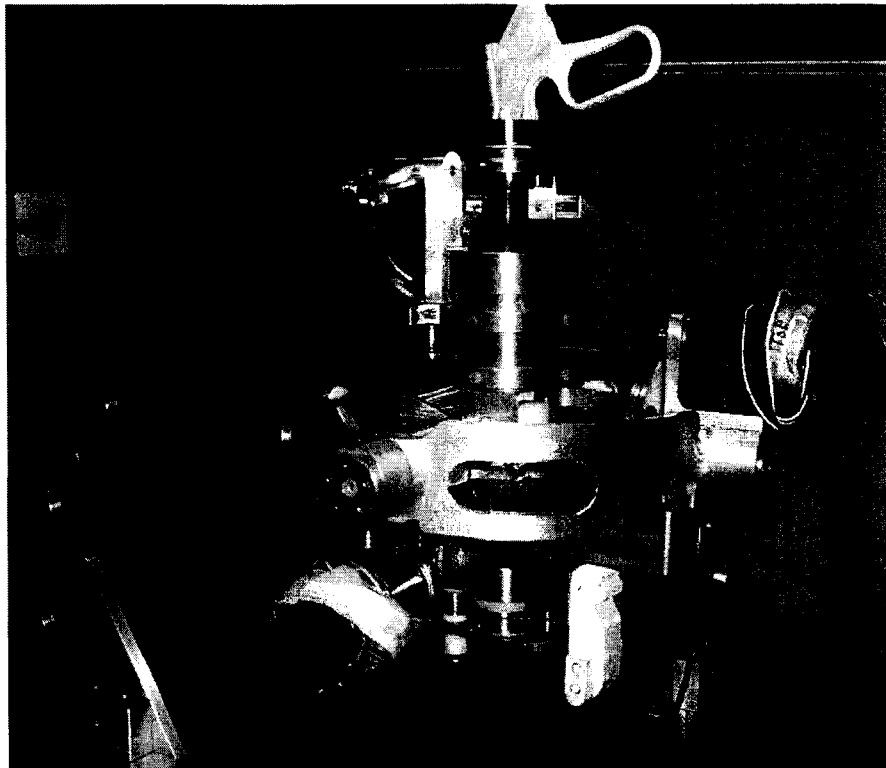


Figure 3-7 Prototype of RFGT (Photo I)

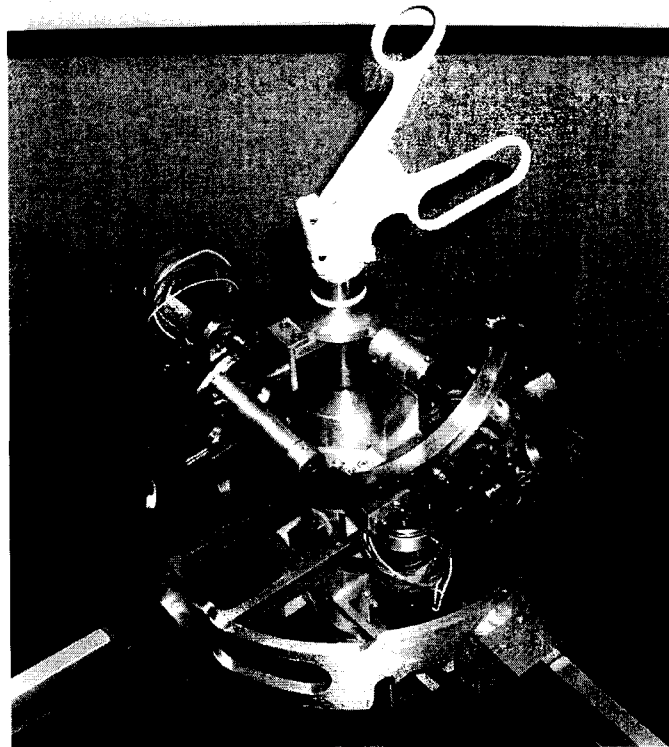
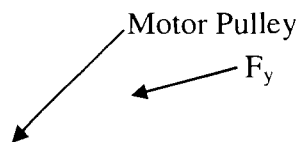


Figure 3-8 Prototype of RFGT (Photo II)

Shown in Figure 3-9, the stationary motor (Maxon EC118891) of X-axis has the radius ratio (ratio of motor pulley and cam) of 12.5:50 (1: 4). The stall torque of motor is 480 mNm. With this ratio, the motor provides 1920 mNm torque to the primary bracket. The force (F_y) along Y-axis yields to

$$f_y = \frac{\text{torque}}{\text{length}} = \frac{1920(\text{mNm})}{l(\text{mm})},$$

l being the distance between handle to the pivot center (mm).



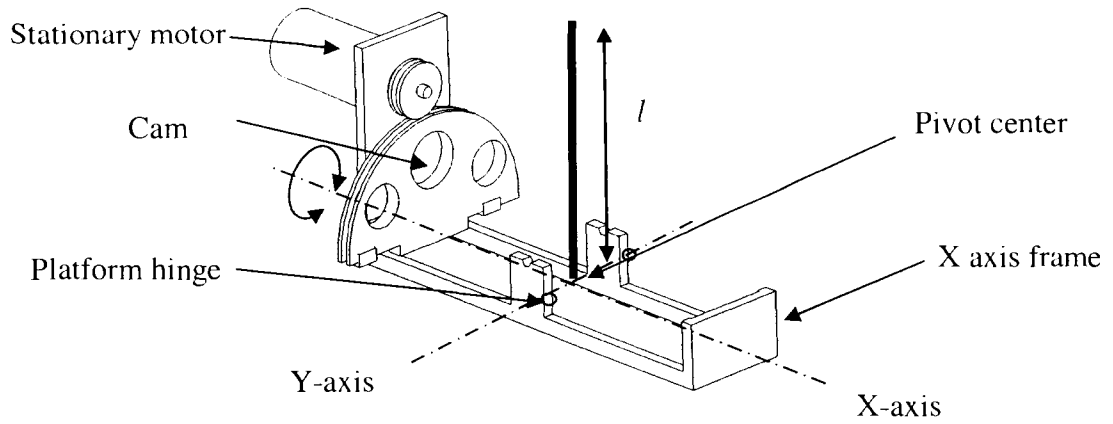


Figure 3-9 Lower frame assembly of RFGT

Shown in Figure 3-10, the platform provides one rotational and one linear force feedback. Maxon motors (EC118752) are installed on both sides of the bracket to counterbalance static weight. The rotation motor is mounted on the lower left side and turns the pulley to provide force feedback for Z-axis rotation. The motor for linear motion is mounted on the opposite side and is connected to the cam by a cable. Using the cam design takes advantage of gear ratio and scales the force/ torque to 12:1. The bracket can provide two-DOF for the handle; therefore, a customized bearing is designed.

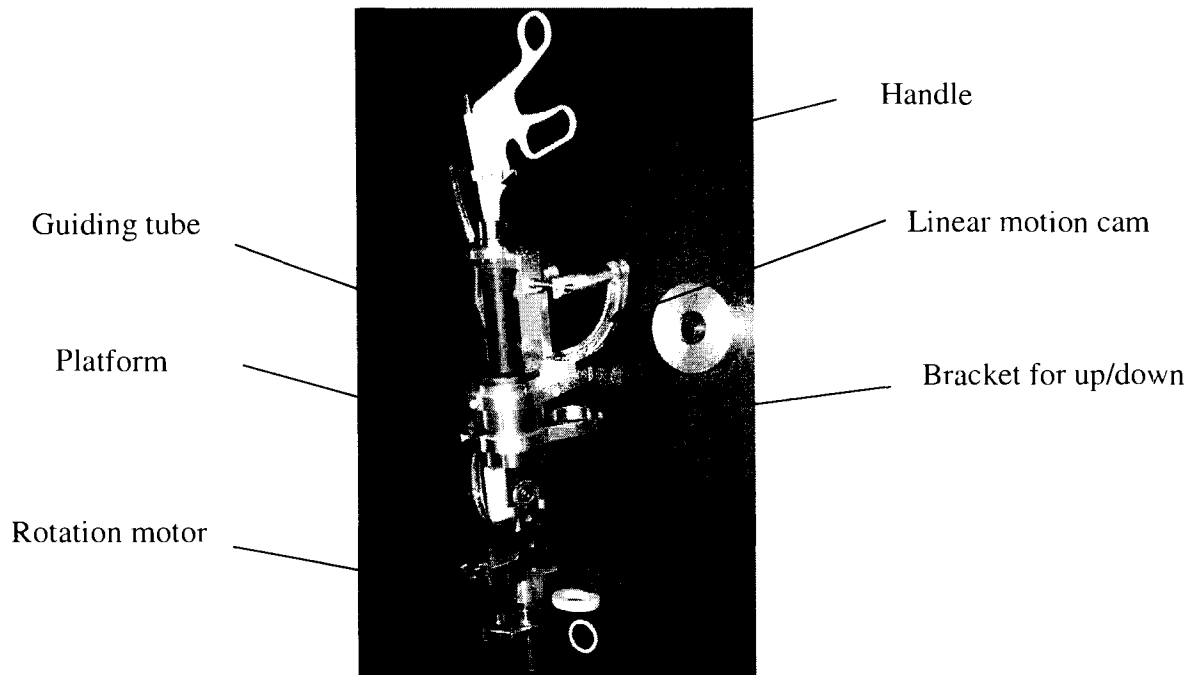


Figure 3-10 Two-DOF platform with handle of RFGT

A crank slider mechanism has a four bar linkage with three revolute joints and one prismatic joint. It converts rotary motion into reciprocating linear motion, or vice versa. While designing the linear motion stroke, the longer the crank the further the slider will move. As shown in Figure 3-11 (a), the motor rotates link 1 in (crank) while the slider reciprocates. The end effector (handle) can be attached to slider to move up and down. As shown in Figure 3-11 (b), the cam replaces link1 in order to magnify torque. The magnification ratio is based on the radius of cam and motor pulley. The advantages of crank slider include 1) less friction than wire pulley type, 2) small backlash, 3) magnification of the torque in the small motor.

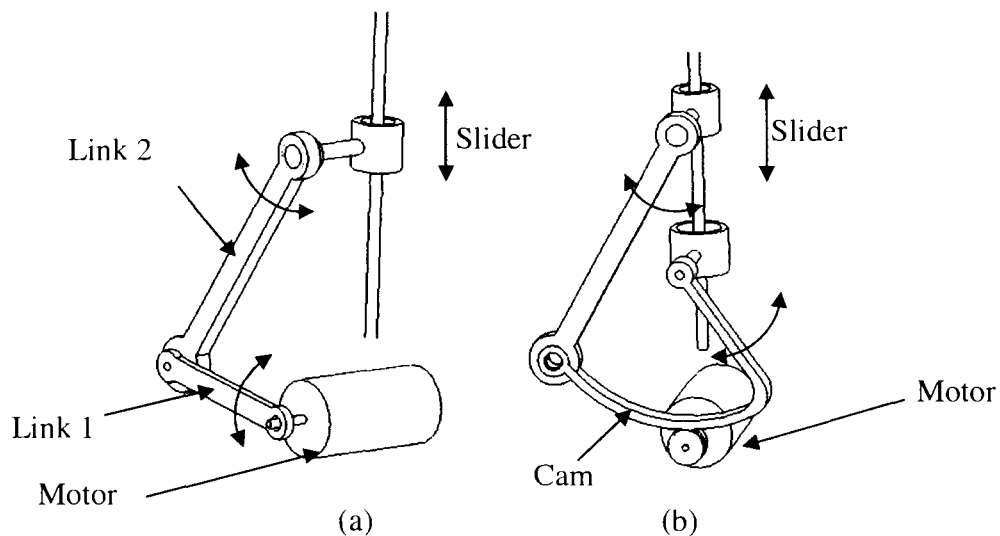


Figure 3-11 Crank slider type (a) and (b)

Limitation of the crank slider includes: 1) could be bulky; the stroke length is based on link length, 2) the crank slider linkage may interfere with other components, 3) force component along the sliding axis is dependant on the slider position. Shown in Figure 3-12, the motor torque is (M) and the radius of cam is (r). The out put force (f) of cam can be expressed as $f = \frac{M}{r}$ which is the linear force that the user can feel. The

magnitudes of the component force (f_y) can be expressed as $f_y = f \sin(\theta)$. Then, the linear force can be obtained as $f_y = \frac{M}{r} \sin(\theta)$. Also, $f_x = f \cos(\theta)$ is the normal force applied to linear axis that will increase friction.

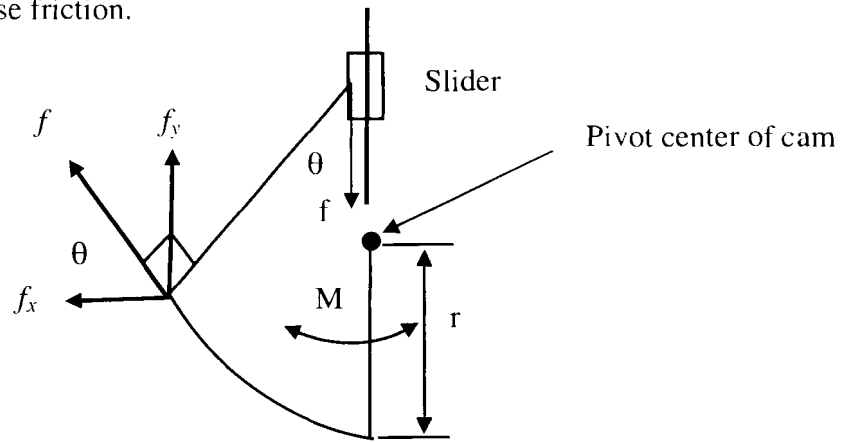


Figure 3-12 Force component of crank slider

Shown in Figure 3-13 (a), the prototype of crank slider utilizes the cam to move the handle up and down. In this design, the motor axis is parallel to linear motion and the torque is transmitted by the wire between the motor and the cam. When the cam rotates, the slide holder moves the handle up and down. A deep groove ball bearing is installed between the handle and slide holder to provide one rotation DOF because ball bearing accepts radial load and thrust load in either direction, or a combination of loads. Figure 3-13 (b) shows that the handle stem is able to rotate inside the slide holder while moving up and down.

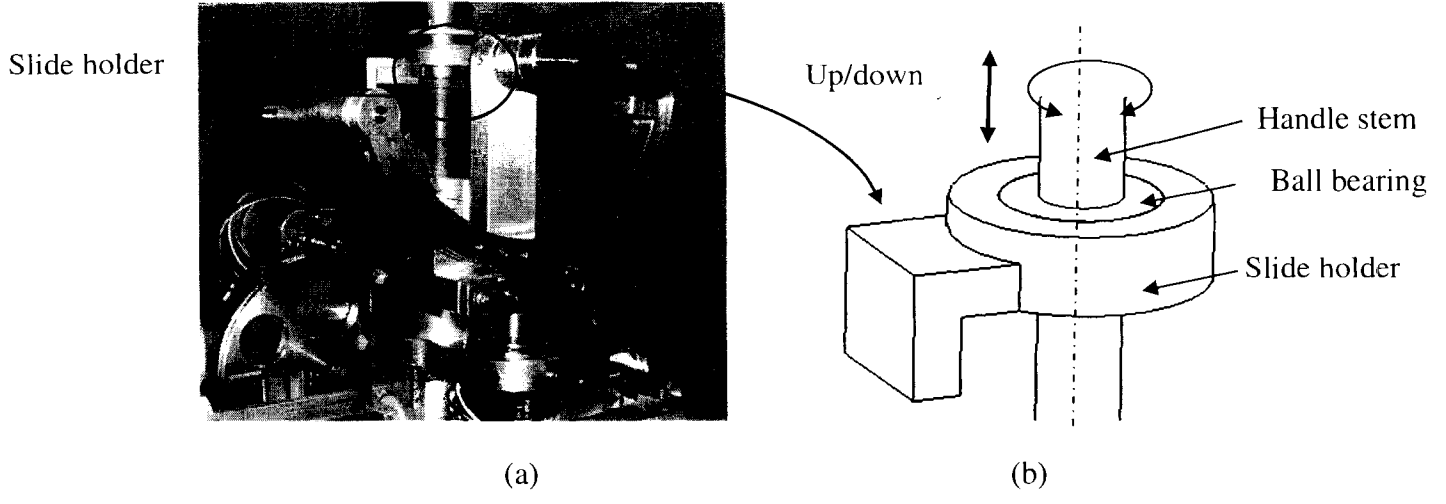


Figure 3-13 Prototype of crank slider type and close view of slider

To provide the rotational DOF along tool axis (Z-axis), the Maxon motor (EC118752) is installed on the bottom. Shown in Figure 3-14, the motor offers force feedback through the pulley wire design. In addition, a counterbalance weight block is installed to provide static balance of the bracket.

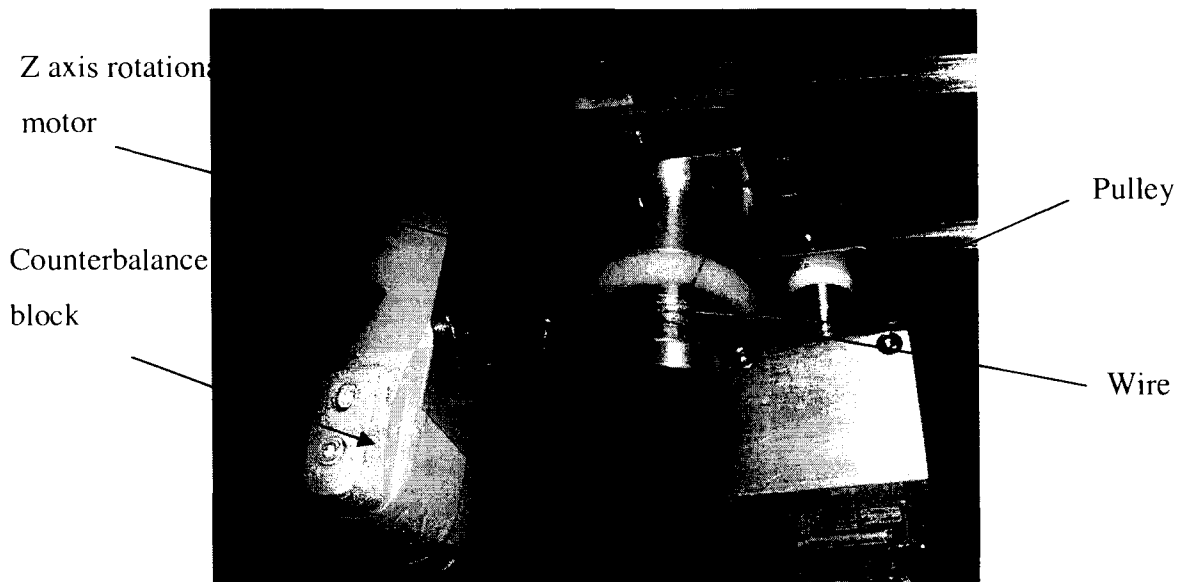


Figure 3-14 Motor and pulley system for Z-axis

Advantages of RFGT include larger workspace and static balance. RFGT is able to reach the design workspace that rotational DOF along X and Y-axis achieves +/- 80° from vertical axis. The Z-axis rotation is able to reach +/- 180 from neutral position. The linear motion is 220 mm which is longer than the design goal. The platform with crank slider is balanced and the center of mass is (12, 18, 22) mm from the pivot center.

Features that can be improved are the 1.5 kg platform (with linear mechanism and the motor), which is much heavier than 0.60 kg of SFGT. The platform, with crank-slider-cam design, contains more than 30 parts to provide two-DOF force feedback. Both SFGT and RFGT contain two movable motors on the platform to provide one linear and one rotational DOF force feedback. These motors increase overall movable weight and the complexity in design for rotation and linear motion. Therefore, a different approach of decoupling two-DOF platform into one rotation DOF and one linear DOF reduces the number of parts and keeps the kinematic design simple. The different kinematic structure is proposed that is based on a spherical parallel mechanism that is able to relocate one movable motor to be stationary in order to reduce over all movable weight.

3.2.3. Hybrid Parallel Support Type (HPST)

Shown in Figure 3-15, the CAD model of hybrid parallel support type (HPST) contains a three rotational DOF platform with one DOF linear mechanism. The platform connected to a base is a parallel mechanism and the linear motion is a serial mechanism so that the device is a hybrid parallel-serial type. Comparing with SFGT and RFGT, this mechanism has two benefits of lower inertia and simpler platform structure. The lower inertia is achieved by reducing movable weight that only one movable motor is on the platform for linear motion. Simpler platform design is achieved by one DOF linear mechanism. The platform of SFGT or RFGT provides two-DOF to the handle so that the design contains more mechanical parts than the platform with only linear motion.

Figure 3-16 shows the rendering image of side and top view and Figure 3-17 shows the photograph of HPST prototype. HPST contains a moving platform connected to the base by three identical branches and a passive supporting mechanism. A linear motion mechanism is attached to the platform to provide four DOF force feedback.

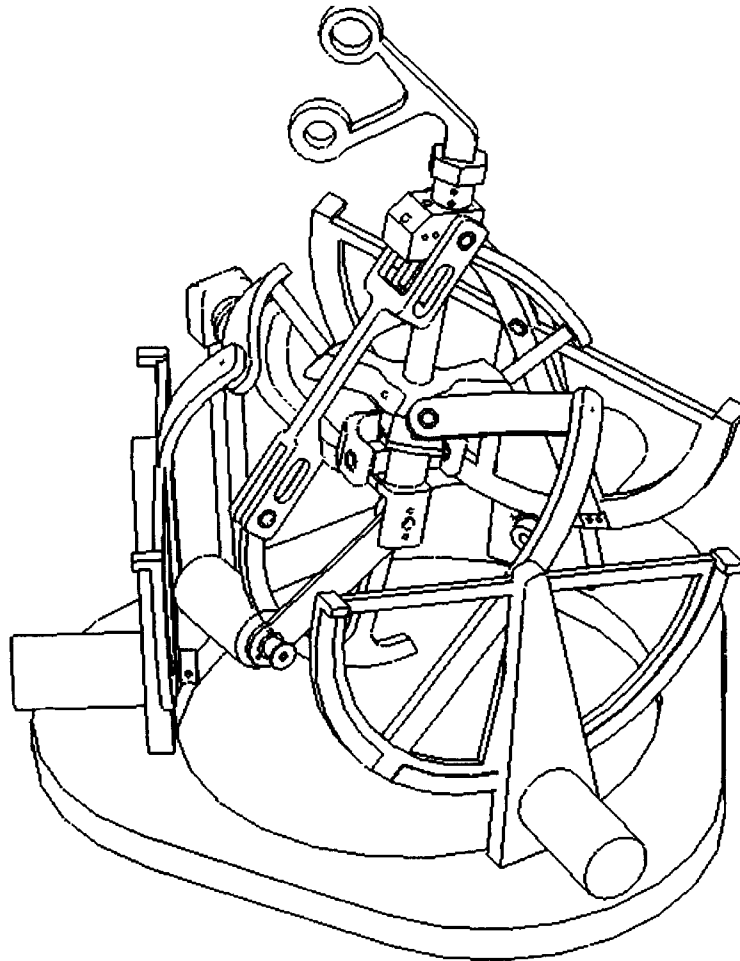


Figure 3-15 CAD model of HPST

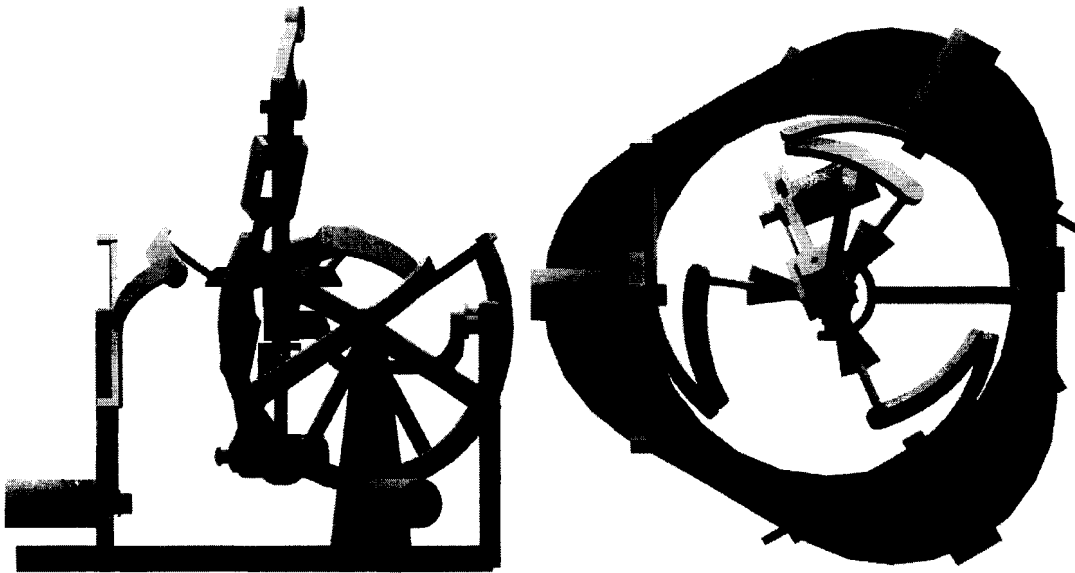


Figure 3-16 Rendering image from side and top view

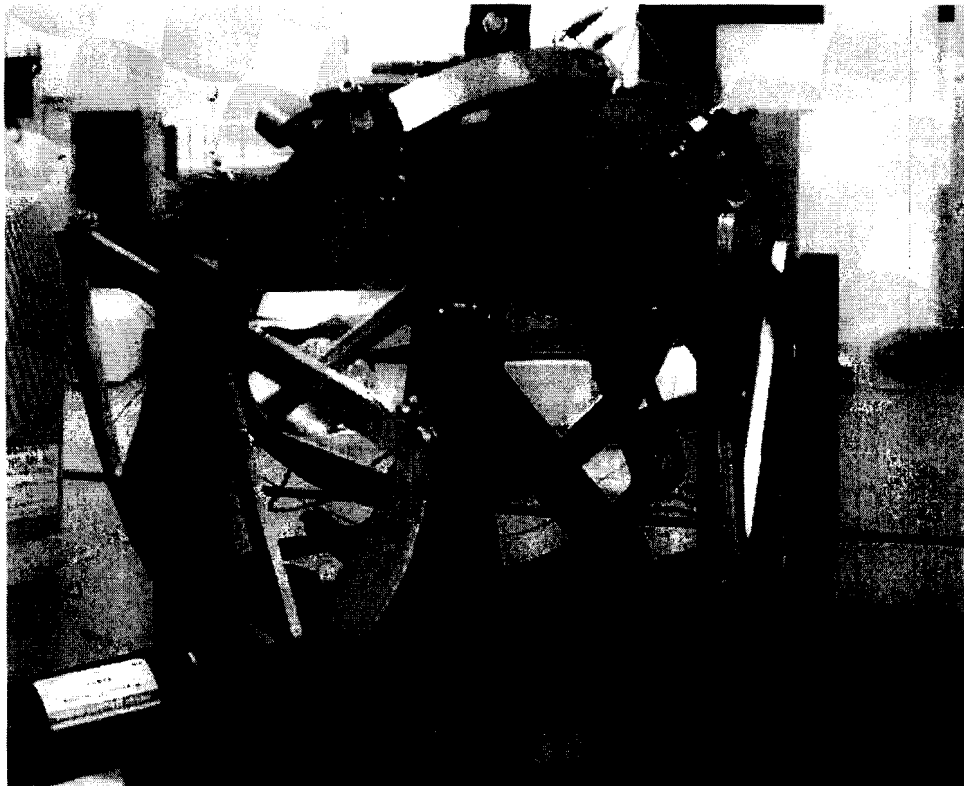


Figure 3-17 Photograph of HPST prototype

Features of the mechanical design:

As shown in Figure 3-18, each branch contains an active cam, an active link and a passive link. The active cam is mounted on the motor bracket by bearing to pivot and actuate the active link. This link lays on a groove of the cam. The active and passive links are connected by a ball joint. The passive link and the platform are connected by a revolute joint. In addition, the platform is supported by three DOF passive support to ensure spherical motion.

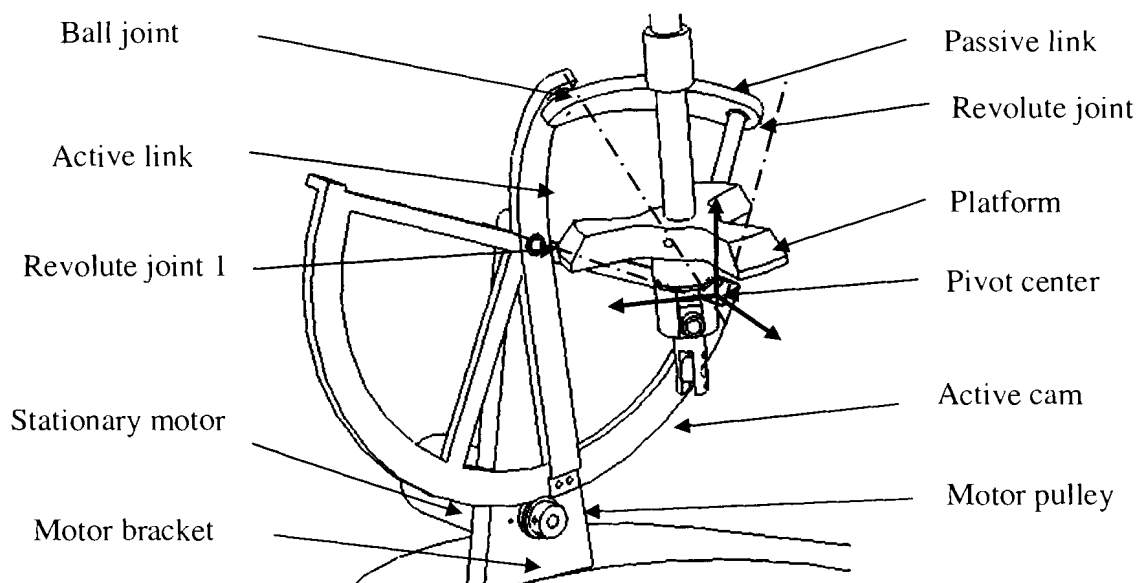


Figure 3-18 Design of one branch of HPST

Linear motion mechanism: Shown in Figure 3-19 is the linear motion applied crank slider mechanism to move the end effector (handle) up and down. The linear link is a yoke type link that is connected to both sides of the holder. This design maintains the balanced

force transition without generating bending moment on the linear guide. A 12.7 mm diameter aluminum shaft with ceramic-coated finish was installed on the platform as the linear guide which is able to reduce linear friction. The 160 mm radius cam is able to provide 150 mm linear stroke. There is a radius ratio (12:1) between cam and motor pulley so that the stall torque of motor is 243 mNm which can be magnified to 2.9 Nm. The center of mass of the platform with linear mechanism is (28.75, -5.27, -0.49) mm from origin point and the mass is 490 grams.

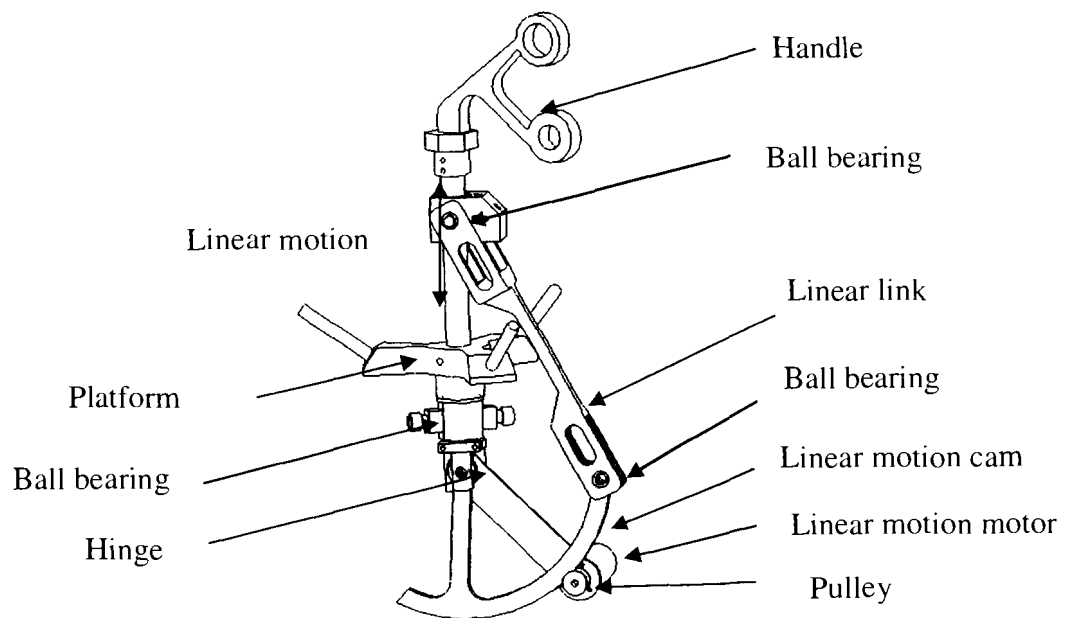


Figure 3-19 Linear motion design

Passive supporting mechanism: Shown in Figure 3-20, a three DOF passive mechanism is fixed on the base to support the load. The mechanism supports the weight of platform, linear linkage, motor and applied force which benefits the load of the stationary motor. If the load is not supported, weight and forces are transmitted to the links that will add extra load to the motor. Two sleeve bearings are used for X and Z-axis supports. Two deep groove ball bearings are installed at both ends of the yoke to reduce friction forces of Y-axis. Two different types of bearings are chosen. Ball bearing takes heavier load than sleeve bearing while sleeve bearings are used for their small size. This supporting

mechanism reduces the workspace of the platform because the linear cam/rod may cause interference with supporting mechanism.

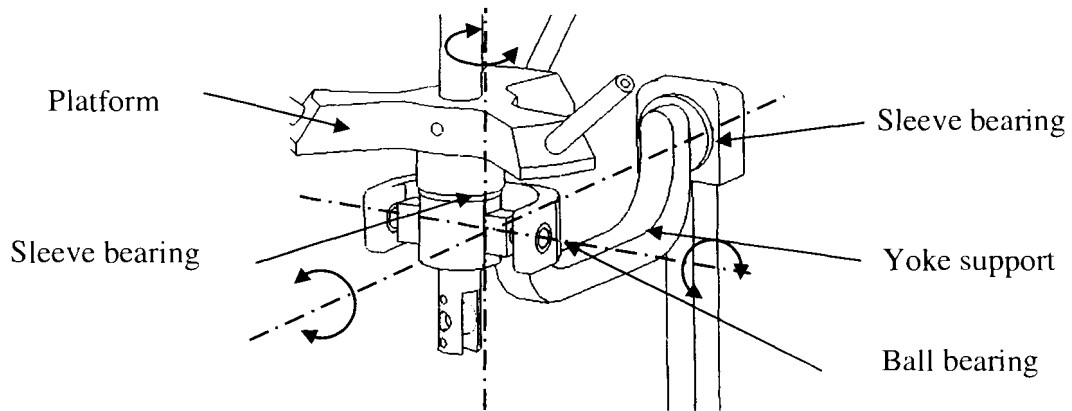


Figure 3-20 Three rotational DOF yoke type passive supporting mechanism

Figure 3-21 shows three stationary motors located on symmetrical and co-planar axes so that the motor axes intersect at the center point. This symmetrical layout ensures the maximal workspace of the three rotational DOF. In addition, the kinematic motion and force distribution is even. If the structure is not symmetrical, the unbalanced weight increases the inertia which defeats the haptic purpose.

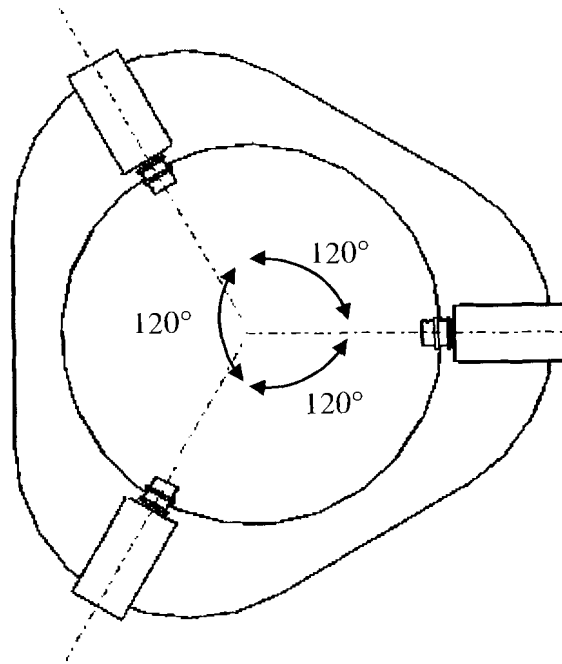


Figure 3-21 Symmetrical motor alignment

Gear ratio cam: Gear reduction between motor and active cam is 1:16. The motor stall torque is 480 mNm. Ceramic-coated aluminum shaft with linear bushing: A ½” aluminum shaft with ceramic-coated finish was installed on the platform to guide linear motion and reduce linear friction. Guiding groove of cam: The wire sets on the thin edge of cam. Any slippage or misalignment may cause loss of wire. A 2 × 2 mm guiding groove keeps the wire to retain accurate position.

Low inertia is an advantage of HPST that is achieved by 1) reducing platform weight from 1.5 kg of RFGT to 0.49 kg, 2) using passive supporting mechanism, 3) maintaining center of mass close to the pivot point. Static balance is achieved by symmetrical branches and platform.

Limitations that can be improved include interference between linear cam, spherical linkages, and yoke support limits workspace. Especially, Z-axis motion is limited within

$\pm 35^\circ$ which is lower than designated range of $\pm 180^\circ$. The passive support can be improved from several perspectives: 1) by relocation of position to reduce interference, 2) by reduction of part numbers.

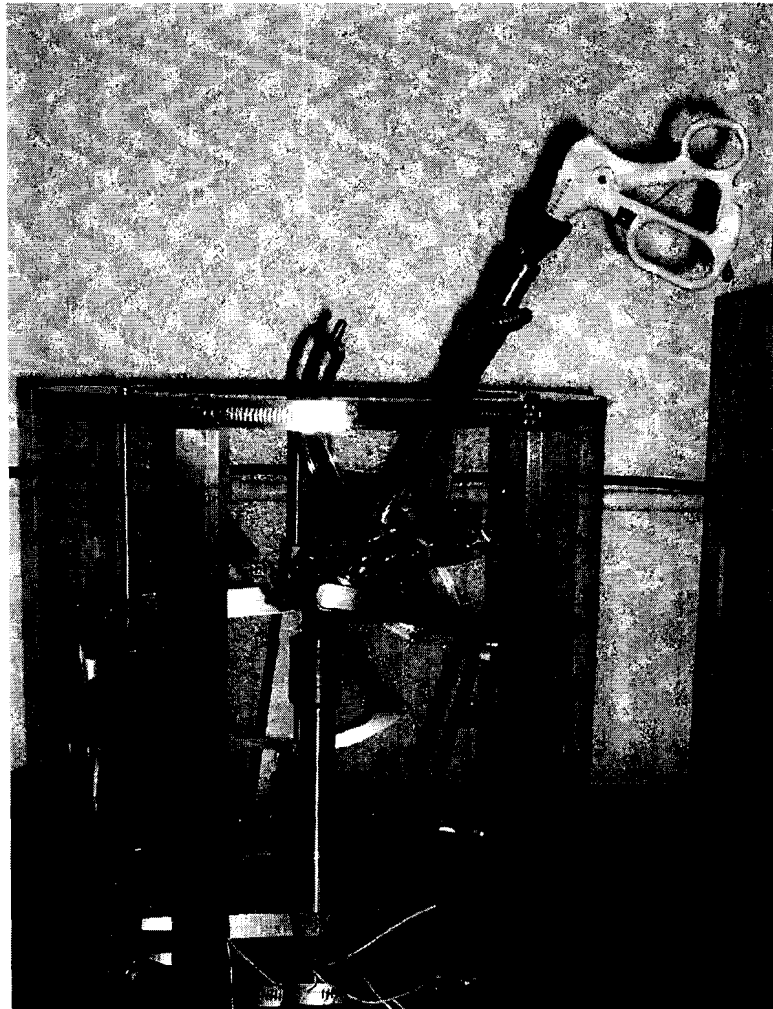


Figure 3-22 Prototype of HPSTA

The kinematics structure of HPSTA is a spherical parallel mechanism. Shown in Figure 3-22, HPSTA contains a spherical supporting joint fixed on the base frame center. The linear motion mechanism was relocated above the platform to avoid interference with the support. For HPSTA, the linear motion cam above the platform would increase the

height to make it 250 mm taller than HPST. Three rotational DOF motors relocated to inside of the frame.

3.2.4. Spherical Parallel Ball Support Type (SPBS)

The spherical parallel ball support type haptic device is a hybrid mechanism that contains a three DOF spherical parallel platform with one linear DOF handle. The device incorporates the benefits of both serial and parallel manipulator.

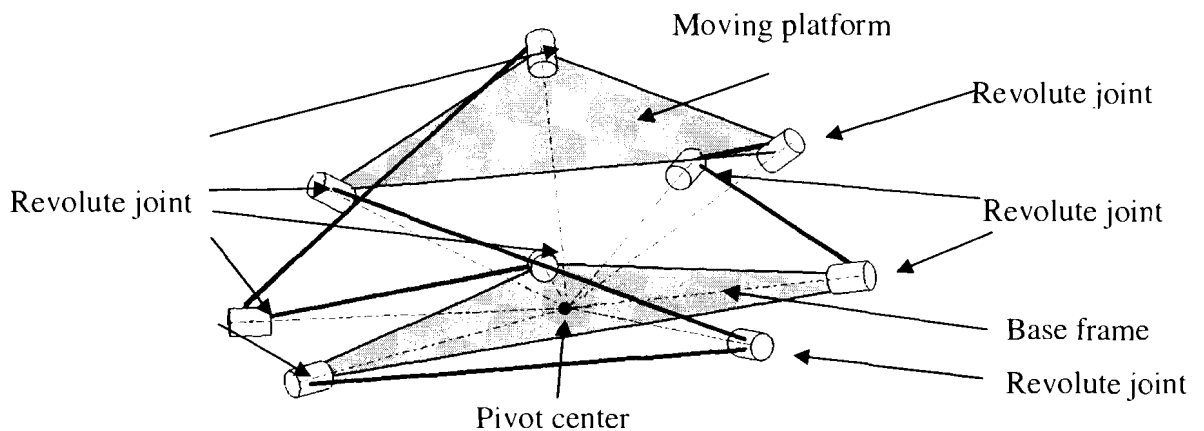


Figure 3-23 Schematic diagram of the spherical parallel platform

The schematic diagram of the spherical parallel platform is shown in Figure 3-23. The three rotational DOF platform is connected to the base frame via three branches. Each branch contains two links with three revolute joints. All of the nine revolute joint vectors intersect at the pivot center point. This point is the insertion point of the VR surgical training environment.

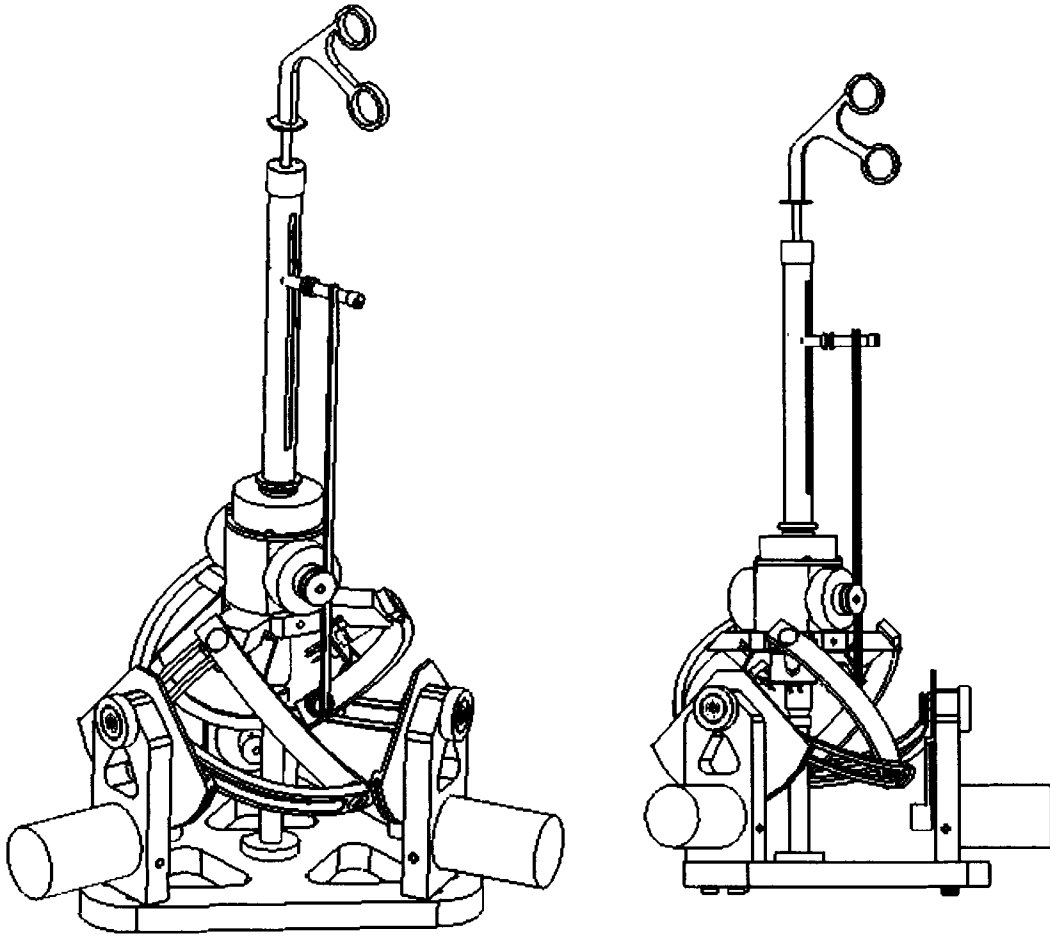


Figure 3-24 CAD model of SPBS (iso and front view)

Figure 3-24 shows the CAD model of SPBS. The moving platform is constrained to three rotational DOF. SPBS contains a three rotational DOF platform and one translational DOF. The platform is connected to the base frame via three identical branches and a passive spherical joint. Figure 3-25 shows each branch contains a motor, an active cam, an active link, and a passive link. There is one revolute joint between the motor bracket and the active cam. The second revolute joint is located between the active and the passive link. The third revolute joint is between the platform and the passive link. All revolute joint vectors intersect at the origin which is also the spherical support center. For HPST, the second joint is a ball joint that replaces a revolute joint.

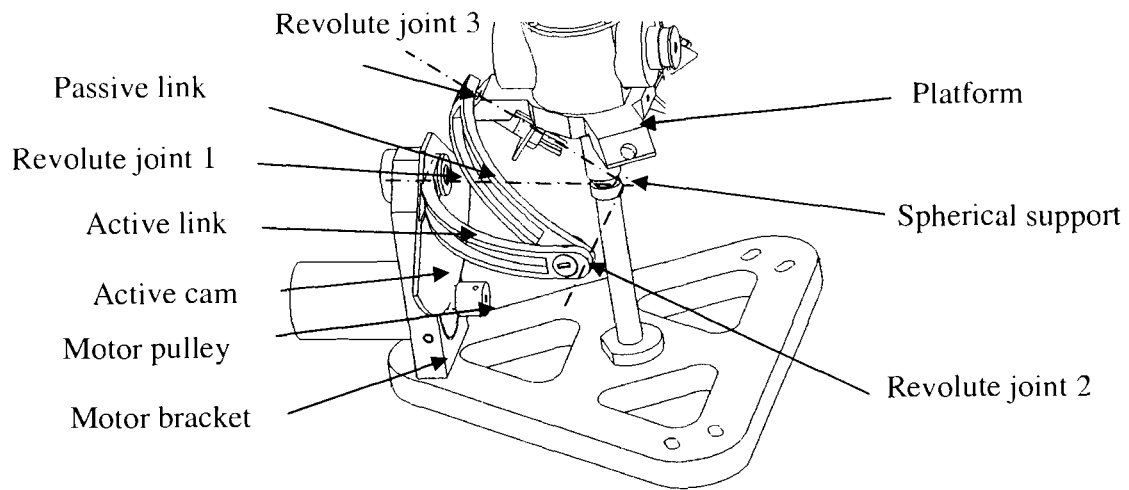


Figure 3-25 Mechanical structure of SPBS (one branch)

The moving platform contains eight links, nine revolute joints, and one spherical joint.

The mobility equation is used to predict the mobility of platform as:

$$F = \lambda(l - j - 1) + \sum_{i=1}^j f_i = 3(8 - 10 - 1) + 9 + 3 = 3$$

Figure 3-26 shows the photograph of SPBS that contains three stationary motors to provide force feedback for rotational DOF. A movable motor is located on the top center of the platform to provide force feedback for linear motion. In addition, the center of mass of movable motor is positioned at the center of the platform. The radius of active link is 60 mm which is 50% smaller than HPST and the platform diameter is reduced from 100 mm to 60 mm.

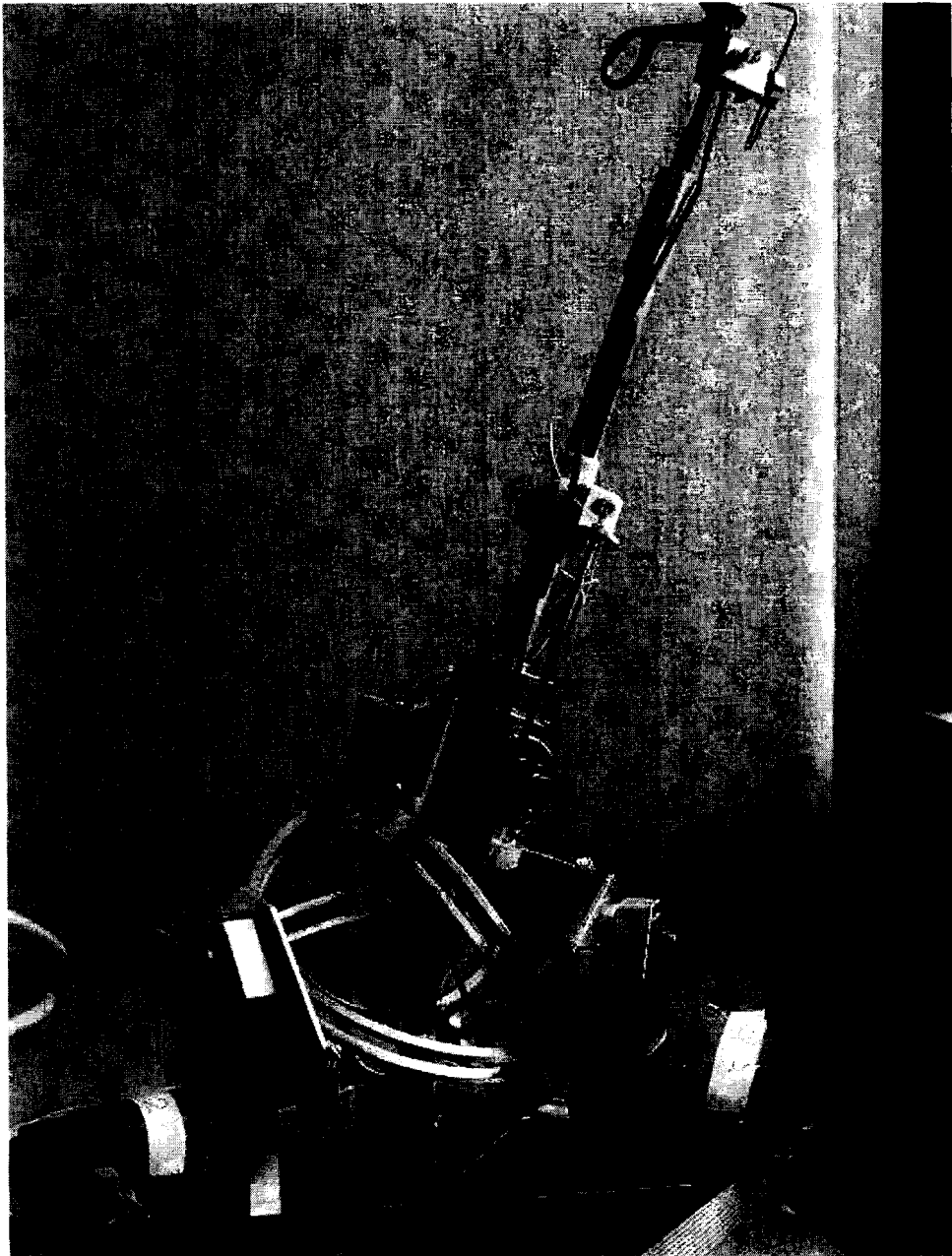


Figure 3-26 Photograph of SPBS prototype

Mechanical design features:

Passive support: A spherical passive support is fixed on the base center to support weight and forces. The 10 mm diameter stainless ball support is an improved version of the HPST. The ball support is compact and adjusts easily to ensure accuracy position. As

compared to the yoke support in HPST, ball support is easier to manufacture because yoke support contains fourteen parts while spherical support contains only four parts. The part number reduction for manufacturing is discussed in chapter 4.

Gear ratio: The gear ratio between motor pulley and cam is 10:1. The Maxon 118891 motor is able to generate 483-mNm stall torque. After magnification by the gear ratio, the applied torque of active link is 4800 mNm. Figure 3-27 shows the relationship between torque and applied force. 80 N force is needed to balance the torque.

$$Force_{stall-torque} = \frac{stall - torque}{length} = \frac{4800mNm}{60mm} = 80N$$

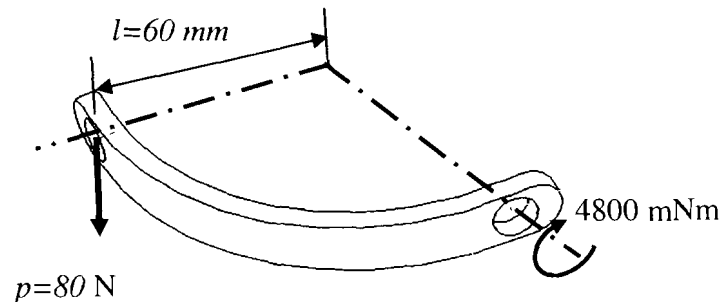


Figure 3-27 Torque and force of active link

Linkage weight reduction: The weight of an active link will be 19g without a weight reduction slot. After applying the slot, the weight will be 10g. The material of the link is aluminum alloy which has a density of 2.7 g/mm^3 . The weight of the link is now reduced by 50% and it is strong enough to avoid any major deflection. A loading example case was calculated to determine the maximum displacement for the active link. In order to calculate the maximum displacement, assuming that the revolute joint I is fixed and a load (100 N) is applied on the distal end. This 100 N force is based on the stall torque and a safety factor of 25%. As shown in Figure 3-28, the maximum displacement (δ_{max}) of the active link can be expressed as

$$\delta_{\max} = \frac{pl^3}{3EI} \quad (3-1)$$

Where p is the load on the end of the active link (N), l is the length of the active link (mm), E is the Young's Modulus of material Aluminum 6061-T6 (73.1GPa), I is the moment of inertia. $I = \frac{bh^3}{12}$ (for link without reduction slot) and $I = \frac{b}{12}(h_2^3 - h_1^3)$ (for link with weight reduction slot).

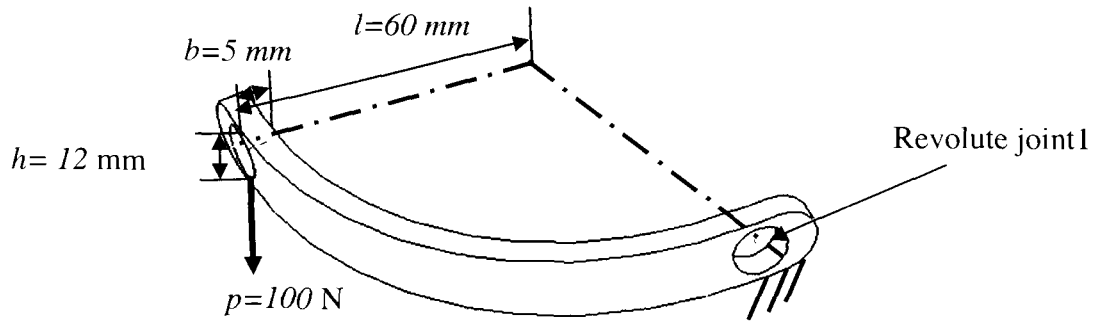


Figure 3-28 Displacement calculation of active link

Substituting p , l , E and I into (3-1) leads to

$$\delta_{\max} = \frac{p \times l^3}{3 \times E \times \frac{b \times h^3}{12}} = \frac{100 \times 60^3}{3 \times 73.1 \times 10^3 \times \frac{5 \times 12^3}{12}} = 1.08e^{-2} \text{ (mm)}$$

For link with slot, the moment of inertia can be expressed as $I = \frac{b}{12}(h_2^3 - h_1^3)$, then maximum displacement of 100 N applied force on distal end can be obtained as

$$\delta_{\max} = \frac{p \times l^3}{3 \times E \times \frac{b \times (h_2^3 - h_1^3)}{12}} = \frac{100 \times 60^3}{3 \times 73.1 \times 10^6 \times \frac{5 \times (12^3 - 8^3)}{12}} = 7.76e^{-1} \text{ (mm)}$$

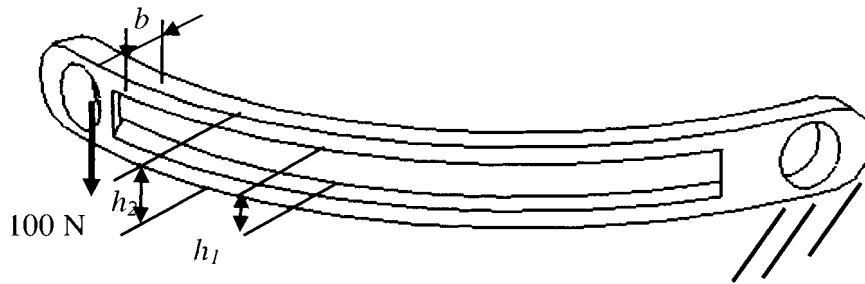


Figure 3-29 The active link with slot

The maximum deflection of active link under 100 N load is $1.08e^{-2}$ mm (without slot) and $7.76e^{-1}$ mm (with slot). According to the calculation, the deflection affected by weight reduction slot is insignificant. This calculation shows that the link is able to provide enough stiffness with less deformation which is an important feature of haptic device and the parallel mechanism.

Increased workspace: The linear motor is located on top of the platform and the linear link slides up and down along the platform to avoid collision with the link while the platform rotates. Therefore, the workspace can reach $\pm 85^\circ$ for X and Y-axes. The rotation along Z-axis can reach $\pm 135^\circ$. The linear motion range is within 180 mm which can be extended if necessary. The linear motion device is mounted on the platform: therefore, modification of the stroke length is independent of the rotational parts.

Symmetrical active axes: Active joint vectors are symmetrical and co-planar. Mechanical limit: Small mechanical limits are installed on both sides of the cam to constrain the motion range of cam within $\pm 60^\circ$. These limits maintain the platform within the workspace without singularity. In addition, it can adjust the tension on the wire.

The center of mass of the platform with linear mechanisms is (0.5, 1.5, 62.5) mm from origin point and the movable weight supported by spherical joint is 325 grams.

Advantages of SPBS include low inertia, large workspace, simple design and compact size.

Limitation of SPBS is complex direct kinematics with no closed-form solution. Details of direct kinematics are discussed in later section. The complex direct kinematics of parallel manipulator without additional analysis is not suitable for real time application.

3.2.5. Two handed Type (THT)

Shown in Figure 3-31, the prototype contains two-handed setup so that the user can manipulate with both hands. The kinematics structure of THT is also spherical parallel mechanism with different linear motion design.

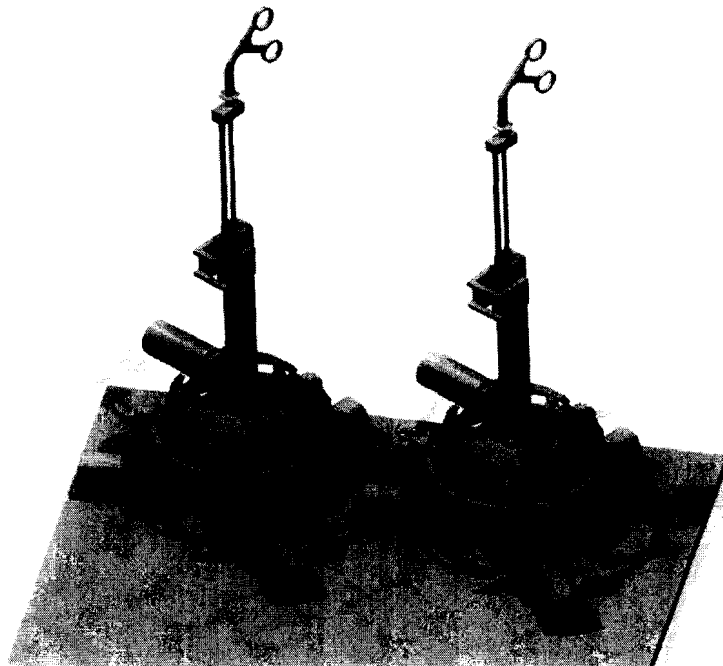


Figure 3-30 CAD model of two-handed type

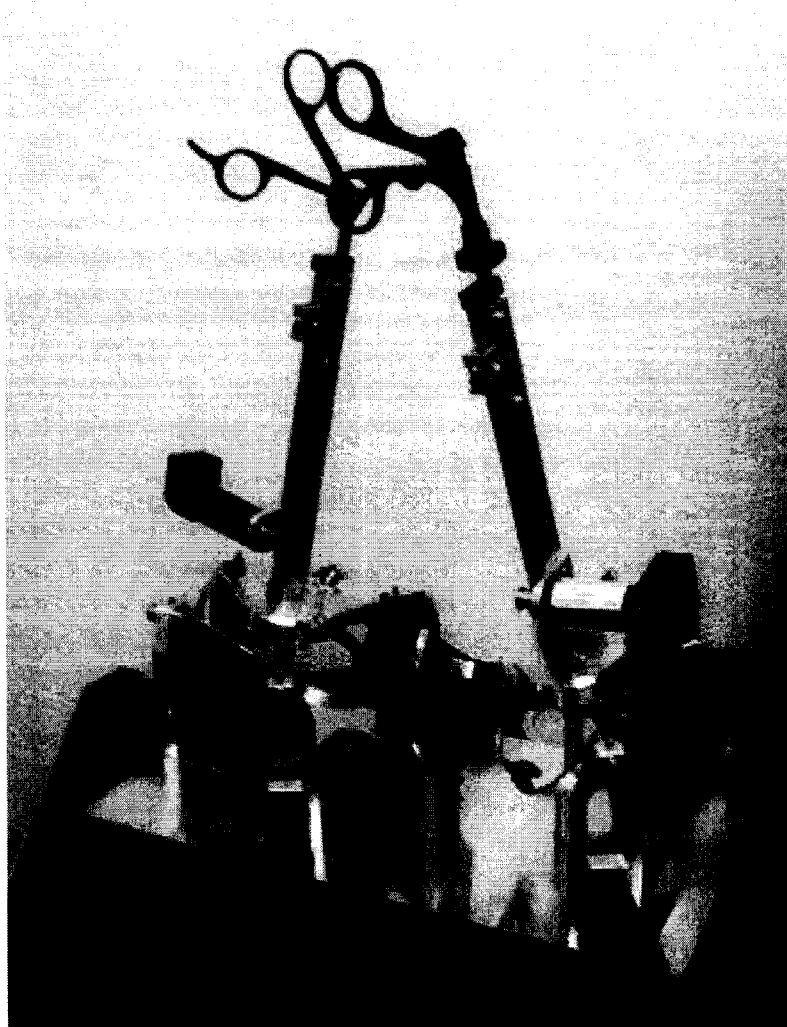


Figure 3-31 Prototype of two-handed type

Mechanical design features:

Connecting pins: Figure 3-32 shows the stainless steel ball support and three connecting pins touching the ball surface. These pins provide rigid and frictionless support.

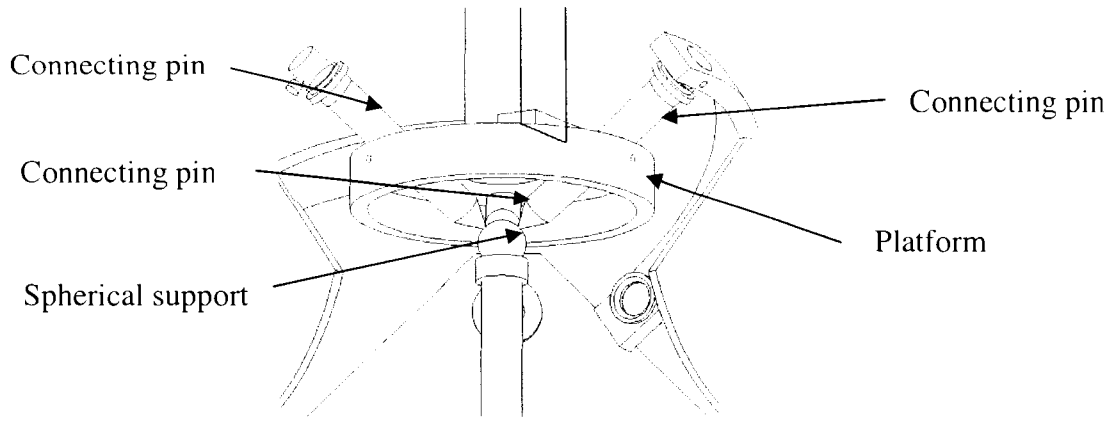


Figure 3-32 Connecting pin of Two handed type

Advantages of THT include low inertia and simple platform design. Limitation includes unbalanced platform weight caused by movable motor. The center of mass of the THT platform is $(-18.4, 32.7, -71.3)$ mm and the weight of platform is 345 grams.

Comparing SPBS and THT, the platform weight, linear motion mechanism and motor mechanism are similar (325 and 345 gram). The weight distribution of SPBS is superior to THT because the center of mass of SPBS is 60 mm above the pivot center. The center of mass of THT platform is 80 mm from pivot center. The spherical support is able to share the weight with static weight balance and lower inertia. THT contains the motor which is hanging on the linear motion frame, thus causing the center of mass to move away from pivot point.

3.3. *Kinematic Modeling*

The kinematic symbols and geometrical model of SPBS are introduced in this section. World coordinate frame (W) is a fixed frame to which all other frames are referred. Figure 3-33 shows the origin of world coordinate frame located at the pivot center of

platform. X_w , Y_w and Z_w provide three axes of world coordinate frame. Shown in Figure 3-34, the platform coordinate frame (P) is attached to the moving platform and defined by X_p , Y_p and Z_p axes passing through three revolute joints of platform. The platform coordinate frame shares its origin point with that of the world coordinate frame and rotates with respect to world coordinate frame without any translation. X_p , Y_p and Z_p axes are perpendicular to each other.

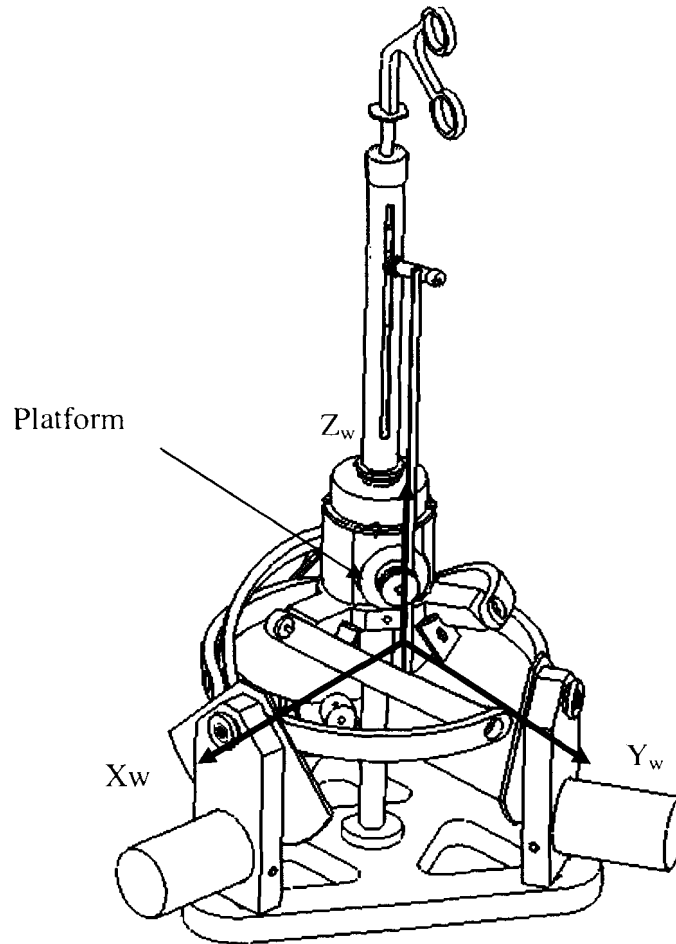


Figure 3-33 World coordinate frame

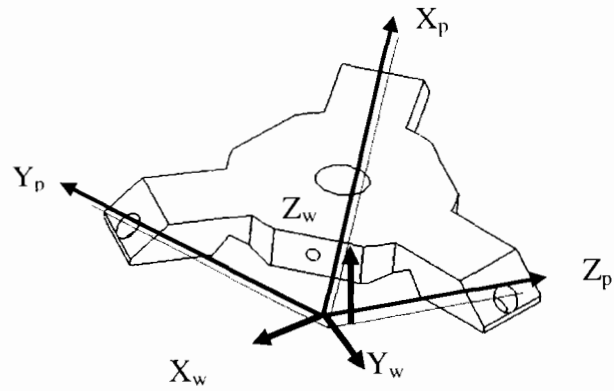


Figure 3-34 World coordinate frame and Platform coordinate frame

Handle coordinate frame (H): As shown in Figure 3-35, handle coordinate frame is attached to the surgical tool handle because it is convenient to describe tool motion with respect to tool coordinate frame rather than the world coordinate frame. The handle has only one linear DOF with respect to the platform and four DOF with respect to the world frame. A special feature about the handle coordinate frame is that the Z-axis (Z_h) is always passing through the origin point O. The origin O is on the intersection of X-axis (x_w), Y-axis (y_w) and Z-axis (z_w) of world frame as show in Figure 3-31 which demonstrates that the handle contains one linear DOF with respect to the platform.

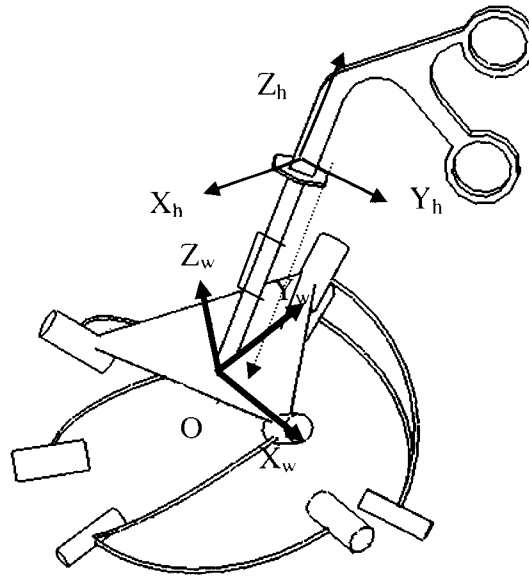


Figure 3-35 Handle coordinate frame

Shown in Figure 3-36, active joint vectors (v_{a1} , v_{a2} , v_{a3}) are unit vectors representing axis of rotation of the motor. These unit vectors are co-planar and symmetrical so that $v_{a1} = [\cos 0^\circ, \sin 0^\circ, 0]^T$, $v_{a2} = [\cos 120^\circ, \sin 120^\circ, 0]^T$ and $v_{a3} = [\cos 240^\circ, \sin 240^\circ, 0]^T$. This symmetrical features balance the link weight which lowers the inertia.

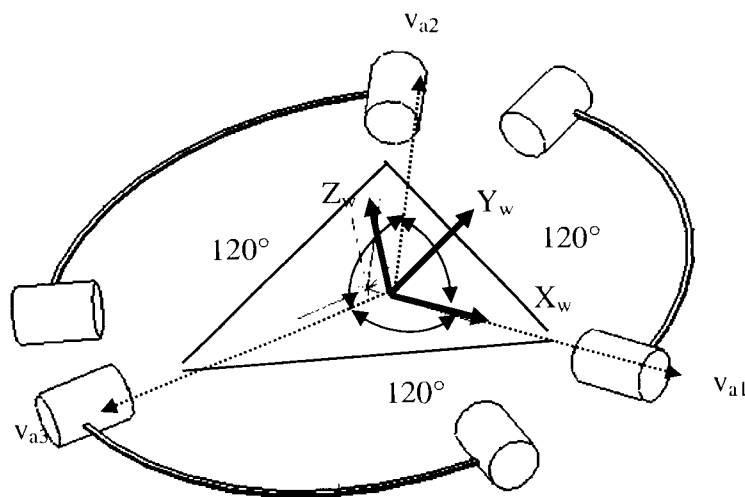


Figure 3-36 Kinematic notation diagram of SPBS

Middle joint vector (m_1, m_2, m_3): unit vectors represent the direction of the middle revolute joint. This vector can be calculated by the revolute joint angle.

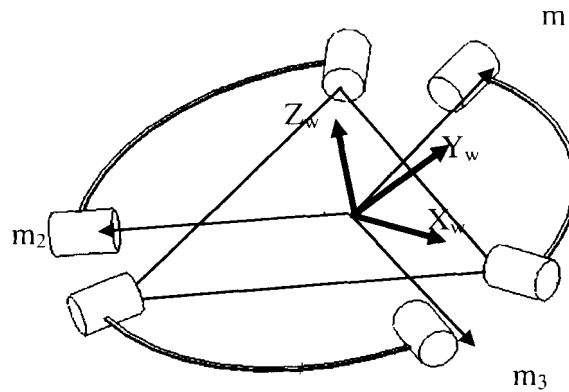


Figure 3-37 Middle joint vector of SPBS

Platform joint vector (p_1, p_2, p_3): unit vectors represent the direction of X, Y and Z-axis of platform. Link arc angles ($\alpha_{11}, \alpha_{12}, \alpha_{21}, \alpha_{22}, \alpha_{31}, \alpha_{32}$): These six angles represent the arc angles of passive and active links. The passive link angles α_{11}, α_{21} and α_{31} are measured between joint axis of the moving platform and the corresponding middle revolute joints. $\alpha_{12}, \alpha_{22}, \alpha_{32}$ are the active link angles measured between the middle revolute joints and active axis. All of the link arc angles are 90° .

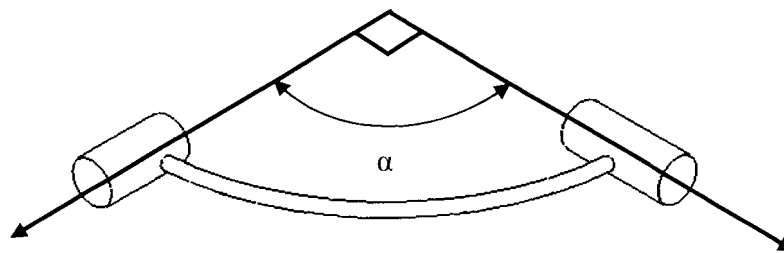


Figure 3-38 Link arc angle

Active angles ($\theta_{1a}, \theta_{2a}, \theta_{3a}$): represent the active link rotation angle. Active angles are 0 at home position. Middle joint angles ($\theta_{1m}, \theta_{2m}, \theta_{3m}$): These angles are measured between passive link and active link. Middle joint angles cannot be controlled directly as their middle joints are un-actuated.

3.3.1. Inverse Kinematic of SPBS

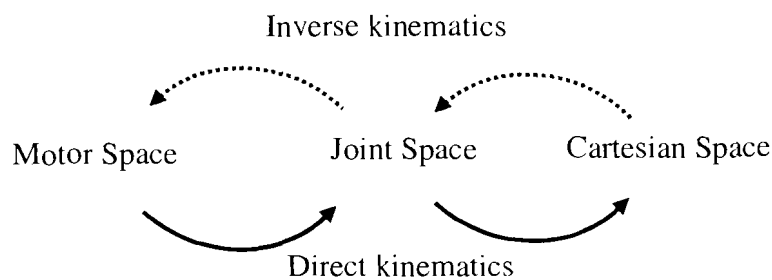


Figure 3-39 Mapping between kinematic

As shown in Figure 3-39[45], the relationship between Cartesian space, joint space and motor space can be used to express the kinematic of SPBS. In SPBS, the Cartesian space is the orientation and position of the end effector (handle). Joint space is the revolute joint vectors and joint angles while motor space includes the motor angles. For inverse kinematics, the dotted line shows that the Cartesian space is known and the motor angle can be calculated. For direct kinematics, the motor angles are known and the Cartesian space of end effector needs to be calculated. When the user moves the handle, direct kinematics is used to calculate the position and the orientation of the handle in Cartesian space.

Once the position and orientation of the end effector is assigned, inverse kinematics, (IK) is needed to solve the corresponding joint variables. In order to solve IK problem, world coordinate frame, Denavit Hartenberg (DH) parameters, active joint vector and link angles must be defined. DH parameters are defined in Table 3-1 that the link angles (α_{1i} , α_{2i} , α_{3i}) are 90 degrees (in Figure 3-38). The middle joint vectors $m_1 [m_{1x}, m_{1y}, m_{1z}]^T$, $m_2 [m_{2x}, m_{2y}, m_{2z}]^T$ and $m_3 [m_{3x}, m_{3y}, m_{3z}]^T$ (in Figure 3-37) are of unit length.

$$|m_1| = m_{1x}^2 + m_{1y}^2 + m_{1z}^2 = 1$$

$$|m_2| = m_{2x}^2 + m_{2y}^2 + m_{2z}^2 = 1$$

$$|m_3| = m_{3x}^2 + m_{3y}^2 + m_{3z}^2 = 1$$

Table 3-1 Denavit Hartenberg table of SPBS

Branch 1				Branch 2				Branch 3			
a_1	α_{1i}	D_1	θ_1	a_2	α_{2i}	d_2	θ_2	a_3	α_{3i}	d_3	θ_3
0	90	0	θ_{1a}	0	90	0	θ_{2a}	0	90	0	θ_{3a}
0	90	0	θ_{1m}	0	90	0	θ_{2m}	0	90	0	θ_{3m}

The end effector (handle) of SPBS contains three rotational DOF and one translational DOF. While calculating the IK, the linear motion of end effector can be isolated from rotation because the end effector is attached to the three rotational platform. Linear motion affects only the distance between the end effector and origin and does not change the orientation. The rotational DOF of end effector depends on the orientation of the platform. The platform rotation matrix (R_h) can be expressed by platform joint vectors $p_1 [p_{1x}, p_{1y}, p_{1z}]^T$, $p_2 [p_{2x}, p_{2y}, p_{2z}]^T$ and $p_3 [p_{3x}, p_{3y}, p_{3z}]^T$.

$$\text{Rotation matrix } R_h = \begin{bmatrix} p_{1x} & p_{2x} & p_{3x} \\ p_{1y} & p_{2y} & p_{3y} \\ p_{1z} & p_{2z} & p_{3z} \end{bmatrix}$$

Once platform joint vectors p_i , ($i=1, 2, 3$) are defined, middle joint vectors m_i , ($i=1, 2, 3$) can be solved by cosine laws. The middle joint vectors $m_i [x_{mi}, y_{mi}, z_{mi}]^T$ can be obtained by the following equations:

$$\cos \alpha_{1i} = p_i \cdot m_i = 0 \quad (3-2)$$

$$\cos \alpha_{i2} = v_{ai} \cdot m_i = 0 \quad (3-3)$$

$$m_{ix}^2 + m_{iy}^2 + m_{iz}^2 = 1 \quad (3-4)$$

Hence, for each given platform joint vector, two possible solutions exist. As shown in Figure 3-40, two solutions of middle joint vectors satisfy one branch; therefore, eight possible configuration solutions fit for previous equations. To identify the physical solution, the device need to be checked in order to find the correct solution set that meets the physical model.

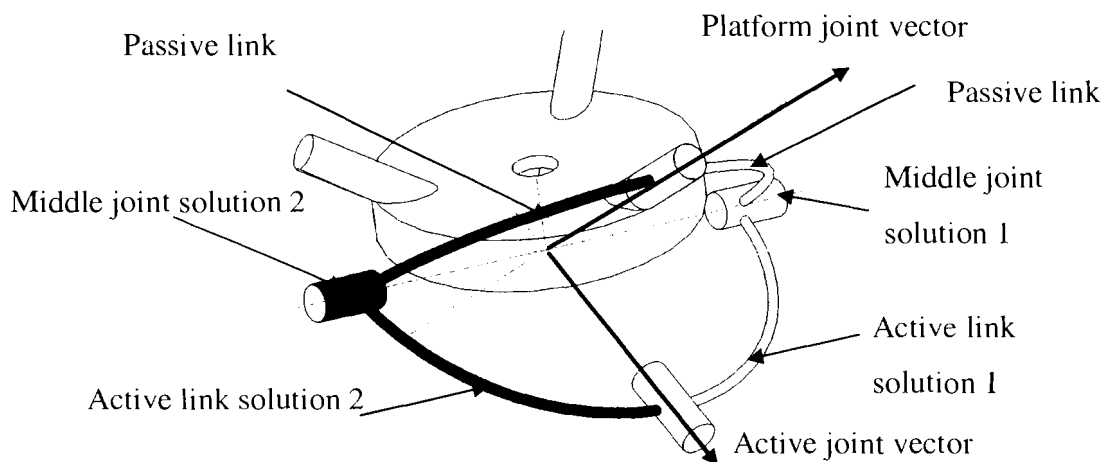


Figure 3-40 Two possible solutions of middle joint vector

At home position, the motor angle is defined to be 0. If the middle joint vector is not at home position, the active angle can be solved by comparing the middle joint vector with the home position. Active rotation angle (θ_i) can also be solved after solving middle joint vectors. Shown in Figure 3-41, $\Delta\theta_i$ is the active angle from start position m_i to new position m_{in} which can be determined by cosine law and expressed as

$$\theta_i = a \cos(m_i \cdot m_{in}) \quad (3-5)$$

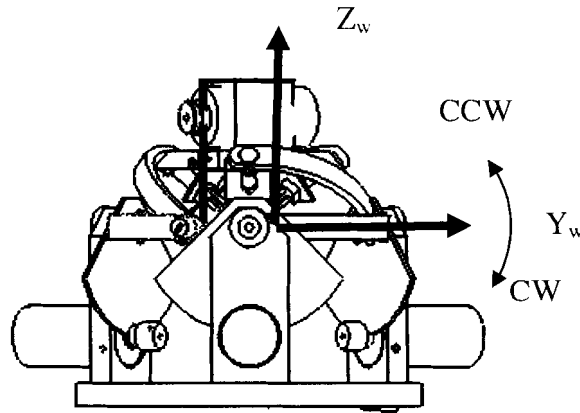


Figure 3-41 Active cam rotation direction

After solving for the active angle, the next step is to determine the rotation direction of the active cam. As shown in Figure 3-41, if the active cam rotates clockwise then the z value of middle joint vector decreases. Gear ratio (10:1) between motor and active cam is converted to obtain corresponding motor angle to reach the new position. The direction of rotation of the motor is the opposite direction of the cam.

$$\Delta\theta_{motor_i} = -\Delta\theta_i \cdot 10 \quad (3-6)$$

3.3.2. Numerical Example of Inverse Kinematics

In this section, a numerical example is introduced to illustrate the procedures of solving IK defined in section 3.3.1. At home position, the top surface of platform is parallel to

the base. Figure 3-42 (a) shows the front view of home position with the platform parallel to the base frame. As shown in Figure 3-42 (b), the platform joint vector p_1 lays on the XZ plane. The home position can be positioned easily because of its condition.

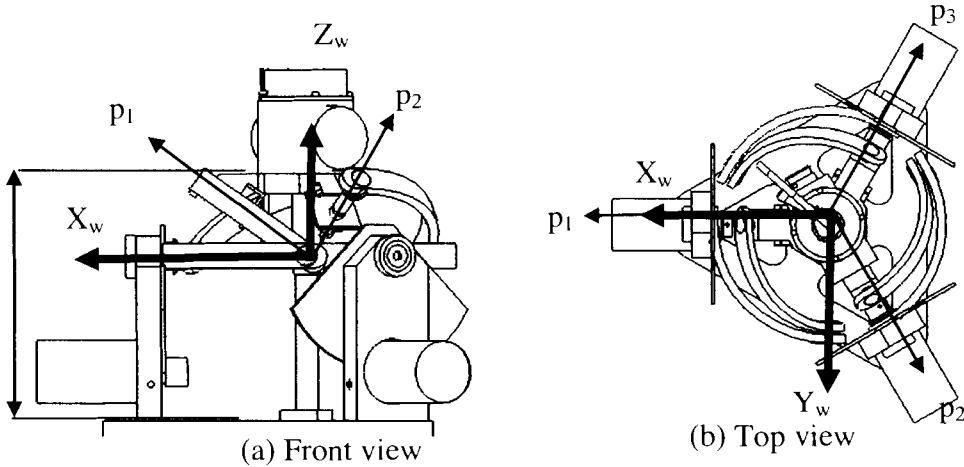


Figure 3-42 Front and top view of home position

The orientation of the platform for home position can be expressed in terms of a rotation matrix. However, in order to give it an angular expression, X-Y-Z fixed angles are used to describe the orientation of the platform. The derivation of the equivalent rotation matrix is straightforward because all rotations occur about the axes of the world coordinate frame. At the initial position, the platform coordinate frame (P) is coincident with the world coordinate frame (W). First, rotate P about X_w by an angle γ , and then rotate about Y_w by an angle β and the rotate about Z_w an angle α . The platform rotation matrix (R_h) can then be expressed by X-Y-Z fixed angles as

$$\begin{aligned}
 R_h &= R_z(\alpha)R_y(\beta)R_x(\gamma) \\
 &= \begin{bmatrix} c\alpha & -s\alpha & 0 \\ s\alpha & c\alpha & 0 \\ 0 & 0 & 1 \end{bmatrix} \begin{bmatrix} c\beta & 0 & s\beta \\ 0 & 1 & 0 \\ -s\beta & 0 & c\beta \end{bmatrix} \begin{bmatrix} 1 & 0 & 0 \\ 0 & c\gamma & -s\gamma \\ 0 & s\gamma & c\gamma \end{bmatrix} \\
 &= \begin{bmatrix} c\alpha c\beta & c\alpha s\beta s\gamma - s\alpha c\gamma & c\alpha s\beta c\gamma + s\alpha s\gamma \\ s\alpha c\beta & s\alpha s\beta s\gamma + c\alpha c\gamma & s\alpha s\beta c\gamma - c\alpha s\gamma \\ -s\beta & c\beta s\gamma & c\beta c\gamma \end{bmatrix}
 \end{aligned}$$

$$\beta = A \tan 2(-r_{31}, \sqrt{r_{11}^2 + r_{21}^2}),$$

$$\alpha = A \tan 2\left(\frac{r_{21}}{c\beta}, \frac{r_{11}}{c\beta}\right), \quad (3-7)$$

$$\gamma = A \tan 2\left(\frac{r_{32}}{c\beta}, \frac{r_{33}}{c\beta}\right)$$

At home position, the rotation matrix of platform can be expressed as

$$R_n = \begin{bmatrix} 0.8165 & -0.4082 & -0.4082 \\ 0 & 0.7071 & -0.7071 \\ 0.5773 & 0.5773 & 0.5773 \end{bmatrix} \quad (3-8)$$

Substituting (3-8) into (3-7), the X-Y-Z fixed angles of the platform at home position can be obtained as $\beta = -35.2619^\circ$, $\alpha = 0^\circ$, $\gamma = 45^\circ$. This is referred as roll, pitch and yaw angles at home position of the platform.

The platform joint vectors are $p_1 [0.8165, 0, 0.5773]^T$, $p_2 [-0.4082, 0.7071, 0.5773]^T$ and $p_3 [-0.4082, -0.7071, 0.5773]^T$. The active joint vectors are $v_{a1} [1, 0, 0]^T$, $v_{a2} [-0.5, 0.866, 0]^T$ and $v_{a3} [-0.5, -0.866, 0]^T$. Next step is to solve middle joint vectors m_1, m_2, m_3 .

Substituting p_1 and v_{a1} into equation (3-2) to (3-4) yields

$$.08165 \cdot m_{1x} + 0 \cdot m_{1y} + 0.5773 \cdot m_{1z} = 0$$

$$1 \cdot m_{1x} + 0 \cdot m_{1y} + 0 \cdot m_{1z} = 0$$

$$m_{1x}^2 + m_{1y}^2 + m_{1z}^2 = 1$$

The middle joint vector m_1 can be solved $[0, 1, 0]^T$, $[0, -1, 0]^T$

Substituting p_2 and v_{a2} into equation (3-2) to (3-4) yields

$$-0.4082 \cdot m_{2x} + 0.7071 \cdot m_{2y} + 0.5773 \cdot m_{2z} = 0$$

$$-0.5000 \cdot m_{2x} + 0.8660 \cdot m_{2y} + 0 \cdot m_{2z} = 0$$

$$m_{2x}^2 + m_{2y}^2 + m_{2z}^2 = 1$$

The middle joint vector m_2 can be solve as $[-0.866, -0.5, 0]^T$, $[0.866, 0.5, 0]^T$

Substituting p_3 and v_{a3} into equation (3-2) to (3-4) yields

$$-0.4082 \cdot m_{3x} - 0.7071 \cdot m_{3y} + 0.5773 \cdot m_{3z} = 0$$

$$-0.5 \cdot m_{3x} - 0.866 \cdot m_{3y} + 0 \cdot m_{3z} = 0$$

$$m_{3x}^2 + m_{3y}^2 + m_{3z}^2 = 1$$

The middle joint vector m_3 can be solved $[0.866, -0.5, 0]^T$, $[-0.866, 0.5, 0]^T$

Each branch contains two solution sets that can satisfy kinematics polynomial equations. However, $m_1=[0, 1, 0]^T$, $m_2=[-0.866, -0.5, 0]^T$ and $m_3=[-0.866, 0.5, 0]^T$ fit the physical model configuration.

By rotating the platform along Y-axis clock wise 15° and the platform rotation matrix can be expressed as

$$R_{new} = R_y \cdot R_h = \begin{bmatrix} \cos(-15^\circ) & 0 & \sin(-15^\circ) \\ 0 & 1 & 0 \\ -\sin(-15^\circ) & 0 & \cos(-15^\circ) \end{bmatrix} \begin{bmatrix} 0.8165 & -0.4082 & -0.4082 \\ 0 & 0.7071 & -0.7071 \\ 0.5773 & 0.5773 & 0.5773 \end{bmatrix} \quad (3-9)$$

$$= \begin{bmatrix} 0.6392 & -0.5437 & -0.5437 \\ 0 & 0.7071 & -0.7071 \\ 0.7690 & 0.4520 & 0.4520 \end{bmatrix}$$

Then, the new platform joint vector p_{in} can be expressed as

$$p_{1n} = \begin{bmatrix} 0.6392 \\ 0 \\ 0.7690 \end{bmatrix}, p_{2n} = \begin{bmatrix} -0.5437 \\ 0.7071 \\ 0.4520 \end{bmatrix}, p_{3n} = \begin{bmatrix} -0.5437 \\ -0.7071 \\ 0.4520 \end{bmatrix}$$

Substituting p_{1n} and v_{a1} into equation (3-2) to (3-4) yields

$$0.6392 \cdot m_{1x} + 0 \cdot m_{1y} + 0.7690 \cdot m_{1z} = 0$$

$$1 \cdot m_{1x} + 0 \cdot m_{1y} + 0 \cdot m_{1z} = 0$$

$$m_{1x}^2 + m_{1y}^2 + m_{1z}^2 = 1$$

Obtaining the new middle joint vectors $m_1 [0, 1, 0]^T$ and $m_1 [0, -1, 0]^T$

Substituting p_{2n} and v_{a2} into equation (3-2) to (3-4) yields

$$-0.5437 \cdot m_{2x} + 0.7071 \cdot m_{2y} + 0.4520 \cdot m_{2z} = 0$$

$$-0.5 \cdot m_{2x} + 0.866 \cdot m_{2y} + 0 \cdot m_{2z} = 0$$

$$m_{2x}^2 + m_{2y}^2 + m_{2z}^2 = 1$$

The new middle joint vector m_2 can be solved to give $[-0.8382, -0.4839, -0.2512]^T$,
 $[0.8382, 0.4839, 0.2512]^T$

Substitute p_{3n} and v_{a3} , into (3-2) to (3-4) yields to

$$-0.5437 \cdot m_{3x} - 0.7071 \cdot m_{3y} + 0.4250 \cdot m_{3z} = 0$$

$$-0.5 \cdot m_{3x} - 0.866 \cdot m_{3y} + 0 \cdot m_{3z} = 0$$

$$m_{3x}^2 + m_{3y}^2 + m_{3z}^2 = 1$$

The new middle joint vector m_3 can be solved to give $[-0.8382, 0.4839, -0.2512]^T$,
 $[0.8382, 0.4839, 0.2512]^T$

In order to solve for the active angle 2, comparing the home position of m_2 $[-0.866, -0.5, 0]^T$ and new position $[-0.8382, -0.4839, -0.2512]^T$

The rotation of active angle 2 can be obtained by

$$\theta_2 = a \cos(m_2 \cdot m_{2n}) = a \cos\left(\begin{bmatrix} -0.866 \\ -0.5 \\ 0 \end{bmatrix} \cdot \begin{bmatrix} -0.8382 \\ -0.4839 \\ -0.2512 \end{bmatrix} \right) = 32^\circ$$

The next step is to determine the direction (clockwise or count-clockwise) for the active link. Since the Z value has decreased, the active link rotates clockwise. The motor angle 2 can be obtained by substituting the active link angle into equation (3-6).

$$\theta_{motor} = -32 \times 10 = 320$$

The motor angle 2 can be obtained as 320° (counter clockwise).

In order to solve the motor angle 3, the home position $m_3 [-0.866, 0.5, 0]^T$ and new position $[-0.8382, 0.4839, -0.2512]^T$ are compared.

The rotation angle of active link 3 can be obtained by

$$\theta_3 = a \cos(m_3 \cdot m_{3n}) = a \cos\left(\begin{bmatrix} -0.866 \\ 0.5 \\ 0 \end{bmatrix} \cdot \begin{bmatrix} -0.8382 \\ 0.4839 \\ -0.2512 \end{bmatrix}\right) = 32^\circ$$

The next step is to determine the direction (CW or CCW) for the active link 3. Since the Z value has decreased, the active link rotates clockwise. The motor angle can be obtained by substituting the active link angle into equation (3-6)

$$\theta_{motor} = -32 \times 10 = 320$$

The motor 3 turns 323° (CCW direction).

In this case, the platform rotated along Y-axis clockwise 15° from home position to a new position. The motor angle 1 has remained as it was and middle joint vector is unmoved. Both motor2 and motor 3 rotate 320° counter-clockwise to rotate active angle 32° clockwise. It can be observed that the active link angle is 90° and the active joint vector is $[1, 0, 0]^T$; therefore, the middle joint vector m_1 moves on $x=0$ plan. This means that the x value of m_1 is always 0.

3.3.3. Direct Kinematics of SPBS

The direct kinematic (DK) equations define the function between Cartesian space the position and the orientation and the space of joint positions[98]. DK of manipulator is known as the joint angle and is used to calculate the position and orientation of the end effector. Gosselin [47] [69] [99] solved the DK problems for spherical parallel mechanism and pointed out that the characteristic polynomial of the three DOF spherical mechanisms has a degree of eight. Merlet [67] proposed both iterative and reduced

schemes to solve the DK of parallel manipulators. Ji [71] studied the direct kinematics for a three DOF spherical parallel manipulator which consisted of two tetrahedrons and found a direct algebraic solution for it.

In general, the IK for the parallel spherical mechanism is unique and can be easily computed. However, the solution to the direct kinematic problem offers some unique challenges for solving a set of nonlinear equations[100]. Numerical methods such as Newton's method need to be implemented to solve the nonlinear equations. Newton's method has high computation time.

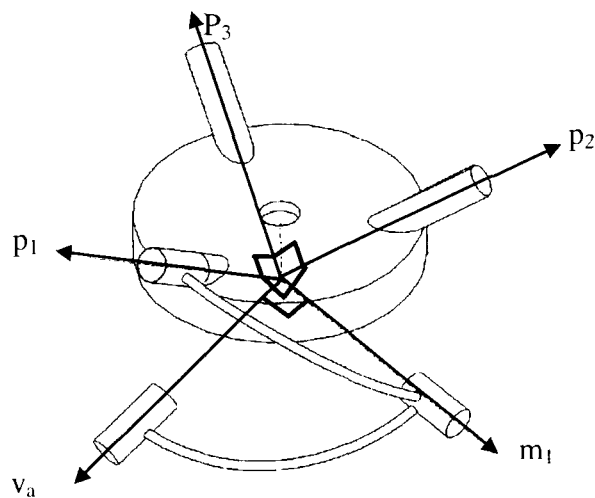


Figure 3-43 Direct kinematics link angle (shown on one branch)

Middle joint vectors are $m_1 [m_{1x}, m_{1y}, m_{1z}]^T$, $m_2 [m_{2x}, m_{2y}, m_{2z}]^T$ and $m_3 [m_{3x}, m_{3y}, m_{3z}]^T$.

Shown in Figure 3-43, the 90° angle between active vector and middle joint vector leads to

$$p_1 \cdot m_1 = \cos \alpha_{11} = \cos(90^\circ) = 0 \quad (3-10)$$

$$p_2 \cdot m_2 = \cos \alpha_{21} = \cos(90^\circ) = 0 \quad (3-11)$$

$$p_3 \cdot m_3 = \cos \alpha_{31} = \cos(90^\circ) = 0 \quad (3-12)$$

As shown in Figure 3-43, p_i ($i=1, 2, 3$) are perpendicular to each other ($p_1 \perp p_2 \perp p_3 \perp p_1$). The orthogonal rotation matrix $R = [p_1, p_2, p_3]$ has the special property of

$R_h^T R_h = I$; therefore, it can be expressed as

$$\begin{bmatrix} p_{1x} & p_{2x} & p_{3x} \\ p_{1y} & p_{2y} & p_{3y} \\ p_{1z} & p_{2z} & p_{3z} \end{bmatrix} \begin{bmatrix} p_{1x} & p_{1y} & p_{1z} \\ p_{2x} & p_{2y} & p_{2z} \\ p_{3x} & p_{3y} & p_{3z} \end{bmatrix} = \begin{bmatrix} 1 & 0 & 0 \\ 0 & 1 & 0 \\ 0 & 0 & 1 \end{bmatrix}$$

This yields

$$p_{1x} \cdot p_{1x} + p_{2x} \cdot p_{2x} + p_{3x} \cdot p_{3x} = 1 \quad \checkmark$$

$$p_{1x} \cdot p_{1y} + p_{2x} \cdot p_{2y} + p_{3x} \cdot p_{3y} = 0 \quad \checkmark$$

$$p_{1x} \cdot p_{1z} + p_{2x} \cdot p_{2z} + p_{3x} \cdot p_{3z} = 0 \quad \checkmark$$

$$p_{1x} \cdot p_{1y} + p_{2x} \cdot p_{2y} + p_{3x} \cdot p_{3y} = 0$$

$$p_{1y} \cdot p_{1y} + p_{2y} \cdot p_{2y} + p_{3y} \cdot p_{3y} = 1 \quad \checkmark$$

$$p_{1x} \cdot p_{1z} + p_{2x} \cdot p_{2z} + p_{3x} \cdot p_{3z} = 0 \quad \checkmark$$

$$p_{1y} \cdot p_{1z} + p_{2y} \cdot p_{2z} + p_{3y} \cdot p_{3z} = 0$$

$$p_{1x} \cdot p_{1z} + p_{2x} \cdot p_{2z} + p_{3x} \cdot p_{3z} = 0$$

$$p_{1z} \cdot p_{1z} + p_{2z} \cdot p_{2z} + p_{3z} \cdot p_{3z} = 1 \quad \checkmark$$

Three of these equations are repeated and only six-marked \checkmark are distinct. Therefore, combining these six equations with (3-10), (3-11) and (3-12) to obtain the following equations

$$p_{1x} \cdot m_{1x} + p_{1y} \cdot m_{1y} + p_{1z} \cdot m_{1z} = 0$$

$$p_{2x} \cdot m_{2x} + p_{2y} \cdot m_{2y} + p_{2z} \cdot m_{2z} = 0$$

$$p_{3x} \cdot m_{3x} + p_{3y} \cdot m_{3y} + p_{3z} \cdot m_{3z} = 0$$

$$p_{1x} \cdot p_{1y} + p_{2x} \cdot p_{2y} + p_{3x} \cdot p_{3y} = 0$$

$$p_{1y} \cdot p_{1z} + p_{2y} \cdot p_{2z} + p_{3y} \cdot p_{3z} = 0$$

$$p_{1x} \cdot p_{1z} + p_{2x} \cdot p_{2z} + p_{3x} \cdot p_{3z} = 0$$

$$p_{1x} \cdot p_{1x} + p_{2x} \cdot p_{2x} + p_{3x} \cdot p_{3x} = 1$$

$$p_{1y} \cdot p_{1y} + p_{2y} \cdot p_{2y} + p_{3y} \cdot p_{3y} = 1$$

$$p_{1z} \cdot p_{1z} + p_{2z} \cdot p_{2z} + p_{3z} \cdot p_{3z} = 1$$

Platform joint vector p_1, p_2, p_3 can be solved from previous equations. There is no closed-form solution for the non-linear equations. With an iterative approach, the problem can be solved by numerical methods such as Newton Raphson Method. Numerical iterative methods are computationally expensive and therefore cannot be used in real time applications. Therefore, the kinematics solution of spherical parallel manipulator cannot be use in real time application by solving non-linear equations.

3.3.4. Numerical Example of Direct Kinematics

The numerical example of SPBS is presented in order to illustrate the DK procedures described in section 3.3.1. In the example, the active joint vectors are $v_{a1} [1, 0, 0]^T$, $v_{a2} [-0.5, 0.866, 0]^T$ and $v_{a3} [-0.5, -0.866, 0]^T$. Figure 3-44 shows the home position of SPBS that middle joint vectors are $m_1 [0, 1, 0]^T$, $m_2 [-0.866, -0.5, 0]^T$, $m_3 [0.866, -0.5, 0]^T$. Three platform joint vectors can be obtained by cosine law.

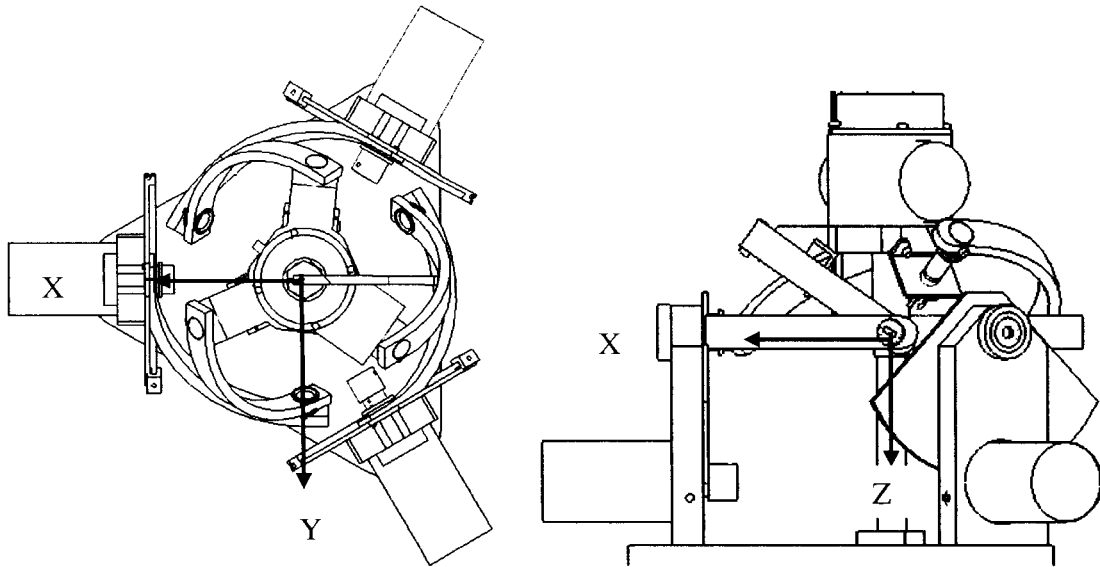


Figure 3-44 Home position of SPBS (top and side view)

The home position of branch 1 and the middle joint vector m_1 are defined and the relation between m_1 and p_1 is expressed in (3-10).

Substituting $m_1 [0, 1, 0]^T$ into equation (3-10) yields

$$p_{1x} \cdot m_{1x} + p_{1y} \cdot m_{1y} + p_{1z} \cdot m_{1z} = 0$$

$$p_{1y} = 0 \quad (3-13)$$

Substituting $m_2 [-0.866, -0.5, 0]^T$ into equation (3-11) yields

$$p_{2x} \cdot m_{2x} + p_{2y} \cdot m_{2y} + p_{2z} \cdot m_{2z} = 0$$

$$-0.866 p_{2x} + (-0.5) p_{2y} = 0 \quad (3-14)$$

Substituting $m_3 [0.866, -0.5, 0]^T$ into equation (3-12) yields

$$p_{3x} \cdot m_{3x} + p_{3y} \cdot m_{3y} + p_{3z} \cdot m_{3z} = 0$$

$$0.866 p_x + (-0.5) p_{3y} = 0 \quad (3-15)$$

$$p_{1y} = 0 \quad (3-13)$$

$$-0.866p_{2x} + (-0.5)p_{2y} = 0 \quad (3-14)$$

$$0.866p_{3x} + (-0.5)p_{3y} = 0 \quad (3-15)$$

$$p_{1x} \cdot p_{2x} + p_{1y} \cdot p_{2y} + p_{1z} \cdot p_{2z} = 0 = 0 \quad (3-16)$$

$$p_{2x} \cdot p_{3x} + p_{2y} \cdot p_{3y} + p_{2z} \cdot p_{3z} = 0 \quad (3-17)$$

$$p_{1x} \cdot p_{3x} + p_{3y} \cdot p_{1y} + p_{3z} \cdot p_{1z} = 0 \quad (3-18)$$

$$p_{1x} \cdot p_{1x} + p_{2x} \cdot p_{2x} + p_{3x} \cdot p_{3x} = 1 \quad (3-19)$$

$$p_{1y} \cdot p_{1y} + p_{2y} \cdot p_{2y} + p_{3y} \cdot p_{3y} = 1 \quad (3-20)$$

$$p_{1z} \cdot p_{1z} + p_{2z} \cdot p_{2z} + p_{3z} \cdot p_{3z} = 1 \quad (3-21)$$

Numerical software, Maple, is used to solve equations (3-13) ~ (3-21). Eight solution sets are obtained from the previous equations. The numerical results are shown in Table 3-2 and Figure 3-45 illustrates configurations corresponding to these solutions. Since there are eight possible solution sets, it is necessary to check the physical device to identify the real position matches the numerical solution.

Table 3-2 Position of the moving platform of the eight solutions

	Branch 1	Branch 2	Branch 3
1	$[-.8165, 0., .5773]$	$[-.4083, .7071, -.5773]$	$[-.4083, -.7071, -.5773]$
2	$ [.8165, 0., .5773]$	$ [.4083, -.7071, -.5773]$	$ [.4083, .7071, -.5773]$
3	$ [.8165, 0., .5773]$	$ [-.4083, .7071, .5773]$	$ [-.4083, -.7071, .5773]$
4	$ [-.8165, 0., .5773]$	$ [.4083, -.7071, .5773]$	$ [.4083, .7071, .5773]$
5	$ [.8165, 0., -.5773]$	$ [-.4083, .7071, -.5773]$	$ [-.4083, -.7071, -.5773]$
6	$ [-.8165, 0., -.5773]$	$ [.4083, -.7071, -.5773]$	$ [.4083, .7071, -.5773]$
7	$ [-.8165, 0., -.5773]$	$ [-.4083, .7071, .5773]$	$ [-.4083, -.7071, .5773]$
8	$ [.8165, 0., -.5773]$	$ [.4083, -.7071, .5773]$	$ [.4083, .7071, .5773]$

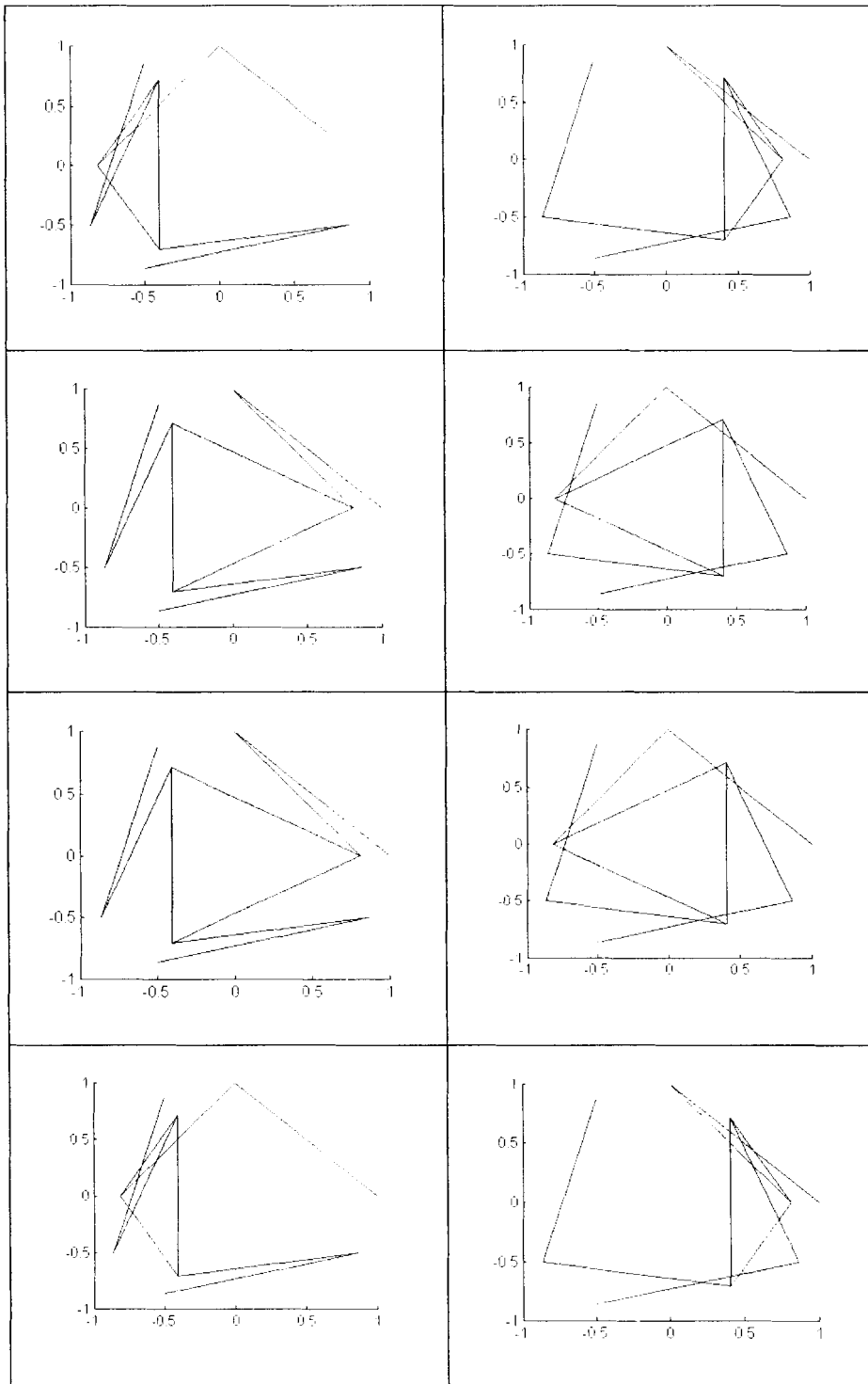


Figure 3-45 The configurations corresponding to the eight solution

The eight solution sets of CAD model are shown in Figure 3-46. By observing this figure, It is found out that only 1 and 5 are physical practical solution. 2, 3, 4, 6, 7 and 8 cause interference between links and platform.

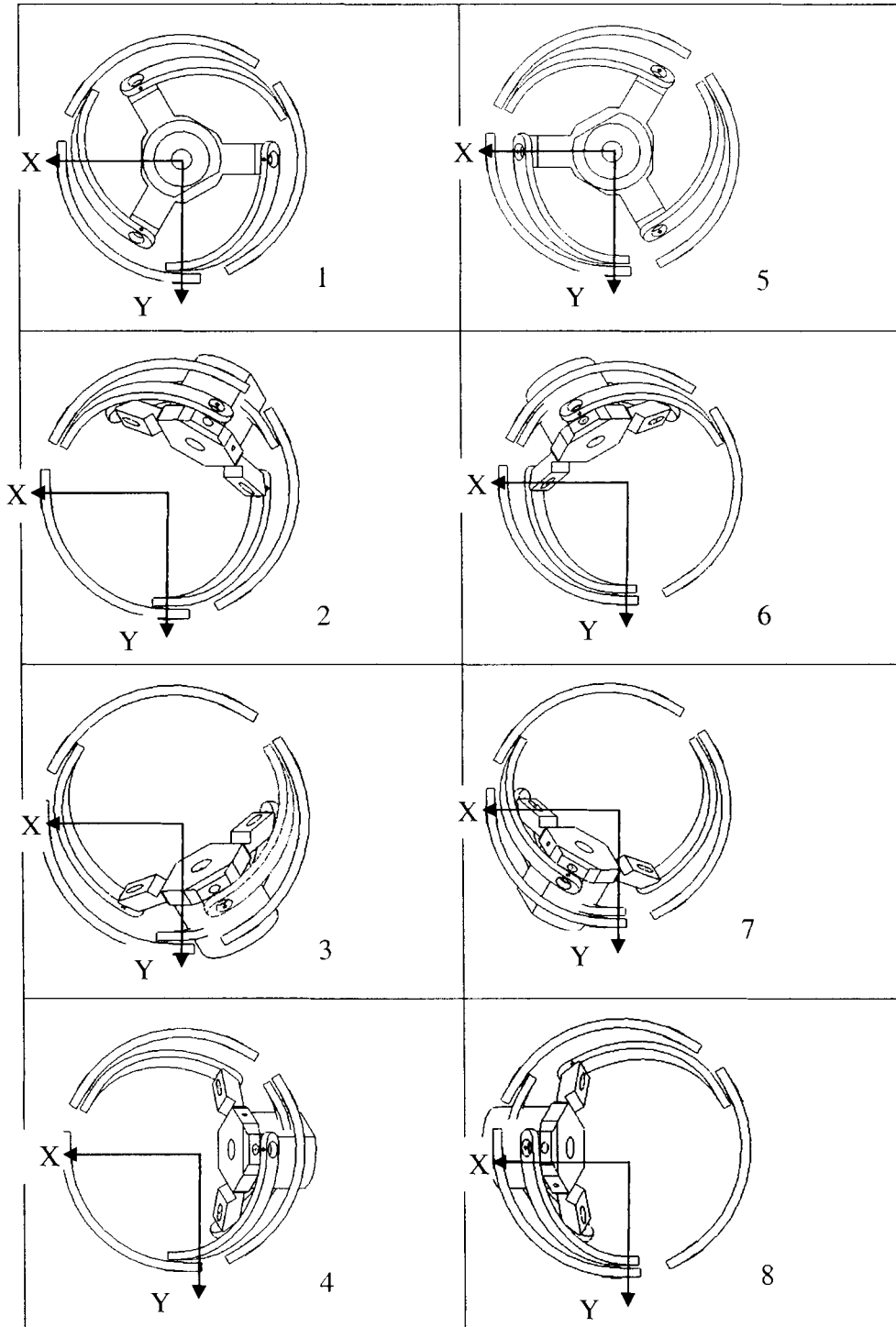


Figure 3-46 The CAD model of corresponding solutions

3.3.5. Experimental setup and measurement result

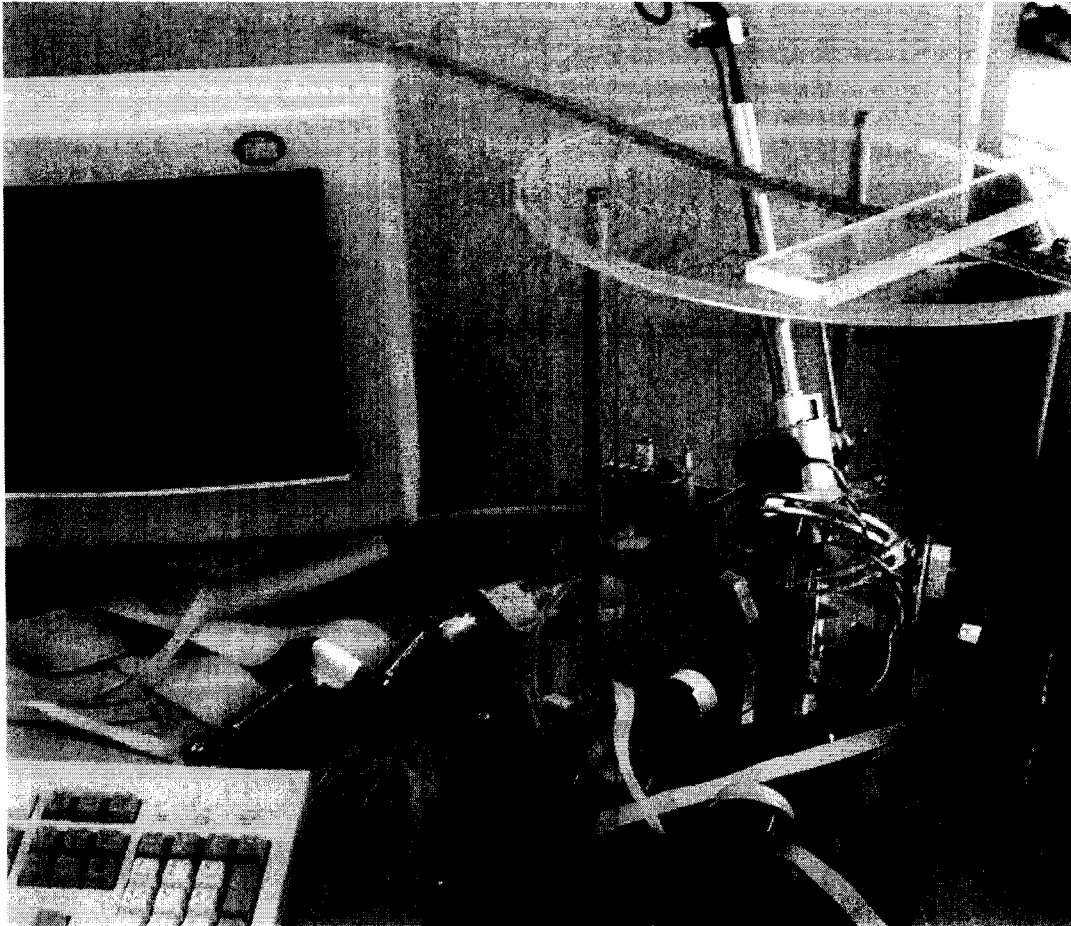


Figure 3-47 Experimental setup for measurement

Shown in Figure 3-47, the experimental hardware setup includes haptic device, motor, encoder, counter board, and I/O card: This setup has four Maxon EC 118891 motors. The encoders used for the haptic device are HEDS 5540 with 5v supply voltage and 500 counts per turn resolution. Counter board (MC-4 A4) counts the encoder pulses. The encoder of each channel is connected to this card. The I/O card, CYDDA 06, consists of two parts: 6 channels of Digital-to-Analog converter (DAC) and a digital I/O. DAC is used for controlling the speed of the motors, where the digital I/O controls the direction which each motor rotates. The output current of the board is not enough to drive the

motors so the outputs go through an amplifier and then go to the motors. Potentiometer (3310 - 9 mm Square Sealed Panel Control): There are four potentiometers attached to the haptic device for identifying the position of the platform. These potentiometers are connected to the CYDDA card.

The software setup in QNX UNIX based pc has two files to run the setup. The header file contains functions for initializing the system, reading the encoder counts, setting the speed and direction of the motors, sending commands to the motors and so on. The main program calls the functions of header file. The encoder channels can be read and can display the count on the screen. There are also functions for sending commands to the motors which get the speed and the channel number and direction and send a voltage to the specified motor.

Measuring the position displacement is easier than that of angles α and β ; therefore, the (x, y) position of the end effector is measured instead of the angles. After obtaining the position of the end effector, the associated angles α and β can be determined uniquely from the following equation, $\alpha = \tan^{-1} \frac{y}{L}$ and $\beta = \tan^{-1} \frac{x}{L}$

In addition, the rotation matrix R is obtained as $R = \begin{bmatrix} \cos \beta & \sin \beta \sin \alpha & \sin \beta \cos \alpha \\ 0 & \cos \alpha & -\sin \alpha \\ -\sin \beta & \cos \beta \sin \alpha & \cos \beta \cos \alpha \end{bmatrix}$

The measurement of distance X and Y with respect to the motor angle is shown in Table 3-3. These measurement data are used for training data set of the neural network in section 3.3.6.

Table 3-3 Samples of the measuring data for NN training

X axis	Y axis	Motor 1 encoder	Motor 2 encoder	Motor 3 encoder
0	-3.5	61	13	65
1	-3.5	62	-10	77
2	-3.5	62	-41	82
3	-3.5	62	-69	87
4	-3.5	59	-98	100
5	-3.5	57	-120	101
6	-3.5	51	-150	104

3.3.6. Neural Network Method to solve DK

The direct kinematics of SPBS requires solving a number of nonlinear equations which is not practical for real time application. In this section, neural networks (NN) are trained to compute the DK of SPBS and the purpose of introducing NN is for real time application. Instead of solving nonlinear equations for the DK, neural networks are used to map the input angles of revolute joints to the orientation of the platform. The training data are obtained from inverse kinematic relationships and measured from the experimental prototype model of the platform. Levenberg-Marquardt (LM) algorithm is used to train the neural networks. This model achieves fast convergence. The trained neural networks are used in the real time interface between the graphical model and a SPBS. Simulation and experiments are carried out to verify the performance of the proposed model.

Other approaches for solving the DK problems are based on learning methods. For example, feedforward neural network was used to model the DK of Steward Platform in [101]. Backpropagation learning strategy was used to train the network which resulted in a model where the direct solutions were accurate within a finite bound.

An improved strategy was then proposed by using mapping offset adjustment, which gave better mapping results on the training data set. In [102], polynomial networks were used to model the DK of parallel manipulators, testing was carried out on circular trajectories.

For the case of parallel spherical manipulator, it was found that this model is not suitable for the surgical training application, since the end effector (handle) of the device needs to be positioned in an arbitrary configuration in the workspace instead of following a given trajectory. This means there is no real time solution of DK of the device. However, real time solution is necessary. Furthermore, no experimental studies were carried out in previous works such as [101] and [102].

For the real time surgical training application, model of DK is needed to interface the haptic device and the graphic model. Two tasks are considered for this application. One is to model the DK and the other task is to implement the model to the environment in real time. The relationship of these two tasks is shown in Figure 3-48. The goal of modeling is mapping the motor angles to position and orientation of platform in the workspace. Data are collected either from inverse kinematics model or directly from the experiment prototype of the mechanism. Three motor angles are read from the encoders of these motors through the computer interface. LM algorithm is used to train the networks. After training, a NN model is obtained which can be used for the real time implementation.

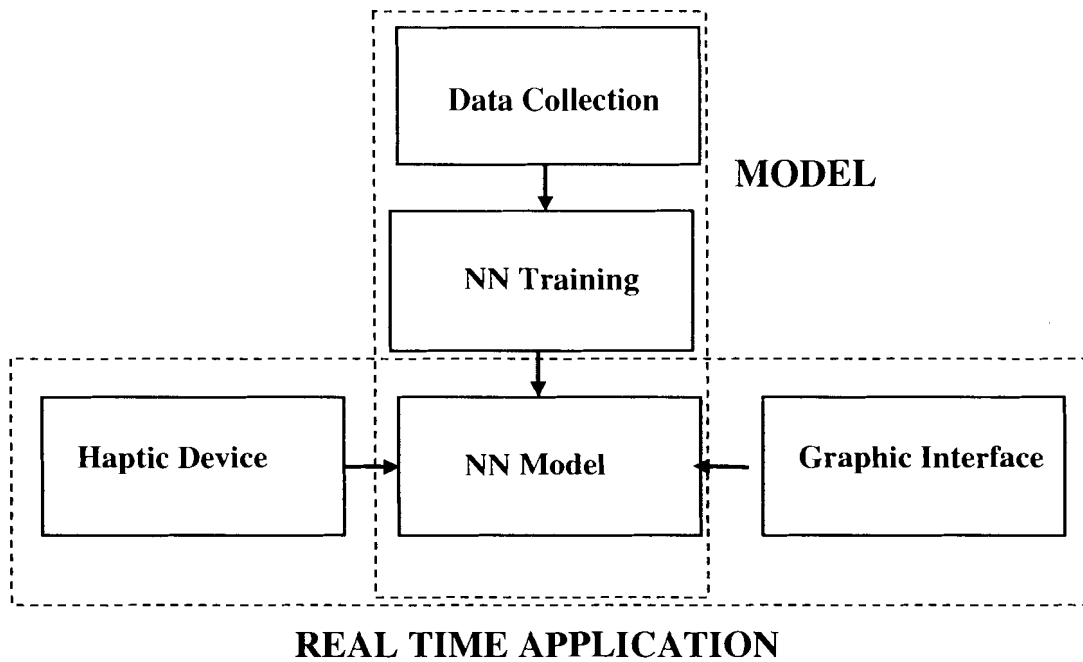


Figure 3-48 Diagram of the neural network for haptic device

The direct kinematics equations of a manipulator express the orientation of the platform frame as a function of the joint variables, as discussed in previous section. For a given configuration of platform as (x, y, θ) , the inverse kinematics can be calculated. In the first trial, a spiral trajectory was generated for the platform and the model of IK was used to calculate corresponding motor angles.

Given the position of N on a unit sphere with respect to the world frame, i.e. (x, y) and the orientation angle of the platform φ along N, the motor angles $(\theta_1, \theta_2, \theta_3)$ can be generated. These data are used to train the proposed networks. In the training process, the angles θ_1, θ_2 and θ_3 are the inputs and the position (x, y) and orientation φ will be the output parameters. The resulting network is used as a model of the DK.

Simulation and experimental results: In order to verify the performance of the proposed NN-based solution methods for DK, simulations and experiments are carried out. In the

simulations, the inverse kinematic equations are used to generate motor angles $\theta_1, \theta_2, \theta_3$. For different platform position and orientation x, y, φ represent in the operation space of SPBS. In the training phase, motor angles are used as input to the networks and orientation of platform form the output. In the testing phase, a new set of input and output data of $\theta_1, \theta_2, \theta_3, x, y, \varphi$ are generated, with $\theta_1, \theta_2, \theta_3$ as input to the trained network, and the output x, y, φ of the network compared to the data generated from inverse kinematic equations to verify the performance of the neural network model.

The test data were generated by using grid of $\Delta x_t, \Delta y_t$, which is different from the training data set. The testing data set is used to verify the generalization capability of the networks. The performance of the model is measured by the following error function

$$err = \sqrt{(x - x_t)^2 + (y - y_t)^2}$$

Where x_t, y_t are the outputs of the network model with the input angles from the testing data set and x, y are true position data used to generate motor angles.

In the first set of simulations, the training data were generated for a fixed orientation of platform $\varphi=0$. In this case, the network has 3 inputs and 2 outputs. The input angles were computed by inverse kinematics equations for given orientation of platform. The training data are generated from the working space $-10 \leq x \leq 10, -10 \leq y \leq 10$ with even grid as Δx_t and Δy_t . After training using the LM algorithm, a neural network model of the DK is obtained. For DK, the inputs are column 3, 4 and 5 of Table 3-3 that is the encoder reading of motor1, 2 and 3. The outputs of column 1 and 2 of Table 3-3 that are the X and Y-axis position of the end effector.

A neural network is trained to model the direct kinematics. The testing results are shown in Figure 3-49. From the figure, it is clear that the NN model gives good approximation of the direct kinematics.

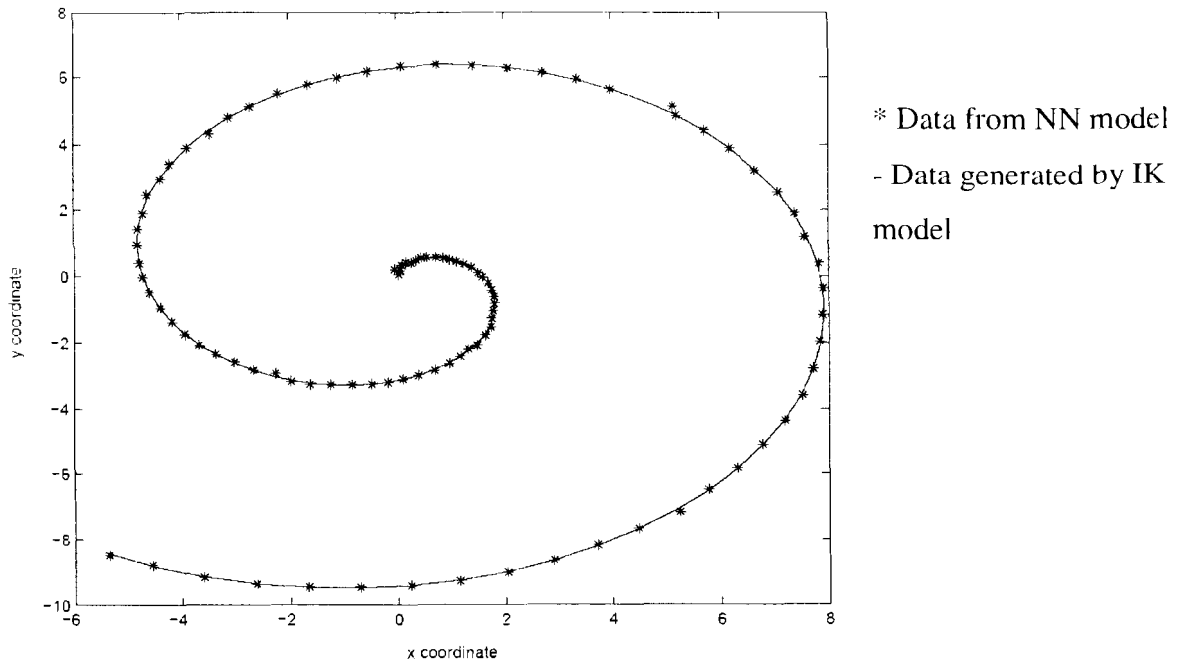


Figure 3-49 Network approximation of spiral trajectory

In the second example, 15 hidden nodes are chosen and initialized the weights and bias of the network randomly, the grid $\Delta x = \Delta y = 1.0$ was used to generate training data. After the training, the neural network model of direct kinematics is obtained. The testing data is generated by using grid of $\Delta x = \Delta y = 0.4$. The mean value of the errors is around 0.3 %. The plot of errors with respect to platform orientation is shown in Figure 3-50 which indicates that the proposed model gives good approximation of the DK of the SPBS.

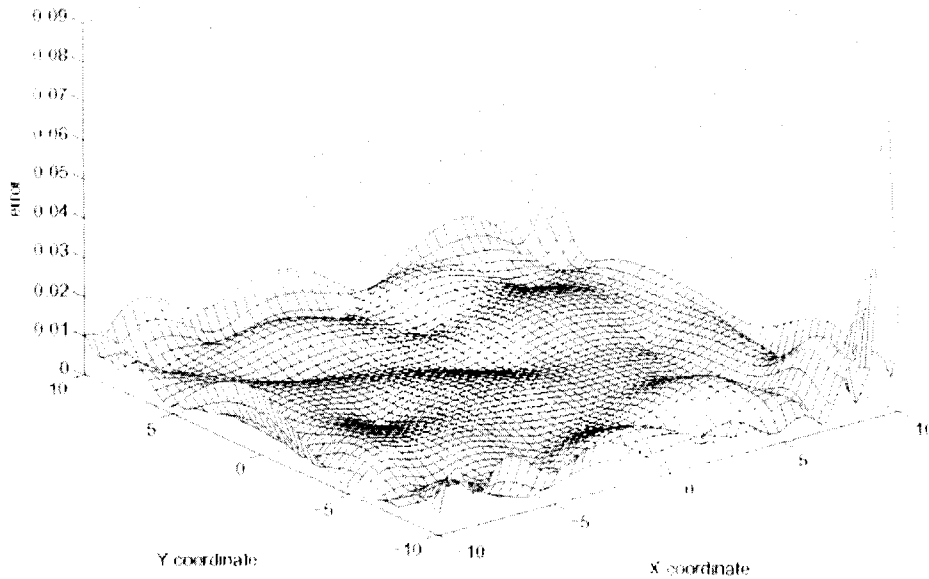


Figure 3-50 Network approximation error of direct kinematics

Furthermore, data from NN model are compared to the experimental data from SPBS. In this comparison, motor angles and orientation of the platform are recorded in the workspace as experimental data. The position data of the model are generated by feeding the angle to the NN model of direct kinematics obtained from training. The (x, y) positions of platform from the model and experiment are shown in Figure 3-51. It shows that for most of the samples, the results from the model match the experimental data well. The approximation error is shown in Figure 3-52. It is found that at the boundary of the workspace, the model error is bigger than that in the middle. The maximum error is around 4 units. This result is expected since the loss of the joints will accumulate error at the boundary. In order to improve the accuracy of the model, experimental measurements are used as training data after which obtained NN model gives better results. The maximum error is about 0.4 units, which is reduced to 10 percent of the NN model obtained from using data from the inverse kinematics.

For haptic device, the errors from NN can be compensated for manually because the user can control the position and orientation of the end effector. For real application of laparoscopic surgery, the error from NN may affect the positional accuracy of the surgical robot. The installation of additional force/pressure sensors on the joint or tool tip increases the positional accuracy of manipulator.

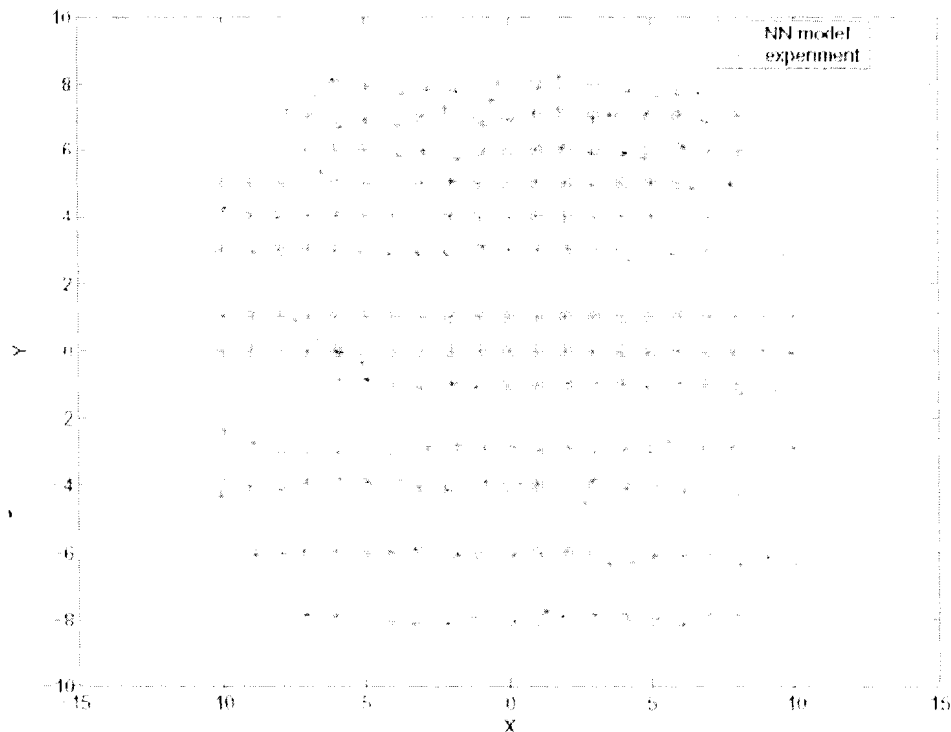


Figure 3-51 Comparison of neural network model and experiment

In this section, neural networks have been used to model the DK of SPBS. It is not necessary to solve non-linear equations. The obtained model gives satisfactory solution for the DK, which suits for real time application. The obtained model can be implemented in SPBS and used in the surgical training environment. This section considered the off line training methods for the model, on line adjustment will be useful for increase the accuracy of the model.

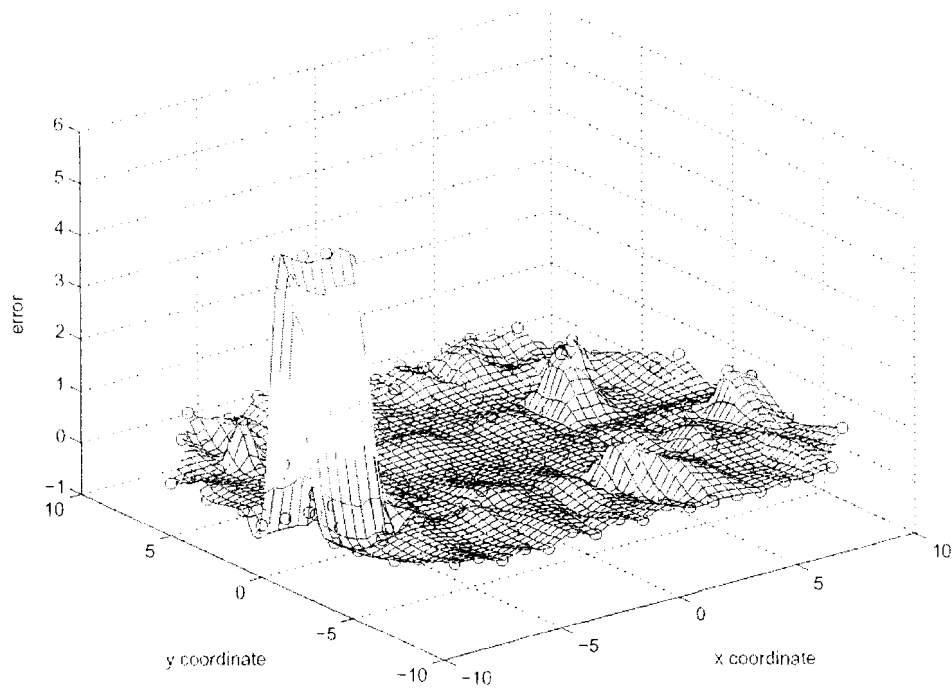


Figure 3-52 Error between neural network model and experiment

3.4. Discussion

Six haptic force feedback devices are proposed, analyzed, designed and manufactured. Different types of motor and linear designs have been synthesized. Electrical motor was selected because of ease of control and non-requirement of extra supplements. For linear motion, both tendon and crank type were built and tested. Wire type offers flexible offset, fast response and small space. Crank slide with cam type occupies bulky space because the link length must be long enough to reach design stroke. The advantage, however, is provision of gear ratio to magnify torque for small motor.

For SFGT and RFGT, the gimbal type structure contains two movable motors that are superior to serial manipulator. Serial manipulators contain only one stationary and three

movable motors for four DOF force feedback. SFGT and RFGT are able to accomplish four DOF functional requirements.

Hybrid spherical parallel mechanism with passive support is a novel design applied to HPST, SPBS, and THT. HPST has a three DOF yoke support to constrain the platform with spherical motion. This constraint can compensate for the misalignment caused by ball joints. However, the rotation motion is not smooth and the user can sense the discontinuities. SPBS and THT are accurate and could operate smoothly that shows later prototypes have better design quality.

SPBS has the advantages of low inertia, lightweight and large workspace that satisfy all the design objectives. SPBS was tested by surgeon who gave positive feedback after manipulation and confirmed the uses of SPBS for surgical simulation. For SPBS, the linear motion guiding tube can be hardened to prevent bending. The linear guide was made from 3/8" aluminum tube and a minor dent on the tube generates resistance when the handle moves up and down. A different material such as stainless steel may substitute for aluminum alloy.

For THT, the movement is smooth and the required machining processes of platform are reduced. However, THT compromised the haptic features. For instance, the movable motor was repositioned from top center of platform to a higher position. This design increases the inertia but reduces the machining processes.

4. Design for Manufacturing

For the development of haptic device, it is important to manufacture the physical hardware for the user to interact with this device. Modeling in CAD software, simulation, and finite element analysis provides visual feedback or theoretical calculations that cannot be replaced by haptic force sensation. “You build a physical prototype to figure out how humans interact with it[103].” The user can interactively manipulate the electro-mechanical haptic device and acquire the force feedback from the device. In addition, the relationship between design and manufacture must be corroborated to build the hardware.

A novel design concept requires multiple developments because of multiple design consideration to become a practical engineering product because of multiple design considerations. For instance, haptic devices are built a various generations with the improvement expressed by the engineering design circles. Figure 4-1 shows the engineering design circle that started with the first design followed by the manufacture and evaluation process. Users can physically interact with the prototype and evaluate the haptic device instead of having it on imagination. Furthermore, the prototype can provide a physical benchmark for implementations with electronic control motors. The design process includes design synthesis, conceptual design, and detail design. The arrow between design and manufacturing illustrates that the design for manufacturing analysis is carried as concurrent engineering. Concurrent engineering (CE) is a method that uses perspective from multiple disciplines to focus on the design and manufacturing sequences. The objective of conducting CE is to avoid production of part features, that are expensive, and to make optimal choices of the materials. This results in improvised quality of early design decisions and a significant impact on the product cost[104]. More than 70 % of the cost is determined in the design stages[105].

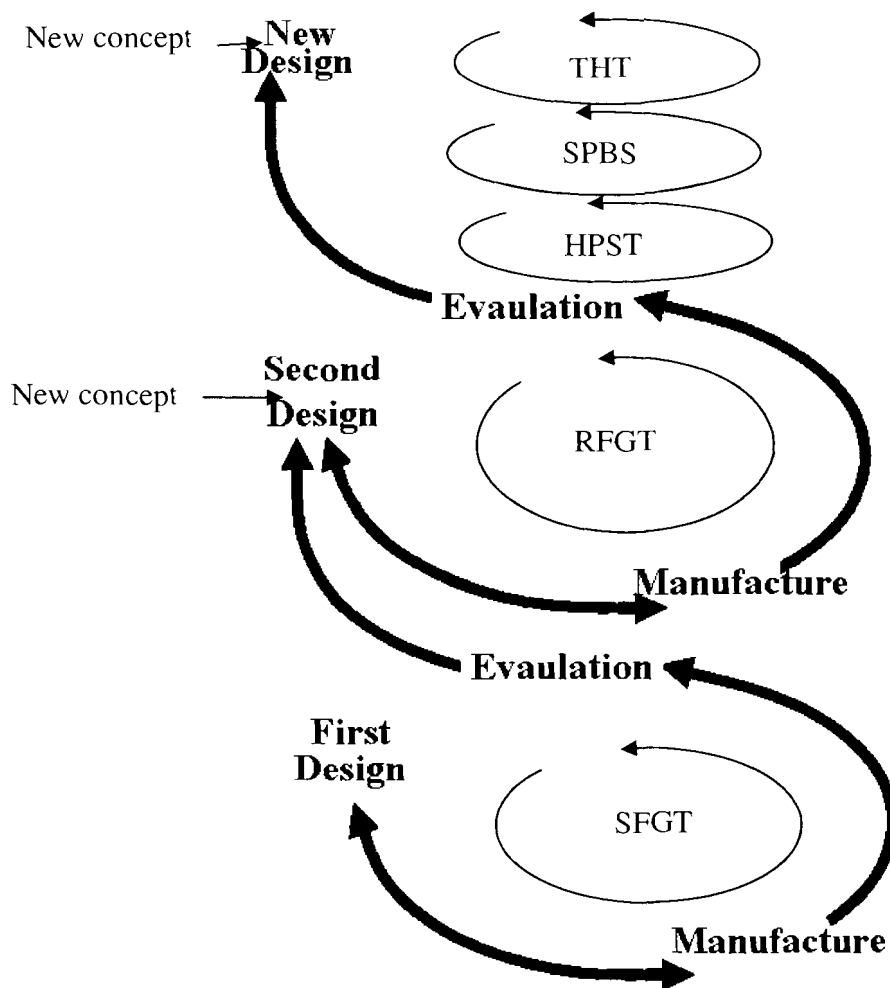


Figure 4-1 Engineering design circles

The CE viewpoint establishes guidelines for intensive involvement of designer (in this case, me) and machine shop in the research, with the goals of improving project coordination and communication. In the early design stage, concept drawings, and sketches are provided to the machine shop. Frequent discussions are developed between designer and manufacturer so that manufacturing site realizes the design concept and provides valuable suggestions from a manufacturing point-of-view.

After building the prototype device, the designated functions are investigated. The investigation includes examination and evaluation to identify advantages and limitations of the prototype. These advantages and limitations of haptic devices have been discussed in chapter 3. The evaluation results are used as a reference for the next design.

Therefore, the next design is developed based on the new design concept as well as the improvement from previous design. The traditional approach to product development requires a substantial amount of time for the product design from its initial configuration to the final product[105].

This chapter is organized as follows: In section 4.1, the guidelines for manufacture and assembly are reviewed and applied to the haptic device. In section 4.2, the bill of materials of SPBS is discussed. In section 4.3, the machining processes for SPBS links are analyzed. In section 4.4, the manufacturing cost structure is analyzed and applied to cost estimation of SPBS. In section 4.5, dimension and tolerance for manufacturing is presented. The accuracy inspection of SPBS is discussed.

4.1. Design Guidelines for Manufacture and Assembly

Otto and Wood conducted a literature review on design for manufacturing and assembly (DFM&A)[106]. Design for manufacturing (DFM) and design for assembly (DFA) are the two components of DFM&A analyses. DFM studies the possibility of minimizing the part numbers of a design while DFA aims at simplifying the methods and/or processes for the attachment of parts. DFA plays an important role in reducing this cost that can reduce the complexity of the assembly process, the number of sub-assemblies, thus reducing the total cost. Although DFM and DFA employ different approaches, their purpose is the same.

The DFA guidelines are the fundamental rules for designers to consider that are listed in Appendix B. Because of the complex mechanical designs, guidelines for both DFM and DFA can be classified into a few categories. For the family of DFM[106], the categories are injection-molded, sheet-formed, cast and machined design guidelines. These guidelines can be used for all mechanical designs. However, only the machined part design guidelines are applied because the first three guidelines are more feasible for

different materials or mass production work. In the design prototype stage, the guidelines for injection molded and casting requires special are applied for mass production. For DFA, the categories include system, handling, insertion, and joining guidelines. The taxonomy of DFM&A guidelines is summarized in Figure 4-2.

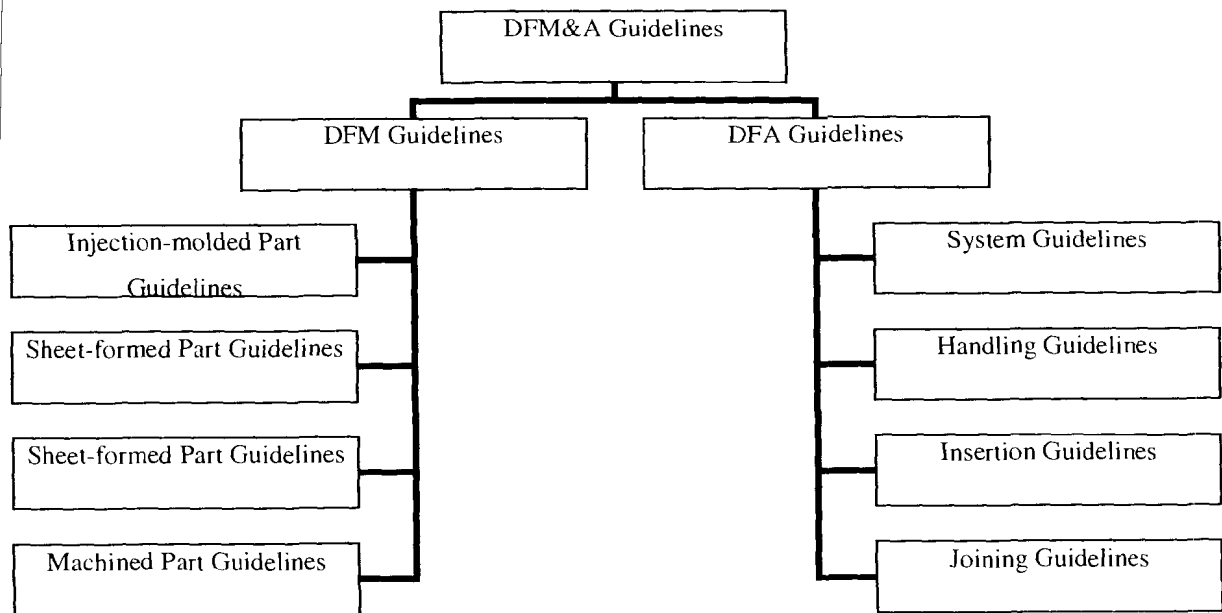


Figure 4-2 Taxonomy of DFM&A Guidelines

Though DFM and DFA share the same purposes, there are potential conflicts between them. For example, a design that combines parts into a module (single part) would simplify the assembly but might complicate the manufacturing of the module. An example of the conflict between SPBS and THT platform is discussed in this section. In the development of haptic devices, the balance among the design for function and manufacturing is necessary. In this research, functions for haptic device such as low inertia, less friction and smooth motion are the important design objectives.

The major manufacturing activities of this research concentrate on machining parts. The applicable guidelines for the haptic devices are in the category of machining DFM and its system and joining for DFA. The following sections analyze the application of these guidelines to the design developed in this research. Comparisons are made between

generations of the device designs and the improvements with the production costs benchmarked.

Based on the characteristic of the research designs, the applicable guidelines for haptic devices are listed below:

- Reduce design production cost
- Enhance design quality
- Symmetrize parts
- Reduce number of parts
- Standardize fastening parts

Enhancing design quality of the haptic device results in low inertia, less friction and less dead weight which is achieved by introducing passive spherical joint. Among these guidelines, reducing the number of parts has the observable effect between the generations of the haptic device designs. Within five generations of haptic designs, the number of custom parts has been reduced from 85 of the first generation to 18 of the fifth generation. The plot of the part number reduction between every two generations is illustrated in Figure 4-3. The part number contains only customized parts but not standard parts such as screws, washer, and motors. These parts can be purchased. Shown in Figure 4-4 , the RFGT contains 68 parts and Figure 4-5 shows the parts of SPBS containing fewer parts than RFGT. In addition, the estimated manufacturing cost is shown in Figure 4-3. This cost is provided by a prototype machine shop. The cost of THT type is based on one piece which means it is single (half of THT).

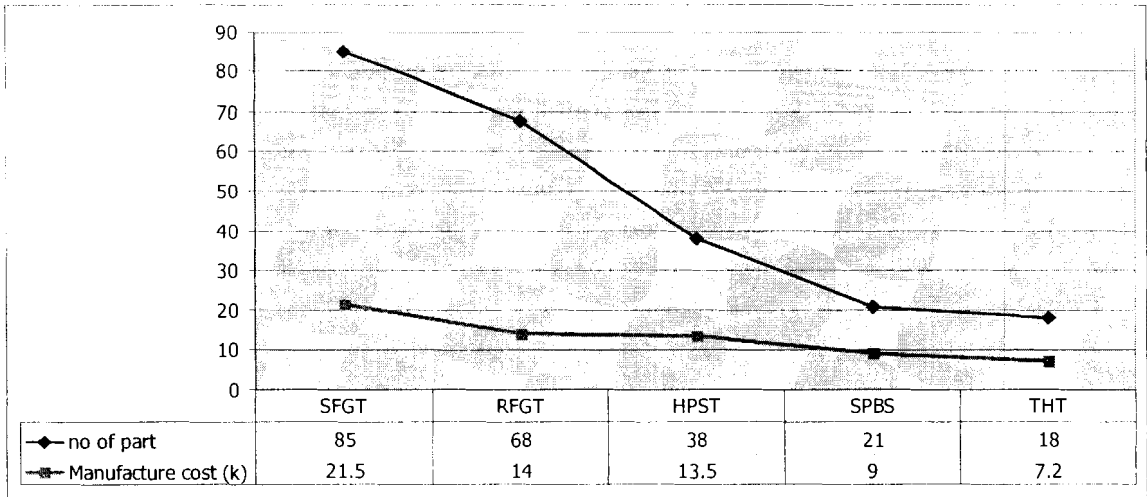


Figure 4-3 Number of parts and manufacturing cost between generations

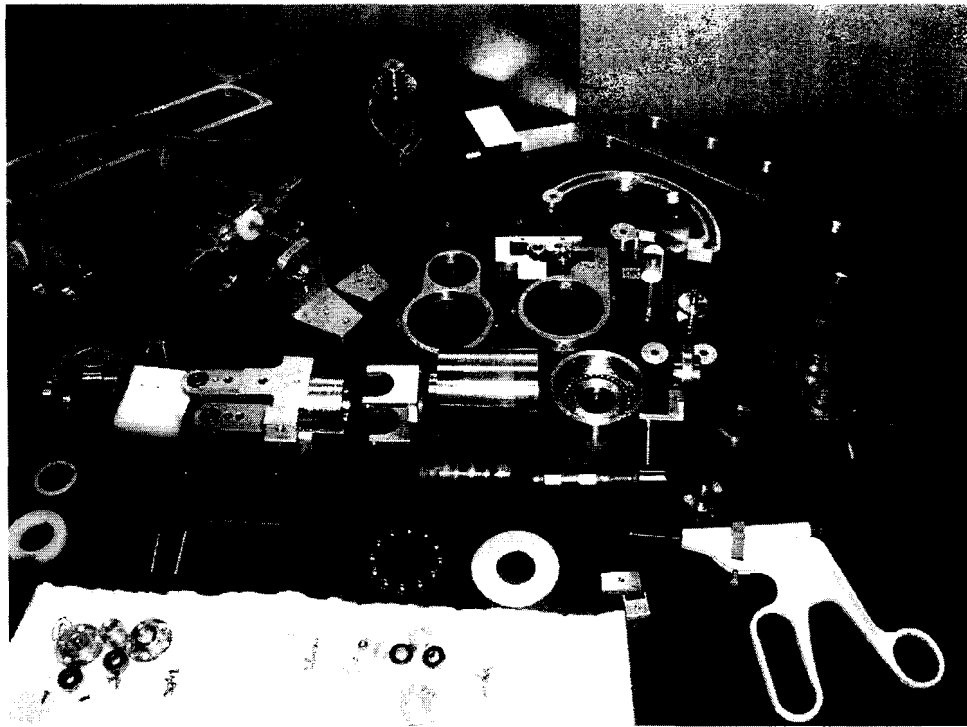
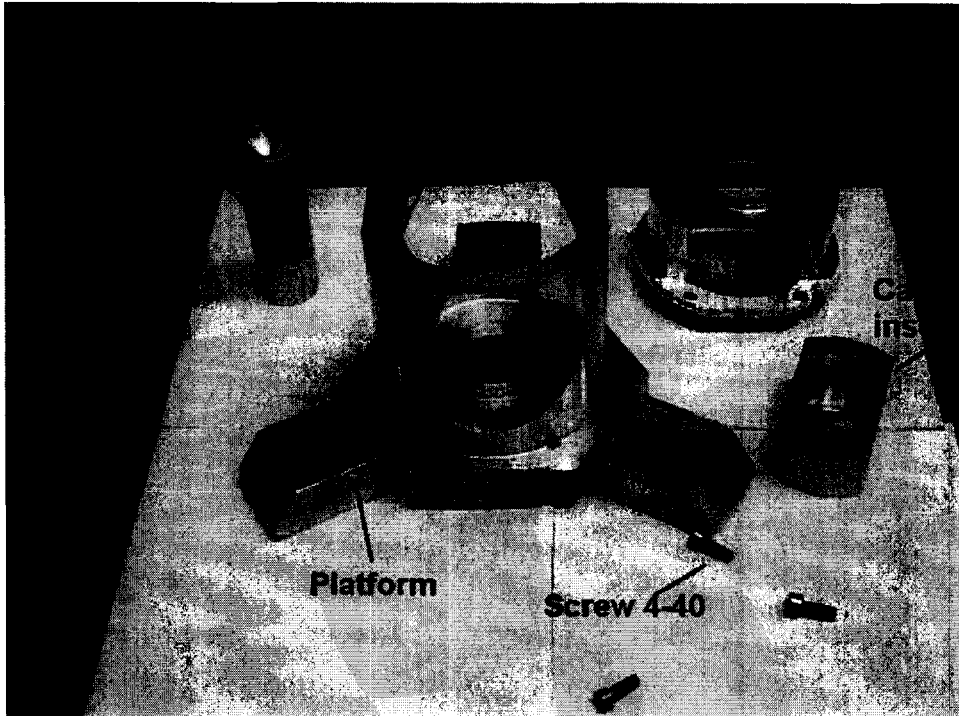
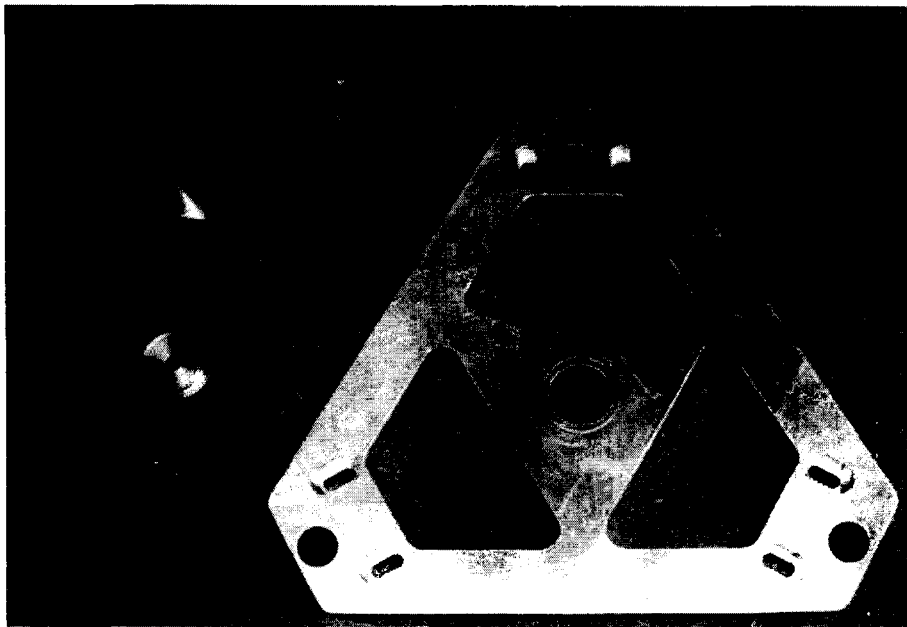


Figure 4-4 Components of RFGT



Components of SPBS platform



Components of SPBS base plate

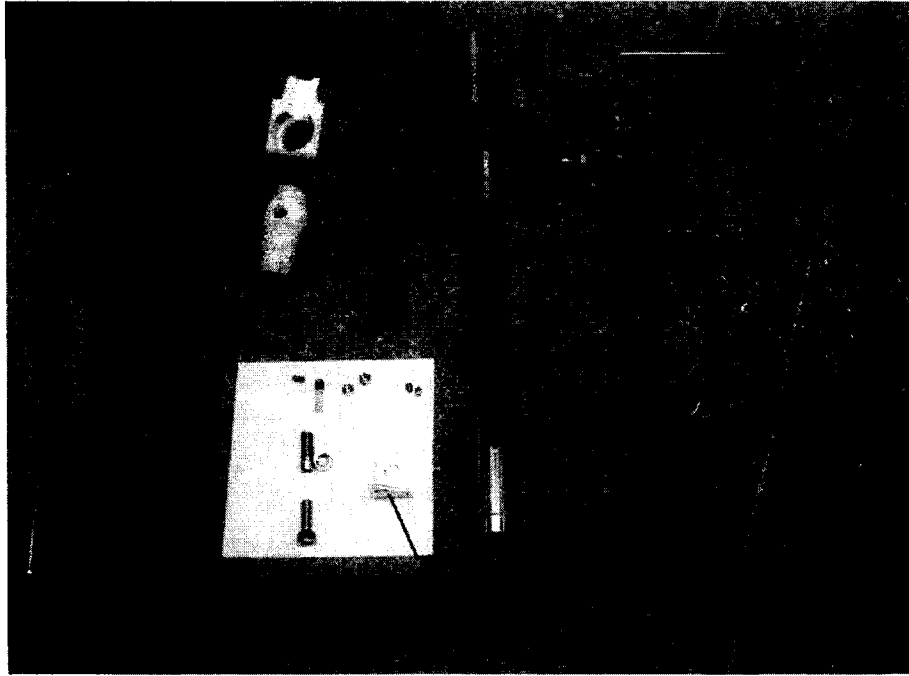


Figure 4-5 Components of SPBS linear guide

The first and second haptic devices, SFGT and RFGT, are designed without considering DFM&A because function generation and concept proofing are the design objectives. At this stage, it is necessary to ensure that function specifications such as low inertia, low friction, and four DOF kinematics motion are satisfied before considering DFM&A. Since DFM&A are not conducted yet, the RFGT contains 68 parts that are three times more than SPBS and THT prototype. As shown in Figure 4-6, the two-DOF bracket of RFGT contains 37 parts. From the functional point of view, the bracket is able to provide smooth force feedback for both rotation and linear motion. From the manufacturing point of view, it contains too many parts, which can be reduced by next design. From the assembly point of view, the customized bearing has more than twenty stainless steel beads that are difficult to assemble.

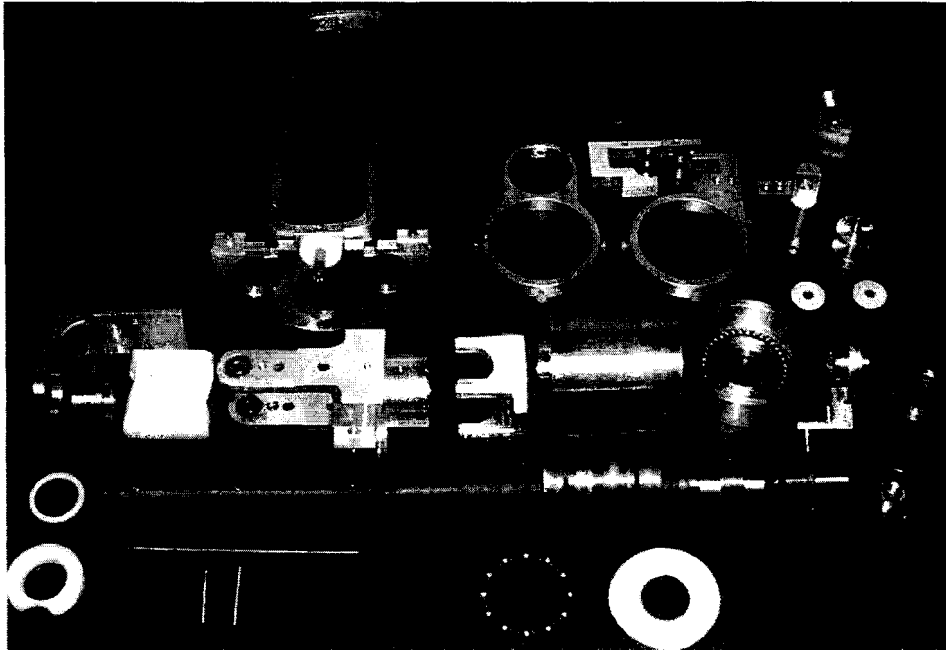


Figure 4-6 Customized bearing and components of RFGT bracket

After evaluating the first two prototypes, the DFM&A are conducted for HPST, SPBS, and THT. The reduction of part numbers results from the following design improvements:

1. Simplify parts
2. Share parts
3. Integrate parts into module

Parts have been simplified, in the aspect of manufacturing, by providing multiple manufacturing options to the machine shop. Simplification of the part for manufacturing does not compromise on functionality of the parts. Symmetrical branches of HPST, SPBS, and THT achieve parts sharing. Shown in Figure 4-7 (a), one branch of SPBS includes inner link, outer link, joints, bushing, cam, pulley, and motor bracket. Shown in Figure 4-7 (b), the top view of SPBS illustrates that the three branches are identical. The revolute joint is composed of bushings, washers, pins, and setscrews that had been modularized to the combination of single bushing and setscrews. In this design, bushing is a special bearing which is a simple bearing without additional components such as ball.

The design follows the guidelines of DFM and the part numbers have been greatly reduced between every generation.

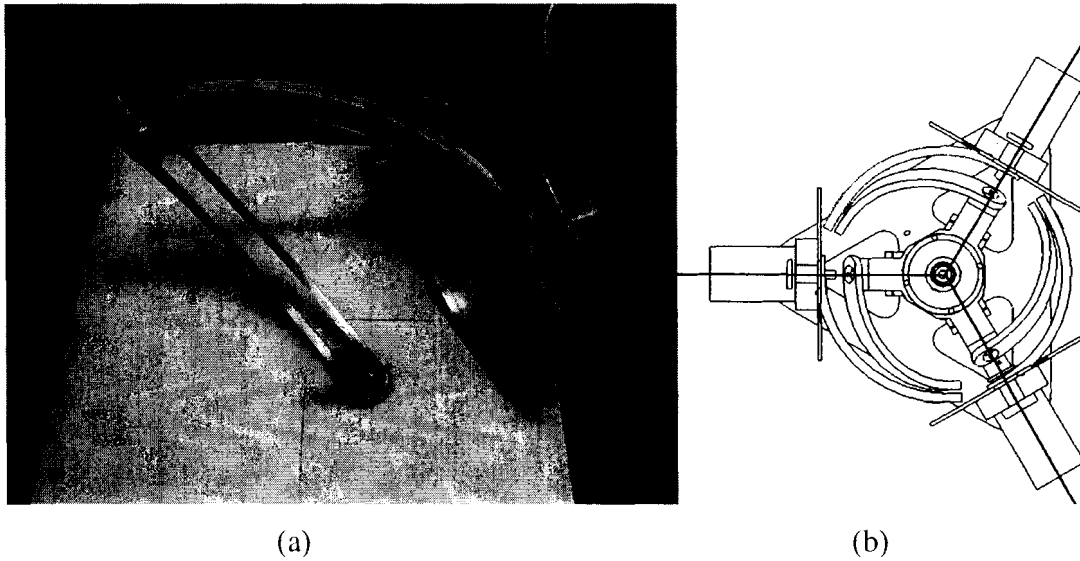


Figure 4-7 Symmetrical branch design of haptic device

As shown in Figure 4-8, the platform of SPBS is machined from one solid aluminum block which requires 6 hours of CNC machining process. The one-piece platform is able to provide firm installation of the linear motor as the installation passes through the center bore. On the right side, the platform of THT is made of a round aluminum plate which can be machined by lathe and milling machine within 1 hour. A motor mount and support is installed for the motor. For SPBS, the motor weight is located on the center of platform, which maintains the balance of the load. For THT, the motor weight is located off-center from the platform center, thus causing unbalance due to hanging weight. The comparison of features of SPBS and THT is listed in Table 4-1.

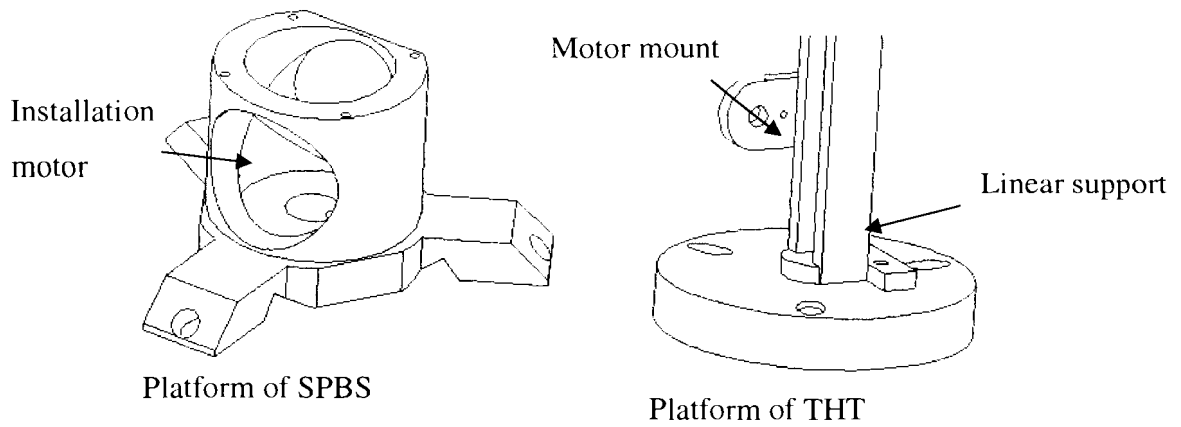


Figure 4-8 Platform of SPBS and THT

Table 4-1 Platform of SPBS and THT

	SPBS	THT
Number of parts	1	3
Machining time (Hr)	6	1
Assembly time (Hr)	0 (does not require assembly)	0.5
Motor weight center (inertia consideration)	On center, low	Off center, high

Compact connecting pin is an example of integration of parts into module. Figure 3-32 shows the stainless steel ball support and three connecting pins. These pins provide rigid and frictionless support to the platform. The connecting pin is a simplified form of the connecting unit of HPST. HPST contains a connecting assembly unit of HPST with a stainless pin, bushing rod, support frame, and washers. The high stiffness stainless steel pin needs to take higher stress because of the tiny contact surface area.

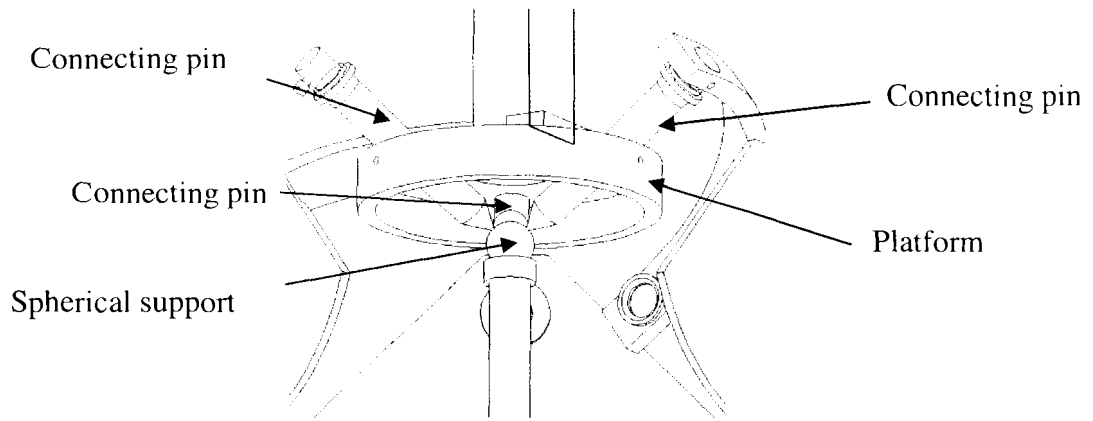


Figure 4-9 Connecting pin of THT

The support of HPST, SPBS, and THT is an example of reducing number of parts guidelines. Figure 4-10 shows the platform support of HPST and THT. The support of HPST contains eleven parts that include base, bushing, yoke fork, bearing, O-ring, and bushing. SPBS and THT platform support contain only three parts that are stainless ball, rod support, and base.

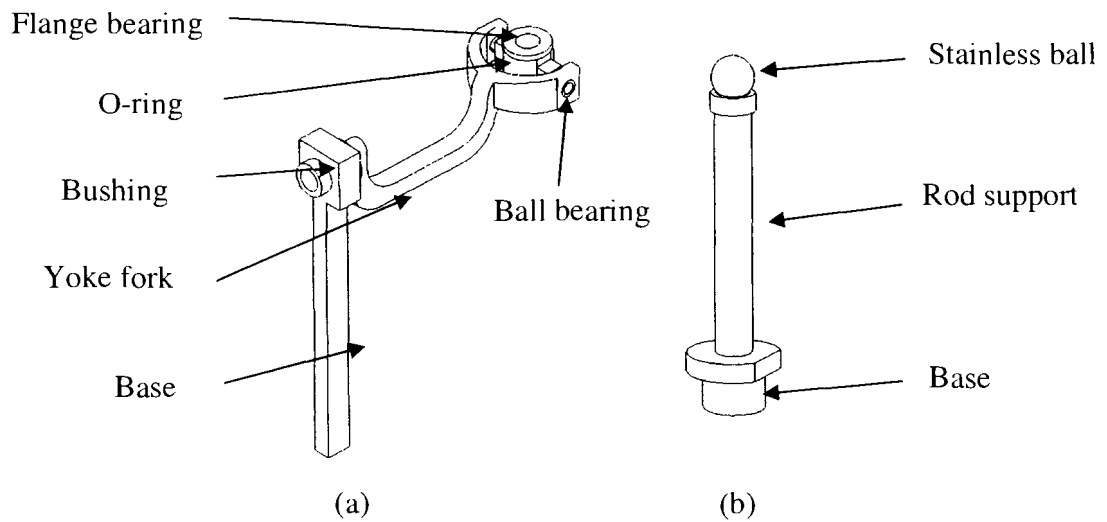


Figure 4-10 Platform support of HPST and THT

4.2. Bill of Materials

Bill of materials (BOM) lists parts, sub assemblies, and raw materials that constitute the assembly. The BOM is an important document associated with the manufacturing process. Maintaining BOM accuracy is essential when considering the substantial impact on cost and production management. The important relationship of cost analysis and engineering bill of materials are discussed by Ostwald[107].

The BOM of SPBS is discussed in this section in order to demonstrate the part construction. Shown in Table 4-2, BOM includes:

1. The total number of components
2. Parts number of each part.
3. Part name, with each name based on its function or shape.
4. The material used for each part, which includes aluminum alloy, brass, stainless steel, and nylon.
5. Customized or stand part; Customized part must be manufactured by machine shop while standard parts, such as screw, nuts, washers and motors, can be purchased.
6. Quantity used for each part.
7. Machining time for each part.
8. Assembling time for each part.
9. Material cost per unit.

Table 4-2 BOM of SPBS

NO	C/S	QTY	Part name	Material	Machining time	Assembly time	Material cost (unit)
1	C	1	Base plate	AL	2	0.25	150
2	S	1	10 24 screw	SS	0	0.1	0.05
3	S	1	Base washer	Brass	0	0.1	0.5
4	C	1	Ball support	SS	1.5	0.5	30
5	C	3	Bracket motor	AL	1.5	0.25	80
6	S	3	Retaining washer	Brass	0	0.25	1
7	C	3	Bracket bushing	AL	0.5	0.25	3
8	C	3	Brass bushing	Brass	0.5	0.25	2
9	S	6	8 32 screw	SS	0	0.1	0.05
10	S	6	4 40 screw	SS	0	0.1	0.05
11	C	3	Cam	AL	1	1	80
12	C	3	Passive link	AL	0.5	0.5	40
13	C	3	Active link	AL	0.5	0.5	40
14	C	1	Platform	AL	6	0.5	60
15	C	1	Rod center	AL	0.5	0.25	50
16	C	1	Cap platform	AL	1	0.1	20
17	C	1	Tube	AL	0.25	0.1	10
18	S	1	Handle	SS	0.25	0.25	50
19	C	1	Up/down pulley	Nylon	1.25	0.5	5
20	C	1	Up/down guide	Nylon	1	0.5	10
21	C	1	Tube cap	Al	1.25	0.25	15
22	S	1	M5 screw	SS	0	0.1	0.5
23	C	3	Link bearing	SS	1.5	0.75	5
24	C	3	Platform link	SS	1.5	1	5
25	C	1	Link up/down	AL	0.75	0.5	10
26	C	3	Sleeve bearing	Nylon	1.5	0.5	5
27	C	4	Motor pulley	Brass	1	0.25	20
28	S	18	M2	SS	0	0.5	0.2
29	C	1	PLT rod	SS	0	0.25	5
30	S	4	Motor		0	0.25	250

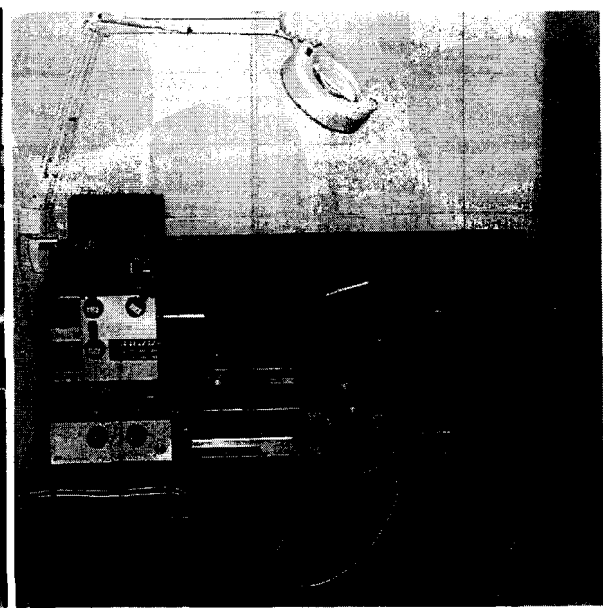
4.3. Machining Processes

In machining processes, both automated machine and non-powered hand tools are used. As shown in Figure 4-11, automated machines include CNC machine center, lathe, and milling machine. The CNC machine center is used for machining most of the customized parts. Lathe machine is used for round parts and milling machine is used for flat surface or/and drill hole.

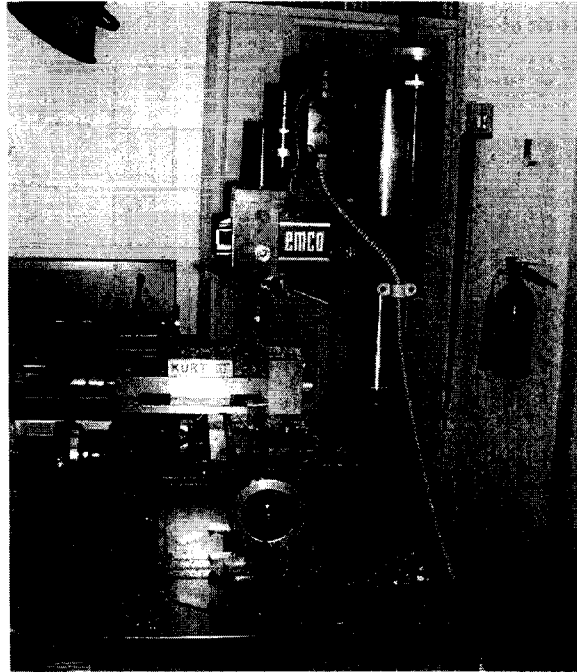
Based on the BOM in previous section, the customized parts of SPBS include platform, base plate, bracket motor, sleeve bearing, ball support, platform link, tube cap, up/down pulley, cam, cap platform, up/down guide, up/down link, passive link and active link that require CNC machine center, lathe, and mill for machining. Bracket bushing, rod center, brass bushing, tube, platform rod, motor pulley, and link bearing require lathe machining.



(a) CNC machine center



(b) Lathe



(c) Milling machine

Figure 4-11 Automated machines

The key design concept for SPBS is in using spherical parallel linkages. In order to achieve the design characteristics, these links require geometrical dimension accuracy in roundness of the arc, and positions of the holes for connection. Accuracy of holes positions on the spherical link is critical to the functionality of the design. The link is designed with two flat ends that can provide ease in measuring position while drilling the bores on both ends.

Shown in Figure 4-12, these links are machined from 1/2-inch thickness aluminum 6061 plate by CNC machine center. The NC files, generated by CAM software, are sent to CNC machine via network. This process conserves the dimensional accuracy in machining process. At the beginning of machining, one side of the aluminum plate is milled to be the datum surface. For each link, three screws are fixed firmly to prevent vibrations while machining. The vibration is caused by the cutting force generated by cutting tool and the force applied on the thin wall (4mm thickness by 12 mm height).

After the CNC machining, the links are machined by milling machine to drill two holes on the ends.

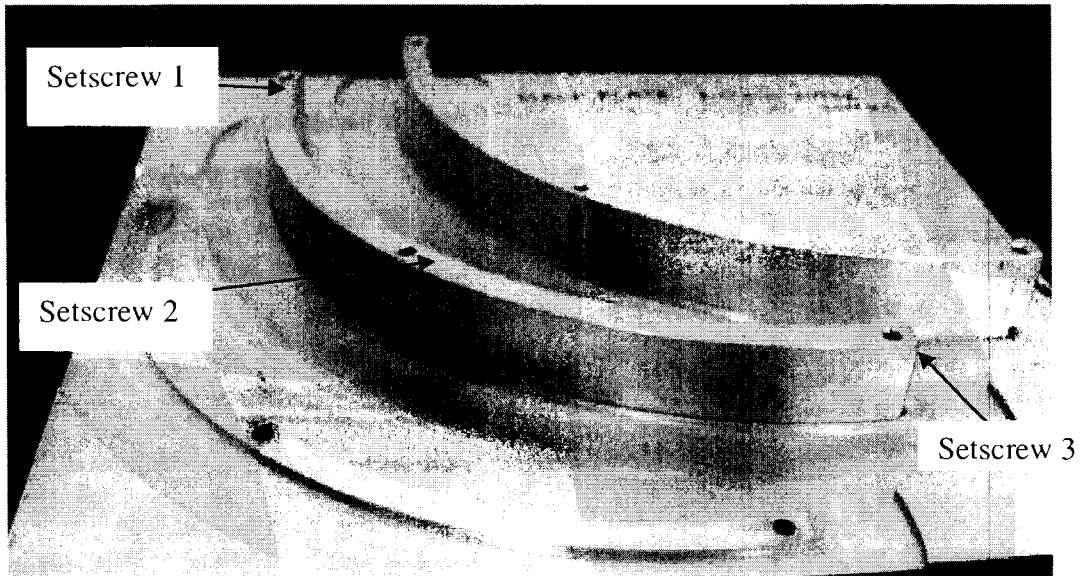


Figure 4-12 Alignment for link arrangement in machining

4.4. Modeling of Manufacturing Cost

The manufacturing cost is modeled to analyze the cost structure of haptic devices. As shown in Figure 4-13, the manufacturing cost can be broken down into piece parts, assembly, and overhead. Piece parts include standard and custom parts. Standard parts can be purchased such as screws, washers, motors, and surgical tools. Custom parts are machined according to design specification. The custom part cost includes material, set up, machining, and tooling. Assembly cost includes labor and tooling. The labor cost could be various and the average labor is 65 ~ 95 CDN per hour. The direct labor machining cost in United States was estimated to be 50 (USD /hr) in 1998[106]. The tooling cost is dependent on the purchase price of the tools and the per-part cost decreases as the total volume increases, which makes it hard to estimate. The overhead

cost includes costs that are not one hundred percent attributable to the activity but are generally associated with the personnel, data processing management, common services, or support of the activity.

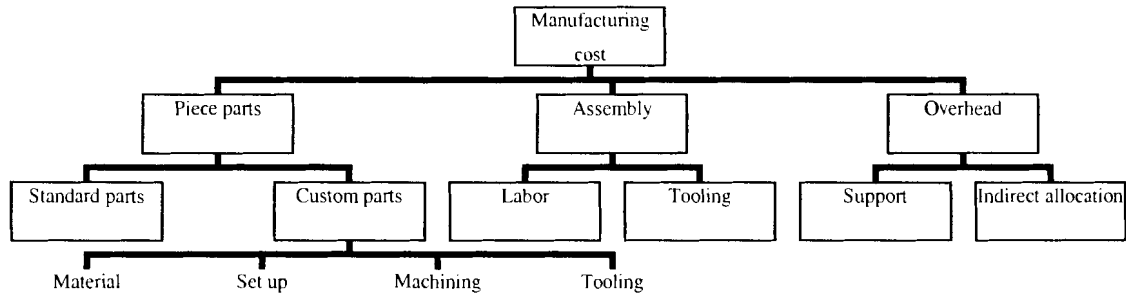


Figure 4-13 Breakdown of manufacturing cost analysis

Based on the BOM and cost structure, the manufacture cost of SPBS is shown in Table 4-3. Those symmetrical parts have three units such as motor bracket, motor pulley, retaining washer, and links. The machining cost in the table is obtained by multiplying the quantity of the parts by the machine cost per unit. The machining cost per unit can be obtained from equation (4-1). The assembly cost in the table is obtained by multiplying the quantity of the parts by the assembly cost. The assembly cost per unit can be obtained from equation (4-2). The part cost in the table is the sum of material cost, machining cost, assembly cost, and setup cost for each part. Cost of machining is the number of hours multiplied with the labor rate per hour.

Table 4-3 List of SPBS manufacturing and materials cost

Name of Part	Q ¹	Setup time	Material cost	Machining cost	Assembly cost	Setup cost	Part cost (\$)
Base plate	1	0.5	150	240	22.5	45	457.5
10 24 screw	1	0	0.05	0	9	0	9.05
Base washer	1	0	0.5	0	9	0	9.5
Ball support	1	0.5	30	180	45	45	300
Motor bracket	3	0.25	150	540	22.5	22.5	735
Retaining washer	3	0	3	0	22.5	0	25.5
Bracket bushing	3	0	9	180	22.5	0	211.5
Brass bushing	3	0.25	6	180	22.5	22.5	231
8 32 screw	6	0	0.3	0	9	0	9.3
4 40 screw	6	0	0.3	0	9	0	9.3
Cam	3	0.25	150	360	90	22.5	622.5
Passive link	3	0.5	120	180	45	45	390
Active link	3	0.5	120	180	45	45	390
Platform	1	0.5	60	600	45	45	750
Center rod	1	0.25	25	60	22.5	22.5	130
Platform cap	1	0.25	20	120	9	22.5	171.5
Tube	1	0.25	10	30	9	22.5	71.5
Handle	1	0.25	50	30	22.5	22.5	125
Pulley up/down	1	0	5	150	45	0	200
Guide up/down	1	0	5	120	45	0	170
Tube cap	1	0	15	150	22.5	0	187.5
M5	1	0	0.05	0	9	0	9.05
Link bearing	3	0.25	10	540	67.5	22.5	640
Platform link	3	0.25	10	540	90	22.5	662.5
Link up/down	1	0.5	10	90	45	45	190
Sleeve bearing	3	0.5	15	540	45	45	645
Motor pulley	4	0.25	20	480	22.5	22.5	545
M2	18	0	0.36	0	45	0	45.36
Platform rod	1	0.25	5	0	22.5	22.5	50
Motor	4	0	1000	0	22.5	0	1022.5
Total		6.25	2000	5490	963	562.5	9015.06

¹ Quantity

The cost structure for manufacture of SPBS is shown in Figure 4-14. The total manufacturing cost includes material, machining, assembly, and set up cost. In this cost analysis, the overhead cost is not included. The machining, assembly, and setup cost is based on equations (4-1), (4-2), and (4-3). The machining cost is 65 % of the total manufacture cost and material cost occupies about 20 %.

$$\text{Machining cost per unit} = \text{Labour rate per hour}^2 \times \text{hours per unit} \quad (4-1)$$

$$\text{Assembly cost per unit} = \text{Labour rate per hour} \times \text{hours per unit} \quad (4-2)$$

$$\text{Set up cost per unit} = \text{Labour rate per hour} \times \text{hours per unit} \quad (4-3)$$

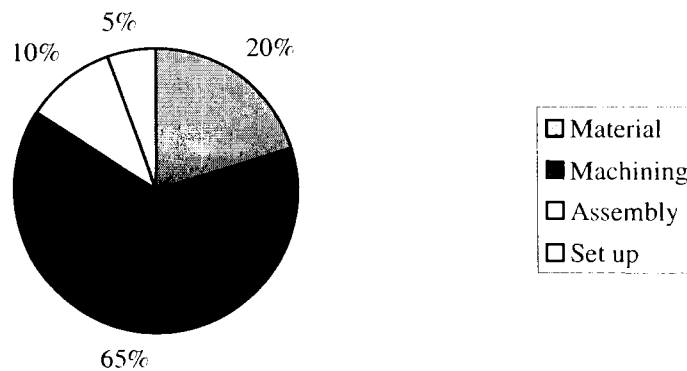


Figure 4-14 Cost structure of SPBS

The manufacturing time (45 Hr) is shown in Figure 4-15. The machining time is around 25 hours which is 60% of the total manufacturing time. Assembly time is 10 hours, dependent on the technology of the machinist. Setup time decreases as the batch size increases because of fewer setup cycles. This manufacturing time structure is for the prototype, which can be reduced for mass production.

² The estimated labor rate per hour is 90 CAD.

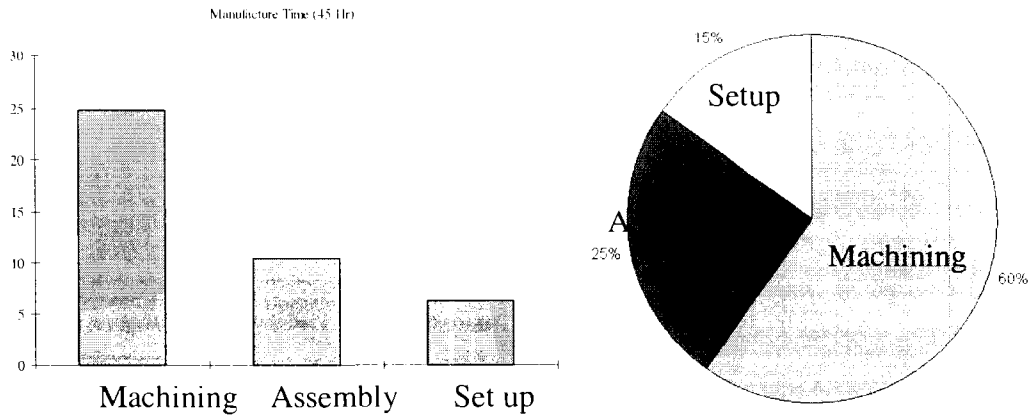


Figure 4-15 Manufacturing time of SPBS

4.5. Tolerance and Accuracy Analysis

In part manufacturing process, several machining steps are involved and datum location is changed as well. Each machining step introduces machining errors that are transformed into next step. New machining errors are introduced as the work piece is moved through the process with changing datum. Machining errors could be created from geometrical and kinematic errors of structural elements, thermal errors, or the static and dynamic errors that have been discussed in Geometric Dimensioning and Tolerancing (GD&T)[108].

Tolerances are used to assure functioning of mechanical parts that are distinct from size or dimensional tolerances. They control the form and orientation (flatness, roundness, perpendicularity) and location (position, concentricity,...) of surfaces and other features as defined in the standard, ANSI Y14.5[109]. The dimensional deviations cause the variation that can be accumulated through an assembly the same as size tolerances. The number of components and geometry variation influence the resultant assembly variations.

The geometric tolerance of haptic device is analyzed in order to calculate the effects on the assemblies along with dimensional variations. For the dimension and tolerance of the design, three type of tolerance are applied. The purpose of choosing different tolerance is for economy. Applying a tighter higher tolerance requires more machining time, special jig, or measurement that means higher expense. In the assembly, different tolerances can be selected to avoid unnecessary waste. As the example of SPBS, the geometric dimensions that effect kinematic motion require higher tolerance. Shown in Table 4-4, three levels of tolerance are chosen. Fine tolerance is applied to the movable parts requiring higher accuracy including, the parts effecting spherical motion such as inner links, outer links and position holes. The middle tolerance is applied to assembly parts that are stationary such as motor bracket and base frame. The non-critical tolerance is applied to dimension which does not require assembly or matching other parts such as the boundary of base frame or the boundary of motor bracket. Details of specifications are shown in engineering drawings of SPBS. A general tolerance associated with manufacturing processes can be referenced as[110].

Table 4-4 Three level machining tolerance

Unit (mm)	Fine (mm)	Middle (mm)	Non critical (mm)
6 ~ 30	(+/-) 0.1	(+/-) 0.2	(+/-) 0.5
30 ~ 120	(+/-) 0.15	(+/-) 0.3	(+/-) 0.8
120 and above	(+/-) 0.2	(+/-) 0.5	(+/-) 1.2

In the application of haptic device, precise end-effector position and orientation are required. The identification of errors in the model will increase the effectiveness of calibration. The geometric errors are the physical parameters that are manufacturing errors such as link length or link angles. Non-geometric errors are generated by control or other reasons. Shown in Figure 4-16, the device error source includes machining, assembly, deflection, measurement, and control errors. In this section, only the geometric errors such as machining and assembly errors are discussed. The deflection of the haptic device is insignificant because of passive support, which was analyzed in chapter 3.

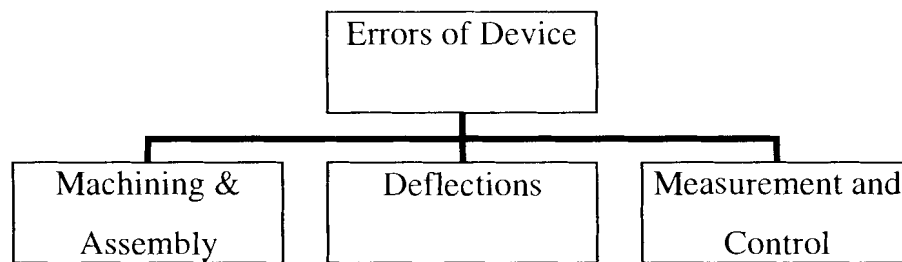


Figure 4-16 Error model of devices

Errors exist in any machined work piece and the actual dimension will be different from nominal dimension. These errors should be within the given limits of tolerance and determined by the dimensional measurement to guarantee accuracy. The links of haptic device are inspection for geometric errors. The purpose of inspection is to verify the difference between design and manufactured values. The reference measuring setup processes was suggested by [111].

The dimensional measurement processes are:

- Create the 1:1 drawing for six links of haptic device from Solid Works
- Plot the drawing
- Measure the drawing to ensure the dimension is 1:1
- Set the datum point and place the link on the drawing as a template
- Check the contour of link for the template
- Set the start and end position of link
- Measure both end of the holes
- Find the center line of both hole
- Find the manufactured angle between two bores
- Compare the manufacture angle with design value

The dimensions of SPBS links are inspected and the errors are shown in Figure 4-17. It shows that the errors of SPBS are less than 1 %, thus satisfying the design of geometrical dimension and tolerance requirements. The kinematic parameters do not have to be

updated for the actual manufactured value to be robust. The result of the experiment shows the kinematics of SPBS has high accuracy[112].

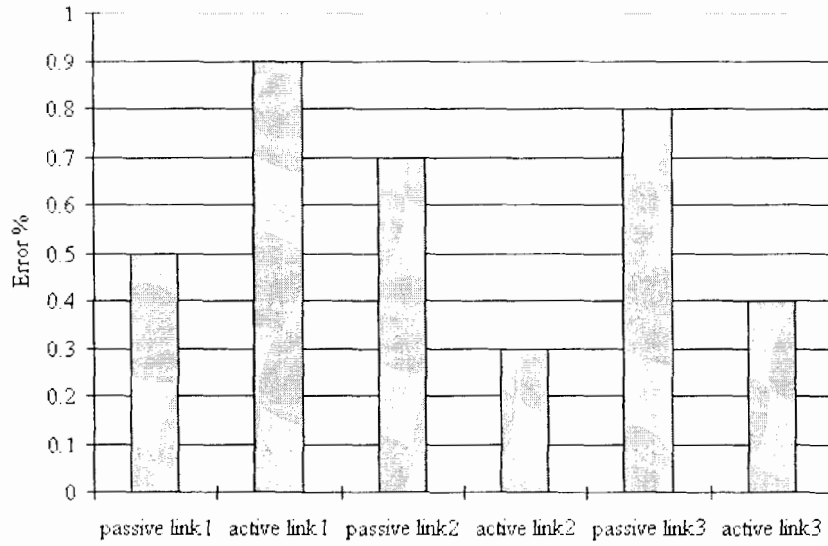


Figure 4-17 percentage of design and manufacturing difference for SPBS

5. Master-slave and Supporting Mechanisms

In chapter 2, tool-holding mechanism is developed, which can be used as a robotic arm to perform a laparoscopic surgery. In chapter 3, it was explained that the haptic devices could be used as surgical training device or master end. The design concepts presented in chapter 2 and 3 can be integrated with supporting mechanisms to enhance the robotic application. These supporting mechanisms are used to assist surgeons for performing complex surgical tasks. In addition, supporting mechanisms are designed that can be used in future applications of laparoscopic surgery or training. The integration of supporting mechanism with the tool holding mechanism or haptic devices can be used as a future base for robotic surgical or training systems. This chapter is to study additional laparoscopic problems and proposes supporting mechanisms to solve these problems. This chapter also includes reviews of prior research, design, and analysis of proposed mechanisms with a discussion of advantages and limitations.

The supporting mechanism is a two-DOF local master slave mechanism which contains a slave end that can pivot as a wrist to achieve pitch and yaw. The slave and master ends are integrated on one surgical tool which is called “local”. The dexterity of mechanism simplifies complex surgical tasks. The second mechanism is the abdominal space maker that can lift a patient’s abdominal wall and create surgical space without using pneumoperitoneum. This mechanism applies a foldable/extendable structure so that it can be inserted into abdominal wall to be expanded.

The problems of laparoscopic surgery are due to indirect access to surgical area that includes limited workspace, and limited vision area, and less dexterity for manipulation. Laparoscopic surgery is limited to four DOF because the surgical tool has a long rigid stem. Therefore, the surgical tool can reach only limited orientation and position. With the limited DOF, the desired position and orientation may not be reached. The concept of designing a flexible stem surgical tool had been proposed in [15],[8]. The flexible stem type is not popular for surgical application. In addition, a new concept of a two-DOF

wrist such as Da Vinci or Zeus has been developed to increase the dexterity. The dexterity and agility can be enhanced by adding a two-DOF joint on the tip of the surgical tool. Therefore, the mechanism with additional DOF can assist surgeon to complete difficult surgical tasks such as suturing.

Adding additional DOF on surgical tool tip increases the dexterity in laparoscopic surgery. Suturing and knotting are considered two of the most difficult and time consuming tasks of endoscopic surgery, detail studies of which can be found in [113]. Shown in Figure 5-1, the suturing task can be broken down into the following five subtasks: 1) stitch (Figure 5-1 a), 2) create a suture loop (Figure 5-1 b, c), 3) develop a knot (Figure 5-1 d, e), 4) place a knot (Figure 5-1 g, f), and 5) secure a knot (Figure 5-1 h). In some circumstances, a specially designed surgical tool such as stapler or suturing device [8] can be used. However, the special purpose tool is able to achieve only certain tasks and is not enough to accomplish all surgical tasks.

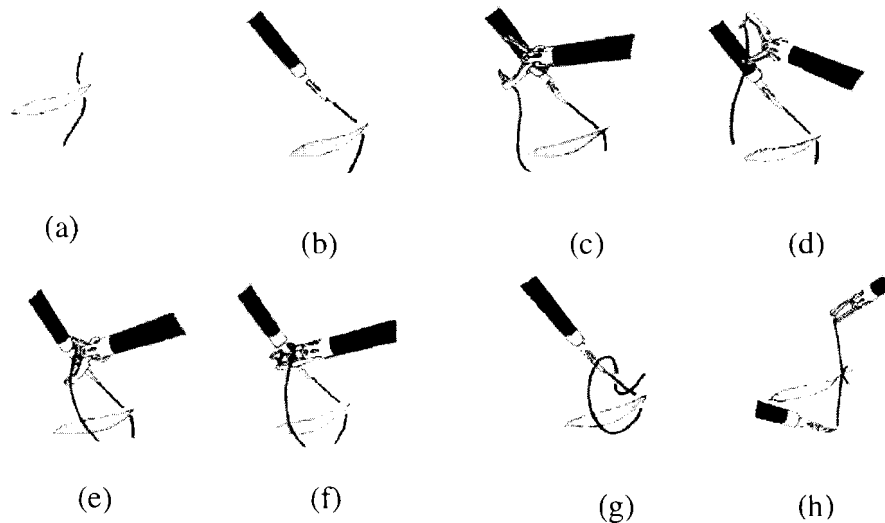


Figure 5-1 Suturing tasks

The robotic surgical systems developed by research or commercial institutes are complex. These systems integrate mechanical devices, electrical control, actuator, computes software. A network is shown in Figure 5-2. There are not many mechanisms developed from mechanical design prospective. This motivates us to design a simple manually

actuated two-DOF mechanism. The benefits include direct control without motor or any electronic devices so that the device can be compact and lightweight.

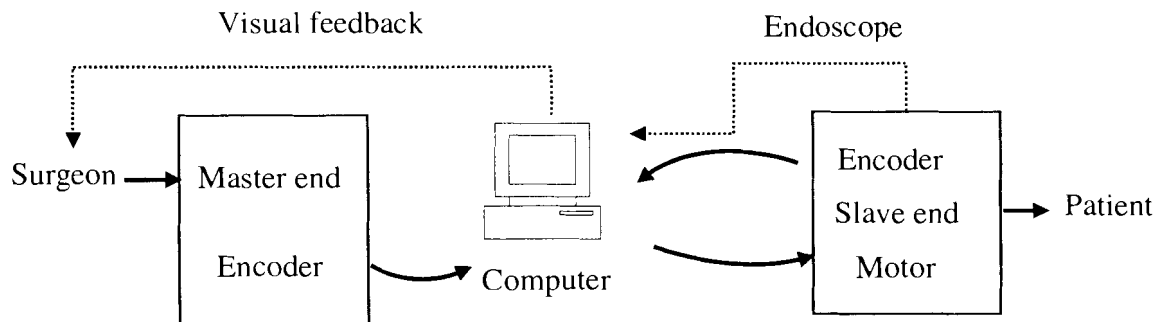


Figure 5-2 schematic of remote master-slave relationship

The motivation is to design a mechanical device to assist surgeon and perform operation fast and easily. For instance, surgical robots enhance minimally invasive surgery by providing a wrist at the end of the instruments to scale motion and filter tremor. Scale motions and tremor filters can augment precision in surgical tasks.

UC Berkeley developed a millirobot with a 15 mm diameter 2 DOF wrist, with yaw and roll axis rotations[82] Figure 5-3. UC Berkeley uses Phantom as the master device to control the slave. Shown in Figure 5-4, the slave manipulator of UC Berkeley laparoscopic telesurgical workstation is actuated through tendons jointly by three DC servomotors. A close up view of the millirobot wrist is shown on the right.

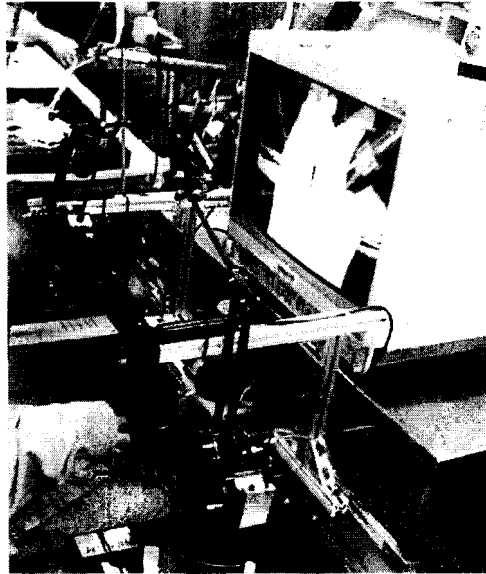


Figure 5-3 Master end of UCB telesurgical workstation

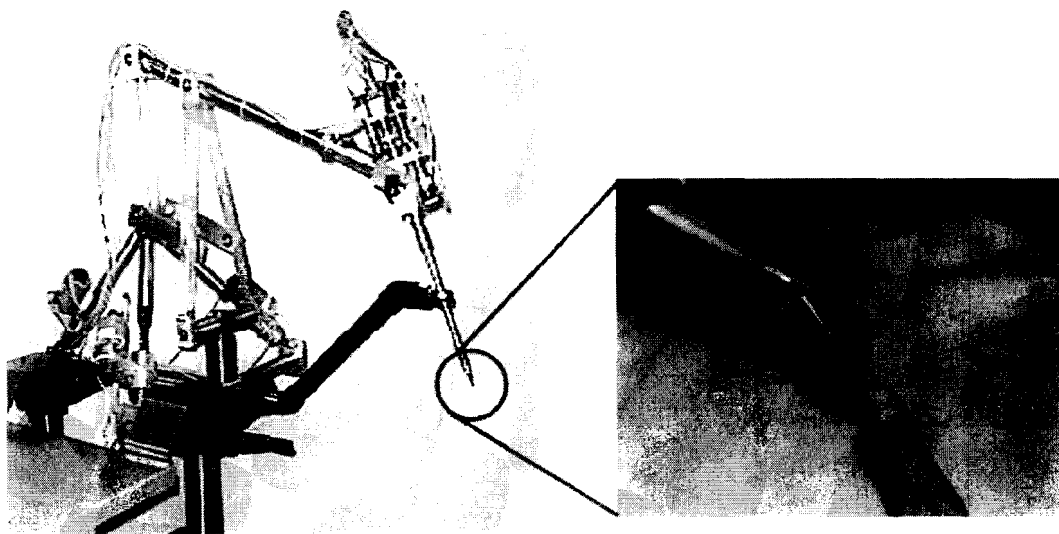
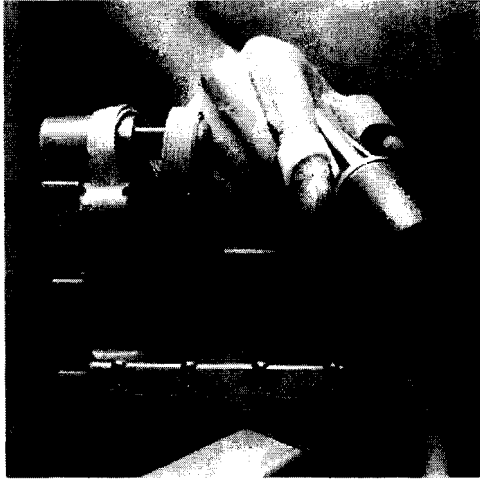


Figure 5-4 Slave manipulator of UCB telesurgical workstation

As shown in Figure 5-5(a), the surgeon's hand control the master device with a finger strip around thumb and index finger. As shown in Figure 5-5(b), the Endo wrist contains two rotational DOF and one pinching that mimics the dexterity of the human wrist. The wrist is remotely driven by actuators at the proximal end of the tool module through tendon drives inside the tool shaft, which is like the cable system used by a robot finger[44]. The surgeon controls the master robot to perform surgery through the slave

device. It is important to ensure the accuracy and real time response between the master device and the Endo wrist. Clamping and suturing tissues are the special surgical missions and the motion range is extensive, allowing precise suturing[114].



(a) Master-end robot



(b) Slave-end device

Figure 5-5 Instuitive surgical master end and Immersion Endo Wrist

The additional DOF master-slave mechanism assists the dexterity of complex surgical tasks developed by UC Berkeley or Immersion. These robotic mechanisms are complex systems integrated with design, manufacture, software development, user interface, control, actuator, communication, and teleoperation. However, there is no surgical tool with additional DOF without motor or actuator to provide similar function as the complex robotic system. Therefore, the novel manual control local master-slave mechanisms are proposed to solve similar surgical problems with less complex mechanism.

5.1. Two-DOF Local Master-Slave Mechanism

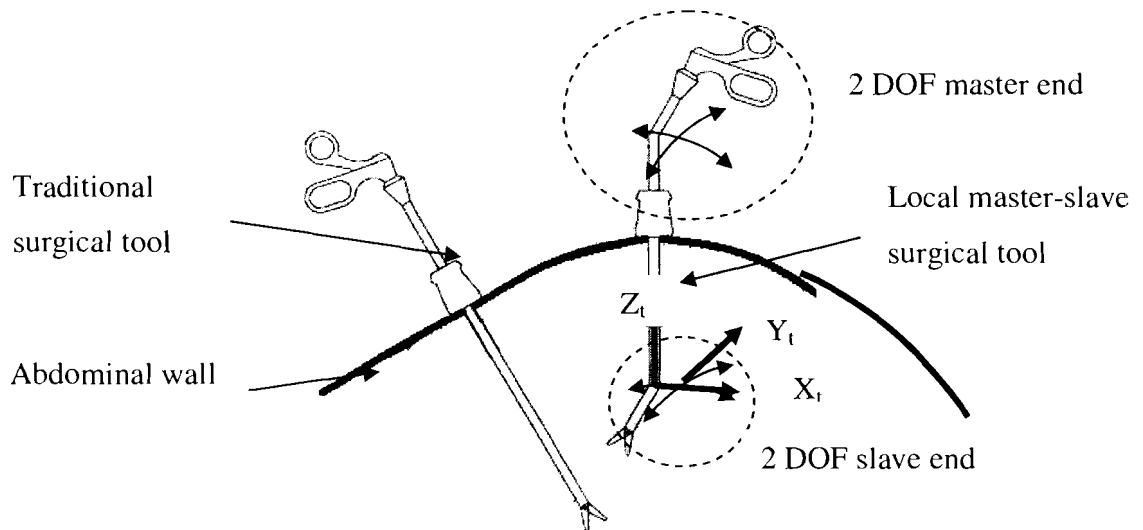
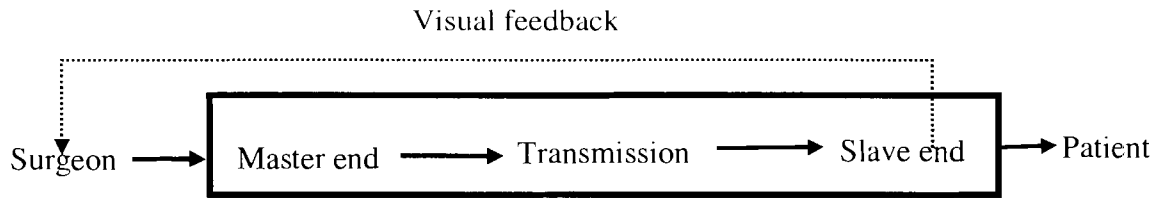


Figure 5-6 Two additional DOF of local master-slave surgical tool

The goal is to design a local master slave mechanism that has two-DOF to pivot like a human wrist. Shown in Figure 5-6, the master end and slave end is integrated on one surgical tool which is “Local master-slave mechanism”. Surgeons can manipulate this mechanism as a surgical tool, directly on the patient. Shown in Figure 5-7, surgeons control the local master-slave mechanism which is integrated as one piece. The transmission system conveys mechanical power from the master end to actuate the slave end. The rotational speed of the master end can be changed, resulting in a different output speed. The transmission can be achieved by cable, wire, pulley, belt, linkage, or gears.



Local master slave on one piece
Figure 5-7 Schematic of local master-slave relationship

In this section, our goal is to design a mechanism that contains two-DOF wrist tool tip for higher dexterity and smooth usage in order to assist surgeons performing complex surgical tasks. The master end contains two rotational DOF to activate pitch and yaw motion of slave end. The master-slave can be manufactured on one-piece tool which is different from these robotic master-slave devices

Mechanical design requirements:

For master end:

- DOF: one rotational about X axis with respect to the tool frame(X_t) (Figure 5-6)
- DOF: one rotational about Y axis with respect to the tool frame (Y_t)
- Finger ring or handle for thumb and index finger

For slave end:

- DOF: one rotational about X axis with respect to the tool frame (X_t) (Figure 5-6)
- DOF: one rotational about Y axis with respect to the tool frame (Y_t)
- Motion range: +/- 45° from center position
- Diameter less than 15 mm

For transmission:

- Transmit the motion between master and slave
- Must fit within 15 mm diameter tool stem

Type synthesis of two-DOF wrists:

Type I: Shown in Figure 5-8, the serial type two rotational DOF master end contains two revolute joints, the revolute joint along X-axis creates first rotational DOF, and the revolute joint along Y-axis creates second rotational DOF. The angle along X-axis and

Y-axis can reach 360°. The advantages include minimal number of links, simple structure, and large workspace. Disadvantage is low rigidity. The rigidity can be increased by applying material with higher strength.

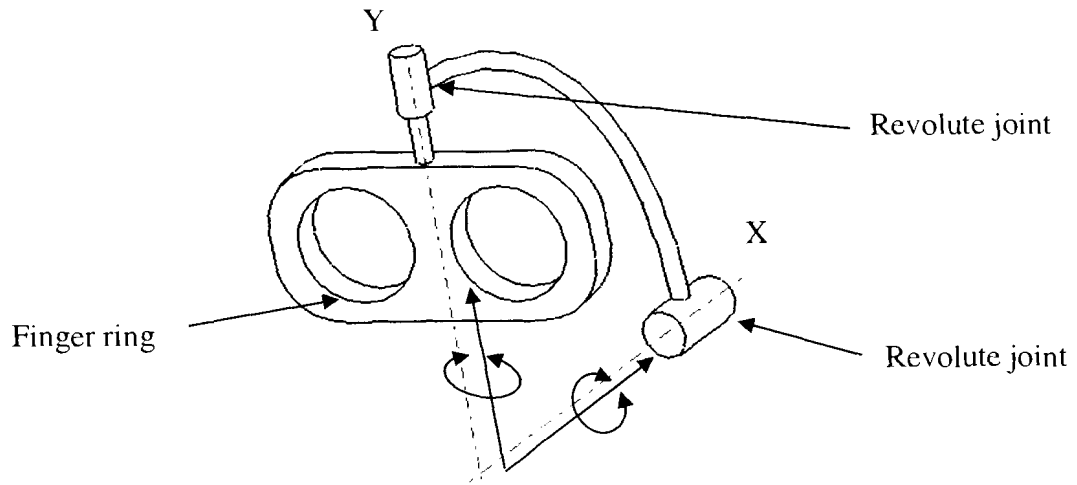


Figure 5-8 Serial type of two-DOF master end

Type II: Shown in Figure 5-9, the second serial two-DOF master is a different version of Figure 5-8, the second revolute joint rotates parallel to Z-axis which makes the pitch and yaw motion. Type I and II are simple structures with minimum number of links. The difference in rotation axes is that type I rotates about X and Y-axes and type II rotates about X and Z-axes.

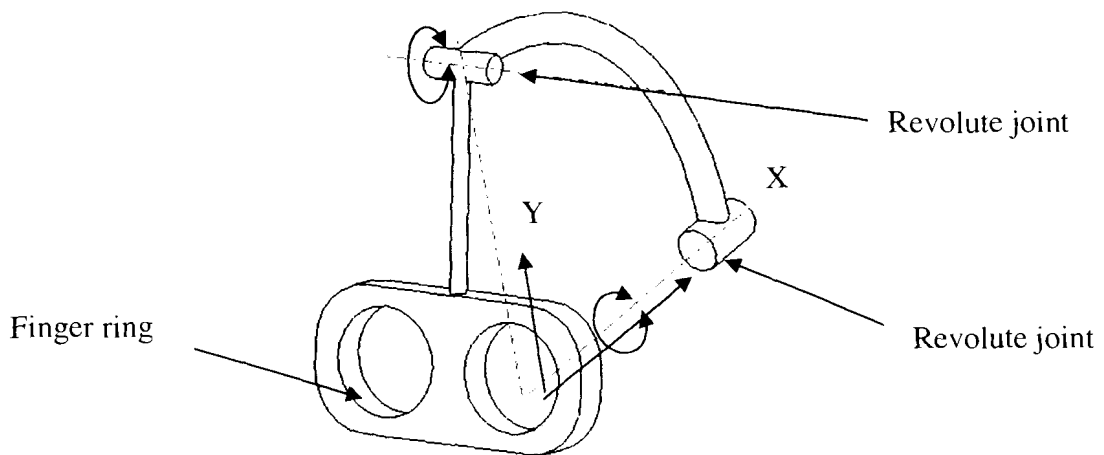


Figure 5-9 Serial type two for X and Z axis rotation

Type III: The parallel type master end is based on a closed loop mechanism. The kinematic motion requires five revolute joints to achieve the two rotational DOF. Shown in Figure 5-10, the finger ring is connected to the ground by two branches. The left branch of the parallel type in Figure 5-10 contains two revolute joints (joint 1 and 2) and the branch on right contains three revolute joints (joints 3, 4 5). That joint 1 and 5 are fixed to the ground and perpendicular to each other. Advantages include higher stiffness and less deflection. Disadvantages include less workspace, more parts, and requirement of higher machining accuracy to assembly.

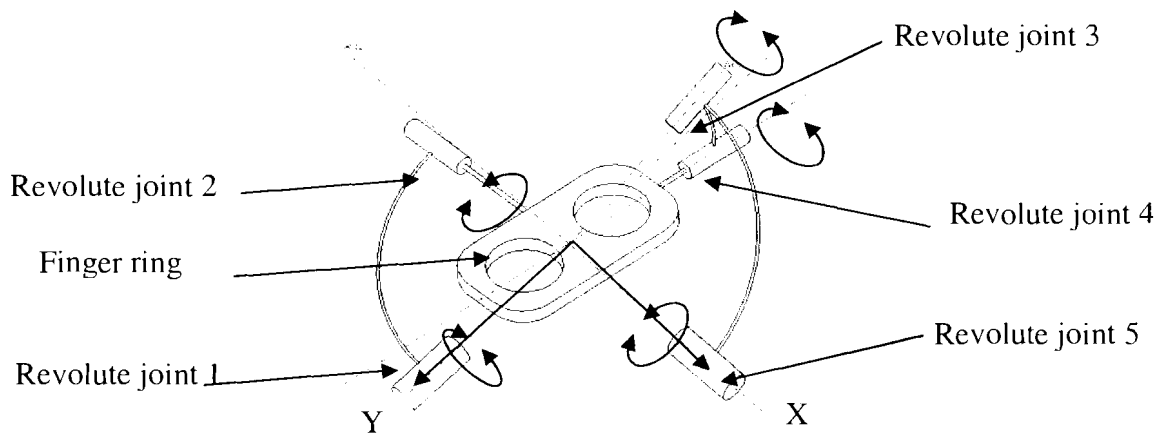


Figure 5-10 Two-DOF spherical parallel type master end

Type IV of master end is shown in Figure 5-11. The finger ring is attached to the base by a spherical joint. Two arc frames of different diameter are hinged to X and Y-axis of the base. The connecting rod of finger ring passes through the arc frame slot. The finger ring pivots the arc frame and pulls the tendon to actuate the slave end. Figure 5-12 show the front and section views of the master end.

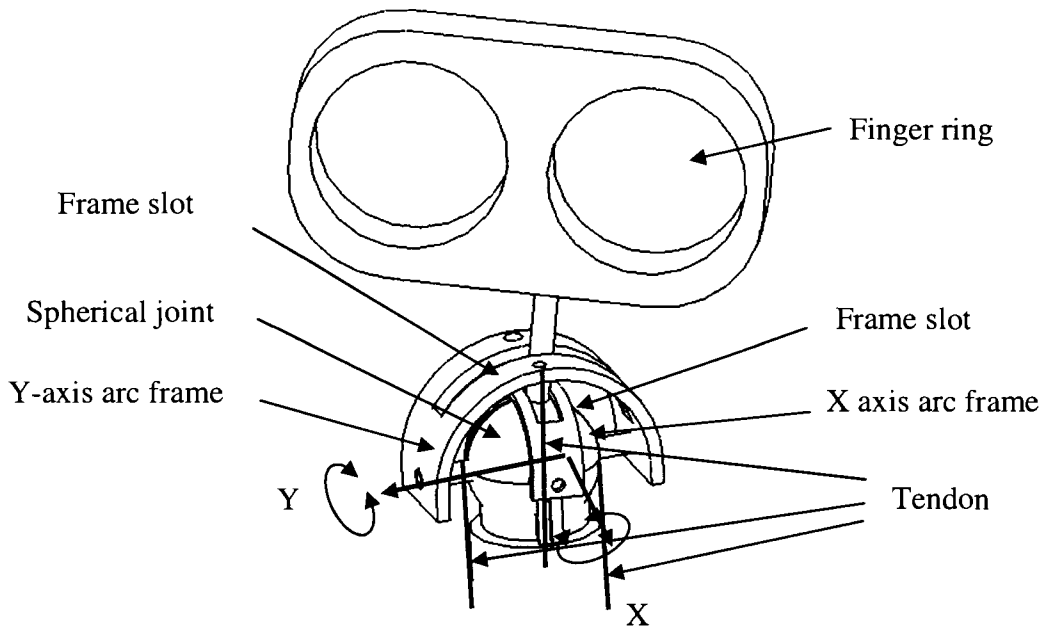


Figure 5-11 Master end spherical joint and arc frame

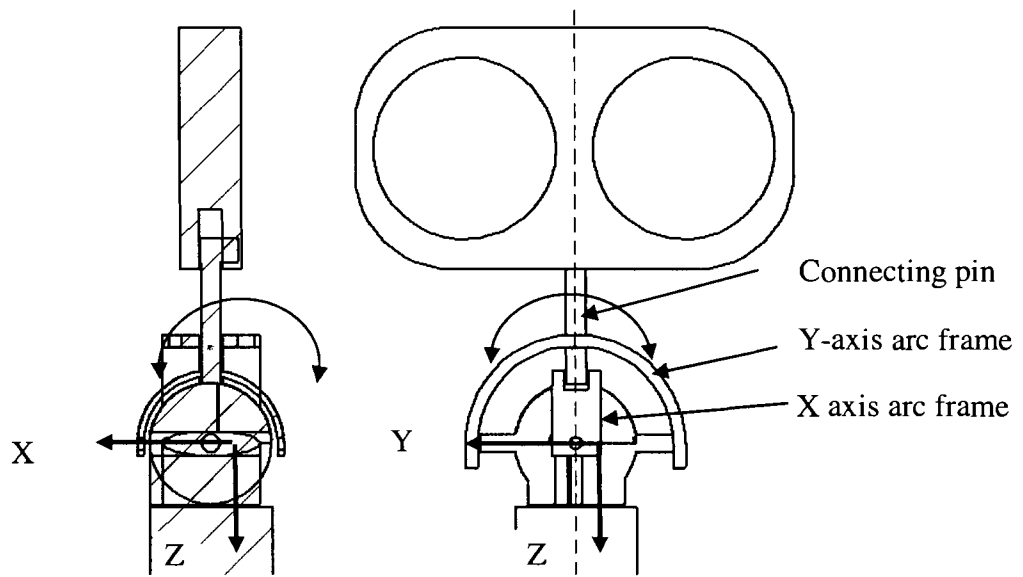


Figure 5-12 Front and section view of master end

Slave End Type I: The slave end design must be small in diameter to be inserted into patient's body through the trocar. Therefore, the slave should be less than 15 mm in diameter. Figure 5-13 shows that the slave end constrains the spherical base with a hemispherical block. Shown in Figure 5-13, there are four bores on the flange of a

hemispherical block for tendon to pass. The tendon pushes or pulls to swivel the hemispherical block along X-axis or Y-axis to create two rotational DOF. The advantages include few parts and simple structure. Limitations include 1) friction force caused by the tendon. The friction force between hemispherical blocks affects the tool tip motion. 2) The tool tip cannot take Z-axis torque which means that it cannot provide the twist motion along Z-axis.

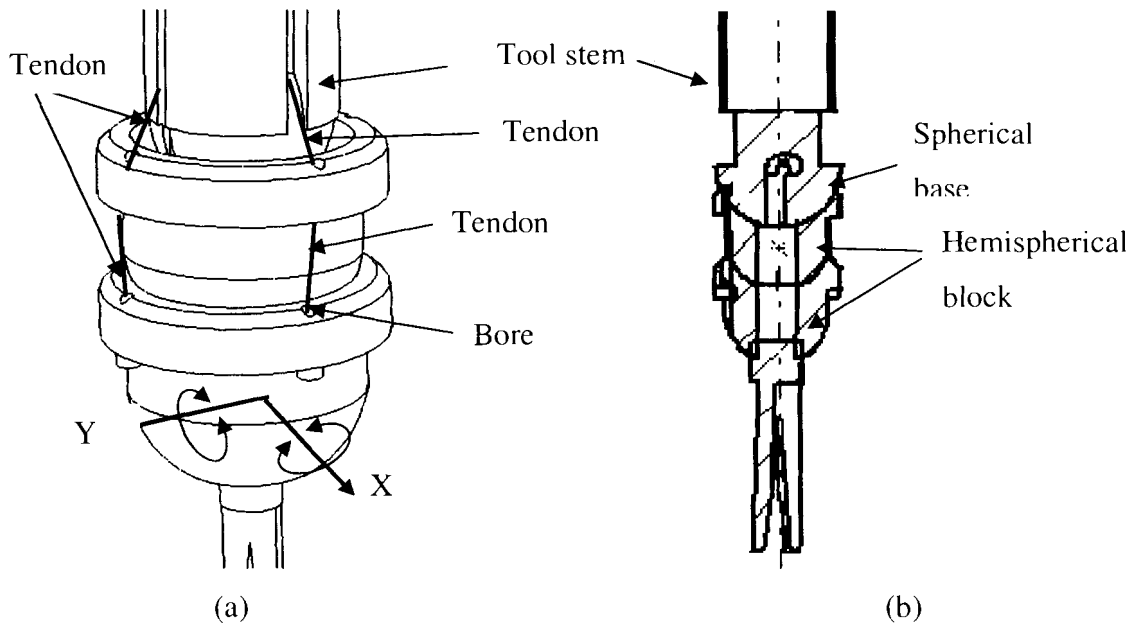


Figure 5-13 First two-DOF slave end with section view

Slave end type II: Figure 5-14 shows the type II, which contains a pulley system to actuate two-DOF. The pulley 1 passes through axis 1 and pivots the link 1 to rotate along X-axis. Second pulley passes through Y-axis and pivots link 2 to rotate along Y-axis. X and Y-axes are perpendicular to create the two rotational DOF wrist motion of tool tip. Nine different postures of slave end are shown in Figure 5-15.

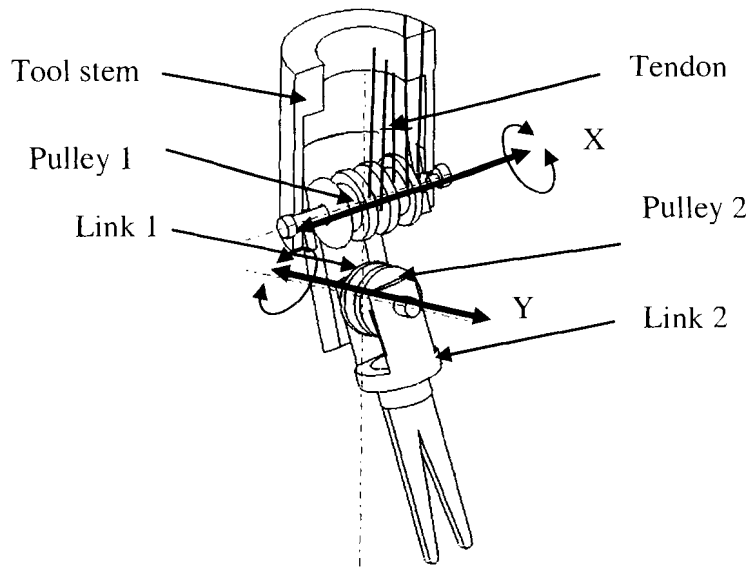
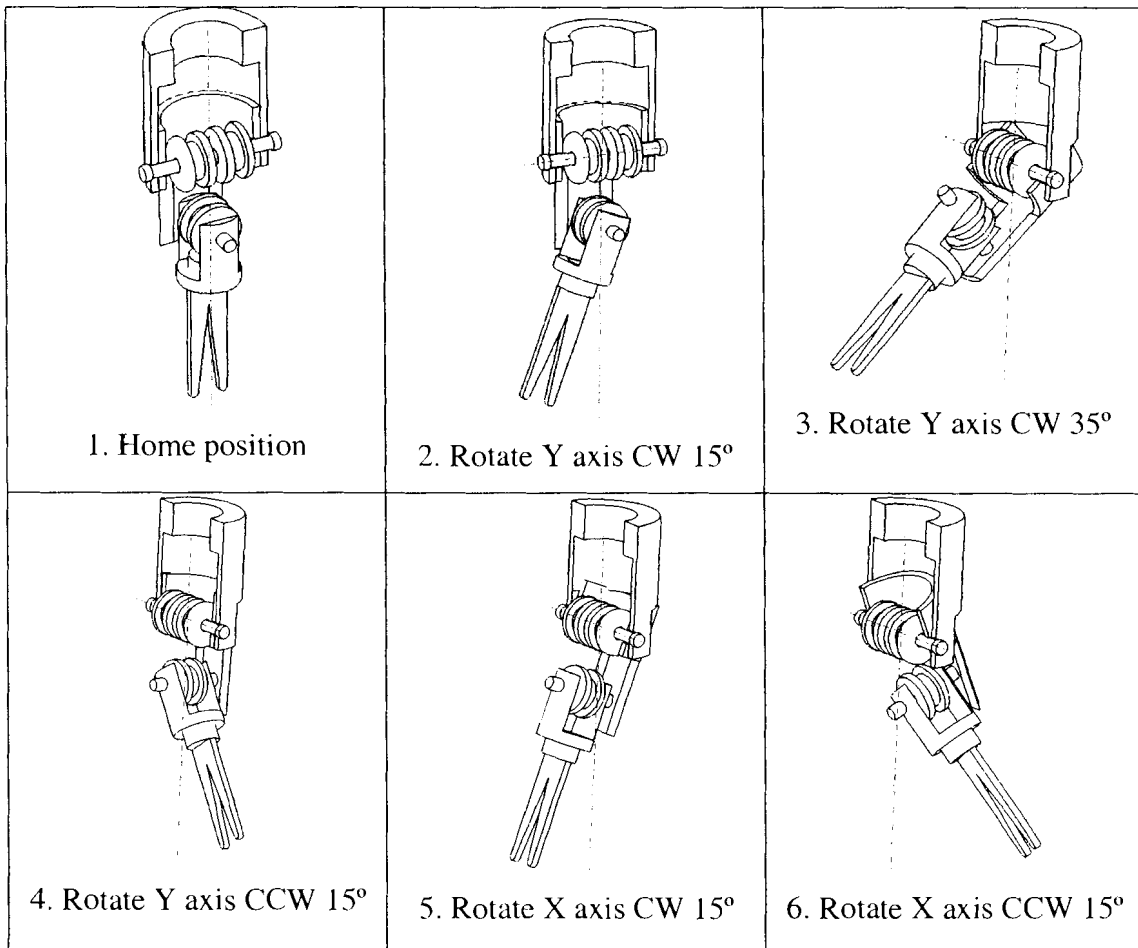


Figure 5-14 Hinge pulley type slave end



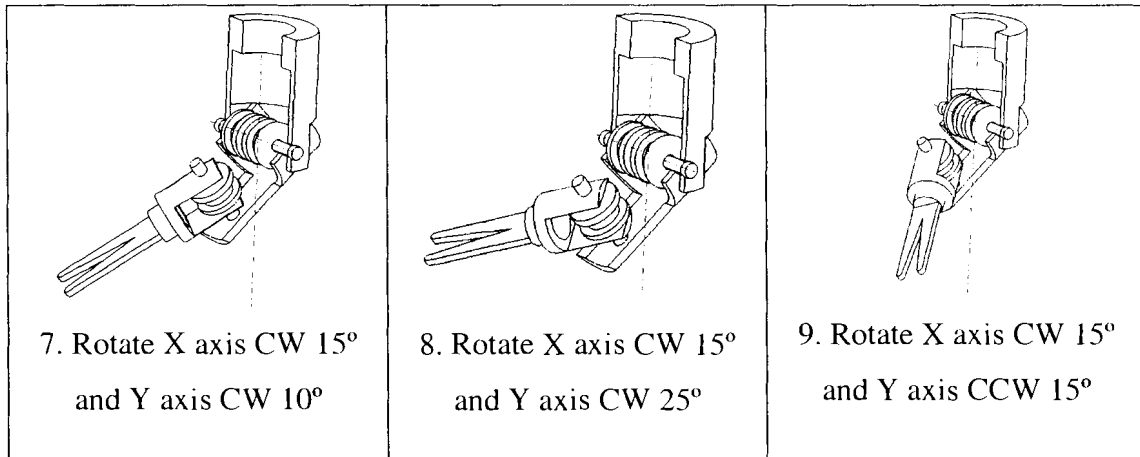


Figure 5-15 Nine different postures of slave end type II³

Transmission: The transmission must be installed inside the surgical tool stem diameter so that linkage or gear type transmissions are not feasible due to dimension. The tendon-driven type has the advantage of compact size and high power-to-weight ratio because actuator can be installed on the fixed base. In addition, a well designed tendon transmission has little back lash[44].

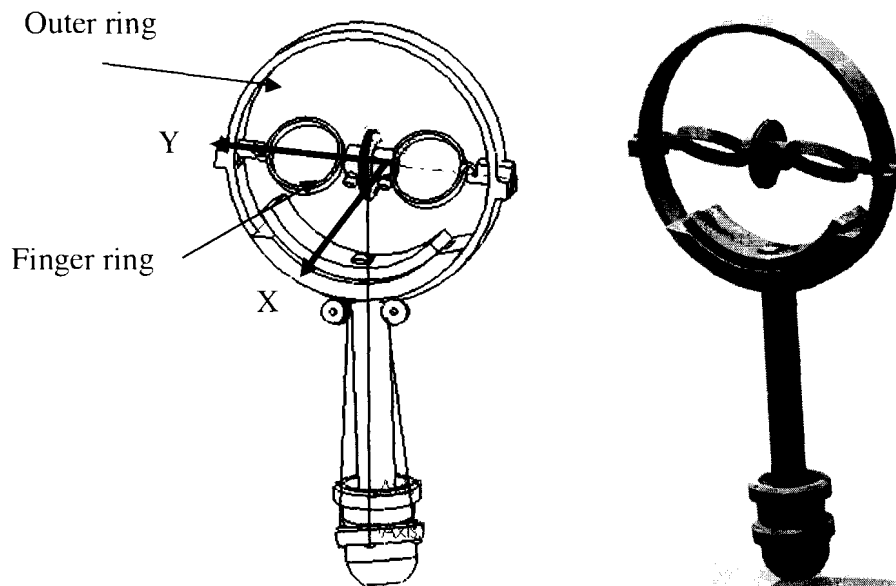


Figure 5-16 Gimbal type local master-slave mechanism

³ CW: Clockwise, CCW: Counter-clockwise

Shown in Figure 5-16, the gimbal type local master-slave mechanism uses the type I master end with type I slave end to integrate as one-piece tool. Gimbal type master end has support for finger ring on both sides so that the problem of low rigidity can be solved. This outer ring limits the rotation angle of finger ring for less than 180° along Y-axis. Motion scale can be achieved by changing the pulley size ratio between master and slave end. The motion control between master and slave is a direct mapping without interference; therefore, the master turns clockwise and the slave turns clockwise as well.

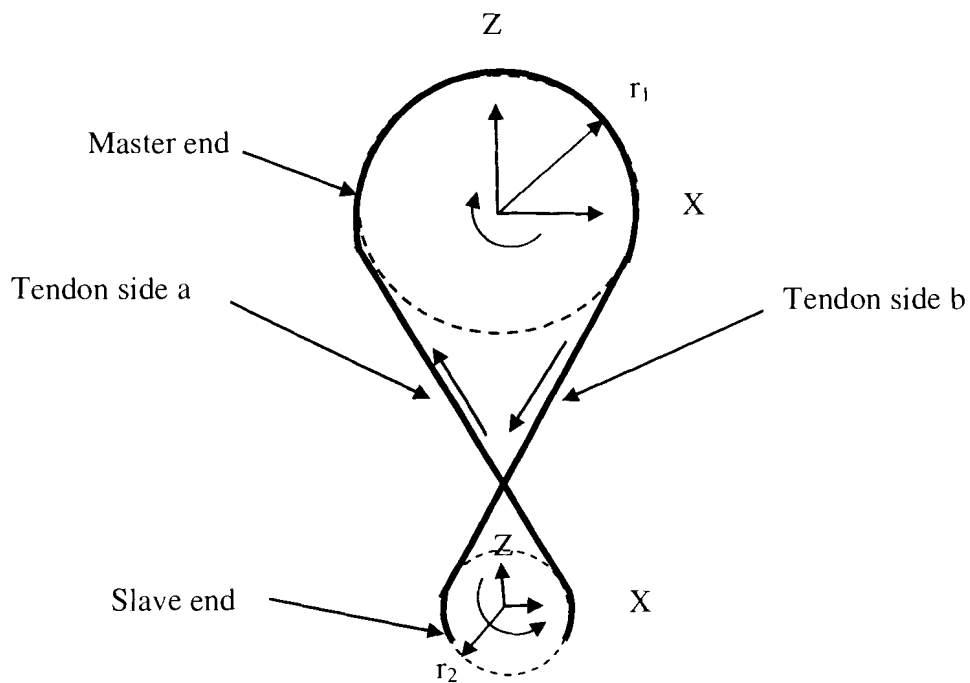


Figure 5-17 Transmission of master-slave

Shown in Figure 5-17, the tendon transmits motion between master and slave ends. When the master end rotates CW, the tendon will rotate the slave end CCW with respect to the pivot center. The motion range and scale can be analyzed between master and slave. From the center position, the required slave end range is 45°. In order to analyze the motion scale between master and slave, the relationship between the X-axis pulley and the diameter of slave end can be expressed as

$$r_1 \times \theta_1 = r_2 \times \theta_2$$

Where

r_1 : the radius of X-axis pulley

θ_1 : rotation angles of master end

r_2 : the radius of slave end spherical (15 mm)

θ_2 : rotation angles of slave end

The rotation range of slave end is 45° from the central position and substituting r_2 (15 mm) into previous equation, the motion range can be expressed as

$$\frac{2\pi r_2}{4} = r_1 \theta_1$$

That can be rewritten as $r_1 \theta_1 = 15.71$ mm

If the motion scale is 1:1, the pulley diameter of master and slave must be the same. If scale motion is considered, the pulley system creates the scale motion by adjusting the radius of r_1 and r_2 .

Advantages of this design include 1) tendon driving direct control from the master end to move slave end without actuator, 2) light weight and compact size. Limitations of this design include uncertainty in the friction force between the hemispherical block, which is affected by the tension force along the tendon.

Shown in Figure 5-18, a second type of local master-slave device uses the gimbal type master and pulley type slave end, yielding the advantages 1) rigid support of master end, 2) slave end is able to take Z-axis torque and have twist motion. The limitation is that the gimbal type master end has different radii for X-axis and Y-axis, causing the motion scale to be unequal on the slave end.

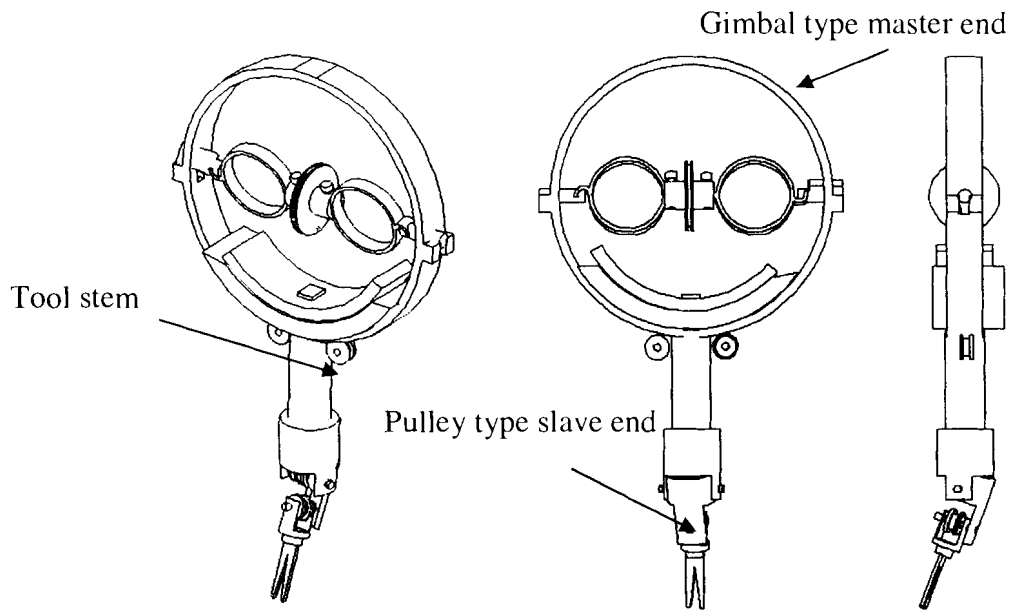


Figure 5-18 Local master-slave type II

Shown in Figure 5-19, a third type of local master-slave mechanism uses spherical ball joint as master end and hemispherical block type as slave end. Type III contains a small master end which is connected to the surgical stem by a spherical joint which offers a 1:1 motion scale between master and slave end.

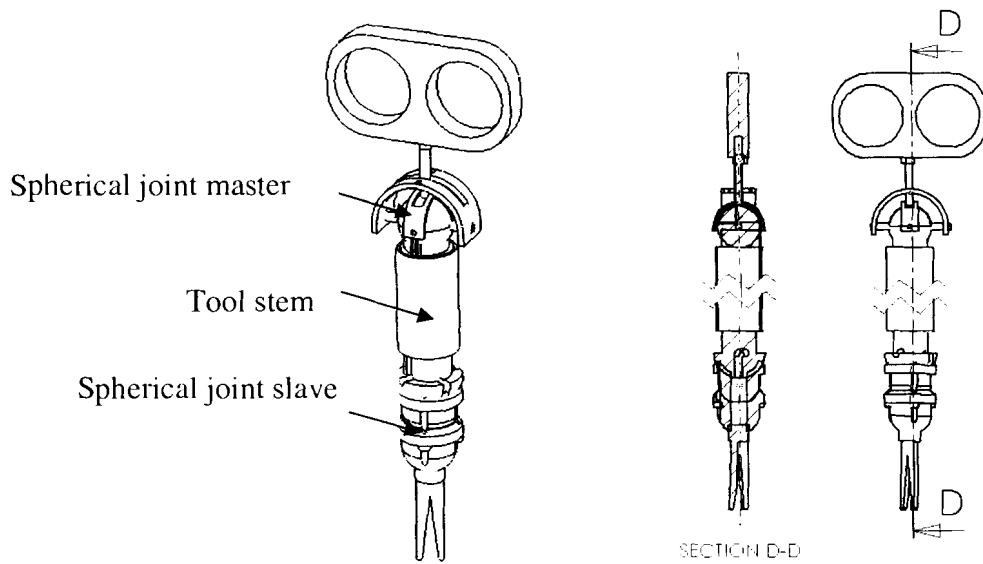


Figure 5-19 Local master-slave type III

The local master-slave mechanism can be divided into two parts to separate master end and slave end. The purpose of separation is for remote control of teleoperation. For the remote master-slave type, potentiometers can be installed on the revolute joint to measure the rotation angle of master end. The rotation angle is used to control the slave end motion. In addition, two motors are required to actuate the tool tip of slave end. The automatic master end uses the same design as local master-slave mechanism. At the master end, two motors are installed to provide the force feedback.

One of the major benefits of the remote master-slave mechanism is the variable motion scale. The motion scale represents the rotation angles ratio between master and slave end. For the local master-slave mechanism, the motion scale is based on the pulley ratio between master and slave end which cannot be changed in operation. The remote master-slave mechanism can use a computer program to change the gear ratio in surgery, because rotation angle of slave end is controlled by motor. The rotation of motor is controlled under the computer program. Figure 5-2 shows this relationship. A second benefit is the filtering of tremor because the slave end can be mounted on a robotic arm. The third benefit is that the surgeon is able to manipulate the master end with a more comfortable posture such as sitting on the chair.

The motor or actuation can be installed on the master end to provide force feedback. Shown in Figure 5-20, the motor Y provides the force back for rotation along Y-axis. That motor X provides the force back for rotation along X-axis.

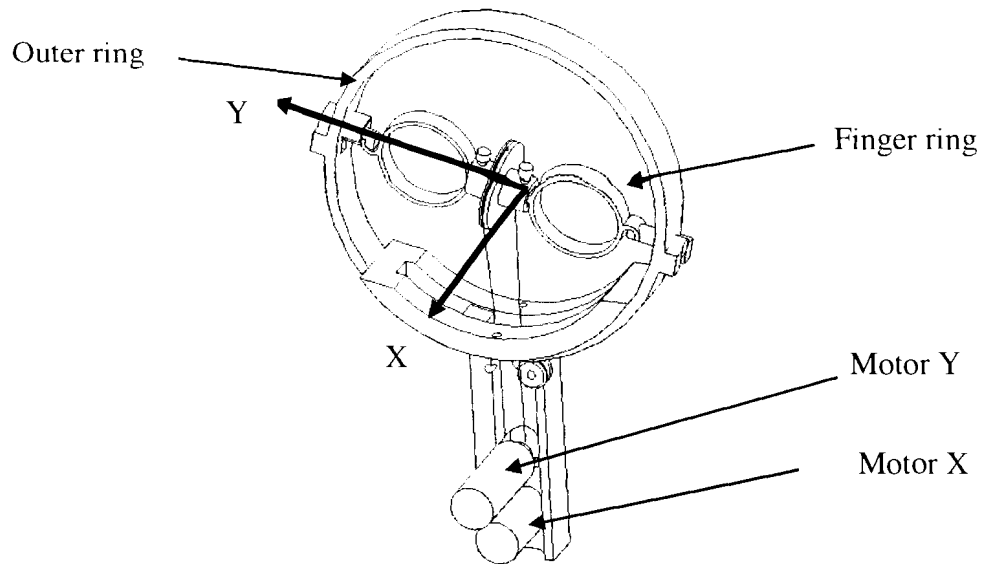


Figure 5-20 Force feedback gimbal type master end

The two-DOF local master-slave device can be integrated with the four DOF haptic device to achieve six DOF kinematic motion. Figure 5-21 shows that the master end is attached to the linear motion part of haptic device. This design creates four DOF with respect to the pivot center and two-DOF at the wrist. Shown in Figure 5-22, the slave end of the master-slave device can be attached on the surgical tool tip and integrated with tool holding mechanism (chapter 2) to be a six DOF robotics arm.

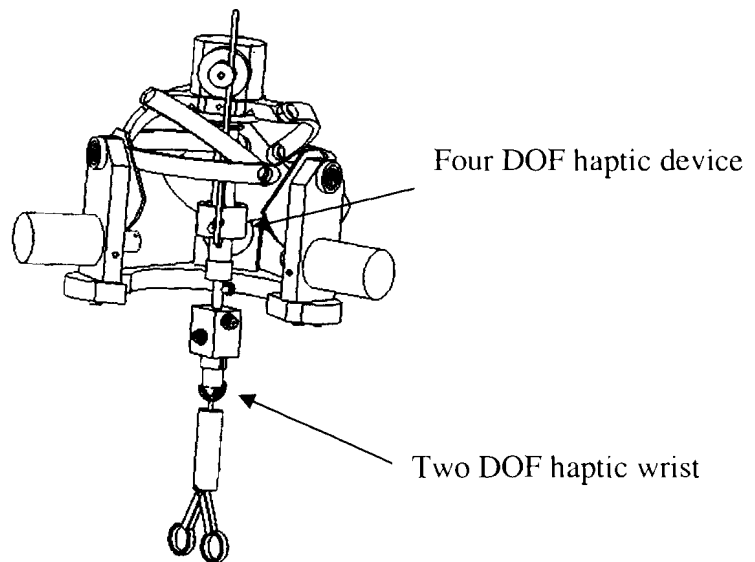


Figure 5-21 Six DOF force feedback haptic device

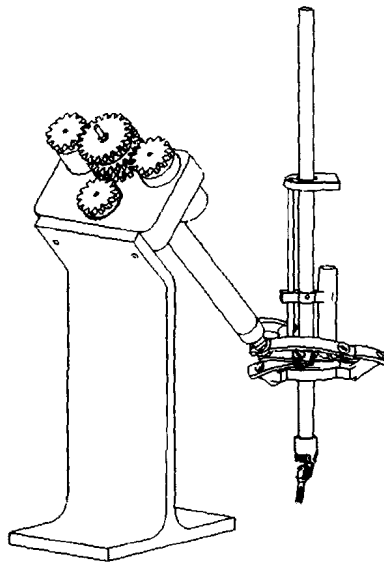


Figure 5-22 Six DOF slave end surgical robot arm

Shown in Figure 5-23, surgeons control the six DOF master end to manipulate the six DOF slave end surgical robot through the computer. In this telesurgery, surgeon and patient can be in the same room or thousands of miles away.

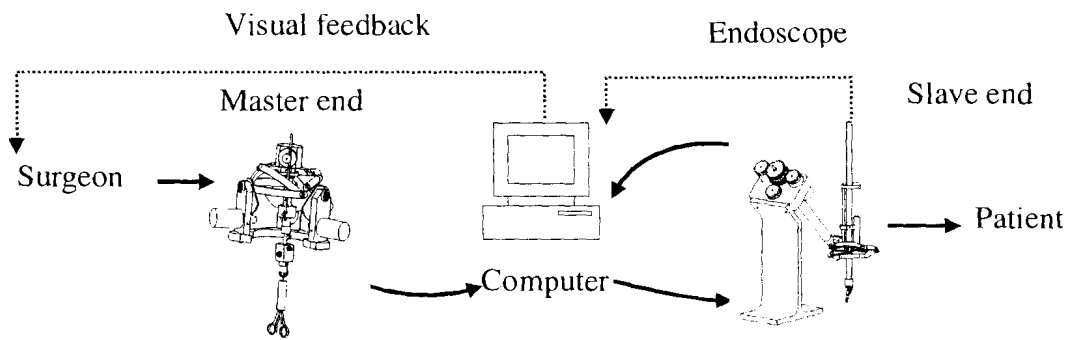


Figure 5-23 Six DOF remote master-slave mechanism schematic

5.2. Abdominal Space Maker

In the laparoscopic surgery, a space must be created inside the patient's body. The insufflations of carbon dioxide gas, pneumoperitoneum, are a routine technique for laparoscopic procedures. The use of carbon dioxide insufflation is safe in a healthy patient, and complications are rare during short procedures. However, the incidence of morbidity increases for prolonged laparoscopic cases and for patients with obstructive pulmonary or cardiac failure[115]. In addition, two major disadvantages of pneumoperitoneum are physiological effects and technical difficulties. The physiological effect drawbacks of carbon dioxide insufflation include gas embolism, hypercarbia, and acidosis. Technical difficulties include sealing and maintaining proper air pressure inside the patient's body. This technology requires additional equipment and carbon dioxide gas supply. Therefore, mechanical abdominal wall lifters are developed to solve previous problems. Research has been conducted with the comparison of gasless and conventional carbon dioxide pneumoperitoneum methods for laparoscopic cholecystectomy and concluded that gasless surgery has faster recovery and late postoperative recovery than conventional pneumoperitoneum surgery [116] and[117]. Therefore, several mechanical retraction devices for lifting abdominal wall are developed[16], [17], [18], and[118].

Shown in Figure 5-24, the devices are made of stainless steel hooks and wires to lift the abdominal wall. These devices occupy space above the abdominal wall that may reduce workspace for surgeons.

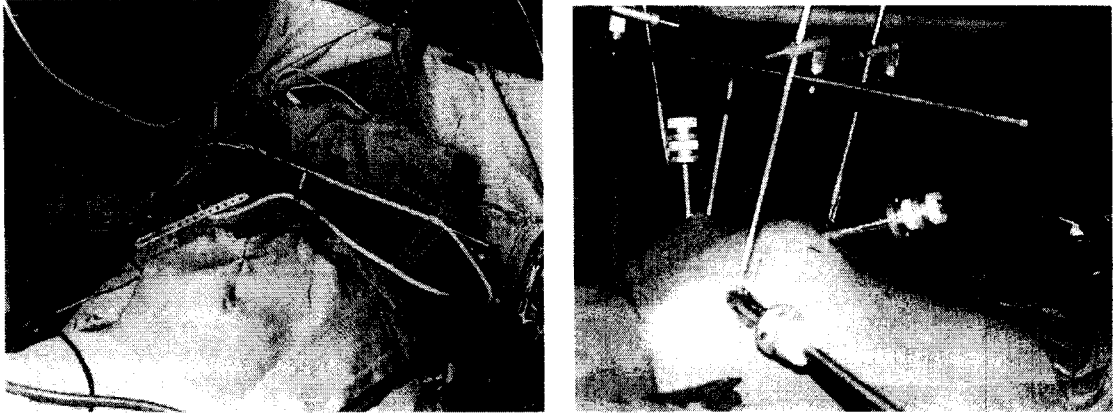


Figure 5-24 Wire and hook type space maker

Shown in Figure 5-25, the fishing-rod-like abdominal wall lifter for gasless laparoscopic surgery consists of 3 mm diameter stainless steel rods and iron lifters that elevate the abdominal wall like a dome-type camping tent, which does not disturb manipulation of scope[119].



Figure 5-25 Fishing rod type abdominal wall lifter

An abdominal wall lifting device consists of three intra-abdominal fan retractors, a winching device and a lifting bar and has been applied in 500 surgical cases in Japan[118]. The advantages are small incision point of 5~ 10 mm. The limitations include 1) assembly with screws is necessary, 2) lifting bar occupies workable space. Figure 5-26 (a) and (b) shows the assembled and disassembled view of the three intra-abdominal fan retractors. Figure 5-26 (c) shows the winching device and lifting base.

The retractor system is attached to a lifting bar and pulled upward with the winching device.

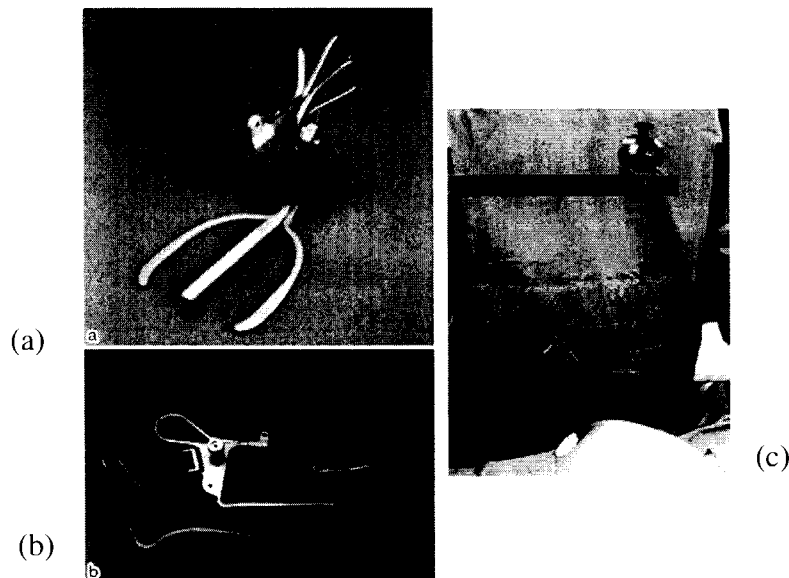


Figure 5-26 Fan type abdominal wall lifting device

These mechanical lifting mechanisms are able to solve the problems caused by pneumatic method. However, these simple rod type mechanism have disadvantages of 1) multiple entrances (4 ~ 6) incision points are necessary to insert the lifting rods or wires that causes additional trauma, 2) the mechanism may disturb maneuverability above the abdominal area by occupying extra space (Figure 5-24).

Therefore, designing new mechanisms to solve the disadvantage of mechanical lifting mechanisms is motivated. To increase the visible and workable space for laparoscopic surgery, two abdominal space makers are proposed that uses a foldable/deployable mechanism. Foldable mechanism can be used for space antenna which can be folded into space shuttle and expanded while needed.

Extendable abdominal space maker (EASM) and deployable abdominal space maker (DASM) are proposed. EASM and DASM can be easily inserted into patient's abdominal wall. This mechanism can be folded into a tube shape before insertion. All of

the main rods and supporting rods can be folded into the sleeve. While folding into the sleeve, foldable hinges do not hold the supporting rod firmly. At this fully expanded status, the foldable hinges hold the supporting rod firmly to make space for surgery. The working space is inside the tripod.

Design Requirements

- Deployable/ Reassemble easily
- Folded within diameter less than 25 mm
- Single point entrance
- No sharp edge or point

EASM type:

Shown in Figure 5-27, the EASM contains three extendable branches with each branch containing an external tube, internal rod, coil spring, and constraining wire. The constraining wire is attached to the distal end of internal rod to control the expansion. In folded status, the coil spring is compressed and the constraining wire limits the expanding force caused by coil spring. As shown in Figure 5-28 (a), in the compressed status of branch, the constraining wire pulls up the internal rod to limit the extension. Shown in Figure 5-28 (b), in the extended status, the coil spring is released to push the internal rod to distal end so that the branch is extended. Figure 5-29, the extended status, shows that the branch is constrained between the internal frame and supporting flange to maintain horizontal position. The fully expanded EASM of branch is 60 mm which can support a 236 mm² area. The EASM can be attached to the platform of tool holding mechanism (chapter 2) to be integrated as a module. The advantages of EASM include: 1) the applying force (the weight of abdominal wall) is perpendicular to the extended branch so that the branch will not be folded back by the weight of abdominal wall, 2) modulated branch so the branch of EASM can be increased to four or five branches. The pressure on abdominal wall can be reduced by increasing contact area.

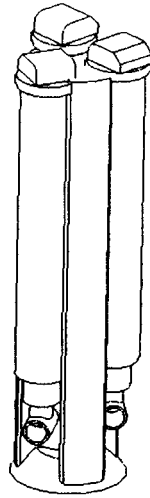


Figure 5-27 Folded EASM status

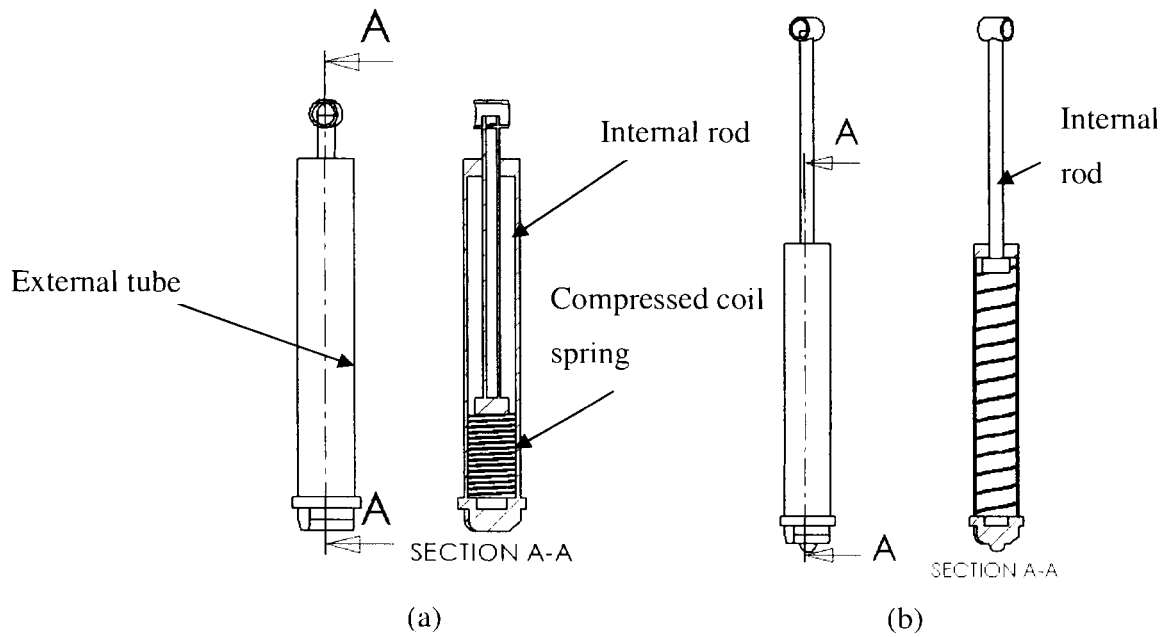


Figure 5-28 Compressed and extended status

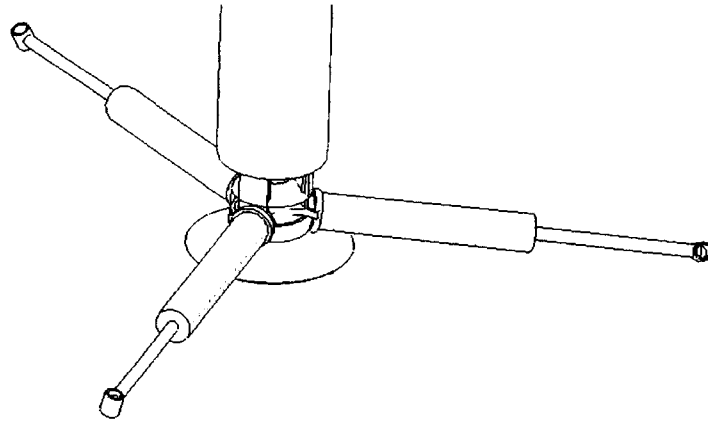


Figure 5-29 EASM Extended status

DASM type:

DASM is a deployable mechanism that uses revolute joints and spherical joints. The structure can be broken into sub assembly links connecting with spherical joint. DASM contains three branches where each branch contains an external tube, coil spring, and internal rod. The external tube uses coil spring to push the inner rod to unfold.

The folded status of DASM is shown in Figure 5-30. Three branches are connected to the center rod by spherical joint. The branch is able to pivot with respect to the spherical joint.

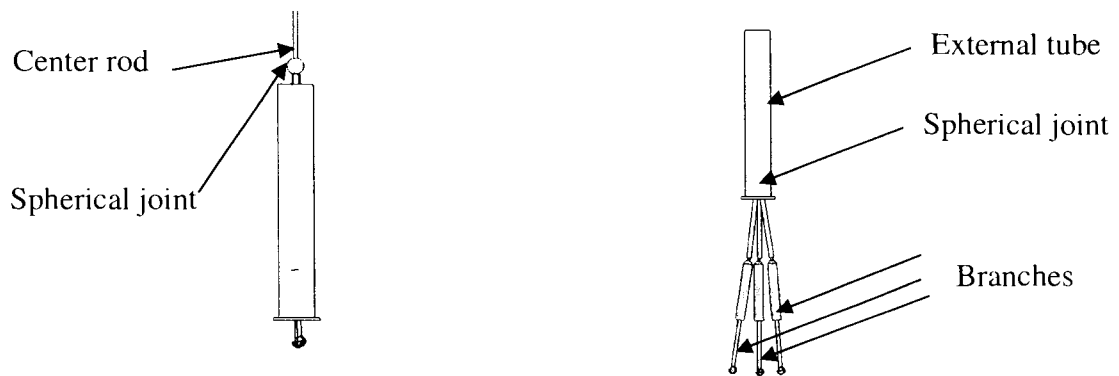


Figure 5-30 Folded DASM

Shown in Figure 5-31 (a), the surgeon manipulates a surgical tool (such as forceps) to hold branch 2 and uses a second surgical tool to connect the hook on the tip of branch 1 to the middle spherical joint of the branches. Shown in Figure 5-31 (b), the hook of branch 1 connects to the middle spherical joint of branch 2. Shown in Figure 5-31 (c), the hook of branch 2 connects to the middle spherical joint of branch 3.

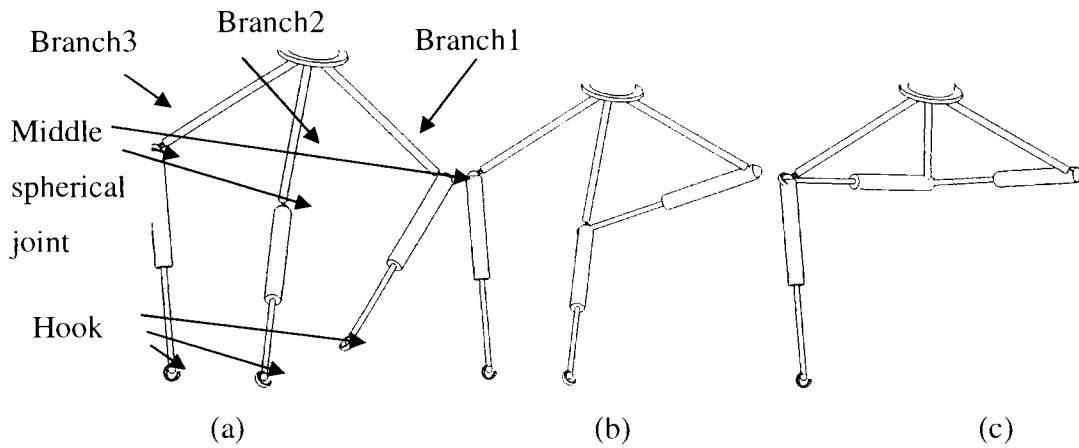


Figure 5-31 DASM semi assembly status

Figure 5-32 shows the assembled status of DASM that is not able to prove a flat surface to support the abdominal wall as EASM. However, the DASM can be located closer to surgical area to create local space which is for surgical area but not the abdominal area.

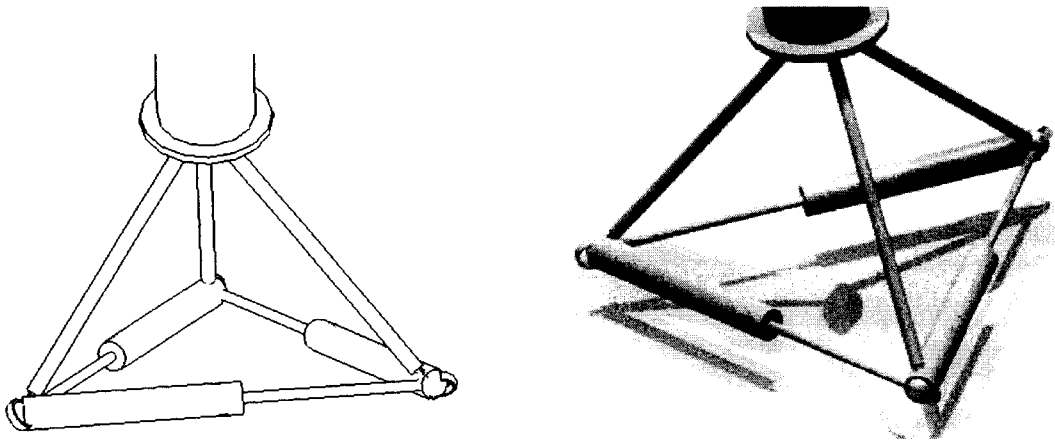


Figure 5-32 DASM assembled status

Advantages of DASM include that the compressed coil spring deploys the branch automatically and the assembly process is very simple for surgeons. Limitations of DASM include 1) the assembly of the middle joint with between branches is necessary so that the surgeons have to complete the connection of structure, 2) under retracting process, it is necessary for surgeon to disassemble the structure, 3) the structure is pyramid shape, so that abdominal wall will be lifted as a pyramid shape, which creates smaller space inside abdominal wall.

5.3.Discussion

An important difference feature between the tool-holding device in chapter 2 and the local master-slave is that the tool-holding device locates away from patient's body. In other words, the tool holding mechanism will not touch patient in laparoscopic surgery and the surgical tool held by the mechanism is inserted into patient's body. The local master slave and abdominal space maker have different features. The slave end of the local master-slave device will be inserted into patient's body in surgery. Nevertheless, the space maker is fully inserted into patient's body and an assembly/disassembly process is necessary to folded/ deploy the DASM. Therefore, the supporting mechanisms need higher safety requirement to ensure patients safety.

Additional considerations include:

1. Sterilization consideration: the master-slave and space maker are not disposable surgical tools. They will be used repeatedly in laparoscopic surgery. Patient's blood or body fluid may remain on the tool. Especially, the blood or body tissue may remain inside the revolute joint or between the moving parts that will be even more difficult to sterilize. It is necessary to find a way to prevent pollution or infection.
2. Fastening consideration: The space maker is a deployable structure that contains coil spring and retaining wire in the external tube of each branch. It is necessary to

consider an additional safety consideration for fastening the mechanism so that the moving parts are secured.

3. **Material selection:** For being sterilized, so a material such as stainless steel, titanium alloy could be used for laparoscopic surgical tool.
4. **Trauma on the abdominal wall caused by the mechanical space maker** will be greater than traditional pneumoperitoneum method because the folded diameter of space maker is 25 mm, which is greater than the 15 mm trocar diameter. In addition, a space maker made with small metal tubes, rods, and wires will have small contact area with abdominal wall that will cause high pressure on contact area and cause tissue damage. A less traumatic balloon type retractor that crease surgical space is proposed to reduce trauma[120].
5. Nothing is more important than safety of the human while the surgical robot interacts with human patients. However, it has not been considered because this research is at experimental stage. Safety should be considered in further development. Ikuta [121] suggested the weight, cover, surface, joint compliance, and shapes are related to patient safety.
6. **Stiffness consideration for space maker:** Since the deployment mechanism and the structural member is a thin tube with springs inside, it is desirable for the stiffness of the mechanism to be comparable to the stiffness of the structural member. Mechanisms exhibit low stiffness due to the use of thin tube. The stiffness can be increased by selecting high stiffness materials such as composites material or titanium.
7. The kinematics of laparoscopic surgery is constrained because the surgical tool must pass through the incision point on abdominal wall. In the surgical process surgeon manipulates a traditional surgical tool so the direction or orientation of the tool tip will not change with respect to the tool stem. However, the two DOF local master-slave mechanism has the kinematic problems of multiple solutions. The tool tip has

infinite solution to approach the same goal position. Four solution sets are shown in Figure 5-33 to reach the same goal point. However, the orientation of tool tip is able to determine a kinematic solution.

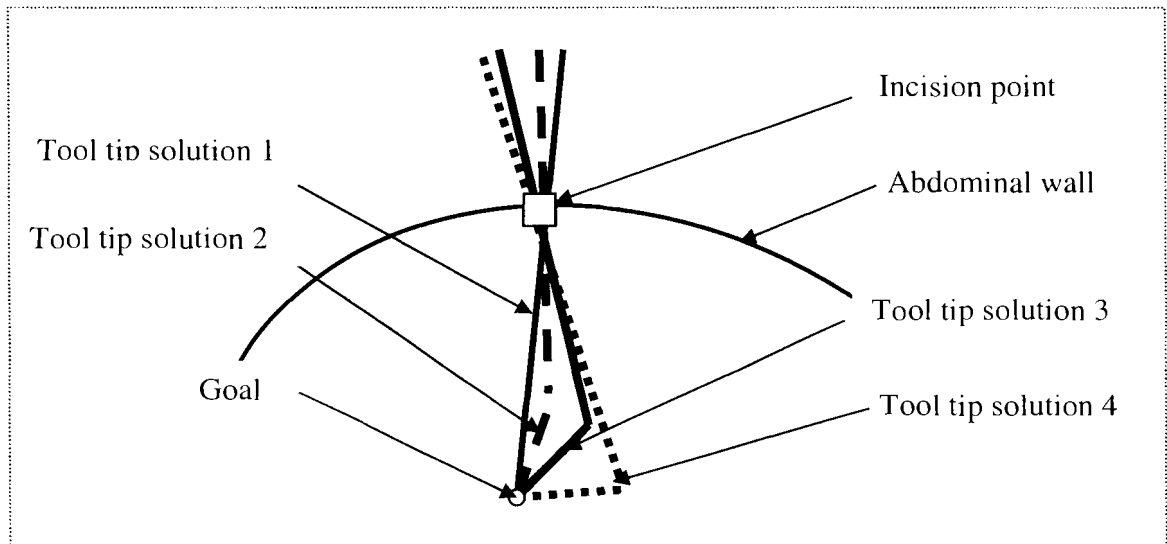


Figure 5-33 kinematic of local master-slave mechanism

6. Conclusion

6.1. Summary and Contributions

The indirect access of laparoscopic surgery causes surgical problems that have been discussed in section 1.2 and this research work solves position of endoscopic/tools, lack of force/tactile feedback, reduced dexterity and pneumoperitoneum problems. This research work focuses on synthesis, design, and development of new robotic mechanisms that solve previous surgical problems. The major research work is listed as:

- Synthesis, design, and development of new surgical tool-holding mechanisms those are able to automate position as a four DOF robotic arm.
- Synthesis, design, and development of new haptic devices those are able to provide four DOF force feedback or work as a master device for telesurgery.
- Design for manufacturing and costs analysis for haptic devices.
- Design of supporting mechanism for local master-slave mechanism and abdominal surgical space maker.

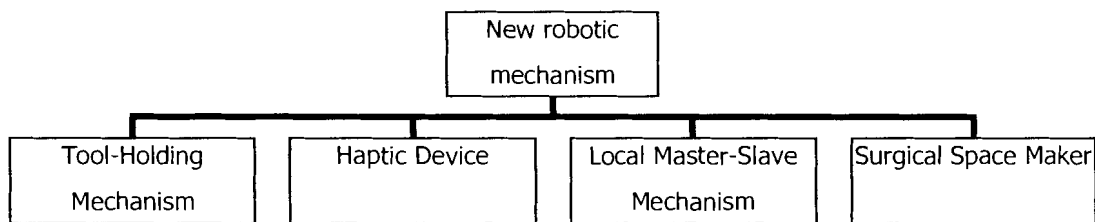


Figure 6-1 Integration of research objective

After developing previous work, this research provides a number of contributions that are listed as:

I. Tool-holding mechanism (chapter 2): The tool-holding mechanism [122] [123] [124] holds laparoscopic instrument to position as a four DOF robotic arm that contains following features:

1. New kinematic mechanism[122]:

The contribution is introducing a new spherical parallel mechanism that automated positions of a surgical tool. It contains a three DOF rotational platform with one linear DOF mechanism to achieve a four DOF conical shape workspace that meets laparoscopic surgery kinematic constraints. This is a first application of spherical parallel mechanism to hold and position a laparoscopic surgical tool.

2. Remote motor allocation and concentric actuating axis:

Three driving motors are fixed on a distal plate to provide more workspace for surgeons. This feature offers more space to solve the bulky size problem of current surgical robots. This new application utilizes parallel manipulator instead of serial manipulator for laparoscopic tool-holding mechanism. Conduct a new design of concentric actuating axis that is first used in surgical tool holding mechanism to transmit motion from the motor to the platform with 19 mm diameter concentric rod that does not use tendon driven with minimal space. This leads to a compact robotic arm size without cable.

3. Nested links:

The links of tool-holding mechanism have different radii. These nested links can avoid collision between links and increase workspace while rotating. This unique design is applied in spherical parallel mechanism.

4. Optimized workspace volume:

The basic design parameters of tool-holding mechanism are obtained from GA. These parameters are calculated based on the maximal workspace volume[64]. This calculation and optimization of GA contributes the optimization ideal between design parameters and the workspace.

5. The kinematic model of this tool-holding mechanism has been developed as a foundation for motion control. The inverse kinematics are investigated and analytically solved[73]. In addition, numerical examples of inverse kinematics are presented.

II. Four DOF Haptic devices (Chapter 3): In the field of haptic force feedback, there are contribution in a number of new design and developments.

6. New gimbal type haptic devices:

SFGT and RFGT are gimbal type haptic devices designed with a two-rotational-DOF platform that contains additional one linear and one rotational force feedback with total of four DOF force feedback[124]. This contributes to a new design for haptic devices which is suitable for three-rotational-DOF application

7. The spherical parallel type manipulators:

The spherical parallel type mechanisms contain three rotational DOF and one linear motion haptic device. These mechanisms introduce an innovative design that uses parallel manipulator feature with three stationary motors. This feature contributes to lower inertia and provides higher force feedback with smaller motor.

8. New passive support component:

The haptic force feedback device with passive support component enhances haptic design features. The passive support holds platform weight, shares load and increases structure stiffness, reducing the deflection to ensure low inertia and low friction. This passive support concept is a unique design concept and first used in haptic force feedback device.

9. New linkage mechanism:

These haptic force feedback devices eliminate the cable or tendon problems by using a linkage to transmit torque from motor to the end effector. This is a main contribution to introduce a new concept in developing design features of haptic device. This is a first

surgical haptic force feedback device with minimal tendon usage which is a contribution to develop the linkage transmission.

10. Both direct and inverse kinematic problems of spherical parallel haptic device are solved[112]. The direct kinematics is necessary to solve the corresponding position of the surgical tool handle. In addition, the numerical examples are presented

11. Neural Network method solving DK[112]:

The contribution is that applying a neural network model to solve the direct kinematic for real time application (section 3.3.5). Instead of solving nonlinear equations for the direct kinematics, NN algorithm is used to train the neural networks. Simulation and experiment are carried out to demonstrate the performance and accuracy.

III. Design for manufacturing (Chapter 4): The DFM guidelines are applied to the design for haptic devices to reduce design production cost, increase design reliability, enhance design quality, symmetrize parts, reduce number of parts, and standardize fastening parts. This contribution leads a new concept to engineering research that mechanical design must consider manufacture ability in design stage. DFM guidelines have been implemented in this research work which presents a foundation for the future development of practical engineering product.

IV. Local master-slave and supporting mechanisms (Chapter 5): Two-DOF local master-slave mechanisms are designed to increase the dexterity for complex surgical tasks. The local master-slave mechanism contains a tool tip that pivots as a two-DOF wrist. Both slave and master end are integrated on one-piece surgical tool, which uses a tendon to actuate. The contribution is proposing a compact manually actuated two-DOF surgical instrument. Additional supporting mechanism such as surgical abdominal space maker is designed to create the surgical space inside patient's body that eliminates

difficulties of pneumatic method. The contribution is developing new foldable mechanism that creates surgical space inside the abdominal wall.

6.2.Future Work Suggestion

The surgical robotic mechanism is developing rapidly so many research topics need to be explored. The future for robotic surgery is based on new development of engineering technology. While robotic mechanisms for laparoscopic surgery are proposed and implemented, developments can be expanded in the future based on the current research achievement.

1. **Single modular arm for tooling-holding:** the tool-holding mechanism is compact in size and the major components of tool-holding mechanism are mounted on the distal plate. Therefore, several of these mechanisms can be integrated into a single modular arm to hold three or four surgical instruments and one laparoscope at same time. After integration, only one surgical arm (Figure 6-2) is needed to manipulate three or four surgical tools. This robotic arm can be attached to the surgical table. Integrating multiple arms into single arm can also reduce the possibility of interference between arms.

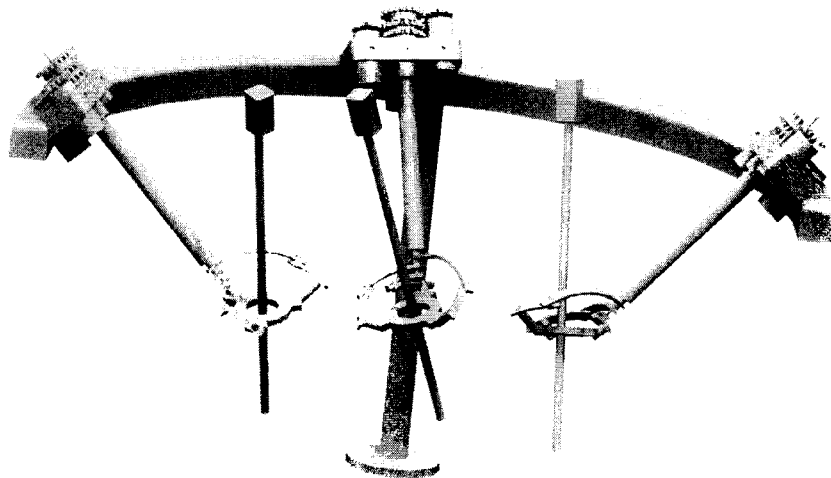


Figure 6-2 Design of single surgical arm with three tools

As shown in Figure 6-3, the four DOF tool-holding arm can be integrated with the four DOF haptic device for telesurgery.

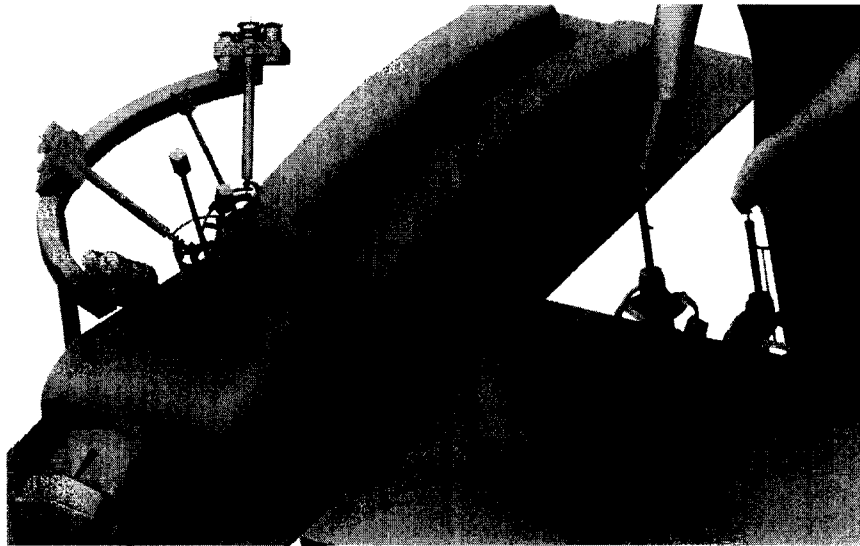


Figure 6-3 Integration of 4 DOF haptic device with tool-holding mechanism for teleoperation

2. **Six DOF haptic force feedback device:** Adding the two-DOF local master-slave mechanism (chapter 5) on the four DOF haptic device (chapter 3) to be a six DOF force feedback device. This device enables surgeon to gain the force feedback for robotic surgery and controls the surgical robot (chapter 2) to position the surgical instrument and laparoscope. A further step of robotic surgery can be implemented of haptic devices and surgical tool-holding mechanism. As shown in Figure 6-4, a surgeon manipulates the six DOF haptic devices as the master to control the slave tool-holding mechanism to teleoperate the surgical tasks on the patient. The robotic surgery requires the integration of software, control, and network for completed surgical robotic system.

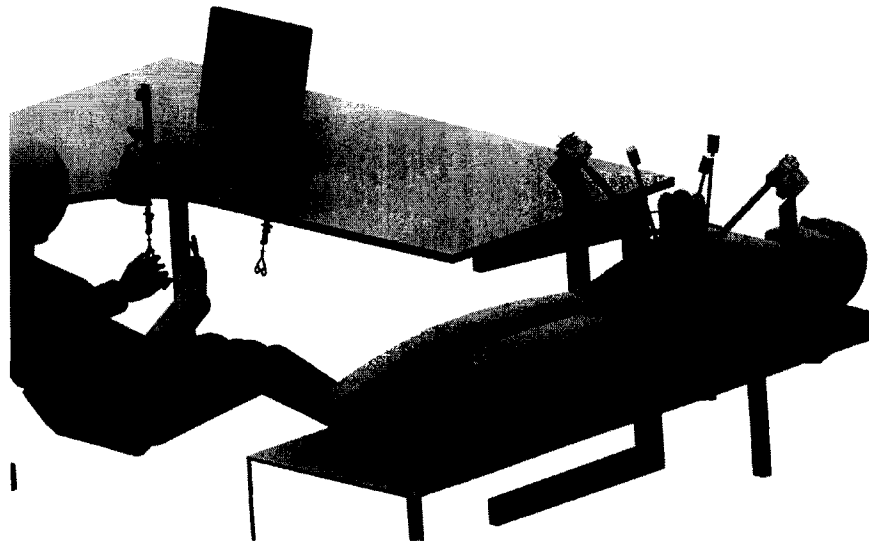


Figure 6-4 The integration of tooling-holding and haptic device

3. **Design for manufacturing analysis of mass production:** In chapter 4, the DFM is analyzed for the prototyping development. In the point of view of engineering product, there are different DFM guidelines that are not being used because these guidelines are for mass production. For instance, the materials used include aluminum alloy that may be replaced by engineering plastic for mass production. Therefore, a further study about the production, scheduling for manufacturing can be explored.

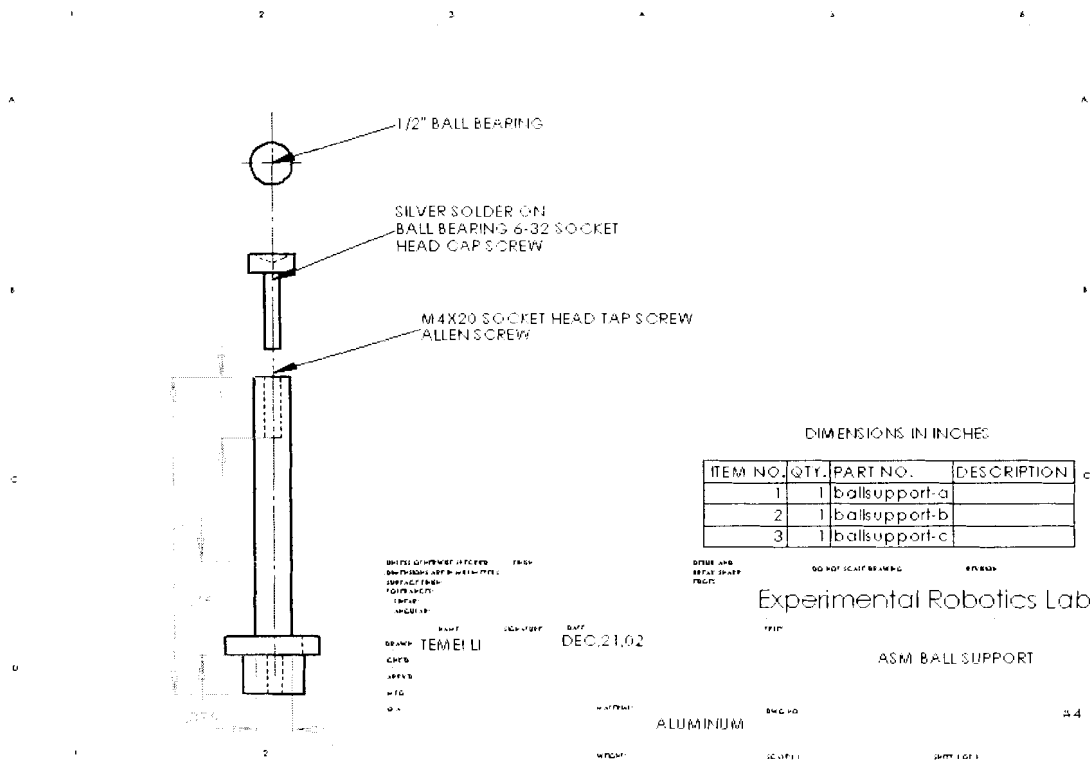
4. **Haptic force feedback gripper or handle:** For the handle of the local master-slave devices (Chapter 5), gripper or pinching function can be integrated. The gripper can provide grasping or clipping motion which can be used for biopsy. The challenge is to integrate one DOF (gripping or pinching) force feedback with the two rotational DOF to become a three DOF force feedback device which is more complex than the current one DOF gripper of Faraz's design [8] or Immersion LSW. By adding this three DOF (one gripping and two rotational DOF) master-slave to the four DOF tool-holding mechanism, the surgical robotic arm has seven DOF.

5. **Modular utilization:** The designed mechanisms are based on the laparoscopic surgery with four DOF kinematic constraints. The laparoscopic surgical mechanism contains more DOF than the requirement of other MIS. For example, in the closed-chest heart surgery the surgical instruments are inserted into chest through the space between ribs. This constrained the tool to only two-DOF (in/out, rotational along insertion axis). Brain surgery, nasal endoscopic surgery, or laser eye surgery are also constrained to two-DOF kinematic motion. By reviewing the previous designs (Chapter 2, and 3), the design of tool-holding and haptic devices can be broken down into modules such as One DOF linear (L) motion, two-DOF (LR) motion, Two rotational (RR) DOF motion, three rotational (RRR) DOF motion. The modular devices can be integrated as a new application in MIS such as heart surgery, eye surgery.

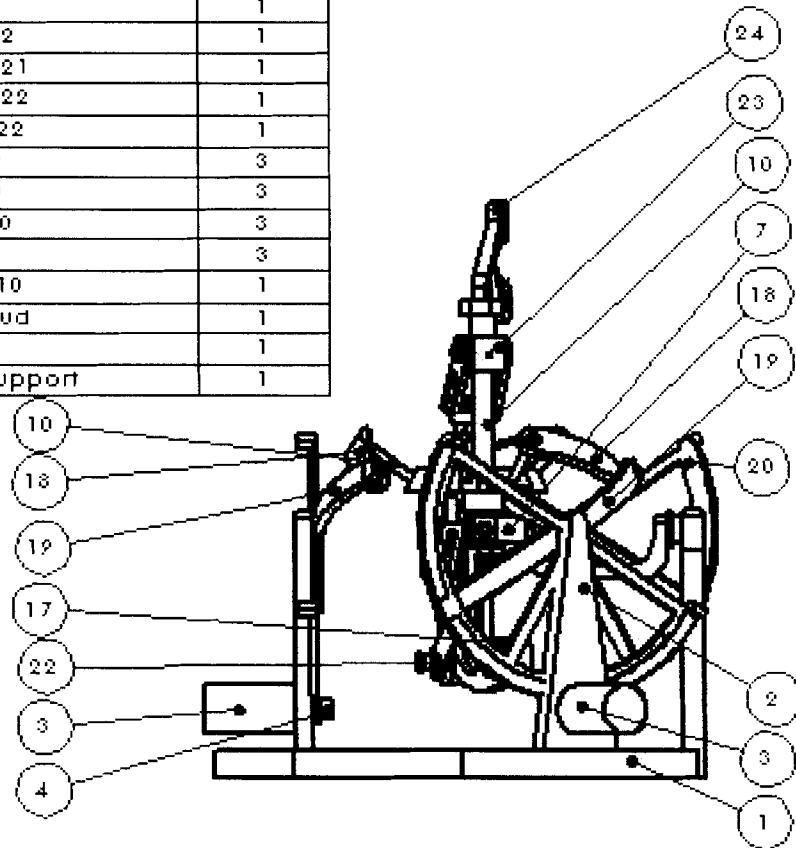
Appendix A Drawings of Assembly and Parts

The drawings of following designs of joints and grasper are included in this appendix

1. Assembly drawing of ball support of SPBS
2. Assembly drawing of HPST
3. Assembly drawing of SPBS
4. Assembly drawing of THT

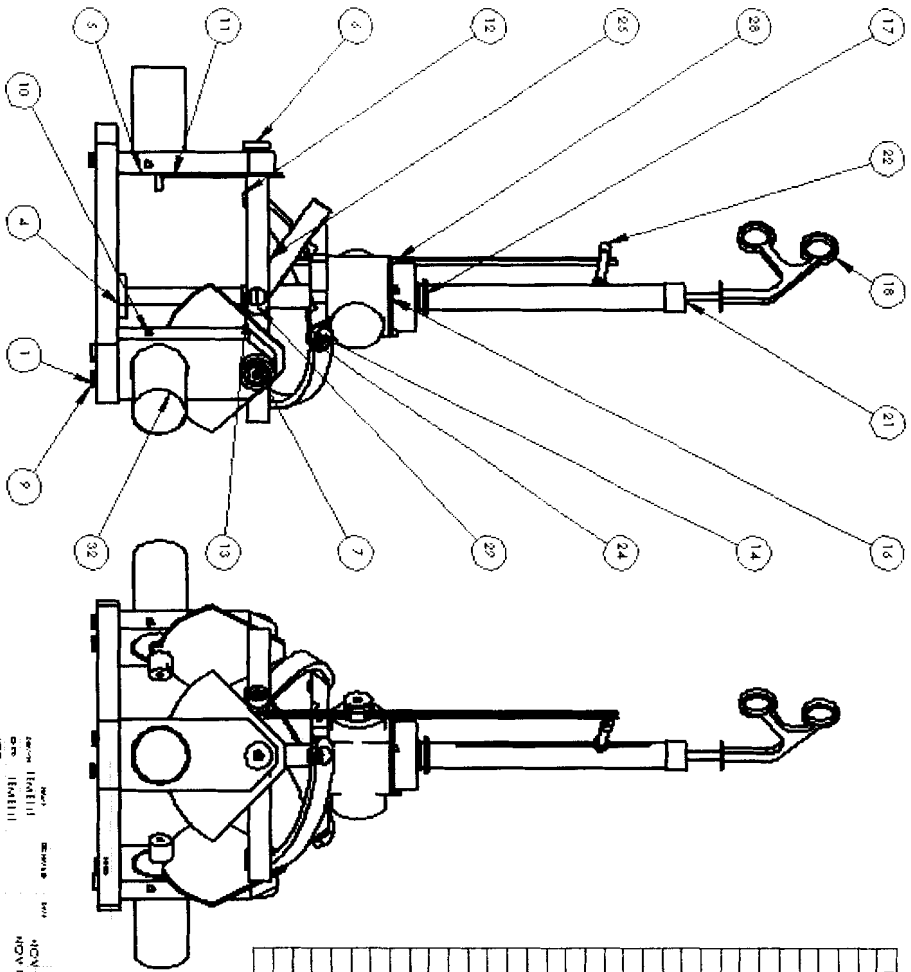


ITEM NO.	PART NUMBER	QTY.
1	bottom-plate	1
2	brkt-lm f	3
3	motor-3s	3
4	pulley-1s	3
5	screw-m 5	6
6	bearingps0812-08	2
7	yoke	1
8	bearingps0406-02	13
9	shaft-pltfm	1
10	pltfm-hap3	1
11	bearingps0812-08	1
12	fork	1
13	cam 85	1
14	brkt-m t2	1
15	brkt-m t21	1
16	brkt-m t22	1
17	motor-22	1
18	am 110	3
19	am 120	3
20	cam 120	3
21	ball3-8	3
22	pulley-10	1
23	holder-ud	1
24	handle	1
25	hap3-support	1



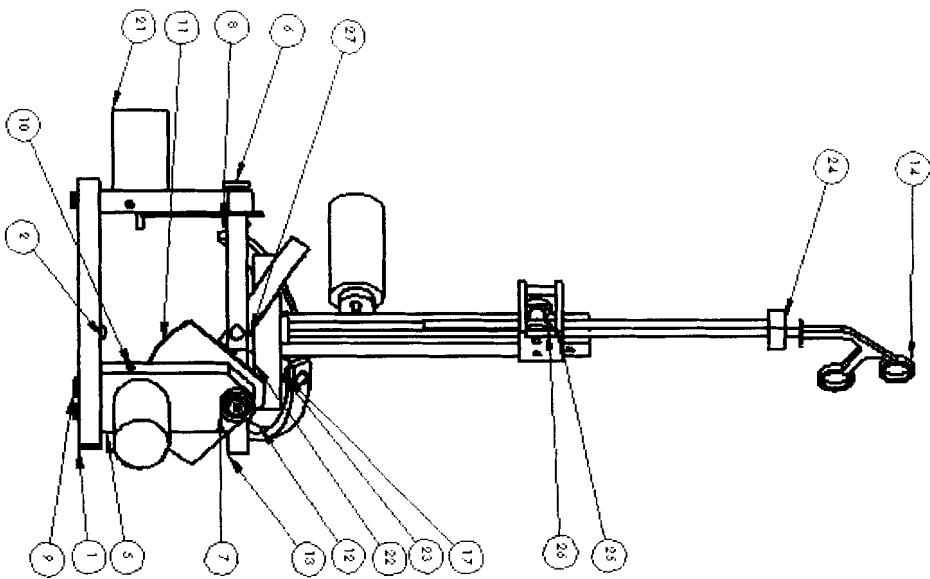
Experimental Robotics Lab

DATE: JUN, 13, 01
 NAME: TEMELLI
 AS M- HPST
 A 4



ITEM NO.	PART NUMBER	QTY.
1	Dose plate	1
2	10-24 nut-head	1
3	Dose-washer	1
4	asm-ballsupport	1
5	Bracketmotor	3
6	Retaining-washer	3
7	Bracketbushing	3
8	brass-bushing	3
9	6-32	4
10	4-40-set	4
11	cam-50	3
12	link-passive-4	3
13	link-active-4	3
14	platform	1
15	rod-ent	1
16	cap-pitmm-ong	1
17	tubular	1
18	handlem	1
19	pluresy/pdown	1
20	guide-up/down	1
21	cap-tube	1
22	m5	1
23	asm-link-bearing-unit	3
24	asm-platform-link-unit	3
25	link-up/down	1
26	asm-sleeve-bearing-unit	3
27	pulley/nt	3
28	m2	3
29	pit/rod	1
30	bracket/pot	3
31	pot	3
32	motor/mg-xon-32	4

DRAWING NO. 1001-1001-1001-1001
 REV. 1
 DATE 11/11/11
 DESIGNED BY J. H. H. H.
 CHECKED BY J. H. H. H.
 APPROVED BY J. H. H. H.
 PART NO. 1001-1001-1001-1001
 QTY. 1001-1001-1001-1001
 ASM-SPBS
 9/11/11



ITEM NO.	PART NUMBER	QTY
1	base-plate-naps	1
2	top-24-link-rod	1
3	base-washer	1
4	asm-bol-support	1
5	bracket-motor	3
6	retaining-washer	3
7	bracket-pushing	1
8	brass-bushing	3
9	8-32	6
10	4-40-set	4
11	cam-50	3
12	link-in-17-naps	3
13	link-out-naps	3
14	rod-naps	1
15	pulley-up-down-naps	1
16	asm-link-bearing-unit	3
17	asm-plate-form-link-unit	3
18	asm-sleeve-bearing-unit	3
19	pulley-in-naps	3
20	m2	1
21	motor-32-holder	4
22	plthm-snap's	1
23	linear-sprt-snap's	1
24	linear-guide	1
25	line-guide-pulley	1
26	line-pulley	1
27	pin-rod-naps	3
28	center-clip	1
29	pin	1

DRAWN BY: TEMELI
 DATE: FEB 04 04
 CHECKED BY: [blank]
 DATE: [blank]

ASMA-THT
 204

Appendix B-Design for Manufacturing Guidelines

DFM and DFA are the integration of product design and process planning into one common activity. The goal is to design a product that is easily and economically manufactured. The core of design for manufacturing system is groups of design guidelines that assist the designer reduce the cost and difficulty of manufacturing an item. DFM guidelines can be found from many reference and the following is a listing of these rules used in this research.

1. Reduce the total number of parts. The reduction of the number of parts in a product is the best opportunity for reducing manufacturing costs. Less parts implies less purchases, inventory, handling, processing time, development time, equipment, engineering time, assembly difficulty, service inspection, testing, etc.
2. Simplify the design and reduce the number of parts because for each part, there is an opportunity for a defective part and an assembly error.
3. Develop a modular design. The use of modules in product design simplifies manufacturing activities such as inspection, testing, assembly, purchasing, redesign, maintenance, service.
4. Design for ease of fabrication. Select the optimum combination between the material and fabrication process to minimize the overall manufacturing cost.

5. Use of standard components. Standard components are less expensive than custom-made items. The high availability of these components reduces product lead times. In addition, their reliability factors are well ascertained.

6. Design within process capabilities and avoid unneeded surface finish requirements. Final operations such as painting, polishing, finish machining, etc. should be avoided.

Reference list

1. Mariani, M.A., et al., *Minimally Invasive Coronary Artery Bypass Grafting Versus Coronary Angioplasty For Isolated Type C Stenosis Of The Left Anterior Descending Artery*. J Thorac Cardiovasc Surg, 1997. **114**(3): p. 434-439.
2. Allen, J.E., *The Economics Of Laparoscopic Surgery*. Jacksonville Medicine, 1997.
3. Tovar, J.A., et al., *Functional Results of Laparoscopic Fundoplication in Children*. Journal of Pediatric Gastroenterology & Nutrition, 1998. **26**(4): p. 429-431.
4. Poole, G., et al., *How much has the introduction of laparoscopic surgery changed open surgery ?* THE NEW ZEALAND MEDICAL JOURNAL, 2003. **116**(1178).
5. Boer, K.T.d., et al., *Peroperative time-motion analysis of diagnostic laparoscopy with laparoscopic ultrasonography*. British Journal of Surgery, 1999. **86**(7): p. 951 - 955.
6. Patkin, M. and L. Isabel, *Ergonomics, engineering and surgery of nonsurgical dissection*. J Royal Coll Surg Edinburgh, 1995. **40**: p. 120-132.
7. Mitchell, T.N., et al., *Three dimensional endoscopic imaging for minimal access surgery*. J Royal Coll Surg Edinburgh, 1993. **38**: p. 285-292.
8. Faraz, A., *Mechanisms and robotic extenders for laparoscopic surgery*. 1998, Thesis Simon Fraser University.
9. Finlay, P., *Robotic controlled endoscopic manipulator*. Technological Advances in Therapeutic Urology, IEE Colloquium, 1996: p. 91-93.
10. Nishikawa, A., et al., *Laparoscope Positioning System with the Surgeon's Face Image-Based Human-Machine Interface*. 2001: p. 166-173.

11. Massie, T.H. and J.K. Salisbury, *The PHANTOM Haptic Interface: A Device for Probing Virtual Objects*. Proceedings of the ASME Winter Annual Meeting, Symposium on Haptic Interfaces for Virtual Environment and Teleoperator, 1994: p. 295-302.
12. Cavusoglu, M.C., et al., *A laparoscopic telesurgical workstation*. Robotics and Automation, IEEE Transactions on, 1999. **15**(4): p. 728-739.
13. Burghart, C., et al., *On-line motion planning for medical applications*. Industrial Electronics Society, IECON, 1998. **4**: p. 2233-2238.
14. Kang, H. and J.T. Wen, *Robotic assistants aid surgeons during minimally invasive procedures*. Engineering in Medicine and Biology Magazine, IEEE, 2001. **20**(1): p. 94-104.
15. Sturges, R.H. and S. Laowattana., *A flexible tendon controlled device for endoscopy*. International Journal of Robotics Research, 1993. **12**(2): p. 121-131.
16. Tsoi, E.K.M. and C.H. Organ, *Abdominal Access in Open and Laparoscopic Surgery*. 1996, New York, NY: Wiley-Liss.
17. Hashimoto, D., et al., *Abdominal wall lifting with subcutaneous*. Surg Today, 1993. **23**: p. 786-790.
18. Hashimoto, D., et al., *Laparoscopic cholecystectomy: an approach without pneumoperitoneum*. Surg Endosc, 1993. **7**: p. 54-56.
19. Kitagawa, M., et al., *Effect of sensory substitution on suture-manipulation forces for robotic surgical systems*. Journal of Thoracic and Cardiovascular Surgery, 2005. **129**(1): p. 151-158.
20. Butner, S.E. and M. Ghodoussi, *Transforming a surgical robot for human telesurgery*. Robotics and Automation, IEEE Transactions on, 2003. **19**(5): p. 818-824.
21. Howe, R.D. and Y. Matsuoka, *Robotic techniques for surgery*. Annul Review Biomed. Eng, 1999. **01**: p. 211-240.

22. Bodner, J., et al., *Mediastinal parathyroidectomy with the da Vinci robot: presentation of a new technique*. Journal of Thoracic and Cardiovascular Surgery, 2004. **127**(6): p. 1831-1832.
23. Mack, M.J., *Minimally Invasive and Robotic Surgery*. American Medical Association JAMA, 2001. **285**(5): p. 568-572.
24. Neisius, B., P. Dautzenberg, and R. Trapp, *Robotic manipulator for endoscopic handling of surgical effectors and cameras*. In first International Symposium on Medical Robotics and Computer Assisted Surgery (MRCAS), 1994: p. 1-7.
25. Kornsuthisopon, S., *New release of the Boonpong laparoscopic camera holder*. Aust N Z J Surg, 1999. **69**(2): p. 141-143.
26. Berkelman, P., et al., *LER: the light endoscope robot*. IEEE/RSJ International Conference on Intelligent Robots and Systems, 2003. **3**: p. 2835-2840.
27. Phillips, W.G. and T. Thieme, *DA VINCI SURGICAL ROBOT*. Popular Science, 2002. **260**(3): p. 73.
28. Guthart, G.S. and J.K. Salisbury, Jr., *The Intuitive telesurgery system: overview and application*. International Conference on Robotics and Automation, 2000. **1**: p. 618-621.
29. Hanly, E.J., et al., *Multiservice laparoscopic surgical training using the daVinci surgical system*. The American Journal of Surgery, 2004. **187**(2): p. 309-315.
30. Casadei, C., S. Martelli, and P. Fiorini, *A Workcell for the Development of Robot-Assisted Surgical Procedures*. Journal of Intelligent and Robotic Systems, 2000. **28**(4): p. 301-324.
31. Omote, K., et al., *Self-guided robotic camera control for laparoscopic surgery compared with human camera control*. The American Journal of Surgery, 1999. **177**(4): p. 321-324.
32. Sackier, J.M., et al., *Voice Activation of a Surgical Robotic Assistant*. The American Journal of Surgery, 1997. **174**(4): p. 406-409.

33. Zhang, X.L., *Application of image tracking and 3D image reconstruction for laparoscopic surgery*, in *School of Engineering Science*. 2002, Thesis Simon Fraser University: Burnaby, BC, Canada.
34. Eykhoff, P., *System Identification: Parameter and State Estimation*. 1974, London: John Wiley and Sons Inc.
35. Angeles, J., *Spatial kinematic chains : analysis, synthesis, optimization*. 1982, Berlin ; New York: Springer-Verlag.
36. Erdman, A.G. and G.N. Sandor, *Mechanism design: analysis and synthesis*. 1991, Englewood Cliffs, N.J.: Prentice Hall.
37. Yan, H.S., *Creative Design of Mechanical Devices*. 1998, Tainan, Taiwan: Springer Verlag.
38. Dukkupati, R.V., *Spatial mechanisms: analysis and synthesis*. 2001, New Delhi: CRC Press.
39. Tsai, L.W., *Mechanism design : enumeration of kinematic structures according to function*. 2001, Boca Raton, FL: CRC Press.
40. Waldron, K.J. and G.L. Kinzel, *Kinematics, dynamics, and design of machinery*. 1999, New York ; Chichester England: Wiley.
41. Miles, A.R., *Spherical electric motors*. Potentials, IEEE, 1990. **9**(3): p. 47-48.
42. Freudenstein, F. and E.R. Maki, *Creation of Mechanisms According to Kinematic Structure and Function*. Journal of Environmental and Planning B, 1979. **6**: p. 375-391.
43. Merlet, J.P., *Parallel Robots*. 2000, Dordrecht, Netherlands: Kluwer Academic.
44. Tsai, L.W., *Robot analysis : the mechanics of serial and parallel manipulators*. 1999, New York ; Chichester England: Wiley.
45. Craig, J.J., *Introduction to robotics: mechanics and control*. 2nd ed. Addison-Wesley series in electrical and computer engineering. Control engineering. 1989, Reading, Mass.: Addison-Wesley.

46. Gosselin, C.M. and E. Lavoie, *On the kinematic design of spherical three degree-of-free manipulators*. The International Journal of Robotics Research, 1993. **12**(4): p. 394-402.
47. Gosselin, C.M., E.S. Pierre, and M. Gagne, *On the Development of the Agile Eye*. IEEE 96 Robotics and Automation Magazine, 1996. **3**(4): p. 29-37.
48. Birglen, L., et al., *SHaDe, a new 3-DOF haptic device*. Robotics and Automation, IEEE Transactions on, 2002. **18**(2): p. 166-175.
49. Cauche, N., et al., *Rotational force-feedback wrist*. IEEE International Symposium on Assembly and Task Planning, 2003: p. 210-215.
50. Liu, X.J., Z.L. Jin, and F.U.R. Gao, *Optimum design of 3-DOF spherical parallel manipulators with respect to the conditioning and stiffness indices*. Mechanism and Machine Theory, 2000. **35**(9): p. 1257-1267.
51. Stewart, D., *A platform with 6 degrees of freedom*. Proc. Of the Institution of mechanical engineers, 1965. **1**: p. 317 -386.
52. Koseki, Y., et al., *Simulation and computer-aided design of spherical parallel manipulators*. Robotics and Automation, 1998. Proceedings IEEE International Conference, 1998: p. 1340-1345.
53. Sciavicco, L. and B. Siciliano, *Modeling and control of robot manipulators*. McGraw-hill electrical and computer engineering series. 1996, New York: McGraw-Hill Companies Inc.
54. Oblak, D. and D. Kohli, *Boundary surfaces, limit surfaces, crossable and noncrossable surfaces in workspace of mechanical manipulators*. ASME Journal of Mechanisms, Transmissions, and Automation in Design, 1988. **110**: p. 389-396.
55. Hay, A.M. and J.A. Snyman, *Methodologies for the optimal design of parallel manipulators*. International Journal for Numerical Methods in Engineering, 2003. **59**(1): p. 131 - 152.

56. Liu, X.-J., J. Wang, and F. Gao, *Workspace Atlases for the Design of Spherical 3-DOF Serial Wrists*. Journal of Intelligent and Robotic Systems, 2003. **36**(4): p. 389-405.
57. Majid, M.Z.A., Z. Huang, and Y.L. Yao, *Workspace Analysis of a Six-Degrees of Freedom, Three-Prismatic-Prismatic-Spheric-Revolute Parallel Manipulator*. The International Journal of Advanced Manufacturing Technology, 2000. **16**(6): p. 441- 449.
58. Stamper, R.E., L.-W. Tsai, and G.C. Walsh, *Optimization of a three DOF translational platform for well-conditioned workspace*. IEEE Robotics and Automation, 1997. **4**: p. 3250-3255.
59. Holland, J.H., *Adoption in Natural and Artificial Systems*. 1975, Ann Arbor, MI: The University of Michigan Press.
60. Goldberg, D., *Genetic Algorithms in Search, Optimization, and Machine Learning*. 1989, Reading, MA: Addison-Wesley.
61. Gill, M.A.C. and A.Y. Zomaya, *A parallel collision-avoidance algorithm for robot manipulators*. IEEE Parallel & Distributed Technology, 1998. **6**(1): p. 68-78.
62. Tian, L., C. Collins, and R. Chu, *Optimal trajectory planning of redundant manipulators in constrained workspace*. Electronics Letters, 2002. **38**(14): p. 762-764.
63. Lee, Y.H., A.C. Marvin, and S.J. Porter, *Genetic algorithm using real parameters for array antenna design optimisation*. High Frequency Postgraduate Student Colloquium, 1999: p. 8-13.
64. Li, T. and S. Payandeh. *Application of Genetic Algorithms to Design of Spherical Mechanical in Laparoscopic Surgery*. in *Processing of the international Conference on Mathematics and Engineering Techniques in Medicine and Biological Science*. 2001. Las Vegas, NV, USA.

65. GIRAUD-MOREAU, L. and P. LAFON, *A COMPARISON OF EVOLUTIONARY ALGORITHMS FOR MECHANICAL DESIGN COMPONENTS*. Engineering Optimization, 2002. **34**(34): p. 307-322.
66. Angeles, J., *Fundamentals of robotic mechanical systems : theory, methods, and algorithms*. 2nd ed. 2003, New York: Springer.
67. Merlet, J.P., *Direct kinematics of parallel manipulators*. Robotics and Automation, IEEE Transactions on, 1993. **9**(6): p. 842-846.
68. Meng-Shiun Tsai, T.-N.S., Yi-Jeng Tsai, Tsann-Huei Chang, *Direct kinematic analysis of a 3-PRS parallel mechanism*. Mechanism and Machine Theory, 2002. **38**: p. 71-83.
69. Gosselin, C.M., J. Sefrioui, and M.J. Richard, *On the Direct Kinematics of Spherical Three-Degree-of-Freedom Parallel Manipulators of General Architecture*. ASME Journal of Mechanical Design, 1994. **116**(2): p. 594-598.
70. Nielsen, J. and B. Roth, *On the Kinematic Analysis of Robotic Mechanisms*. The International Journal of Robotics Research, 1999. **18**(12): p. 1147-1160.
71. Ji, P. and H. Wu, *Algebraic solution to forward kinematics of a 3-DOF spherical parallel manipulator*. Journal of Robotic Systems, 2001. **18**(5): p. 251-527.
72. Hsu, J., *Integration and control of the laparoscope holding robot*, in *Engineering Science*. 2003, Thesis Simon Fraser University: Burnaby.
73. Hsu, J.K., T. Li, and S. Payandeh, *On Integration of a Novel Minimally Invasive Surgery Robotic System*. ICAR, 2005: p. 437-444.
74. Roth, Z.S., B.W. Mooring, and B. Ravani, *An Overview of Robot Calibration*. IEEE J. of Robotics and Automation, 1987. **3**(5): p. 377-384.
75. Gosselin, C. and J. Angeles, *Singularity analysis of closed-loop kinematic chains*. Robotics and Automation, IEEE Transactions on, 1990. **6**(3): p. 281-290.
76. Angeles, J., G. Yang, and I.-M. Chen, *Singularity analysis of three-legged, six-DOF platform manipulators with URS legs*. Mechatronics, IEEE/ASME Transactions on, 2003. **8**(4): p. 469-475.

77. Goldsmith, P.B., *Design and kinematics of a three-legged parallel manipulator*. Robotics and Automation, IEEE Transactions on, 2003. **19**(4): p. 726-731.
78. Voglewede, P.A. and I. Ebert-Uphoff, *Overarching framework for measuring closeness to singularities of parallel manipulators*. Robotics, IEEE Transactions on [see also Robotics and Automation, IEEE Transactions on], 2005. **21**(6): p. 1037-1045.
79. Parenti-Castelli, V., R.D. Gregorio, and F. Bubani, *Workspace and Optimal Design of a Pure Translation Parallel Manipulator*. Meccanica, 2000. **35**(3): p. 203-214.
80. Burdea, G., *Force and touch feedback for Virtual Reality*. 1996, New York: John Wiley & Sons.
81. Berenji, H.R., et al., *Pitch control of the space shuttle training aircraft*. Control Systems Technology, IEEE Transactions on, 2001. **9**(3): p. 542-551.
82. Cavusoglu, M.C., A. Sherman, and F. Tendick, *Design of Bilateral Teleoperation Controllers for Haptic Exploration and Telemanipulation of Soft Environments*. IEEE Transactions on Robotics and Automation, 2002. **18**(4): p. 641-647.
83. Basdogan, C., C.-H. Ho, and M.A. Srinivasan, *Virtual environments for medical training: graphical and haptic simulation of laparoscopic common bile duct exploration*. Mechatronics, IEEE/ASME Transactions on, 2001. **6**(3): p. 269-285.
84. Chen, E. and B. Marcus, *Force feedback for surgical simulation*. Proceedings of the IEEE, 1998. **86**(3): p. 524-530.
85. Lamata, P., et al., *A New Methodology to Characterize Sensory Interaction for Use in Laparoscopic Surgery Simulation*. 3078 ed. Lecture Notes in Computer Science. 2004. 177-184.
86. Scott, H.J. and A. Darzi, *Tactile feedback in laparoscopic colonic surgery*. British Journal of Surgery, 1997. **84**: p. 1005.
87. Preusche, C., T. Ortmaier, and G. Hirzinger, *Teleoperation concepts in minimal invasive surgery*. Control Engineering Practice, 2002. **10**(11): p. 1245-1250.

88. Wagner, C.R., N. Stylopoulos, and R.D. Howe, *The role of force feedback in surgery: analysis of blunt dissection*. The Haptic Interfaces for Virtual Environment and Teleoperator Systems, 2002: p. 68-74.
89. Kazanzides, P., et al., *Force sensing and control for a surgical robot*. IEEE International Conference on Robotics and Automation, 1992. **1**: p. 612-617.
90. Massie, T.H., *Design of a Three Degree of Freedom Force-Reflecting Haptic Interface*. 1993, Thesis MIT: Boston, MA.
91. Shimoga, K.B., *A survey of perceptual feedback issues in dexterous telemanipulation. II. Finger touch feedback*. Virtual Reality Annual International Symposium, 1993: p. 271-279.
92. Merlet, J.P., *Optimal design for the micro parallel robot MIPS*. IEEE International Conference Robotics and Automation, 2002. **2**: p. 1149-1154.
93. Yoon, J. and J. Ryu, *Design, fabrication, and evaluation of a new haptic device using a parallel mechanism*. Mechatronics, IEEE/ASME Transactions on, 2001. **6**(3): p. 221-233.
94. Lee, J.H., K.S. Eom, and I.I. Suh, *Design of a new 6-DOF parallel haptic device*. IEEE International Conference on Robotics and Automation, 2001. **1**: p. 886-891.
95. Tsumaki, Y., et al., *Design of a Compact 6-DOF Haptic Interface*. Proceedings of the 1998 IEEE International Conference on Robotics and Automation, 1998: p. 2580-2585.
96. Geffard, F., et al., *On the use of a base force/torque sensor in teleoperation*. IEEE Robotics and Automation, 2000. **3**: p. 2677-2683.
97. Baumeister, T., *Marks' standard handbook for mechanical engineers / revised by a staff of specialists ; Eugene A. Avallone, editor; Theodore Baumeister III, editor*. 10th ed. 1996, New York: McGraw-Hill.
98. Spong, M.W. and M. Vidyasagar, *Robot Dynamics and Control*. 1989, New York, NY: John Wiley and Sons.

99. Gosselin, C.M., L. Perreault, and C. Vaillancourt, *Simulation and computer-aided design of spherical parallel manipulators*. Engineering in Harmony with Ocean, 1993. **2**: p. 301-306.
100. Merlet, J.P., *Direct kinematics and assembly modes of parallel manipulators*. Int. J. Robotics, 1992. **11**(2): p. 150-162.
101. Yee, C.S. and K.B. Lim, *Feedforward kinematics solution of Stewart platform using neural network*. Neuralcomputing, 1997. **16**: p. 333-349.
102. Boudreau, R., S. Darenfed, and C.M. Gosselin, *On the computation of the direct kinematics of parallel manipulators using polynomial networks*. Systems, Man and Cybernetics, Part A, IEEE Transactions on, 1998. **28**(2): p. 213-220.
103. Thilmany, J., *A touching sensation*. Mechanical Engineer, 2003: p. 4-7.
104. Wang, H.P., *Concurrent design of products, manufacturing processes and systems*. Automation and production systems. Vol. 3. 1998, Amsterdam: Gordon and Breach Science Pub.
105. Gu, P. and A. Kusiak, *Concurrent engineering: methodology and applications*. Advances in industrial engineering. 1993, New York: Elsevier.
106. Otto, K.N. and K.L. Wood, *Product design: techniques in reverse engineering and new product development*. 2001, Upper Saddle River, NJ: Prentice Hall.
107. Ostwald, P.F. and T.S. McLaren, *Cost analysis and estimating for engineering and management*. 2004, Upper Saddle River, NJ: Pearson Education.
108. ASME, *Geometric Dimensioning and Tolerancing*. 1994, ASME - American Society of Mechanical Engineers National Standards, 1994, ASME Y14.5M.
109. ASME, *Dimensioning and Tolerancing*. 1983.
110. Molloy, O., S. Tilley, and E. Warman, *Design for manufacturing and assembly: concepts, architectures and implementation*. 1998, London; New York: Chapman & Hall.

111. Meadows, J.D., *Measurement of geometric tolerances in manufacturing*. Manufacturing engineering and materials processing;. 1998, New York: Marcel Dekker.
112. Li, T., Q. Li, and S. Payandeh, *NN-based Solution of Forward Kinematics of 3 DOF Parallel Spherical Manipulator*. IROS, 2005 p. 827-832.
113. Cao, C.G.L., *A task analysis of laparoscopic surgery : requirements for remote manipulation and endoscopic tool design*. 1996, Thesis Simon Fraser University.
114. Tewari, A., et al., *Technique of da vinci robot-assisted anatomic radical prostatectomy*. Urology, 2002. **60**(4): p. 569-572.
115. Wittgen, C., et al., *Analysis of the hemodynamic and ventilatory effects of laparoscopic cholecystectomy*. Arch Surg, 1991. **126**: p. 997-1001.
116. Koivusalo, A., et al., *A comparison of gasless mechanical and conventional carbon dioxide pneumoperitoneum methods for laparoscopic cholecystectomy*. Anesth Analg, 1998. **86**(1): p. 153-158.
117. Koivusalo, A.M., I. Kellokumpu, and L. Lindgren, *Gasless laparoscopic cholecystectomy: comparison of postoperative recovery with conventional technique*. Br. J. Anaesth., 1996. **77**(5): p. 576-580.
118. Akira, S., et al., *Gasless Laparoscopic Surgery Using a New Intra-abdominal Fan Retractor System: An experience of 500 Cases*. Journal Nippon Med Sch, 2005. **72**(4): p. 213-236.
119. Nakamura, H., et al., *Fishing-rod-type abdominal wall lifter for gasless laparoscopic surgery*. Surgical Endoscopy, 1996. **10**(9): p. 944-946.
120. Maas, S.M., J.J. Hage, and M.A. Cuesta, *Less traumatic abdominal wall retraction for gasless laparoscopic surgery*. Surgical Endoscopy, 2000. **14**(8): p. 769-770.
121. Ikuta, K., H. Ishii, and M. Nokata, *Safety Evaluation Method of Design and Control for Human-Care Robots*. The International Journal of Robotics Research, 2003. **22**(5): p. 281-297.

122. Li, T. and S. Payandeh, *Design of spherical parallel mechanisms for application to laparoscopic surgery*. Robotica, 2002. **20**: p. 133-138.
123. Li, T. *Special purpose mechanism for minimally invasion surgery*. in *12th Annual Canadian Conference on Intelligent System*. 2002. Calgary, AB, Canada.
124. Payandeh, S. and T. Li, *Toward new designs of haptic devices for minimally invasive surgery*. Computer Assisted Radiology and Surgery., 2003: p. 775-781.